

Award Number: W81XWH-12-1-0591

TITLE: Organizing the Cellular and Molecular Heterogeneity in High-Grade Serous Ovarian Cancer by Mass Cytometry

PRINCIPAL INVESTIGATOR: Garry P. Nolan, Ph.D.

CONTRACTING ORGANIZATION: The Leland Stanford Junior University
Stanford, CA 94305-2004

REPORT DATE: October 2013

TYPE OF REPORT: Annual

PREPARED FOR: U.S. Army Medical Research and Materiel Command
Fort Detrick, Maryland 21702-5012

DISTRIBUTION STATEMENT: Approved for Public Release;
Distribution Unlimited

The views, opinions and/or findings contained in this report are those of the author(s) and should not be construed as an official Department of the Army position, policy or decision unless so designated by other documentation.

REPORT DOCUMENTATION PAGE

Form Approved
OMB No. 0704-0188

Public reporting burden for this collection of information is estimated to average 1 hour per response, including the time for reviewing instructions, searching existing data sources, gathering and maintaining the data needed, and completing and reviewing this collection of information. Send comments regarding this burden estimate or any other aspect of this collection of information, including suggestions for reducing this burden to Department of Defense, Washington Headquarters Services, Directorate for Information Operations and Reports (0704-0188), 1215 Jefferson Davis Highway, Suite 1204, Arlington, VA 22202-4302. Respondents should be aware that notwithstanding any other provision of law, no person shall be subject to any penalty for failing to comply with a collection of information if it does not display a currently valid OMB control number. **PLEASE DO NOT RETURN YOUR FORM TO THE ABOVE ADDRESS.**

1. REPORT DATE 01/Oct/2013			2. REPORT TYPE Annual		3. DATES COVERED 30 Sep 2012 – 29 Sep 2013	
4. TITLE AND SUBTITLE Organizing the Cellular and Molecular Heterogeneity in High-Grade Serous Ovarian Cancer by Mass Cytometry					5a. CONTRACT NUMBER	
					5b. GRANT NUMBER W81XWH-12-1-0591	
					5c. PROGRAM ELEMENT NUMBER	
6. AUTHOR(S) Garry P. Nolan, Ph.D. Wendy J. Fantl, Ph.D. E-Mail: gnolan@stanford.edu					5d. PROJECT NUMBER	
					5e. TASK NUMBER	
					5f. WORK UNIT NUMBER	
7. PERFORMING ORGANIZATION NAME(S) AND ADDRESS(ES) The Leland Stanford Junior University Stanford, CA 94305-2004					8. PERFORMING ORGANIZATION REPORT NUMBER	
9. SPONSORING / MONITORING AGENCY NAME(S) AND ADDRESS(ES) U.S. Army Medical Research and Materiel Command Fort Detrick, Maryland 21702-5012					10. SPONSOR/MONITOR'S ACRONYM(S)	
					11. SPONSOR/MONITOR'S REPORT NUMBER(S)	
12. DISTRIBUTION / AVAILABILITY STATEMENT Approved for Public Release; Distribution Unlimited						
13. SUPPLEMENTARY NOTES						
14. ABSTRACT Primary ovarian cancer (OC) represents a complex set of stem cell and cancer cell phenotypes embedded in a mixture of stromal and infiltrating immune cells. This grant develops techniques and approaches using mass cytometry that organize the heterogeneity within and between patient tumors to enlighten mechanisms and clinical opportunities in the apparent chaotic structure of the cancer. (1) A preliminary mass cytometry OC dataset by a "social clustering" strategy finds cell neighborhoods in high dimensional space reveals that 18 out of 20 samples had clusters of apparent stem-cell expressing deterministic combinations of stem cell markers. (2) Two high dimensional antibody panels were optimized and assembled to interrogate the tumor and immune cell compartments. (3) Indivumed (Hamburg Germany) is established as source for acquiring high quality HG-SOC primary specimens from single-cell dissociated tumors obtained within 3 hours of resection. (4) A QC procedure was established that surveys tumor samples (including epithelial, mesenchymal and immune cells) prior to their resection (using Abs against cleaved cCaspase 3, cleaved cPARP, vimentin, E-cadherin and CD45) to focus resection procedures on viable non necrotic tissue. (5) Eight key cell lines which bear remarkable genetic similarity to primary HG-SOC tumors have been obtained [1] as standards for primary tumors.						
15. SUBJECT TERMS Tumor initiating cells, Modularity Optimization in Networks of Cellular Phenotypes (MONOCLE), primary diagnostic samples, Indivumed, dissociation conditions, evaluation of viability and apoptosis, immunohistochemistry, validation of tumor antibodies, validation of immune cell antibodies, ovarian cancer cell lines, future plans.						
16. SECURITY CLASSIFICATION OF:				17. LIMITATION OF ABSTRACT	18. NUMBER OF PAGES	19a. NAME OF RESPONSIBLE PERSON
a. REPORT U	b. ABSTRACT U	c. THIS PAGE U	USAMRMC			
				UU	107	19b. TELEPHONE NUMBER (include area code)

Table of Contents

	<u>Page</u>
Introduction.....	4
Body.....	5
Key Research Accomplishments.....	10
Reportable Outcomes.....	10
Conclusion.....	11
References.....	12
Appendices.....	14

INTRODUCTION

High-grade serous ovarian cancer (HG-SOC) is the most common form of ovarian cancer and the majority of patients presenting with the disease respond well to initial treatment. However 70-90% of patients subsequently relapse and die of their disease [2, 3].

At present there is no consensus regarding the cell type that gives rise to HG-SOC. Several hypotheses have been proposed including ovarian surface epithelia and the fimbriae epithelia of the fallopian tube [4-6]. What is apparent is the diverse pathophysiology of the disease-- with ovarian cancer demonstrating a multitude of molecular and cellular alterations. This so-called heterogeneity has confounded attempts to establish the cellular origin of HG-OC and the differentiation stages at which "stemness" arises has hampered the search for successful treatment regimens, and begs the question of how we will bring order to this heterogeneity.

Therefore, with a need to organize the diverse nature of OC as the driving force for our research strategy, our approach has been to dismantle the tumor into its constituent single cells, to undertake deep phenotyping of each based on as many as 40 features per cell in a high throughput format, and then compare cell types both within as well as across tumors. *To ultimately tackle both these issues my lab is using a transformative proteomics technology termed mass cytometry, (aka **Cytometry by Time of Flight (CyTOF)**) which permits simultaneous measurements of up to 40 parameters per single-cell (expected to increase to ~70 primary channels and 200 or more pseudo channels), to provide a system-wide view of HG-SOC.* Constituent single cells from disaggregated ovarian tumors are analyzed to enable the delineation of the molecular and cellular basis of tumor heterogeneity in HG-SOC. This information is essential for permitting early diagnosis, chemoprevention, risk assessment, development of new therapies and personalized treatment regimens for this deadly disease.

BODY

D.1 Background

Single mass cytometry facilitates high-dimensional, quantitative analysis of the effects of bioactive molecules on cell populations at single-cell resolution. Datasets are generated with antibody panels (upwards of 40) in which each antibody is conjugated to a polymer chelated with a stable metal isotope, usually in the Lanthanide series of the Periodic Table [7-10] and **Appendix A** for copy of reference 8. The antibodies recognize surface markers to delineate cell types, such as immune, epithelial, mesenchymal, and intracellular signaling molecules demarcating multiple cell functions such as survival, DNA damage, cell cycle and apoptosis. By measuring all these parameters simultaneously, the signaling network state of an individual cell can be measured. A proof-of-principle for this technology described the immune continuum within a healthy bone marrow sample [11].

The body of the text will discuss progress over the last year (and current ongoing efforts) which pertains largely to **Task 1**. Specifically:

- **Subtask 1a:** Establish conditions for dissociation of solid tumors into single cells.
- **Subtask 1b:** Select a panel of extracellular modulators with which to measure signaling responses (done in the context of titrating the antibodies).
- **Subtask 1c:** Select two panels of ~60 antibodies each (*this should have been 40 in the original SOW*).
- **Subtask 1d:** We have submitted and *gained approval* for the necessary HRPO (IRB) and the ACURO.
- **Subtask 1e:** Acquire 10 primary diagnostic (no treatment) ovarian tumor or ascites samples with matched blood samples (Neel lab at UHN Toronto, and Berek at Stanford). In a new development we are now acquiring samples from Indivumed in Hamburg Germany.
- **Subtask 1f:** Develop and apply new informatics tools and algorithms.
- **Subtask 2b:** Cell line validation of monitoring reagents for extracellular modulators of signaling pathways.

D.2 Foundational Experiments

In earlier studies that were foundational for this award the *Neel lab* performed high throughput screening of surface marker expression in primary HG-SOC samples by fluorescence-based flow cytometry. The data identified a number of markers that were either expressed consistently in low percentages of cells (“minority markers” n=65) or were variably expressed in different cells (“variable markers” n=35) across different samples. Such markers would either represent spurious expression of proteins with little to no relevance to OC, or potentially represented markers associated with rare subpopulations of some benefit to the continuance of the tumor. A CyTOF panel was assembled, comprised of thirty-one metal-conjugated antibodies, against a set of these markers (from the high throughput screen) in combination with Pax-8, (a transcription factor representing cells of Mullerian origin), potential stem cell markers (e.g., Sox2, Nanog, Bmi-1, unphospho β -Catenin) and DNA damage (pATM, pH2AX) and cell cycle proteins (cyclin B1, pRb and pH3) for experimentation and analysis of 21 primary HG-SOC tumors and 30 ovarian cancer cell lines carried out in the *Nolan Lab* at Stanford.

In order to capture the depth of information that a CyTOF dataset provides there are informatics challenges at several levels. These include the multi-dimensional nature of the data, which results in the need to analyze millions of single-cell measurements, the distorted space of the data distribution, owing to the differential dynamic range of each antibody, differences in cell size, etc.), and the possibility that sub-populations assume different shapes in multi-dimensional space and include vastly different numbers of cells. It is therefore necessary to have a number of complementary, overlapping and mutually exclusive computational approaches for analyzing CyTOF data. To date there have been several approaches taken to analyze CyTOF data [12-15].

The *Pe'er Lab* developed a new algorithm Modularity Optimization in Networks of Cellular Phenotypes (MONOCLE) that adapts network theory to analyze mass cytometry data, employing a “Facebook”-like strategy. First, “k-neighborhoods” are assigned for each single-cell measurement (in 31 parameter-space). A pilot density of k = 20-50 is employed (i.e., the 20-50 nearest cells) and Mahalanobis, rather than Euclidean, distances are used to identify neighbors in the distribution. This innovation deals with the different dynamic ranges of antibody intensity/cell size defined above. A “Similarity Score,” defined as the intersection of k-neighborhoods, is

then calculated for each pair of points. The Louvain method of community detection is then employed to identify clusters in the network.

Preliminary data, applying MONOCLE to the CyTOF data resulted in the identification of 34 clusters of cells. Seven of these were CD45+, representing the immune cell infiltration in the primary tumors; gratifyingly, these clusters were recognized as distinct from the cell lines and the other, non-lympho-hematopoietic cells in the primary tumor samples. Six other clusters were Vimentin+, which could indicate infiltrating stroma or epithelial-mesenchymal-like properties in the primary tumor. The remaining clusters varied in size, but four were generally small and enriched in stem cell markers. Remarkably, 18/20 primary sample had significant populations of at least one of these “stem cell-like” clusters, and in most samples, these clusters were mutually exclusive (i.e., the sample had one or at most two types of clusters, but not all four).

These findings are intriguing for several reasons. First, they are consistent with previous work from the *Neel lab* indicating that the surface phenotype of tumor initiating cells (TIC) from HG-SOC is heterogeneous [16]. Second, they emphasize the potential benefit of coupling analysis of putative functional stem cell markers (e.g., SOX2, etc.) to surface antibody assessment. Third, and most interestingly, they suggest clear sorting strategies for enriching such clusters from primary HG-SOC samples, experiments of which are in progress in the *Neel lab*.

Given the above results, and the potential advantage of using functional markers to identify/enrich for TIC, the *Neel lab*, is taking several additional approaches in parallel. Studies in hematopoietic stem cells, T cell-ALL and other malignancies suggest that low ROS (reactive oxygen species) might be associated with the stem cell state. Indeed, in initial experiments, the *Neel lab* has found that sorting for cells with low ROS using the fluorescence marker H(2)DCF-DA (dihydrodichlorofluorescein diacetate (DCF) enriches for cells with Sox2 and ASCL1 transcripts. We are currently examining testing whether low ROS levels can be used to enrich for TIC (using our xenograft assay[16]), as well as searching directly for additional surface markers that correlate with SOX2 expression and/or ROS levels. Such markers will be iteratively incorporated into CyTOF experiments in collaboration with the *Nolan lab* to optimize our ability to identify, quantify, and study the properties of HG-SOC TIC.

D.3 Parallel Studies in the Nolan Lab Landscaping HG-SOC primary samples

Using an alternative and complementary strategy, the Nolan Lab is analyzing primary diagnostic ovarian tumor samples using an antibody panel designed to interrogate the biology based on prior knowledge in the literature. In this first year we have taken considerable measures to ensure data collected is of high value. *This means strict control over the sample acquisition process, stage-specific tests during the protocol to ensure we are working with live cells, and testing of every single reagent for its validity to bind the epitope against which it was originally raised. We believe these initial steps—though tedious—are critical to “trusting” the data from such precious samples as those obtained from patients with fatal diseases.*

D.3.1 Acquisition of primary diagnostic HG-SOC samples from Indivumed, Hamburg Germany

Indivumed (Indivumed.com), based in Hamburg, Germany has developed a biobank in which stringent processing protocols are applied to fresh primary human samples (mostly tumors) such that they retain comparable patterns of biomolecules (DNA, RNA and protein) as they were in the human body. Importantly, sample collection is based on the following criteria:

- Team of on-call nurses
- Tight communication **and timing** with surgery team
- Present during entire surgery
- Record data such as blood supply clamping, etc.
- First to handle tissue samples after surgery
- All processing done on-site, in room adjacent to OR – **tight timing**
- Record observations, location of sample collection, timing, etc.
- Full clinical annotation

Sample ID	TB Neg	Fixed Samples		Viably Frozen Samples	
		Aqua-	Aqua-/PARP-	Aqua-	Aqua-/PARP-
4079	37%	58%	15%	11%	4%
4080	90%	-	-	42%	11%
4081	86%	87%	13%	33%	12%
B1930 lib	79%	78%	26%	-	-
B1930 milt	77%	84%	27%	-	-
R847 lib	77%	76%	21%	30%	11%
R847 milt	80%	-	-	14%	4%

Table 1: Viability of CRC samples fixed and frozen post-dissociation (Aqua) match viability post-dissociation (TB: trypan blue), although PARP cleavage is high. Viable freezing results in large decrease in viability. See text.

In her prior employment in the Biotech arena, Dr Fantl worked with Indivumed and therefore capitalized on a former very productive relationship to establish a new collaboration to procure high quality HG-SOC samples for this award. One hurdle to overcome was the preparation of viable single cells from solid tumors. Preparatory experiments were performed in the Nolan lab testing a matrix of conditions, based on enzymatic and mechanical dissociation protocols using human ovarian tumor samples from mouse xenografts. A graduate student from the *Nolan Lab* spent one week at Indivumed to optimize and transfer the procedure “on-site”. In summary, given the prevalence of colorectal cancer (CRC) cases over ovarian, the dissociation conditions were established at Indivumed using CRC samples. Importantly, CRC and HG-SOC are considered “soft tumors”. No ovarian cases presented during our post-doc’s visit to Indivumed. Based on a comparison of conditions, in our current protocol samples are dissociated mechanically in a Milteny “gentleMACS” dissociator in the presence of a Milteny proprietary protease mix and then incubated with rotation for 30 minutes all according to the manufacturer’s instructions. *Importantly single cell suspensions of HG-SOC were generated within 3 hours post resection. This will be standard operating procedure for acquisition of all our primary tumor samples.*

D.3.2. Testing samples for viability post-dissociation

By way of introduction, we are using trypan blue, Aqua (for fluorescence-based flow cytometry) and cisplatin (for CyTOF) to measure the viability status of the samples. These reagents operate on the principle that a compromised cell with a damaged plasma membrane permits reagent entry into the cytoplasm, whereas a healthy cell with an intact plasma membrane does not. Good viability therefore correlates with *lack* of staining. At Indivumed, immediately after dissociation, the viability of the cells was determined by trypan-blue counting of a small aliquot. Samples were then exposed briefly to aqua or cisplatin, reagents that allow viability to be determined by fluorescence or mass cytometry respectively at Stanford [17]. At Indivumed, samples were either fixed in paraformaldehyde (PFA) and frozen or viably frozen in DMSO/fetal bovine serum as per *Nolan lab* established protocols [18]. Several important observations were made, primarily with the colon samples (**Table 1**), but relevant to the HG-SOC samples of which six are now at Stanford. 1) *Trypan Blue staining demonstrates that cells are viable post-dissociation.* 2) *Fixation and freezing immediately post-dissociation results in “capturing” cells in a viable form suitable for cytometry (Aqua- column, red outline)* 3) *Significant cell death (apoptosis and necrosis) occurs after a “viable” freezing procedure (blue outline around last two columns).* **We also have this information for 4 ovarian samples in which the Aqua- cells were ~ 10% for 2 samples and ~60% for another 2.** 4) *In spite of good viability of fixed samples post thaw, a percentage of cells have undergone apoptosis (aqua-/PARP-column within red outline).* **Note: number of initial samples represents initial studies that set the groundwork for later experimental design.**

D.3.3. Cells undergoing apoptosis pre-exist in primary tumors *in situ*

That levels of cleaved PARP were increased in Aqua negative cells led to the question of whether this “apoptotic state” pre-exists within the tumor or is introduced during the single-cell dissociation procedure. To evaluate this possibility, immunohistochemistry was performed with an antibody against cCaspase 3 on formalin fixed paraffin embedded sections (FFPE) at Indivumed. Apoptotic cells were detected in 7 ovarian cancer cases, whereas one case was completely negative for cleaved Caspase-3. Two cases (R873 and R892) exhibited maximal 5% of apoptotic cells. In further two cases (X2617 and x2619) 10% of apoptotic cells

Sample no.	Tissue type	Staining Intensity	Positive cells (%)	Compartment			Comment
				Tumor	Stroma	Inflammatory cells	
R866-Tp13	ovarian cancer	0	0	0	0	0	
R873-Tp11	ovarian cancer	1+	≤5	x	0	0	only surface tumor epithelium weak positive
R892-Tp11	ovarian cancer	1+	≤5	x	0	x	some inflammatory cells and detritus positive
X2617-Tp12	ovarian cancer	2+	10	0	x	x	mainly inflammatory cells positive
X2619-Tp12	ovarian cancer	2+	10	0	x	x	mainly inflammatory and stroma cells positive, only single tumor cells positive
X2623-Tp111	ovarian cancer	1+	30	x	x	x	tumor cells partly very weak positive, majority only with nonspecific background
Z289-Tp111	ovarian cancer	1+	20	x	x	0	mainly tumor cells positive (very weak)
Z301-Tp111	ovarian cancer	2+	50	x	x	x	mainly tumor cells positive (weak to moderate)

Table 2 Histopathological evaluation of anti-Caspase-3, cleaved immunohistochemistry. (0 = negative, 1+ = weak, 2+ = moderate, 3+ = strong, x = positively stained)

were detected. A high percentage (20%, 30% and 50%) of apoptotic cells was determined in three cases (Z289, 2623 and Z301). The results for HG-SOC samples were evaluated independently by two pathologists (**Table 2**). These samples will be evaluated by flow in the coming weeks.

D.3.4. Reagent validation and characterization

Antibodies: We have developed two antibody panels against tumor cells and one against the infiltrating immune cells. Antibodies were either, purchased as metal-conjugates, or conjugated by us to metal-chelating polymers and were all titrated against positive and negative controls to optimize signal to noise (see appendix for titrations). Multiple antibody clones were tested from different vendors, the details of which are given in **Table 3** (Tumor antibody panel) and **Table 4** (Immune panel). Two exemplar titrations are shown for CD133, a stem cell surface marker (**Figure 1a**) and pH2AX, a transducer of DNA damage (**Figure 1b**), both critical components of ovarian cancer biology. Our complete sets of titrations are in Appendix A.

Multiple antibody clones were tested from different vendors, the details of which are given in **Table 3** (Tumor panel) and **Table 4** (Immune panel). Two exemplar titrations are shown for CD133, a stem cell surface marker (**Figure 1a**) and pH2AX, a transducer of DNA damage (**Figure 1b**), both critical components of ovarian cancer biology. Our complete sets of titrations are in **Appendix B and C** respectively.

Mass	Element	Antibody	Clone	Vendor	Catalogue Number	Titration Cell Lines
113	In	Not used				
115	In	Vimentin	D21H3	CST	5741BF	OVCAR3, NIH3T3
139	La	CD45	H130	Biologend	304002	OVCAR3, PBMCs
141	Pr	N Cadherin	8C11	BD	561553	HeLa, OVCAR
142	Nd	c-Casp 3	C92-605	BD	624084	Jurkat, 24hr Etoposide +/-
143	Nd	CA125	X75 (3C8/4)	Gen Way	GWD-17DD7A	U937, OVCAR3
144	Nd	CD90	5E10	Biologend	328102	K562, Jurkats
145	Nd	p-AMPK (pT172)	40H19	CST	2535BF	U937, 24hr AICAR+/-
146	Nd	p-ATM (pS1981)	10H11.E12	Millipore	05-740	Jurkat, 4hr Etoposide +/-
147	Sm	p-H2AX (pS139)	JBW301	Millipore	05-636	Jurkat, 4hr Etoposide +/-
148	Nd	Total Cyclin B1	GNS-1	BD	554176	HCT116, Nocodazole +/-
149	Sm	p-NFkB (pS529)	K10-895.12.50	BD	558393	Jurkat, TNF +/-
150	Nd	pBCL2 (S70)	5H2	CST	2827BF	OVCAR3, Taxol +/-
151	Eu	p-ERK (pT202/pY204)	DA3.14.4E	CST	4370BF	U937, PMA +/-
152	Sm	Ki67 (total)	B56	BD	556003	HCT116, Nocodazole +/-
153	Eu	p-CHK2 (pT68)	C13C1	CST	2661BF	HCT116, Nocodazole +/-
154	Sm	pSTAT3(Y705)	4 P-STAT3	BD	6240484	Jurkats, PVO4 +/-
155	Gd	CD133	AC133	Miltenyi	130-090-422	Jurkats, CaCo
156	Gd	CD10	H110a	Biologend	312202	Jurkats, REH
157	Gd	SNAIL	20C8	eBiosciences	14-9859-82	HCT116, NIH3T3
158	Gd	E-Cadherin	2.40E+11	CST	3195BF	Jurkats, OVCAR3
159	Tb	p-Akt (pS473)	D9E	CST	4060BF	Jurkat, PVO4 +/-
160	Gd	Sox2	O30-678	BD	561469	ESC, +/- LIF
161	Dy	cMYC	D84C12	CST	5605BF	MEF, + DOX (Day 2)
162	Dy	pSTAT5(Y694)	47	BD	6240484	Jurkats, PVO4 +/-
163	Dy	Endoglin	43A3	Biologend	323202	U937, HELA
164	Dy	CD24	ML5	Biologend	311102	PBMCs, B vs T.
165	Ho	p-Rb (pS807/811)	J112-906	BD	558389	HCT116, Nocodazole +/-
166	Er	CD44	BJ18	DVS	3166001B	PBMCs, T vs Monos
167	Er	PAX8	polyclonal	Abcam	ab97477	Jurkats, OVCAR3
168	Er	CD13	L138	BD	624084	PBMCs
169	Tm	p-CHK1 (pS345)	133D3	CST	2348BF	Jurkat, Etoposide +/-
170	Er	Non-phos β -Catenin	D10A8	CST	8480BF	HCT116, 293 +/- LiCl
171	Yb	c-PARP (N214)	624084	BD	624084	Jurkat, 24hr Etoposide +/-
172	Yb	pS6 (pS235/pS236)	N7-548	BD	624084	Jurkats, PMA +/-
173	Yb	Mesothelin	MB-G10	Rockland	200-301-A87	OVCAR, HeLa
174	Yb	pCREB (S133)	8763	CST	9198BF	Jurkat, PMA +/-
175	Lu	Total p53	1C12	CST	2524BF	Jurkat, Etoposide +/-
176	Yb	pHH3 (S28)	HTA28	Biologend	641002	HCT116 Cells +/- Nocodazole

Table 3: Tumor antibody Panel: Antibodies from DVS were purchased as metal conjugates. All others were conjugated and titrated in the Nolan Lab.

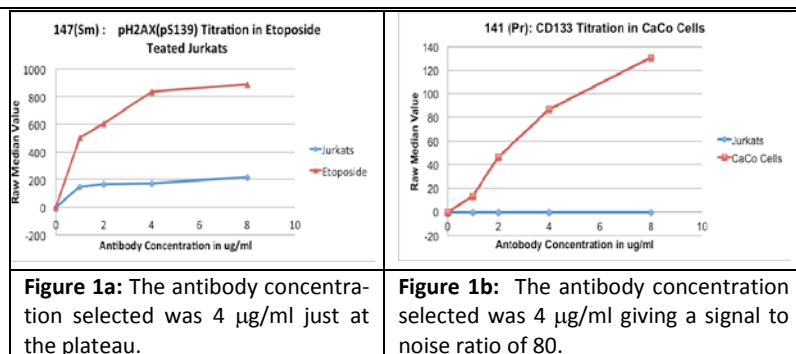


Figure 1a: The antibody concentration selected was 4 μ g/ml just at the plateau.

Figure 1b: The antibody concentration selected was 4 μ g/ml giving a signal to noise ratio of 80.

Acquisition of ovarian cancer cell lines

In a recent publication, a panel of 47 ovarian cancer cell lines from the Broad-Novartis Cancer Cell Line Encyclopedia (CCLE) were analyzed in order to identify those with highest genetic similarity to primary HG-SOC tumours [1, 19]. The study compared copy-number changes, mutations and mRNA expression profiles of with primary HG-SOC samples from The Cancer Genome Atlas (TCGA) database [20]. Unexpectedly, the findings revealed pronounced differences in molecular profiles between commonly used ovarian cancer-cell lines and HG-SOC tumor samples. Furthermore, several rarely used cell lines were identified that more closely resemble cognate tumor profiles than commonly used cell lines.

Therefore, we worked closely with the Japanese Collection of Research Biosources, part of the National Institute of Biomedical Innovation in Osaka, Japan, Public Health England, Fox Chase Cancer Center, and ATCC to procure 8 (KURAMOCHI, OVSAHO, COV362, OVCAR4, TYKNU (platinum-sensitive and resistant), OVKATE, CAOVS) of the 13 cell lines that feature as bearing the greatest similarity to primary HG-SOC tumors (**Figure 2**). We are acquiring SNU119 from Korea. These cell lines will always we included with any batch of primary HG-SOC tumor samples that are analyzed by mass cytometry.

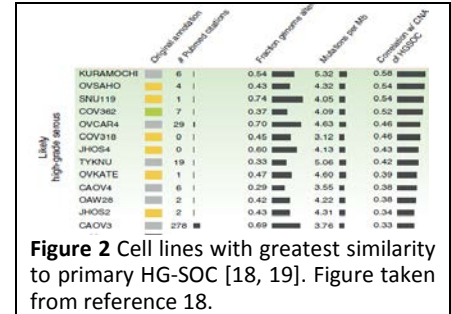


Figure 2 Cell lines with greatest similarity to primary HG-SOC [18, 19]. Figure taken from reference 18.

E. FUTURE PLANS

Over the past year, we have performed extensive validation of reagents and experimental procedures. Within the next year, we anticipate performing CyTOF analysis on 20 to 30 primary tumors (Indivumed) and 10 to 20 ascites that will be acquired at Stanford. We will determine both the tumor and infiltrating immune cell landscape.

For each primary tumor sample, IHC will be performed on FFPE samples prepared immediately post tumor resection with antibodies against CD45 (to gate immune

Mass	Element	Antibody	Clone	Vendor	Catalogue Number	Titration Cell Lines	
113	In	CD61	VI-PL2	BD	555752	PBMCs, Mono/ CD4+	
113	In	CD235ab	H1R2	Biolegend	306602	Human Bone Marrow	
115	In	HLA-DR	L243	Biolegend	307602	PBMCs, B cells/ CD3+	
139	La	CD45	H130	Biolegend	304002	OVCAR3, PBMCs	
141	Pr	CCR6	G034E3	DVS	31410034	PBMCs, B cells/ CD4+	
142	Nd	pMAPKAPK2 (pT344)	27B7	CST		U937, TNFa +/-	
143	Nd	pSTAT1 (pY701)	4a	BD	624084	Splenocytes, IFNa +/-	
144	Nd	CD11b	IRCF44	DVS	3144001B	PBMCs, Mono/ CD4+	
145	Nd	CD4	RPA-T4	DVS	3145001B	PBMCs, CD3+/ CD8+	
146	Nd	CD8	RPA-T8	DVS	3146001B	PBMCs, CD3+/ CD4+	
147	Sm	p-H2AX (pS139)	JBW301	Millipore	05-636	Jurkat, 4hr Etoposide +/-	
148	Nd	CD123	6H6	Biolegend	306002	PBMCs, Mono/ CD3+	
149	Sm	p-NFkB (pS529)	K10-895.12.50	BD	558393	Jurkat, TNFa +/-	
150	Nd	CD206		19.2	BD	555953	PBMCs, 72hr GM-CSF +/-
151	Eu	pERK (pT202/pY204)	DA3.14.4E	CST	43708F	U937, PMA +/-	
152	Sm	Ki67 (total)	B56	BD	556003	HCT116, Nocodazole +/-	
153	Eu	CD45RA	H1100	DVS	3153001B	PBMCs, CD8 /CD45RO +/-	
154	Sm	pSTAT3 (Y705)	4 P-STAT3		624084	Jurkat, PVO4 +/-	
155	Gd	CD19	H1B19	BD	555410	PBMCs, B cells/CD8+	
156	Gd	B2CA2	201A	Biolegend	354202	PBMCs, pDCS/B cells	
157	Gd	CD11c		3.9	Biolegend	301602	PBMCs, Mono/CD3+
158	Gd	CD33	WM53	DVS	3158001B	PBMCs, Mono/CD14-	
159	Tb	CCR7		150503	R&D systems	MAB197-500	PBMCs, CD8+/CD3-
160	Gd	CD14	M5E2	DVS	3160001B	PBMCs, CD33 +/-	
161	Dy	CD66b	G10F5	Biolegend		305102	Whole blood, CD45low/B cells
162	Dy	pSTAT5 (Y694)		47	624084	624084	Jurkat, PVO4 +/-
163	Dy	CXCR3	G025H7	Biolegend	353702	PBMCs, B cells/NK cells	
164	Dy	ICOS	C398.4A	Biolegend	313502	PBMCs, CD8 24hr PMA/Iono +/-	
165	Ho	CD16	3G8	DVS	3165001B	PBMCs, Mono/CD14-	
166	Er	FoxP3	PCH101	Ebioscience	14-4776-82	PBMCs, CD4/CD8	
167	Er	CD163	GHI/61	BD	556017	PBMCs, Mono/CD3+	
168	Er	CD68	Y1/82A	Biolegend	333802	PBMCs, Mono/CD3+	
169	Tm	CD25	2A3	DVS	3169003B	PBMCs, CD8 24hr PMA/Iono +/-	
170	Er	CD3	UCHT1	DVS	3170001B	PBMCs, CD14-/CD14+	
171	Yb	pPARP (N214)	F21-852	BD	624084	Jurkat, 24hr Etoposide +/-	
172	Yb	pS6 (pS235/pS236)	N7-548	BD	624084	Jurkat, PMA +/-	
173	Yb	LAG-3	N/A	R&D systems	AF2319	PBMCs, CD8 PMA/Iono +/-	
174	Yb	pCREB (S133)	87G3	CST	91988F	Jurkat, PMA +/-	
175	Lu	PD1	EH12.2H7	DVS	3175008B	PBMCs, 24hr PMA/Iono +/-	
176	Yb	CD56	NCAM16.2	BD	559043	PBMCs, CD3-/Mono	

Table 4: Immune cell antibody panel: Antibodies from DVS were purchased as metal conjugates. All others were conjugated and titrated in the Nolan Lab.

and non-immune cell types, cPARP and cCaspase 3 (to determine the extent of apoptosis) and vimentin and E-cadherin to determine potential epithelial and mesenchymal compartments. Furthermore, a small aliquot will be evaluated by fluorescence-based flow cytometry which along with cell scatter properties will be compared with the IHC data. The remainder of the sample will be designated for CyTOF analysis with the two panels. Wherever possible, triplicates for each sample will be analyzed. These analyses are designed to serve four purposes:

- 1) Determine how comparable the sample being analyzed is to the tumor *in situ*
- 2) Enumerate the immune and non-immune component of each tumor sample
- 3) Landscape the surface phenotype and basal signaling states of the markers with potential information to be gained about: epithelial and mesenchymal cells as well as transitional EMT states (vimentin, e-cadherin, endoglin, snail), TICs (NFkB, Sox2, Myc, β -catenin), cell of tumor origin (CA125 and mesothelin),
- 4) The immune cell landscape in terms of specific immune cell subsets within and between different tumor and ascites samples.

We are in regular contact with the Neel Lab to allow each group to incorporate relevant antibodies revealed their TIC studies. Efforts are also placed on improving the viability of cells post freezing in DMSO/serum. This allows us to expose viable cells to stimuli, such as cytokines, growth factors and drugs, capitalizing on past work from the Nolan Lab that demonstrated how the magnitude of an evoked response by a cell can be correlated with clinical features [21-24]

Additional CyTOF antibody panels will be built, based on what we learn from experiments in the Neel and Nolan labs, and also with emphasis on the stromal compartment.

F. KEY RESEARCH ACCOMPLISHMENTS

- Identification of stem-like clusters in 18/20 primary samples from the Neel/Nolan dataset
- Application of MONOCLE to look at cell neighborhoods (Pe'er lab)
- Identification and validation of Individumed as a reliable source of high quality human specimens (supplies numerous Biotechs, Pharma and the NIH)
- Validation and optimization of ~ 80 antibodies that have been assembled into a "tumor" and "immune cell" panel
- Acquisition of relevant HG-SOC cell lines [18]

G. REPORTABLE OUTCOMES

G.1a MANUSCRIPTS FUNDED BY THIS RESEARCH

Bjornson, Z.B., G.P. Nolan, and W.J. Fantl, *Single-cell mass cytometry for analysis of immune system functional states*. *Curr Opin Immunol*, 2013. **25**(4): p. 484-94.

G.1b ABSTRACTS AND PRESENTATIONS

Nolan: European Congress of Immunology, September 5-8, 2012 From Immune-Monitoring to Health Policy – What is the Future?, Glasgow, Scotland

Nolan: From the laboratory to the clinic, September 10-13, 2012 A definable "structure" for the immune system and cancers at the single cell level, Trinity College, Oxford, England

Nolan: Scripps Research Institute Guest Speaker, January 17, 2013, A Systems Structure for Immunity and Cancer at the Single Cell Level, Jupiter Beach, FL

Nolan: CELLTech 2013, January 23, 2013, Single Cell Systems-Structured View of Immunity & Cancer, San Diego, CA

Nolan: Personalized Medicine World Congress, January 28-29, 2013, The Network as Symptom, Sentinel, Diagnostic & Target, Mountain View, CA

Nolan: 9th Spring School on Immunology, March 12-14, 2013, A Definable "Structure" for the Immune System and Cancers at the Single Cell Level, Ettal, Germany

Nolan: *LINCS Data Forum*, March 20-21, 2013, **Without DEVIATION from the norm there can be no Evolution**, Boston, MA

Nolan: *American Association for Cancer Research Annual Meeting*, April 7-10, 2013, **A systems-level view of ovarian cancer and AML at the single cell level by mass cytometry**, Washington, DC

Nolan: *Karolinska Institutet*, May 31, 2013, **Mass Cytometry: Next generation flow cytometry**, Stockholm, Sweden

Nolan: *3rd Annual Cambridge Stem Cell Institute International Symposium*, July 8, 2013, **Single Cell Systems Structure View of Stem Cells and Cancer** Cambridge University, England

Nolan: *Frontiers of Single Cell Analysis Conference*, September 5-7, 2013, **A single cell systems view of cancer and immunity**, Stanford, CA

Fantl: *Systems Medicine in Cancer*, June 14-15, 2013 **Deep Single Cell Profiling by Mass Cytometry**, Langenbeck-Virchow-Haus Berlin

Fantl: *Molecular Therapeutics of Cancer Gordon Conference*, July 14 – 18, 2013 **Deep Single Cell Profiling by Mass Cytometry**, Boulder, Colorado

Neel: *Advances in Ovarian Cancer Research, AACR*, September 18 – 21, 2013 **Analyzing the Cellular Basis for Heterogeneity in Serous Ovarian Carcinoma**, Miami, FL

G.2 LICENSES APPLIED FOR AND/OR ISSUED

N/A

G.3 DEGREES OBTAINED OR SUPPORTED BY THIS AWARD

N/A

G.4 DEVELOPMENT OF CELL LINES, TISSUE OR SERUM REPOSITORIES

N/A

G.5 INFORMATICS SUCH AS DATABASES AND ANIMAL MODELS, etc.

All data from these studies is available on Cytobank.org

G.6 FUNDING APPLIED FOR BASED ON THIS AWARD

N/A

G.7 EMPLOYMENT OR RESEARCH OPPORTUNITIES APPLIED FOR AND/OR RECEIVED BASED ON EXPERIENCE/TRAINING SUPPORTED BY THIS AWARD

N/A

H. CONCLUSION

The preliminary data have identified: i) the experimental variables to be addressed ensuring rigor and consequently confidence in understanding the biology of the disease (rather than experimental artifacts) ii) a new algorithm identified potential stem-like cell subsets in a preliminary study with primary samples. This critical information has been incorporated into the design of the upcoming experiments. Thus addressing the point of “so what”, we are set to carry out studies on high quality viable HG-SOC single cells prepared from clinically annotated samples where the parameters measured at the single-cell level will provide critical information about the disease and actionable steps to benefit patients.

I. REFERENCES

1. Domcke, S., et al., *Evaluating cell lines as tumour models by comparison of genomic profiles*. Nat Commun, 2013. **4**: p. 2126.
2. Coticchia, C.M., J. Yang, and M.A. Moses, *Ovarian cancer biomarkers: current options and future promise*. J Natl Compr Canc Netw, 2008. **6**(8): p. 795-802.
3. Gardner, G.J. and E.L. Jewell, *Current and future directions of clinical trials for ovarian cancer*. Cancer Control, 2011. **18**(1): p. 44-51.
4. Auersperg, N., *Ovarian surface epithelium as a source of ovarian cancers: unwarranted speculation or evidence-based hypothesis?* Gynecologic oncology, 2013. **130**(1): p. 246-51.
5. Auersperg, N., *The origin of ovarian cancers--hypotheses and controversies*. Front Biosci (Schol Ed), 2013. **5**: p. 709-19.
6. Flesken-Nikitin, A., et al., *Ovarian surface epithelium at the junction area contains a cancer-prone stem cell niche*. Nature, 2013. **495**(7440): p. 241-5.
7. Ornatsky, O., et al., *Highly multiparametric analysis by mass cytometry*. J Immunol Methods, 2010. **361**(1-2): p. 1-20.
8. Bendall, S.C., et al., *A deep profiler's guide to cytometry*. Trends Immunol, 2012. **33**(7): p. 323-32.
9. Bjornson, Z.B., G.P. Nolan, and W.J. Fantl, *Single-cell mass cytometry for analysis of immune system functional states*. Curr Opin Immunol, 2013. **25**(4): p. 484-94.
10. Tanner, S.D., et al., *An introduction to mass cytometry: fundamentals and applications*. Cancer Immunol Immunother, 2013. **62**(5): p. 955-65.
11. Bendall, S.C., et al., *Single-cell mass cytometry of differential immune and drug responses across a human hematopoietic continuum*. Science, 2011. **332**(6030): p. 687-96.
12. Amir el, A.D., et al., *visSNE enables visualization of high dimensional single-cell data and reveals phenotypic heterogeneity of leukemia*. Nat Biotechnol, 2013. **31**(6): p. 545-52.
13. Linderman, M.D., et al., *CytoSPADE: High-Performance Analysis and Visualization of High-Dimensional Cytometry Data*. Bioinformatics, 2012.
14. Newell, E.W., et al., *Cytometry by time-of-flight shows combinatorial cytokine expression and virus-specific cell niches within a continuum of CD8+ T cell phenotypes*. Immunity, 2012. **36**(1): p. 142-52.
15. Qiu, P., et al., *Extracting a cellular hierarchy from high-dimensional cytometry data with SPADE*. Nat Biotechnol, 2011. **29**(10): p. 886-91.
16. Stewart, J.M., et al., *Phenotypic heterogeneity and instability of human ovarian tumor-initiating cells*. Proc Natl Acad Sci U S A, 2011. **108**(16): p. 6468-73.
17. Fienberg, H.G., et al., *A platinum-based covalent viability reagent for single-cell mass cytometry*. Cytometry A, 2012. **81**(6): p. 467-75.
18. Krutzik, P.O., et al., *Analysis of protein phosphorylation and cellular signaling events by flow cytometry: techniques and clinical applications*. Clin Immunol, 2004. **110**(3): p. 206-21.
19. Barretina, J., et al., *The Cancer Cell Line Encyclopedia enables predictive modelling of anticancer drug sensitivity*. Nature, 2012. **483**(7391): p. 603-7.
20. *Integrated genomic analyses of ovarian carcinoma*. Nature, 2011. **474**(7353): p. 609-15.
21. Irish, J.M., et al., *Single cell profiling of potentiated phospho-protein networks in cancer cells*. Cell, 2004. **118**(2): p. 217-28.
22. Kornblau, S.M., et al., *Dynamic single-cell network profiles in acute myelogenous leukemia are associated with patient response to standard induction therapy*. Clin Cancer Res, 2010. **16**(14): p. 3721-33.

23. Palazzo, A.L., et al., *Association of reactive oxygen species-mediated signal transduction with in vitro apoptosis sensitivity in chronic lymphocytic leukemia B cells*. PLoS ONE, 2011. 6(10): p. e24592.
24. Rosen, D.B., et al., *Distinct patterns of DNA damage response and apoptosis correlate with Jak/Stat and PI3kinase response profiles in human acute myelogenous leukemia*. PLoS ONE, 2010. 5(8): p. e12405.

Appendix A —

Single-cell mass cytometry for analysis of immune system functional states

Zach B Bjornson, Garry P Nolan and Wendy J Fantl



ELSEVIER

Single-cell mass cytometry for analysis of immune system functional states

Zach B Bjornson, Garry P Nolan and Wendy J Fantl

Mass cytometry facilitates high-dimensional, quantitative analysis of the effects of bioactive molecules on cell populations at single-cell resolution. Datasets are generated with panels of up to 45 antibodies. Each antibody is conjugated to a polymer chelated with a stable metal isotope, usually in the lanthanide series of the periodic table. Antibody panels recognize surface markers to delineate cell types simultaneously with intracellular signaling molecules to measure biological functions, such as metabolism, survival, DNA damage, cell cycle and apoptosis, to provide an overall determination of the network state of an individual cell. This review will cover the basics of mass cytometry as well as outline assays developed for the platform that enhance the immunologist's analytical arsenal.

Addresses

Stanford University School of Medicine, Department of Microbiology & Immunology, Baxter Laboratory for Stem Cell Biology, 269 Campus Drive, Stanford, CA 94305-5175, USA

Corresponding authors: Nolan, Garry P (gnolan@stanford.edu) and Fantl, Wendy J (wjfantl@stanford.edu)

Current Opinion in Immunology 2013, **25**:484–494

This review comes from a themed issue on **Host pathogens**

Edited by **Marc Pellegrini** and **Bruce D Walker**

For a complete overview see the [Issue](#) and the [Editorial](#)

Available online 31st August 2013

0952-7915/\$ – see front matter, © 2013 Elsevier Ltd. All rights reserved.

<http://dx.doi.org/10.1016/j.coi.2013.07.004>

Fluorescence-based flow cytometry has proven an invaluable technology for both immunologists and clinicians alike [1]. Importantly, it provides crucial biological information at the single-cell level regarding ploidy, immunophenotype, frequency of cell subsets, expression levels of proteins, as well as functional characterization [2–7]. Furthermore, the potential of this technology can be significantly extended by interrogating single cells not only in their basal state but also after their exposure to exogenous stimuli. The latter has given rise to fluorescence-based phospho-flow cytometry, which has enabled determination of the activity of intracellular pathways [8,9*,10,11,12*,13*,14*,15,16,17]. Interrogated revelation of cellular states is key to the mechanistic understanding of the immune system perturbed during disease, and to elucidating the positive or negative effects on signaling pathways wherein cells have been exposed to

therapeutic and potential therapeutic agents *in vitro* or *in vivo* [14*,18–20].

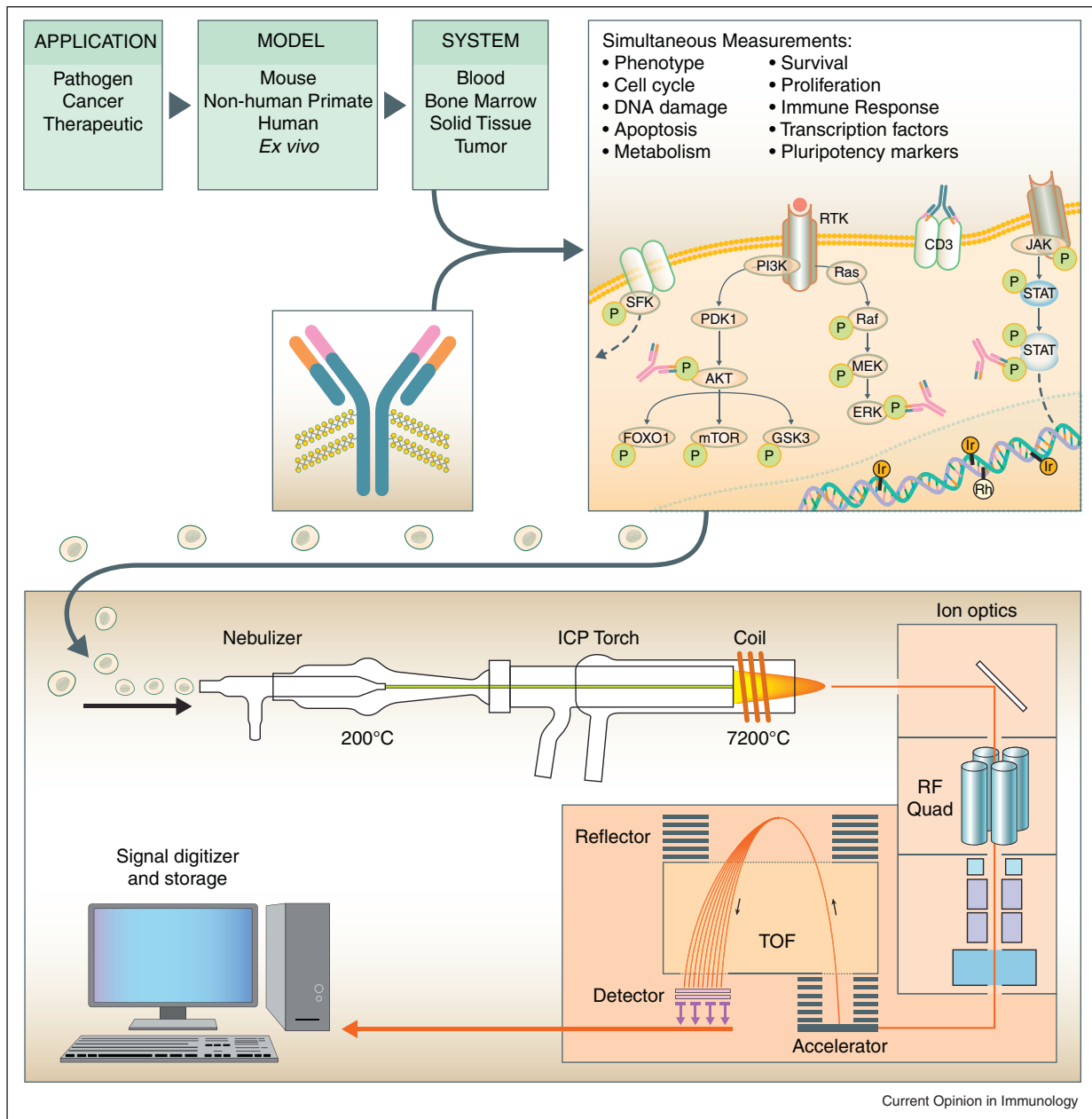
However, as powerful as fluorescence-based flow cytometry can be, it falls somewhat short of uncovering the well-recognized complexity of the immune system when determined simultaneously with intracellular network states. The primary drawback of traditional fluorescence-based flow cytometry is ironically the same tool that has enabled it to be so useful for nearly three decades: the number of markers that can be simultaneously analyzed is inherently limited by spectral overlap. Measurement beyond three fluorophores becomes more complex as more parameters are added, involving corrections for spectral overlap as well as appreciation for the auto-fluorescence of certain cell types [21,22]. Even with such corrections and understanding, the practical limit of flow cytometry is about ten markers wherein significant training or effort is involved in designing such panels. Investigation of intracellular pathways under such restrictions is unwieldy, since the bulk of the parameters for a fluorescence-based analysis will be assigned to surface markers that call out specific cell types, leaving only a few channels to measure phosphorylation states or levels of intracellular proteins. So where do we go from here?

A new generation of single-cell analysis technology called mass cytometry overcomes most of these limitations (Figure 1). The **CyTOF** (**Cytometry by Time Of Flight**) is a mass spectrometer-flow cytometer hybrid instrument that uses stable isotopes instead of fluorophores as reporters [23,24,25,26,27,28*,29,30]. Mass cytometry offers a number of significant advantages compared to fluorescence-based applications. Of foremost importance, due to their discrete readouts, use of isotopes as reporters enables a significant increase in the number of measurable parameters per cell. Furthermore, the platform is quantitatively accurate with linear sensitivity across four orders of magnitude. Further advances such as increased numbers of deployable isotopes, novel nano-crystal configurations and computational tools promise to extend mass cytometry well into the 'omics' arena and provide system-wide views of immune function in healthy donors and patients suffering from infection, inflammation or cancer.

Basic concepts of mass cytometry

To address the limitation of traditional fluorescence-based cytometry, namely the number of simultaneously

Figure 1



Mass cytometry enables high-dimensional analysis of diseases and therapeutic responses. Diseases including cancer and infections perturb cellular signaling. Mass cytometry provides a readout for up to 52 simultaneous measurements, of both disease-induced perturbations and importantly of counter-perturbations induced by candidate therapeutics. Furthermore, the simultaneous inclusion of cell phenotype and cell cycle provide a more detailed picture than possible before. After cells are stained with antibodies and other metallic assay reagents, they are introduced into the mass cytometer as a stream of single cells, then atomized and ionized as they pass through the inductively coupled plasma (ICP) torch. Low-mass elements (including carbon and nitrogen) are filtered out by a radio frequency quadrupole before entering the time-of-flight (TOF) detector. A high-speed, online analysis system produces data equivalent to that of traditional fluorescence-based cytometry.

measured parameters, Scott Tanner and colleagues at the University of Toronto embarked upon a remarkable adaptation of inductively coupled plasma mass spectrometry (ICP-MS). ICP-MS is routinely used in the mining, metallurgy and semi-conductor industries and is the method of choice for measuring the elemental components of

materials since it can detect the contamination of, for example, blood with lead and drinking water with arsenic, beryllium or heavy metals. In ICP-MS, samples are vaporized, atomized and ionized in plasma at temperatures approximating that of the surface of the sun (7500 K). The mass spectrometer can then resolve and quantify

elemental components, on the basis of mass-to-charge ratio (m/z), with a level of sensitivity at parts per quadrillion and with no interference between channels.

Tanner and colleagues realized that incorporating such attributes into flow cytometry might dramatically increase the number of parameters that could be measured per single cell. They reasoned that, rather than being conjugated to fluorophores, antibodies could be conjugated to stable metal isotopes, such as lanthanides, that are absent or at low abundance in biological systems, and then adapt ICP-MS instrumentation for their detection at single-cell resolution [23,27,31–33]. This was the foundational concept upon which the mass cytometer was developed.

By tagging each antibody with a unique lanthanide isotope, the readout from each isotope can be correlated with a particular antibody, which in turn can be correlated to levels of antigen associated with an individual cell. Thus, the number of simultaneously measurable parameters per cell is now only limited by the number of stable isotopes suitable for conjugating to antibody reagents. For this to be accomplished, two fundamental technical challenges needed to be overcome. One was to develop reagents to tag antibodies with stable metal isotopes. Another was to adapt the ICP mass spectrometer to simultaneously detect multiple isotope tags, in the form of an ion cloud, associated with a single cell event.

In many respects the workflow for a mass cytometry experiment is analogous to traditional flow cytometry (Figure 1). By taking advantage of a long history of fluorescence-based innovations, it has been possible to ‘recreate’ the assays of many reagents with isotope-labeled tags. These adaptations as well as novel assays specific to mass cytometry will be outlined below.

Attaching metal-chelating polymers to antibodies

For the attachment of multiple atoms of a given isotope to a selected antibody, acrylic acid polymers were synthesized with a uniform number polymer units and functionalized with multiple copies of a chelator, such as 1,4,7,10-tetraazacyclododecane-1,4,7,10-tetraacetic acid (DOTA) or diethylene triamine pentaacetic acid (DTPA), compatible with the chemistry of trivalent metal lanthanide ions [34]. The resultant chelated lanthanide has a K_d of 10^{-16} and is therefore nearly impervious to losses or exchanges between other chelated metals within an antibody panel. A terminal maleimide group on the polymer permits its conjugation to selectively reduced disulfide groups in the hinge region of the immunoglobulin heavy chain.

Typically four to five polymers bind to each antibody, with each polymer chain capable of carrying up to 30 metal isotopes [32,34]. The first and current generation of isotope-chelating polymers can bear up to 120 lanthanide

ions per antibody molecule [34]. That, combined with the level of ion transmission at 1 in 10,000, means the lower limit of detection for any given cellular parameter is about 300–1000 target protein copies (comparable to many fluorophores by traditional fluorescence). Unlike photomultiplier tubes in photon-driven cytometry which can show non-linear sensitivity across the dynamic range, the sensitivity of the ICP-MS readout is linearly proportional to the number of elemental isotopes conjugated to each antibody. Nevertheless, the sensitivity of lanthanide-conjugated antibodies is currently about two-fold lower than the brightest fluorophores such as phycoerythrin. This will likely be overcome with new modalities that are under investigation to increase the number of metal isotopes linked to an individual antibody [35,36].

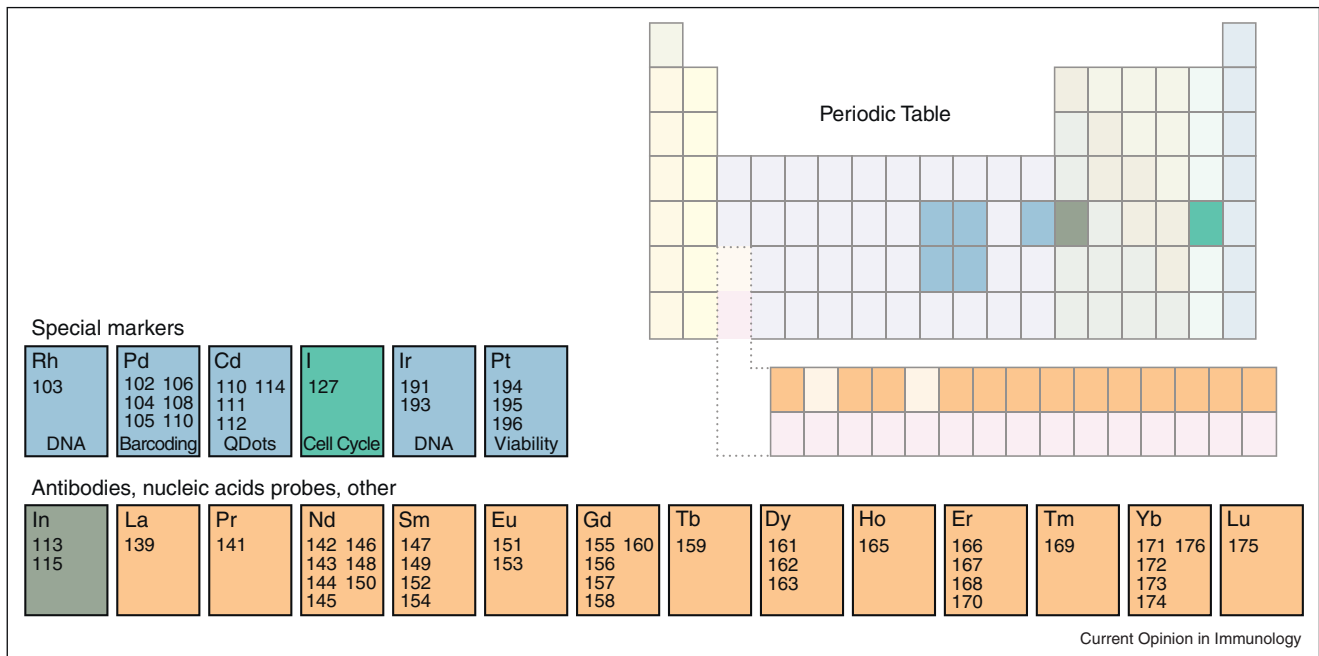
As will be discussed below, the lanthanides dominate as the group of metals compatible with current polymer tag chemistries. However, in order to expand the number of simultaneously measurable parameters, new chelation chemistries are under development with the aim of including isotopes with oxidation states other than +3, such as the noble metals. Their atomic mass falls within the range suitable for mass cytometry and could thus increase the panel of metal-tagged antibodies available for single-cell analysis by 20 or more.

Assigning stable metal isotopes to measurements of cellular parameters

At present, a total of 37 purified, stable lanthanide isotopes are available and compatible with the metal chelating polymer chemistry (Figure 2). Of those, 27 are available at enrichment purities above 97 percent; the rest are available at enrichment purities above 92 percent. Care must be taken when assigning antibodies to isotopes to ensure that impurities in other channels do not result in false-positives during analysis. Additionally, certain metals are prone to oxidation, which results in signal in other channels. For example, measurements of gadolinium 157 are prone to interference from +16 oxidation of praseodymium 141. In addition to the lanthanides, indium, a post-transition metal, has two isotopes that are compatible with the chelating chemistry, but their sensitivity is low and thus only suitable for detection of highly abundant proteins, such as CD45 expressed on leukocytes. One additional parameter can be measured with quantum dots (Q-dots) using the cadmium that is their major constituent.

Given the absence of light scatter properties to record a cell event, measurement of rhodium or iridium DNA intercalators, as well as a cell event-induced ion cloud duration measurement (‘cell length’) can be used to demarcate cells in terms of their DNA content and approximate size, respectively [26,32]. A variety of other measurements (viability, cell cycle and multiplexing barcode reagents) are discussed below, bringing the total

Figure 2



A large number of metals are available for a variety of measurements. The lanthanides provide 37 stable isotopes for measuring antigen-bound antibodies, MHC tetramers and nucleic acid probes with high sensitivity. Indium provides two low-sensitivity channels for highly expressed markers, and quantum dots provide one additional channel (cadmium). Rhodium and iridium, as DNA intercalators, register a cell event. Platinum, in the form of cisplatin:sulfur complexes, is used as a viability marker. Iodine, as iodo-deoxyuridine, is used for cell cycle measurements. Six palladium isotopes allow for mass tag 'barcoding' and multiplexed measurement of samples.

number of quantifiable parameters for a single cell to 52. It might be possible in the future to measure forward and side scatter before introduction of each cell into the ICP-MS plasma. Likewise, it might be possible to sort cells by cleaving the reporter elements from the cells before introduction into the plasma and using those readouts to trigger a standard cell sorter.

Adapting ICP-MS to measuring single-cell ion clouds

It was necessary to adapt the ICP-MS to retain the temporal information of a multi-ion cloud derived from a single cell [23,31,32]. As with conventional ICP-MS, liquid samples, but now containing a cell suspension, are nebulized into single-cell droplets, rapidly dried in a heated spray chamber and then delivered into the central channel of the 7500 K argon plasma where they are vaporized, atomized and ionized to create clouds of ions that correspond to the cells. The ion cloud derived from a single cell has a measurement span of approximately 200–300 microseconds. Therefore, in order to measure the composition of each cloud fully, a fast and simultaneous mass analyzer is required. This ruled out the use of quadrupole and magnetic sector mass analyzers because they detect one isotope at a time and require 200 microseconds or more to switch between measured isotopes.

Instead, a time of flight (TOF) analyzer was used. This measures the complete mass spectra 'simultaneously' in 13 microsecond pulses and captures the entire cohort of ions derived from a single cell over the 200–300 microsecond ion cloud duration. This restricts sample throughput to 1000 cells per second.

Developing the mass cytometry tool kit

Of fundamental importance is the observation that fluorescence and mass cytometry yield very comparable results when analyzed by traditional 2D flow plots, histograms and heat-maps [37^{**},38^{**}]. Yet there are clear differences between the two platforms. Although the deep dive into a single cell at the level of greater than 45 parameters provides an unprecedented level of detail unavailable by fluorescence, the latter platform efficiently determines measures of, for example, cellular calcium and reactive oxygen species, for which as yet there are no mass cytometry equivalents. However, over the past year a number of new reagents have been created for mass cytometry that can now be incorporated into the 'tool kit' as discussed below.

Data normalization with bead standards

As with any quantitative technology, there is a stringent requirement for internal and external reagent standards

for data normalization. In the case of mass cytometry, crucially, variation in instrument performance can be caused by factors such as instrument calibration, fluctuations in plasma and build-up of cellular debris in the sample introduction components. In order to normalize for these factors, polystyrene beads infused with precise amounts of several lanthanide isotopes are acquired simultaneously with every sample. A multiplicative correction derived from the bead signature is now routinely applied to the raw mass cytometry data before any further analysis takes place [39]. The software for its implementation is available at www.cytobank.org/nolanlab.

Increasing throughput and decreasing variability by mass tag barcoding

Amine-reactive fluorescent dyes, such as Pacific Blue, Alexa Fluor 488, Alexa Fluor 700 and Alexa Fluor 750 each attached to N-hydroxysuccinimidyl (NHS) ester, can be used in different combinations for fluorescence ‘barcoding’ of separate samples that are subsequently pooled, stained in a single tube with a fluorescently-tagged antibody panel and analyzed simultaneously on a flow cytometer. Data are then deconvoluted according to the fluorescent barcode signatures of the component samples [40]. There are three significant advantages to sample barcoding: (i) all samples are stained in the same tube with the same antibody mix, eliminating cell-to-antibody ratio-dependent effects on staining, (ii) reduced antibody consumption and (iii) increased sample throughput.

These principles can apply to barcoding reagents available for mass cytometry (mass cell barcoding). In a recent study, metal barcode reagents were prepared by chelating lanthanides with a bifunctional macrocyclic compound, maleimido-mono-amide-DOTA (mDOTA), which labels cells by covalent attachment to intracellular thiol groups. Samples were labeled with a unique binary combination of seven mDOTA-lanthanide reagents, multiplexed and deconvoluted to accurately recover samples with given barcodes. This foundational study lends support to the use of metal barcoding reagents in mass cytometry [41]. Unlike fluorescence-based cytometric analysis, a fluidics purge lasting several minutes is required between sample introductions on the mass cytometer. The throughput gained by barcoding is thus particularly significant. As a refinement of the barcoding reagents used in the published study, the mDOTA-lanthanides have now been replaced with six palladium isotopes. These have masses (102–110) below that of the smallest lanthanide and therefore do not occupy channels that can otherwise be used for metal-tagged antibodies (E. Zunder, G. Behbehani, R. Finck, C. Thom, G. Nolan manuscript in preparation).

Cell viability determinations

A large set of fluorescence-based reagents exists with which to measure cell viability. They operate on the principle that a compromised cell with a damaged plasma

membrane permits reagent entry into the cytoplasm, whereas a healthy cell with an intact plasma membrane does not. Specifically, reagents are available that: (i) intercalate non-covalently into DNA (e.g. 7-aminoactinomycin D (7-AAD) or propidium iodide) [42,43], (ii) covalently attach to DNA (TdT dUTP nick end labeling (TUNEL) [44] (iii) covalently attach to proteins (Invitrogen Fixable LIVE/DEAD1) [45], and (iv) monitor alterations in mitochondrial membrane potential (differences in fluorescence of the monomeric and aggregate forms of 5,5',6,6'-tetrachloro-1,1',3,3' tetraethylbenzimidazolylcarbocyanine iodide (JC-1)) [46]. Similarly, a variety of reagents is available for determination of cell viability by mass cytometry and operates under the same principles as fluorescent reagents, albeit with a different readout. These include rhodium and iridium-containing metal-intercalators [26] and an amine-reactive chelator, 1,4,7,10-tetraazacyclododecane-1,4,7,10-tetraacetic acid mono (N-hydroxysuccinimide ester) (DOTA-NHS-ester) [38]. Recently, a protocol was described for using cisplatin to determine cell viability [47]. Although well known as a chemotherapeutic agent because of its ability to form extremely stable DNA-platinum adducts, cisplatin has an alternative activity in which it reacts on a much more rapid timescale (minutes as opposed to days) with protein thiols, forming covalent platinum–sulfur bonds. Furthermore, in an independent study, acrylamide polymers bearing platinum or palladium recognized non-viable cells [48]. Platinum has six stable isotopes, of which three are dominant (194, 195 and 196 Da) and well separated from the lanthanides, making cisplatin an ideal reagent for determinations of cellular viability by mass cytometry.

Measuring the cell cycle by mass cytometry

No biological evaluation would be complete without including measurements of cell cycle phase. An abundance of fluorophore-based reagents have been used for decades to stage cells on the basis of their DNA content using traditional flow cytometry. Included in the list are supra-vital stains in the Hoechst group, such as 4',6-diamidino-2-phenylindole (DAPI) that bind to A-T-rich regions within the minor groove of DNA, or membrane-impermeable reagents such as propidium iodide and bromo-deoxyuridine [3,49]. These fluorescent stains can all be used with a limited number of antibodies that characterize a specific cell cycle phase.

In a recent study, Behbehani *et al.* designed a panel of metal-chelated antibodies with which to perform a comprehensive analysis of the cell cycle progression machinery [37]. The panel included antibodies against cyclins, phosphorylated retinoblastoma (Rb), phosphorylated Cdk1, phosphorylated histone H3 and Ki67 to denote cells in cycle covering the G0, G1, G2 and M phases. Of its many roles, retinoblastoma is pivotal for cell cycle progression, with a complex mechanism defining its role

in G1 to S progression [50,51]. However, the antibody used here was against an epitope encompassing residues pS807 and pS811, which are substrates for cyclin C/Cdk3 and are necessary for quiescent cells to enter into cycle [52]. To identify cells in S phase, multiple studies have used halopyrimidines (bromo-deoxyuridine, iodo-deoxyuridine and chloro-deoxyuridine) which become incorporated into newly synthesized DNA. Antibodies recognizing these groups necessarily require a DNA denaturation step to gain access to the modified site [53,54]. However, iodo-deoxyuridine, without an accompanying antibody, can be measured directly by mass cytometry: the incorporated iodine in the newly synthesized DNA has an atomic mass of 127, which falls within the requisite range for mass cytometry. Its inclusion in the panel gave a direct and clear measure of the percentage of S-phase cells which was also beneficial in increasing the resolution between the G1 and G2 phases.

Using a variety of cancer cell lines, cycling T lymphocytes and primary human bone marrow, Behbehani *et al.* identified all cell cycle phases with a core panel: p-Rb (pS807/S811), IdU, cyclin B and p-Histone H3 (pS28). Importantly, the cell cycle phases were validated in side-by-side measurements by fluorescence flow cytometry [37**]. The importance of this study lies in the ability to now measure many other biological parameters within the context of the cell cycle. For example, signaling, DNA damage, and metabolic pathways can now be examined at defined phases in the cell cycle (G. Behbehani, W. Fantl, G. Nolan, S. Lowe, P. Mallik, unpublished). In the area of infectious disease, vaccinia, influenza and hepatitis C virus infections are all known to alter cell cycle progression [55–58]. Conversely the host cell cycle affects the replication of viruses such as Ebola virus, in which case the virus depends on actively proliferating host cells for replication itself [59]. This core marker set would be equally significant in the development of therapeutic agents, many of whose activities are known to be influenced by cell cycle state [60–64].

Measurements of cytokines: regulators of immune cell subsets and beyond

Traditional flow cytometry has greatly benefited from single-cell measures of cytokine activity. The cytokine superfamily includes interleukins, chemokines, colony-stimulating factors, interferons, as well as the transforming growth factor and tumor necrosis factor families, all with a large array of diverse biological functions. They have well-described functions in innate immunity (inflammation, chemotaxis, allergy, macrophage and NK cell activation) as well as in adaptive immunity (cellular and humoral) [65–72]. However, cytokines are now known to be produced by and mediate their effects on cells other than immune cells and have been implicated in the pathologies of, for example, cancer, stroke and pulmonary arterial hypertension [73–75].

Thus, given their far-reaching effects in multiple tissues, defining cellular phenotypes based on their cytokine expression is another essential parameter to include in the mass cytometry toolkit. Fluorescence-based flow cytometry protocols have measured cytokine production in a variety of T cell subsets [76–79]. Recently, mass cytometry applied to CD8+ T cells after stimulation with anti-CD3, anti-CD3/anti-CD28 or PMA/ionomycin has remarkably revealed there to be about 200 distinguishable subtypes based on the combinatorial diversity of the nine functional attributes, with even greater diversity revealed when taking into account different expression patterns of surface markers [80**]. This study has set the stage for measuring the functional diversity of both immune and non-immune cell subsets.

Major histocompatibility class-peptide tetramers conjugated to metal-chelating polymers

Antigen-specific T cell subsets are generated when their T cell receptors interact with pathogen-derived peptide-major histocompatibility complexes expressed on antigen presenting cells [81]. At a given moment, there will be numerous T cell subsets throughout the body with different antigen specificities. However, their low frequency and low affinity interaction of their receptor with peptide-bound MHC precluded a detailed characterization of their properties. To circumvent this problem, Altman and Davis constructed a peptide-MHC tetramer in which four identical biotinylated MHC-peptide molecules were complexed with streptavidin conjugated to a fluorophore, resulting in increased avidity [82]. The peptide-MHC complex only binds to the specific T cells that respond to that peptide. The tetramer can then be detected by flow cytometry via the fluorescent label [82,83]. Recently, the fluorophore on streptavidin was replaced by a metal-chelating polymer allowing a multidimensional analysis to be performed by mass cytometry with a panel of cytokine antibodies as described above. In this way it was possible to identify 56–106 combinations of functional attributes for several viral-specific T cell subsets, revealing a far more complex view of the cytokine network than seen before [80**].

Building panels of thirty-something antibodies for deep proteomic profiling

One undisputed advantage of single-cell mass cytometry is the ability to measure multiple parameters on a single-cell basis, without the need to compare smaller panels or computationally join data files from separate smaller antibody panels [5,7]. As mentioned above, most isotopes are assigned to antibodies, as they are at the crux of the mass cytometry ‘tool kit.’ As with any antibody, the conditions for their use must be optimized. The key steps are conjugation to the metal-containing polymer and performing the appropriate titrations to measure signal-to-noise ratios (also referred to as ‘stain index’).

Panels can be designed with up to 45 antibodies focused completely on surface markers to delineate cellular hierarchy, or a combination of surface markers and intracellular signaling molecules. The latter are focused on the activation states of intracellular signaling pathways. This approach has provided new information about established cell types, as well as previously unidentified cell types revealed by new combinations of surface markers. In addition to providing an increased understanding of the immune system, mass cytometry can also provide new information about solid tumors. Using appropriate protocols to dissociate tumors [84,85] into their constituent single cells, new cellular hierarchies have been revealed in ovarian cancer (J. Stewart, B. Neel, B. Bodenmiller, W. Fantl and G. Nolan, unpublished). This increased level of detail regarding signaling potential at the single-cell level, regardless of the tissue of derivation, provides a new backdrop for drug discovery.

Deep proteomic profiling of the human immune system

The first deep proteomic study evaluated signaling responses in specific immune cell subsets within the hematopoietic continuum [28^{*},38^{**}]. Two panels each comprising 31 metal polymer-conjugated antibodies were assembled. The 'phenotypic panel' was designed to measure surface molecules expressed on immune cell subsets, and successfully identified known and distinct immune cell subsets, including B, T, NK and DC cells and monocytes. However, transitional cells were also seen, not previously captured in prior studies, but that are consistent with an immune continuum rather than abrupt conversions to distinct differentiation stages. The second panel maintained 13 surface marker antibodies from the first panel but had an additional 18 intracellular signaling molecules representing the activation status for a number of pathways. Human bone marrow was treated with twenty extracellular modulators including growth factors, cytokines, chemokines and three small molecule kinase inhibitors (dasatinib, Jak1 inhibitor and the U0126 Mek inhibitor). Thus, Ras/Raf/Erk, NF- κ B, p38/MAPKAPK2, STATs 1, 3 and 5, CREB and BCR signaling were all included and measured simultaneously [38^{**}]. Using Spanning-tree Progression Analysis of Density-normalized Events (SPADE, discussed in more depth below) signaling responses were seen within tight cellular boundaries as well as across multiple immune cell types. This system-level view is the first in a series of studies to generate a human immune reference map as a resource for therapeutic and vaccine studies (Z. Bjornson, G. Fragiadakis, M. Spitzer, M. Davis, G. Nolan, unpublished).

This foundational study also demonstrated a paradigm for multi-dimensional analysis of complex primary tissues, namely establishing a phenotypic hierarchy using surface

markers and then selecting a subset of surface marker antibodies to combine with antibodies that measure activated intracellular signaling molecules. Since then, many additional antibody panels have been optimized to interrogate a broad variety of cellular functions including: receptor tyrosine kinase signaling, epithelial-mesenchymal transition, the Wnt pathway, apoptosis, survival, proliferation, DNA damage response, cell cycle, metabolism, embryonic stem cells and induced pluripotent stem cells. The value of this technology platform is in its ability to measure multiple cellular functions, which will be invaluable for understanding disease states. However, it is first necessary to have the tools to analyze high-dimensional data.

Analyzing high-dimensional mass cytometry data

Although mass and fluorescence-based flow cytometry use entirely different instrumentation, the data from both platforms provide equivalent information [37^{**},38^{**}]. However, there are several notable differences in the data. In fluorescence cytometry, significant background signals arise from spectral overlap and auto-fluorescence, the natural fluorescence of cellular structures. In mass cytometry, because 'auto-mass' does not exist, there is minimal background and consequently less spread around zero. Nonetheless, in both cases, a transformation such as the inverse hyperbolic sine function is typically applied to compress values around zero, resulting in a more coherent negative population (one that lacks a marker of interest). However, the standard transformation used with mass cytometry data does not compress the data as strongly as standard transformations for fluorescence data, resulting in data that is truer to the measured signal (Fig. S2 in [38^{**}]).

We and others have adapted a variety of algorithms to the analysis of high-dimensional, single-cell mass cytometry data. One obvious choice for processing large datasets is clustering, the grouping of similar cells, which has been applied extensively to microarray data [86,87]. One of the first algorithms developed to analyze mass cytometry data was SPADE [38^{**},88^{**},89]. It uses hierarchical, agglomerative clustering after performing density-dependent downsampling in an effort to preserve rare cell types that would otherwise be drowned out by far more frequent cell types. The resulting clusters can be placed into a minimum-spanning tree [38^{**}], or into a more highly connected graph with a force-directed layout (E. Zunder and G. Nolan, manuscript in preparation).

Automatic determination of known, biologically relevant clusters is still a difficult problem in flow cytometry data analysis because it is difficult to determine the edge of where one cell population begins and the other ends. This is an especially difficult problem when one considers

transitions and progressions where cells dynamically exist along a framework of cell states. On the one hand, under-segmentation results in clusters containing multiple cell types whereas on the other hand, over-segmentation needlessly divides homogenous cell types. In a new approach, over-segmentation of cell subsets and their subsequent merging by affinity propagation resulted in larger, biologically relevant cell subpopulations [90] (T. Chen, M. Clutter *et al.*, in submission). This technique works especially well for analyzing continuous progressions of cells, such as the cell cycle, where manual demarcation of cell subsets is difficult.

Recently, viSNE, a visualization tool for high-dimensional single-cell data based on the t-distributed stochastic neighbor embedding (t-SNE) algorithm [91,92], was applied to mass cytometry datasets from healthy and leukemic bone marrow [93]. viSNE generates a two-dimensional map that reflects the proximity of cells to one another in high-dimensional space. This approach works well but is currently unable to process a large number of cells. One established statistical tool, principle component analysis (PCA), has also been applied to mass cytometry datasets. It derives summary variables to capture as much variation as possible in as few terms as possible to aid visualization [94]. This technique has successfully been applied to CyTOF data [38**,80**]; however, its ability to fully separate many distinct cell populations remains limited.

Summary and conclusions

Reiterating a central theme of this essay, we have discussed how mass cytometry can be applied to advance traditional flow cytometry assays. Although mass cytometry, as it stands with panels of 45 parameters in routine use, provides a level of detail about protein function not previously possible, further improvements are needed. These include increased sensitivity, changes in the instrumentation to increase sample flow rate and to reduce sample loss as well as new computational tools. Regardless, multi-dimensional, single-cell mass cytometry is currently positioned to have dramatic consequences on drug development and therapeutic programs for multiple indications ranging from infectious disease, cancer, inflammatory conditions and trauma.

Acknowledgements

The authors wish to thank Drs Scott Tanner, Olga Ornatsky, Dmitry Bandura, Mitch Winnik and Mark Nitz for their critical reading of this manuscript. This work was supported by the Rachford and Carlota A. Harris Endowed Chair to GPN as well as NIH grants U19 AI057229, 1R01CA130826, U54CA149145, N01-HV-00242, 5-24927, 5U54CA143907, FDA contract HHSF223201210194C, CIRM grants DR1-01477 and RB2-01592, European Commission grant HEALTH.2010.1.2-1 and a DoD CDMRP Teal Innovator Award. Conflict of interest statement: G.P.N. has personal financial interest in the company DVS Sciences, the manufacturers of the instrument and reagents described in this manuscript.

References and recommended reading

Papers of particular interest, published within the period of review, have been highlighted as:

- of special interest
 - of outstanding interest
1. Chattopadhyay PK, Roederer M: **Cytometry: today's technology and tomorrow's horizons.** *Methods* 2012, **57**:251-258.
 2. Sigal A, Danon T, Cohen A, Milo R, Geva-Zatorsky N, Lustig G, Liron Y, Alon U, Perzov N: **Generation of a fluorescently labeled endogenous protein library in living human cells.** *Nat Protoc* 2007, **2**:1515-1527.
 3. Darzynkiewicz Z: **Critical aspects in analysis of cellular DNA content.** *Curr Protoc Cytom* 2011. Chapter 7:Unit 7 2..
 4. Jacobberger JW, Frisa PS, Sramkoski RM, Stefan T, Shults KE, Soni DV: **A new biomarker for mitotic cells.** *Cytometry A* 2008, **73**:5-15.
 5. Biancotto A, Fuchs JC, Williams A, Dagur PK, McCoy JP Jr: **High dimensional flow cytometry for comprehensive leukocyte immunophenotyping (CLIP) in translational research.** *J Immunol Methods* 2011, **363**:245-261.
 6. Biancotto A, Dagur PK, Fuchs JC, Langweiler M, McCoy JP Jr: **OMIP-004: in-depth characterization of human T regulatory cells.** *Cytometry A* 2012, **81**:15-16.
 7. van Lochem EG, van der Velden VH, Wind HK, te Marvelde JG, Westerdaal NA, van Dongen JJ: **Immunophenotypic differentiation patterns of normal hematopoiesis in human bone marrow: reference patterns for age-related changes and disease-induced shifts.** *Cytometry B Clin Cytom* 2004, **60**:1-13.
 8. Krutzik PO, Irish JM, Nolan GP, Perez OD: **Analysis of protein phosphorylation and cellular signaling events by flow cytometry: techniques and clinical applications.** *Clin Immunol* 2004, **110**:206-221.
 9. Irish JM, Hovland R, Krutzik PO, Perez OD, Bruserud O, Gjertsen BT, Nolan GP: **Single cell profiling of potentiated phospho-protein networks in cancer cells.** *Cell* 2004, **118**:217-228.
 - This showed that perturbation responses in individual cancer cells could be related to leukemia patient clinical outcomes. An advantage of this single-cell approach was that signaling could be characterized in rare populations of cancer cells and contrasted with the bulk cancer cell population. This study revealed and characterized the cell signaling heterogeneity of AML and showed that signaling in individual cancer cells can be closely linked to the clinical behavior of the disease.
 10. Irish JM, Czerwinski DK, Nolan GP, Levy R: **Kinetics of B cell receptor signaling in human B cell subsets mapped by phosphospecific flow cytometry.** *J Immunol* 2006, **177**:1581-1589.
 11. Irish JM, Czerwinski DK, Nolan GP, Levy R: **Altered B-cell receptor signaling kinetics distinguish human follicular lymphoma B cells from tumor-infiltrating nonmalignant B cells.** *Blood* 2006, **108**:3135-3142.
 12. Irish JM, Kotecha N, Nolan GP: **Mapping normal and cancer cell signalling networks: towards single-cell proteomics.** *Nat Rev Cancer* 2006, **6**:146-155.
 - This describes the advantages of single-cell, high-dimensional flow cytometry in translational cancer research. This review defines much of the new language in the field (e.g. 'signaling nodes' and 'signaling profiles') and highlights key challenges in cancer research that can now be addressed using 'single-cell proteomics' approaches like mass cytometry.
 13. Palazzo AL, Evensen E, Huang YW, Cesano A, Nolan GP, Fantl WJ: **Association of reactive oxygen species-mediated signal transduction with in vitro apoptosis sensitivity in chronic lymphocytic leukemia B cells.** *PLoS ONE* 2011, **6**:e24592.

Multi-parametric flow cytometry of primary chronic B-cell leukemia samples identified distinct cell subpopulations, within and between samples. B-cell receptor network proteins of these subpopulations showed varying intracellular signaling responses to *ex vivo* treatment with hydrogen peroxide, a reactive oxygen species which acts as an intracellular second messenger. A link was seen between the magnitudes of these responses

and their apoptotic proficiency after *ex vivo* fludarabine exposure. Such single-cell analysis has the potential to monitor the therapeutic benefit of this standard-of-care drug.

14. Rosen DB, Putta S, Covey T, Huang YW, Nolan GP, Cesano A, Minden MD, Fantl WJ: **Distinct patterns of DNA damage response and apoptosis correlate with Jak/Stat and PI3kinase response profiles in human acute myelogenous leukemia.** *PLoS ONE* 2010, **5**:e12405.
- Multi-parameter flow cytometry of primary acute myeloid leukemia samples revealed multiple distinct cell subpopulations identifiable by their surface marker expression, cytokine and growth factor-mediated signaling pathway responses, as well as their response to DNA-damaging agents. The activation states of the JAK/STAT and PI3 kinase pathways were strongly associated with *ex vivo* and *in vivo* responsiveness to DNA damaging agents.
15. Hotson AN, Hardy JW, Hale MB, Contag CH, Nolan GP: **The T cell STAT signaling network is reprogrammed within hours of bacteremia via secondary signals.** *J Immunol* 2009, **182**:7558-7568.
16. O'Gorman WE, Dooms H, Thorne SH, Kuswanto WF, Simonds EF, Krutzik PO, Nolan GP, Abbas AK: **The initial phase of an immune response functions to activate regulatory T cells.** *J Immunol* 2009, **183**:332-339.
17. O'Gorman WE, Sampath P, Simonds EF, Sikorski R, O'Malley M, Krutzik PO, Chen H, Panchanathan V, Chaudhri G, Karupiah G *et al.*: **Alternate mechanisms of initial pattern recognition drive differential immune responses to related poxviruses.** *Cell Host Microbe* 2010, **8**:174-185.
18. Krutzik PO, Crane JM, Clutter MR, Nolan GP: **High-content single-cell drug screening with phosphospecific flow cytometry.** *Nat Chem Biol* 2008, **4**:132-142.
19. Kornblau SM, Minden MD, Rosen DB, Putta S, Cohen A, Covey T, Spellmeyer DC, Fantl WJ, Gayko U, Cesano A: **Dynamic single-cell network profiles in acute myelogenous leukemia are associated with patient response to standard induction therapy.** *Clin Cancer Res* 2010, **16**:3721-3733.
20. Tong FK, Chow S, Hedley D: **Pharmacodynamic monitoring of BAY 43-9006 (Sorafenib) in phase I clinical trials involving solid tumor and AML/MDS patients, using flow cytometry to monitor activation of the ERK pathway in peripheral blood cells.** *Cytometry B Clin Cytom* 2006, **70**:107-114.
21. Chattopadhyay PK, Price DA, Harper TF, Betts MR, Yu J, Gostick E, Perfetto SP, Goepfert P, Koup RA, De Rosa SC *et al.*: **Quantum dot semiconductor nanocrystals for immunophenotyping by polychromatic flow cytometry.** *Nat Med* 2006, **12**:972-977.
22. Perfetto SP, Ambrozak D, Nguyen R, Chattopadhyay PK, Roederer M: **Quality assurance for polychromatic flow cytometry using a suite of calibration beads.** *Nat Protoc* 2012, **7**:2067-2079.
23. Baranov VI, Quinn Z, Bandura DR, Tanner SD: **A sensitive and quantitative element-tagged immunoassay with ICPMS detection.** *Anal Chem* 2002, **74**:1629-1636.
24. Ornatsky O, Baranov VI, Bandura DR, Tanner SD, Dick J: **Multiple cellular antigen detection by ICP-MS.** *J Immunol Methods* 2006, **308**:68-76.
25. Ornatsky OI, Kinach R, Bandura DR, Lou X, Tanner SD, Baranov VI, Nitz M, Winnik MA: **Development of analytical methods for multiplex bio-assay with inductively coupled plasma mass spectrometry.** *J Anal At Spectrom* 2008, **23**:463-469.
26. Ornatsky OI, Lou X, Nitz M, Schafer S, Sheldrick WS, Baranov VI, Bandura DR, Tanner SD: **Study of cell antigens and intracellular DNA by identification of element-containing labels and metallointercalators using inductively coupled plasma mass spectrometry.** *Anal Chem* 2008, **80**:2539-2547.
27. Razumienko E, Ornatsky O, Kinach R, Milyavsky M, Lechman E, Baranov V, Winnik MA, Tanner SD: **Element-tagged immunoassay with ICP-MS detection: evaluation and comparison to conventional immunoassays.** *J Immunol Methods* 2008, **336**:56-63.
28. Bendall SC, Nolan GP: **From single cells to deep phenotypes in cancer.** *Nat Biotechnol* 2012, **30**:639-647.
- One of the most pressing issues facing next-generation single-cell analysis platforms is addressing the cancer heterogeneity and how it relates to the overall disease progression and outcome. These approaches vary widely, from imaging and mass spectrometry of expressed epitopes and molecules, to molecular and sequencing analysis of gene expression and genomic content. Bendall and Nolan compare and contrast a number of these approaches, providing real-world applications of how they have been used to decipher complex cellular systems.
29. Bendall SC, Nolan GP, Roederer M, Chattopadhyay PK: **A deep profiler's guide to cytometry.** *Trends Immunol* 2012, **33**:323-332.
30. Tanner SD, Baranov VI, Ornatsky OI, Bandura DR, George TC: **An introduction to mass cytometry: fundamentals and applications.** *Cancer Immunol Immunother* 2013, **62**:955-965.
31. Bandura DR, Baranov VI, Ornatsky OI, Antonov A, Kinach R, Lou X, Pavlov S, Vorobiev S, Dick JE, Tanner SD: **Mass cytometry: technique for real time single cell multitarget immunoassay based on inductively coupled plasma time-of-flight mass spectrometry.** *Anal Chem* 2009, **81**:6813-6822.
32. Ornatsky O, Bandura D, Baranov V, Nitz M, Winnik MA, Tanner S: **Highly multiparametric analysis by mass cytometry.** *J Immunol Methods* 2010, **361**:1-20.
33. Tanner SD, Bandura DR, Ornatsky O, Baranov VI, Nitz M, Winnik MA: **Flow cytometer with mass spectrometer detection for massively multiplexed single-cell biomarker assay.** *Pure Appl Chem* 2008, **80**:2627-2641.
34. Lou X, Zhang G, Herrera I, Kinach R, Ornatsky O, Baranov V, Nitz M, Winnik MA: **Polymer-based elemental tags for sensitive bioassays.** *Angew Chem Int Ed Engl* 2007, **46**:6111-6114.
35. Illy N, Majonis D, Herrera I, Ornatsky O, Winnik MA: **Metal-chelating polymers by anionic ring-opening polymerization and their use in quantitative mass cytometry.** *Biomacromolecules* 2012, **13**:2359-2369.
36. Majonis D, Herrera I, Ornatsky O, Schulze M, Lou X, Soleimani M, Nitz M, Winnik MA: **Synthesis of a functional metal-chelating polymer and steps toward quantitative mass cytometry bioassays.** *Anal Chem* 2010.
37. Behbehani GK, Bendall SC, Clutter MR, Fantl WJ, Nolan GP: **Single-cell mass cytometry adapted to measurements of the cell cycle.** *Cytometry A* 2012, **81**:552-566.
- A methodology to allow measurement of all phases of the cell cycle by mass cytometry. This methodology (which utilizes the mass cytometer's ability to directly detect Iodo-deoxyuridine) was extensively compared to standard fluorescent approaches and yielded equivalent results across a range of cell lines and primary cell types. Importantly, mass cytometric cell-cycle analysis allows for the simultaneous measurement of up to 35 additional parameters, permitting the measurement of cell-cycle state with multiple other measurements of cellular function in complex samples. As a proof of principle, the authors simultaneously measured the cell cycle state of 25 different immunophenotypic populations of healthy human bone marrow.
38. Bendall SC, Simonds EF, Qiu P, Amir el AD, Krutzik PO, Finck R, Bruggner RV, Melamed R, Trejo A, Ornatsky OI *et al.*: **Single-cell mass cytometry of differential immune and drug responses across a human hematopoietic continuum.** *Science* 2011, **332**:687-696.
- First large-scale demonstration of developed reagents and analysis methods for single-cell mass cytometry and demonstration of merging multiple datasets through mutual information. Besides being the first practical demonstration of the technology, it also provided an analytical resource of regulatory signaling information in the human hematopoietic and immune system that continues to be utilized in subsequent investigations in a fashion akin to gene expression and genomic sequence repositories (www.cytobank.org/nolanlab).
39. Finck R, Simonds EF, Jager A, Krishnaswamy S, Sachs K, Fantl W, Pe'er D, Nolan GP, Bendall SC: **Normalization of mass cytometry data with bead standards.** *Cytometry A* 2013.
- Bead-based normalization of mass cytometry data uses the signal intensities of metal-embedded beads to account for the effects of instrument variation and thus enables a more accurate interpretation of the biological differences between samples measured on the mass cytometer. The method which is implemented on freely available software applies a multiplicative correction derived from slopes fitted between smoothed

bead signals and their global averages. This expands the types of analyses available using mass cytometry by allowing comparisons to be made across data acquired over periods of weeks or longer.

40. Krutzik PO, Nolan GP: **Fluorescent cell barcoding in flow cytometry allows high-throughput drug screening and signaling profiling.** *Nat Methods* 2006, **3**:361-368.
 41. Bodenmiller B, Zunder ER, Finck R, Chen TJ, Savig ES, Bruggner RV, Simonds EF, Bendall SC, Sachs K, Krutzik PO *et al.*: **Multiplexed mass cytometry profiling of cellular states perturbed by small-molecule regulators.** *Nat Biotechnol* 2012, **30**:858-867.
- A mass tag-based, cellular multiplexing approach (MCB) for mass cytometry was developed to increase measurement throughput and reduce experimental variation. MCB was applied to characterize inhibitor impact on human peripheral blood mononuclear cell signaling networks under 96 conditions, allowing classification of inhibitor and cell-type selectivity. This study demonstrates that high-content, high-throughput screening with MCB can be applied to drug discovery, preclinical testing and mechanistic investigation of human disease.
42. Moore A, Donahue CJ, Bauer KD, Mather JP: **Simultaneous measurement of cell cycle and apoptotic cell death.** *Methods Cell Biol* 1998, **57**:265-278.
 43. Schmid I, Krall WJ, Uittenbogaart CH, Braun J, Giorgi JV: **Dead cell discrimination with 7-amino-actinomycin D in combination with dual color immunofluorescence in single laser flow cytometry.** *Cytometry* 1992, **13**:204-208.
 44. Gavrieli Y, Sherman Y, Ben-Sasson SA: **Identification of programmed cell death in situ via specific labeling of nuclear DNA fragmentation.** *J Cell Biol* 1992, **119**:493-501.
 45. Perfetto SP, Chattopadhyay PK, Lamoreaux L, Nguyen R, Ambrozak D, Koup RA, Roederer M: **Amine reactive dyes: an effective tool to discriminate live and dead cells in polychromatic flow cytometry.** *J Immunol Methods* 2006, **313**:199-208.
 46. Cossarizza A, Baccharani-Contri M, Kalashnikova G, Franceschi C: **A new method for the cytofluorimetric analysis of mitochondrial membrane potential using the J-aggregate forming lipophilic cation 5,5',6,6'-tetrachloro-1,1',3,3'-tetraethylbenzimidazolcarbocyanine iodide (JC-1).** *Biochem Biophys Res Commun* 1993, **197**:40-45.
 47. Fienberg HG, Simonds EF, Fantl WJ, Nolan GP, Bodenmiller B: **A platinum-based covalent viability reagent for single-cell mass cytometry.** *Cytometry A* 2012, **81**:467-475.
- Cisplatin is the viability stain of choice that is compatible with mass cytometry. Since platinum isotopes are not routinely conjugated to antibodies for mass cytometry, no protein measurement channel is lost. Furthermore, although cisplatin is a DNA-damaging agent, cisplatin staining does not induce DNA damage or apoptosis if used in the 'pulse' application that optimally discriminates viable from non-viable cells.
48. Majonis D, Ornatsky O, Kinach R, Winnik MA: **Curious results with palladium- and platinum-carrying polymers in mass cytometry bioassays and an unexpected application as a dead cell stain.** *Biomacromolecules* 2011, **12**:3997-4010.
 49. Darzynkiewicz Z, Crissman H, Jacobberger JW: **Cytometry of the cell cycle: cycling through history.** *Cytometry A* 2004, **58**:21-32.
 50. Sage J: **The retinoblastoma tumor suppressor and stem cell biology.** *Genes Dev* 2012, **26**:1409-1420.
 51. Takahashi C, Sasaki N, Kitajima S: **Twists in views on RB functions in cellular signaling, metabolism and stem cells.** *Cancer Sci* 2012, **103**:1182-1188.
 52. Ren S, Rollins BJ: **Cyclin C/cdk3 promotes Rb-dependent G0 exit.** *Cell* 2004, **117**:239-251.
 53. Burns KA, Kuan CY: **Low doses of bromo- and iododeoxyuridine produce near-saturation labeling of adult proliferative populations in the dentate gyrus.** *Eur J Neurosci* 2005, **21**:803-807.
 54. Svetlova M, Solovjeva L, Blasius M, Shevelev I, Hubscher U, Hanawalt P, Tomilin N: **Differential incorporation of halogenated deoxyuridines during UV-induced DNA repair synthesis in human cells.** *DNA Repair (Amst)* 2005, **4**:359-366.
 55. Wali A, Strayer DS: **Infection with vaccinia virus alters regulation of cell cycle progression.** *DNA Cell Biol* 1999, **18**:837-843.
 56. Yoo NK, Pyo CW, Kim Y, Ahn BY, Choi SY: **Vaccinia virus-mediated cell cycle alteration involves inactivation of tumour suppressors associated with Brf1 and TBP.** *Cell Microbiol* 2008, **10**:583-592.
 57. Jiang W, Wang Q, Chen S, Gao S, Song L, Liu P, Huang W: **Influenza A virus NS1 induces G0/G1 cell cycle arrest by inhibiting the expression and activity of RhoA protein.** *J Virol* 2013.
 58. Kannan RP, Hensley LL, Evers LE, Lemon SM, McGovern DR: **Hepatitis C virus infection causes cell cycle arrest at the level of initiation of mitosis.** *J Virol* 2011, **85**:7989-8001.
 59. Kota KP, Benko JG, Mudhasani R, Retterer C, Tran JP, Bavari S, Panchal RG: **High content image based analysis identifies cell cycle inhibitors as regulators of Ebola virus infection.** *Viruses* 2012, **4**:1865-1877.
 60. Malumbres M: **Cell cycle-based therapies move forward.** *Cancer Cell* 2012, **22**:419-420.
 61. Dent P, Tang Y, Yacoub A, Dai Y, Fisher PB, Grant S: **CHK1 inhibitors in combination chemotherapy: thinking beyond the cell cycle.** *Mol Interv* 2011, **11**:133-140.
 62. Zhang YW, Hunter T, Abraham RT: **Turning the replication checkpoint on and off.** *Cell Cycle* 2006, **5**:125-128.
 63. Malumbres M, Barbacid M: **To cycle or not to cycle: a critical decision in cancer.** *Nat Rev Cancer* 2001, **1**:222-231.
 64. Ewald B, Sampath D, Plunkett W: **H2AX phosphorylation marks gemcitabine-induced stalled replication forks and their collapse upon S-phase checkpoint abrogation.** *Mol Cancer Ther* 2007, **6**:1239-1248.
 65. Melo RC, Liu L, Xenakis JJ, Spencer LA: **Eosinophil-derived cytokines in health and disease: unraveling novel mechanisms of selective secretion.** *Allergy* 2013, **68**:274-284.
 66. O'Shea JJ, Paul WE: **Mechanisms underlying lineage commitment and plasticity of helper CD4+ T cells.** *Science* 2010, **327**:1098-1102.
 67. Liao W, Lin JX, Leonard WJ: **Interleukin-2 at the crossroads of effector responses, tolerance, and immunotherapy.** *Immunity* 2013, **38**:13-25.
 68. Littman DR, Rudensky AY: **Th17 and regulatory T cells in mediating and restraining inflammation.** *Cell* 2010, **140**:845-858.
 69. Cox MA, Kahan SM, Zajac AJ: **Anti-viral CD8 T cells and the cytokines that they love.** *Virology* 2013, **435**:157-169.
 70. Sallusto F, Lanzavecchia A: **Heterogeneity of CD4+ memory T cells: functional modules for tailored immunity.** *Eur J Immunol* 2009, **39**:2076-2082.
 71. Sun JC, Lanier LL: **NK cell development, homeostasis and function: parallels with CD8(+) T cells.** *Nat Rev Immunol* 2011, **11**:645-657.
 72. Takata H, Naruto T, Takiguchi M: **Functional heterogeneity of human effector CD8+ T cells.** *Blood* 2012, **119**:1390-1398.
 73. Coussens LM, Zitvogel L, Palucka AK: **Neutralizing tumor-promoting chronic inflammation: a magic bullet?** *Science* 2013, **339**:286-291.
 74. Shichita T, Ago T, Kamouchi M, Kitazono T, Yoshimura A, Ooboshi H: **Novel therapeutic strategies targeting innate immune responses and early inflammation after stroke.** *J Neurochem* 2012, **123**(Suppl 2):29-38.
 75. Hassoun PM, Mouthon L, Barbera JA, Eddahibi S, Flores SC, Grimminger F, Jones PL, Maitland ML, Michelakis ED, Morrell NW *et al.*: **Inflammation, growth factors, and pulmonary vascular remodeling.** *J Am Coll Cardiol* 2009, **54**:S10-S19.
 76. Sallusto F, Geginat J, Lanzavecchia A: **Central memory and effector memory T cell subsets: function, generation, and maintenance.** *Annu Rev Immunol* 2004, **22**:745-763.

77. Donaldson MM, Kao SF, Eslamizar L, Gee C, Koopman G, Lifton M, Schmitz JE, Sylwester AW, Wilson A, Hawkins N *et al.*: **Optimization and qualification of an 8-color intracellular cytokine staining assay for quantifying T cell responses in rhesus macaques for pre-clinical vaccine studies.** *J Immunol Methods* 2012, **386**:10-21.
78. Lamoreaux L, Roederer M, Koup R: **Intracellular cytokine optimization and standard operating procedure.** *Nat Protoc* 2006, **1**:1507-1516.
79. Lovelace P, Maecker HT: **Multiparameter intracellular cytokine staining.** *Methods Mol Biol* 2011, **699**:165-178.
80. Newell EW, Sigal N, Bendall SC, Nolan GP, Davis MM: **Cytometry by time-of-flight shows combinatorial cytokine expression and virus-specific cell niches within a continuum of CD8+ T cell phenotypes.** *Immunity* 2012, **36**:142-152.
- First description of the development and use of peptide-MHC tetramer staining in conjunction with mass cytometry to identify and profile antigen-specific T cells with a large number of phenotypic and functional markers. Computational methods were applied that provide a new view of the functional and phenotypic diversity of the CD8+ T cell compartment. This analysis shows that CD8+ T cells from normal human donors display a broad continuum of phenotypic profiles with with remarkable diversity in their abilities to produce various cytokines.
81. Blum JS, Wearsch PA, Cresswell P: **Pathways of antigen processing.** *Annu Rev Immunol* 2013.
82. Altman JD, Moss PA, Goulder PJ, Barouch DH, McHeyzer-Williams MG, Bell JL, McMichael AJ, Davis MM: **Phenotypic analysis of antigen-specific T lymphocytes.** *Science* 1996, **274**:94-96.
83. Davis MM, Altman JD, Newell EW: **Interrogating the repertoire: broadening the scope of peptide-MHC multimer analysis.** *Nat Rev Immunol* 2011, **11**:551-558.
84. Panchision DM, Chen HL, Pistollato F, Papini D, Ni HT, Hawley TS: **Optimized flow cytometric analysis of central nervous system tissue reveals novel functional relationships among cells expressing CD133, CD15, and CD24.** *Stem Cells* 2007, **25**:1560-1570.
85. Chang Q, Hedley D: **Emerging applications of flow cytometry in solid tumor biology.** *Methods* 2012, **57**:359-367.
86. Do JH, Choi DK: **Clustering approaches to identifying gene expression patterns from DNA microarray data.** *Mol Cells* 2008, **25**:279-288.
87. Nugent R, Meila M: **An overview of clustering applied to molecular biology.** *Methods Mol Biol* 2010, **620**:369-404.
88. Qiu P, Simonds EF, Bendall SC, Gibbs KD Jr, Bruggner RV, Linderman MD, Sachs K, Nolan GP, Plevritis SK: **Extracting a cellular hierarchy from high-dimensional cytometry data with SPADE.** *Nat Biotechnol* 2011, **29**:886-891.
- SPADE is a cytometry visualization tool that uses a tree-like representation to convey the relatedness of cell phenotypes, including rare cell types. The paper shows how SPADE can be used to identify immune subsets based on non-canonical markers or to compare marker expression under different experimental conditions. SPADE was the first algorithm that was purpose-built for investigating mass cytometry data, and SPADE diagrams have appeared in several subsequent mass cytometry publications.
89. Linderman MD, Bjornson Z, Simonds EF, Qiu P, Bruggner RV, Sheode K, Meng TH, Plevritis SK, Nolan GP: **CytoSPADE: high-performance analysis and visualization of high-dimensional cytometry data.** *Bioinformatics* 2012, **28**:2400-2401.
90. Frey BJ, Dueck D: **Clustering by passing messages between data points.** *Science* 2007, **315**:972-976.
91. van der Maaten LJP: **Learning a parametric embedding by preserving local structure.** In *Proceedings of the Twelfth International Conference on Artificial Intelligence and Statistics (AISTATS)*. 2009:384-391.
92. van der Maaten LJP, Hinton GE: **Visualizing high-dimensional data using t-SNE.** *J Mach Learn Res* 2008, **9**:2579-2605.
93. Amir el AD, Davis KL, Tadmor MD, Simonds EF, Levine JH, Bendall SC, Shenfeld DK, Krishnaswamy S, Nolan GP, Pe'er D: **viSNE enables visualization of high dimensional single-cell data and reveals phenotypic heterogeneity of leukemia.** *Nat Biotechnol* 2013, **31**:545-552.
94. Ringner M: **What is principal component analysis?** *Nat Biotechnol* 2008, **26**:303-304.

Appendix B —

Titration Slides for Tumor Panel

OVCAR Tumor Panel 1 – Metal assignment

In113	Not used
In115	<u>Vimentin</u>
La139	<u>CD45</u>
140Ce	Not used
Pr141	<u>N-cadherin</u>
Nd142	<u>Cleaved-caspase 3</u>
Nd143	<u>CA125</u>
Nd144	<u>CD90</u>
Nd145	<u>pAMPK(T172)</u>
Nd146	<u>pATM(S1981)</u>
Sm147	<u>pH2AX(S139)</u>
Nd148	<u>Cyclin B1</u>
Sm149	<u>p65Rel-A(S529)</u>
Nd150	<u>pBcl-2(S70)</u>
Eu151	<u>pErk(T202Y204)</u>
Sm152	<u>Ki67 (total)</u>
Eu153	<u>Chk2(T68)</u>
Sm154	<u>pSTAT3(Y705)</u>
Gd155	<u>CD133</u>
Gd156	<u>CD10</u>

Gd157	<u>SNAIL</u>
Gd158	<u>E-Cadherin</u>
Tb159	<u>pAkt(473)</u>
Gd160	<u>Sox2</u>
Dy161	<u>Myc</u>
Dy162	<u>pSTAT5(Y694)</u>
Dy163	<u>Endoglin</u>
Dy164	<u>CD24</u>
Ho165	<u>pRb(S807/811)</u>
Er166	<u>CD44</u>
Er167	<u>PAX8</u>
Er168	<u>CD13</u>
Tm169	<u>pChk1(S345)</u>
Er170	<u>Non-phospho-β-catenin</u>
Yb171	<u>cleaved-PARP</u>
Yb172	<u>prpS6(S235/236)</u>
Yb173	<u>Mesothelin</u>
Yb174	<u>pCREB(S133)</u>
Lu175	<u>p53 (total)</u>
Yb176	<u>pHH3(S28)</u>

Blue – surface

Green- transcription

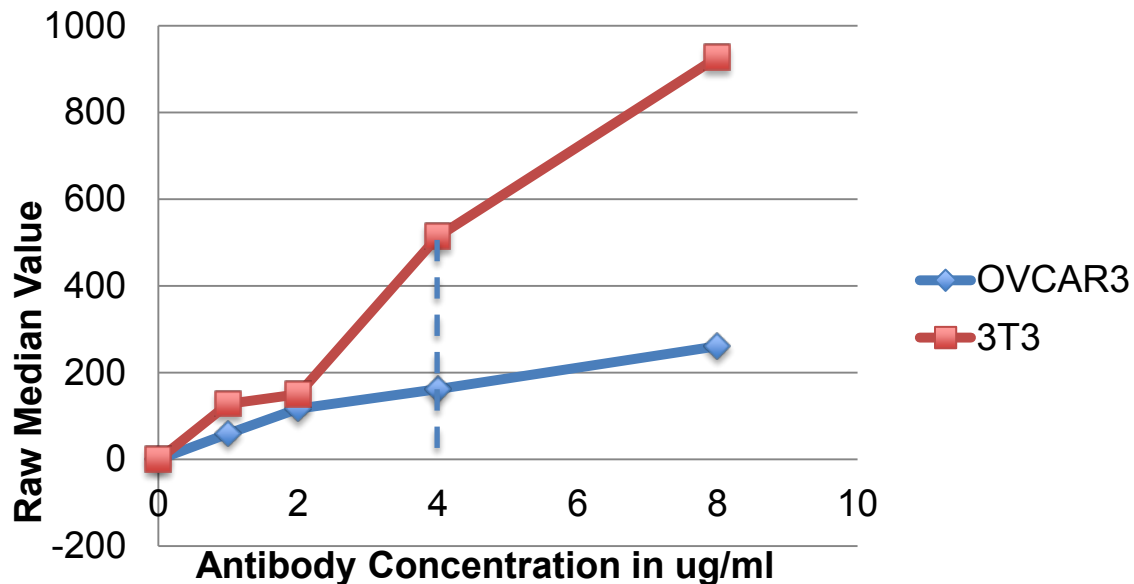
Red – DDR cell cycle

Purple – signaling

Orange - apoptosis

Italics – ovarian-specific

115 (In): Vimentin



115 (In): Vimentin

Date Conjugated: 7/22/13

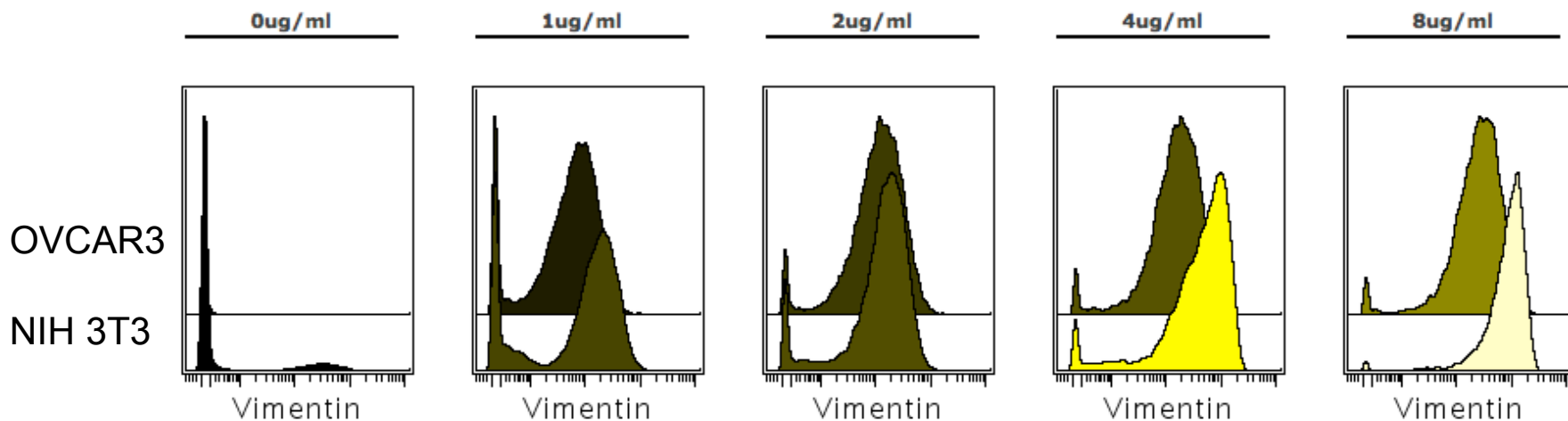
Titration: 8/16/13

CST 5741BF

Clone: D21H3

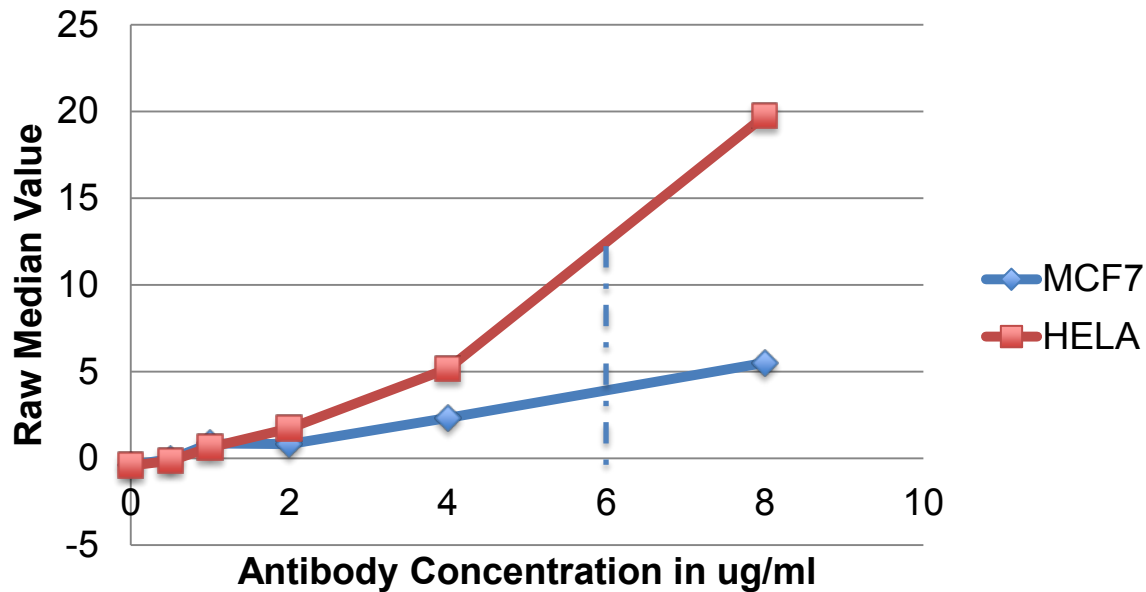
Selected Conc. : **4ug/ml**

	0ug/ml	1ug/ml	2ug/ml	4ug/ml	8ug/ml
OVCAR3	-0.43	59.38	117.34	161.87	260.84
NIH 3T3	-0.3	127.77	150.27	514.28	927.54



Cd45 on 139 from immune panel

141 (Pr): N-Cadherin



141 (Pr): N-Cadherin

Date Conjugated: 9/26/13

Titration: 10/10/13

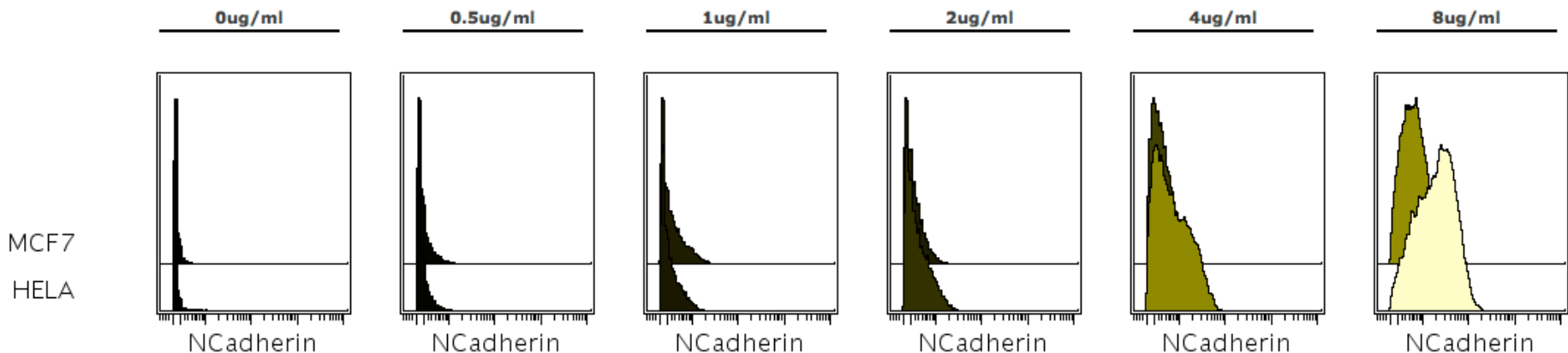
BD 561553

Clone: 8C11

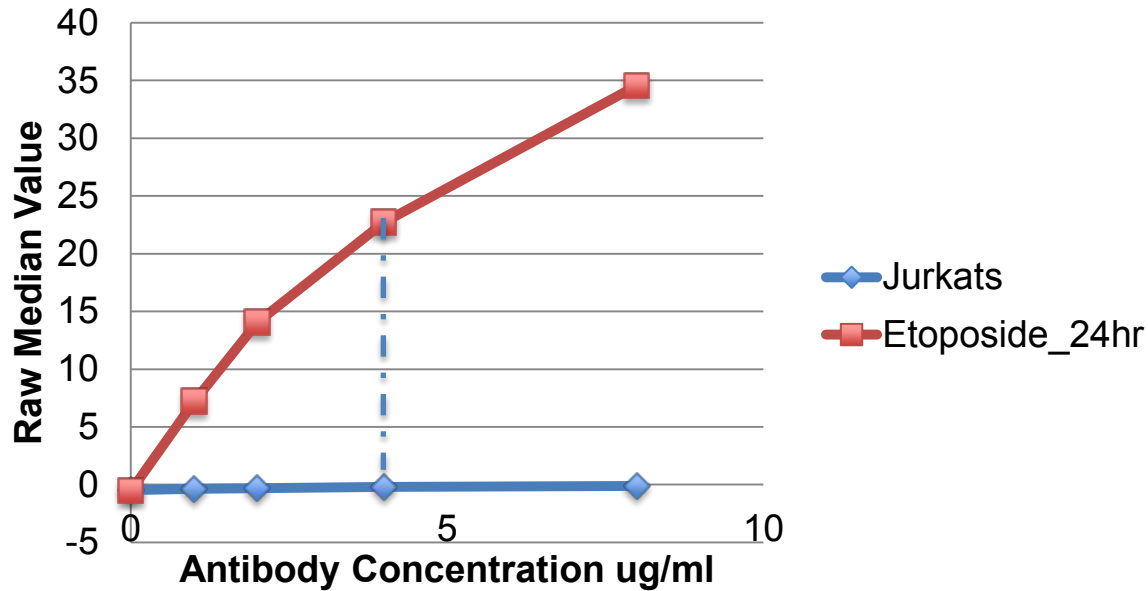
Selected Conc.: **6ug/ml**

	0ug/ml	0.5ug/ml	1ug/ml	2ug/ml	4ug/ml	8ug/ml
MCF7	-0.38	-0.04	0.86	0.83	2.33	5.51
HELA	-0.42	-0.13	0.64	1.73	5.17	19.75

6µg



142 (Nd): cCaspase3



142 (Nd): cCaspase3

Date Conjugated: 2/12/2013

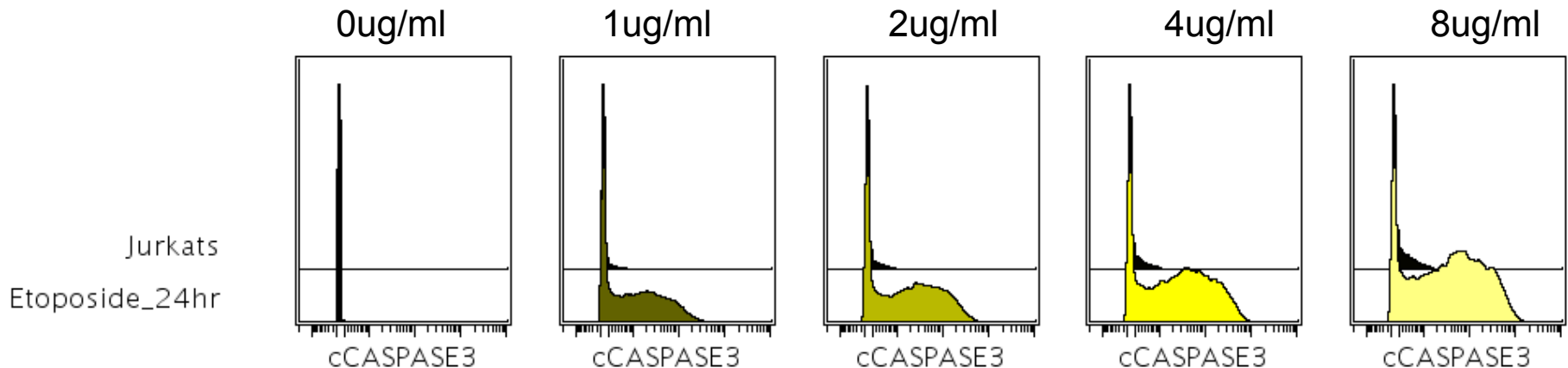
Titration: 3/8/13

BD 624084

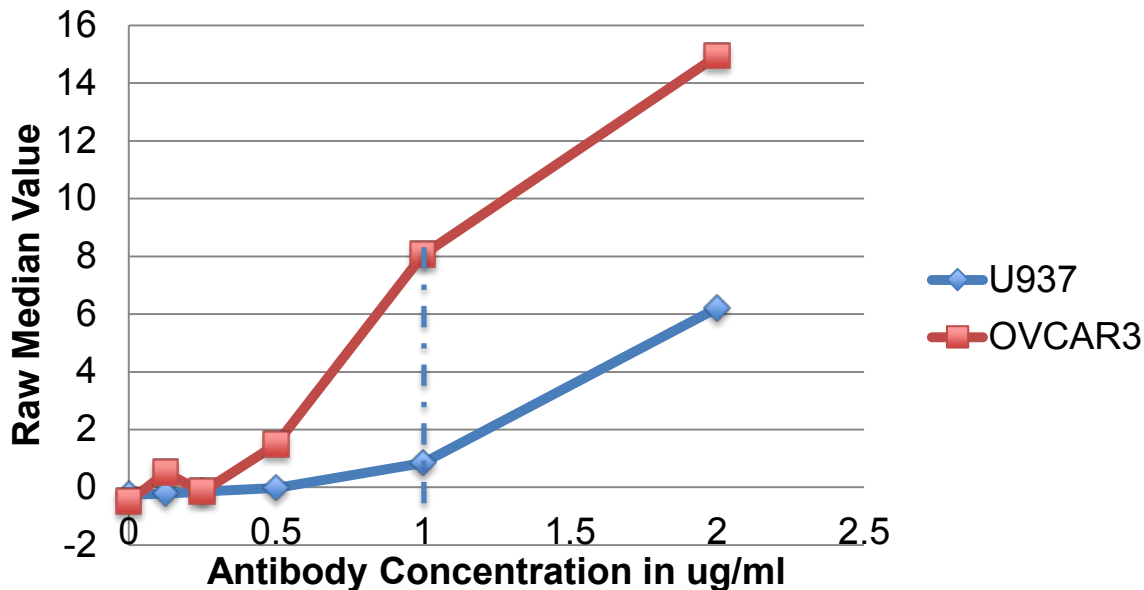
Clone: C92-605

Selected Conc.: **4ug/ml**

	0ug/ml	1ug/ml	2ug/ml	4ug/ml	8ug/ml
Jurkats	-0.47	-0.37	-0.3	-0.21	-0.12
Etoposide_24hr	-0.53	7.19	14.04	22.71	34.55



143 (Nd): CA125

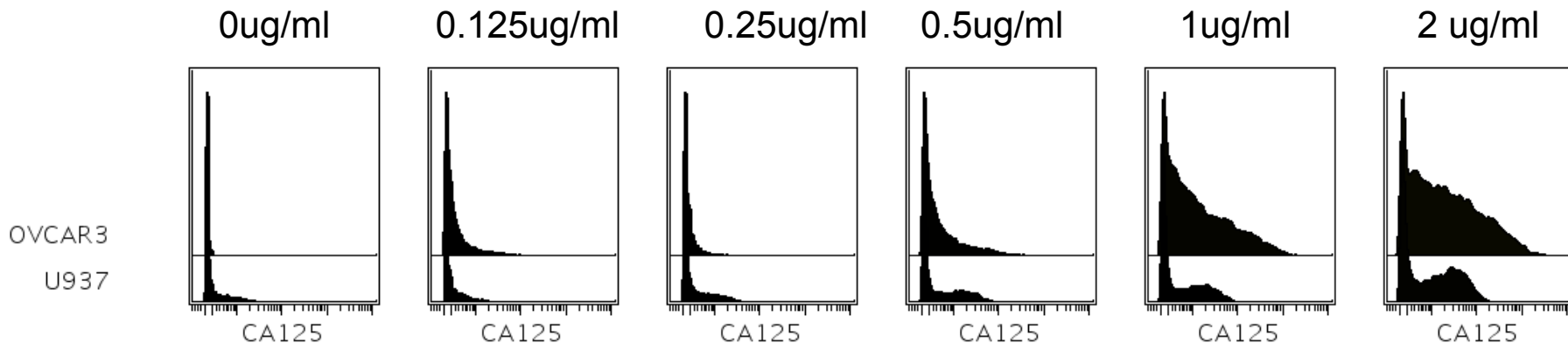


143 (Nd): CA125

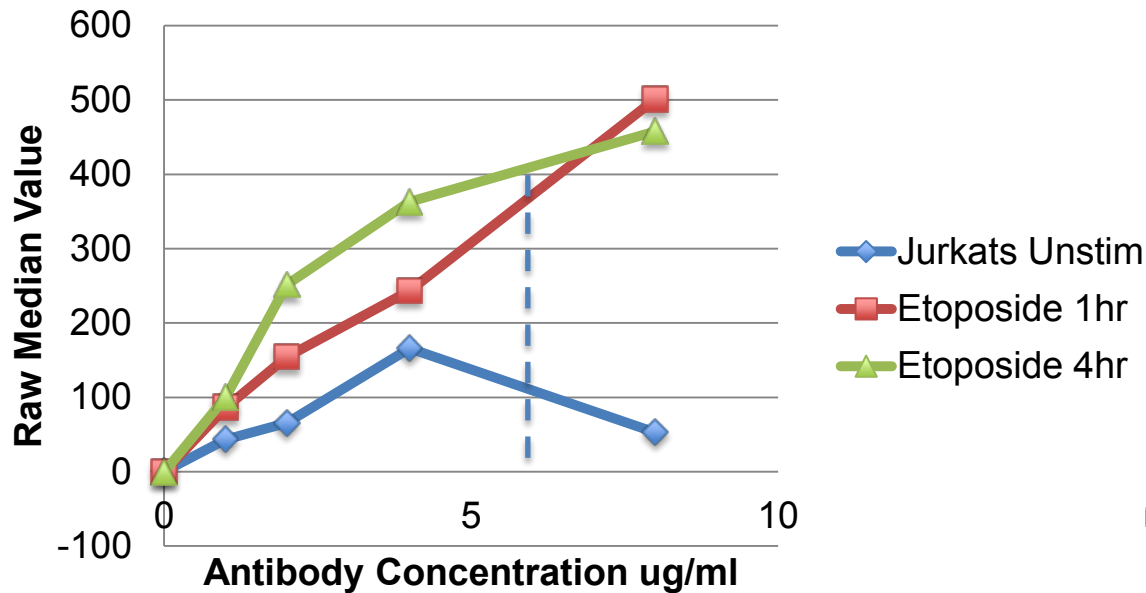
Conjugated: /9/2013
 Titration: 8/28/13
 GenWay GWD-17DD7A
 Clone: X75 (3C8/4)

Selected Conc. : **1ug/ml**

	0ug/ml	0.125ug/ml	.25ug/ml	0.5ug/ml	1ug/ml	2ug/ml
OVCAR3	-0.49	0.51	-0.16	1.48	8.06	14.94
U937	-0.26	-0.22	-0.14	-0.02	0.84	6.21



146 (Nd): pATM pS1981

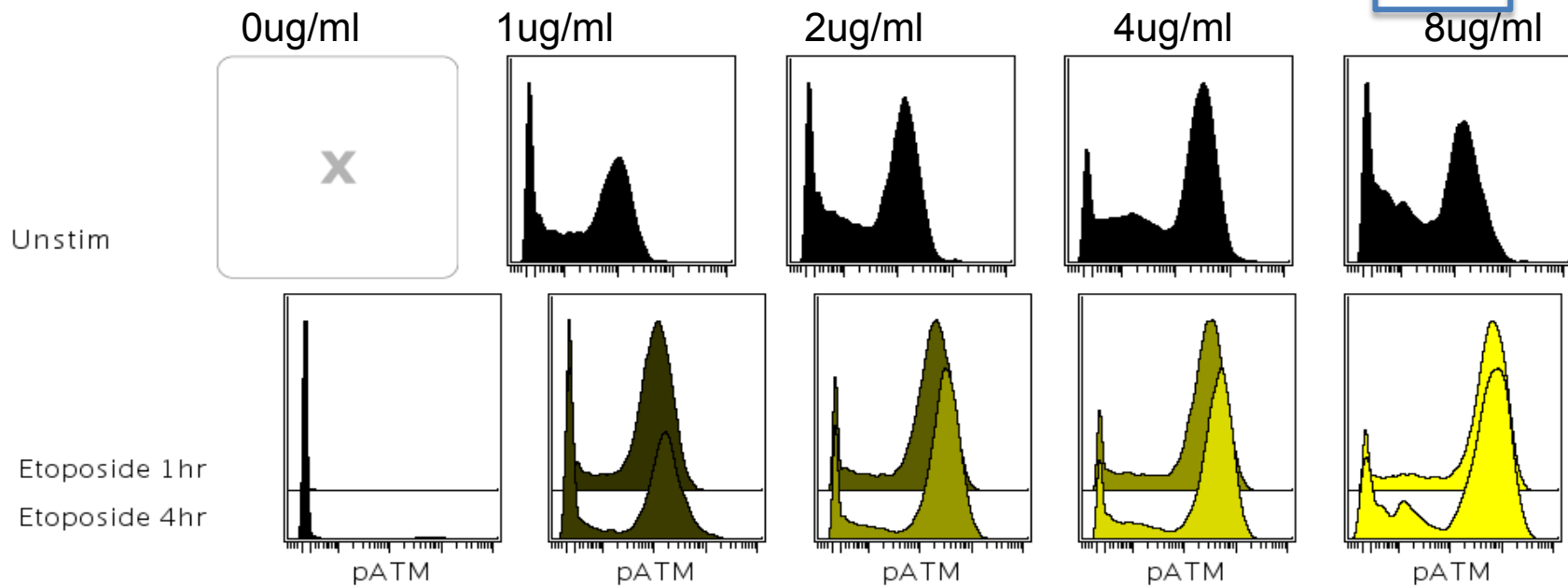


146 (Nd): pATM (pS1981)

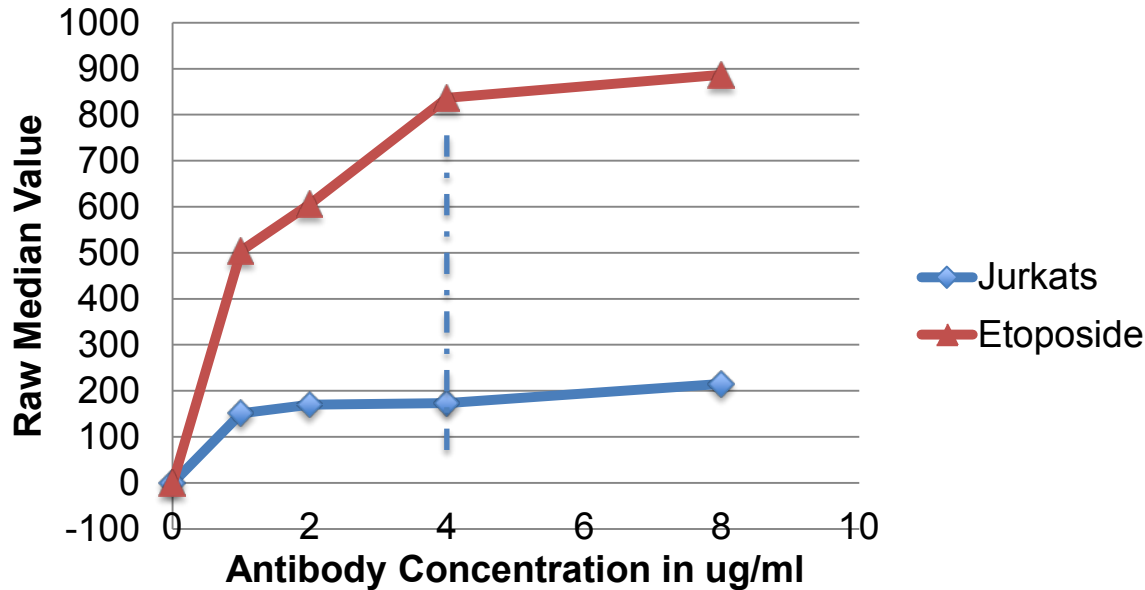
Conjugated: 9/21/12
 Titration: 10/18/12
 Millipore 05-740
 Clone: 10H11.E12

	0ug/ml	1ug/ml	2ug/ml	4ug/ml	8ug/ml
Unstim	X	43.02	65.67	165.85	52.72
Etoposide 1hr	-0.49	86.21	154.41	243.5	501.01
Etoposide 4hr	-0.4	99.8	251.38	363.09	457.84

Selected Conc. : **6ug/ml**



147(Sm) : pH2AX (pS139)

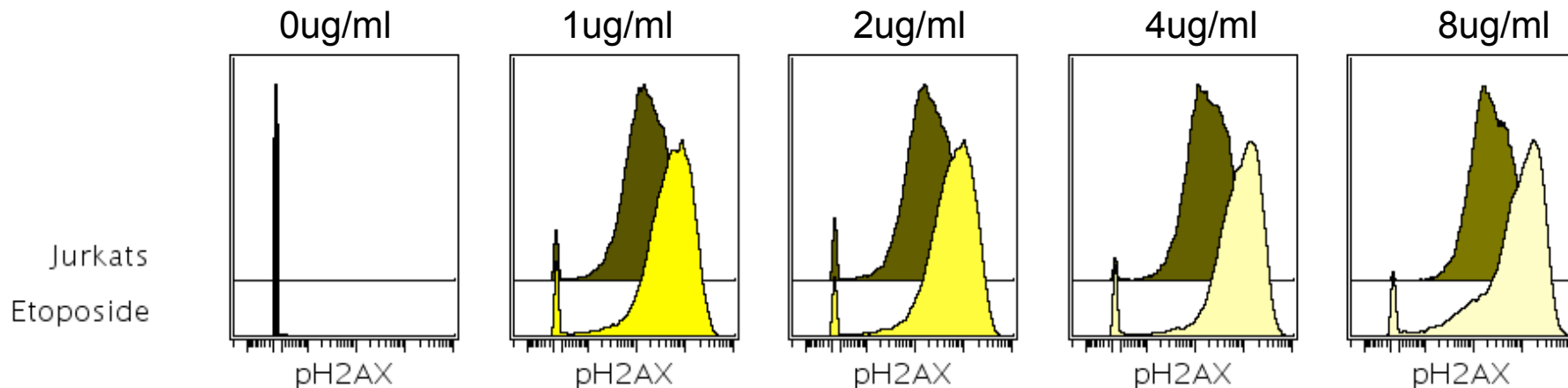


147 (Sm): pH2AX (pS139)

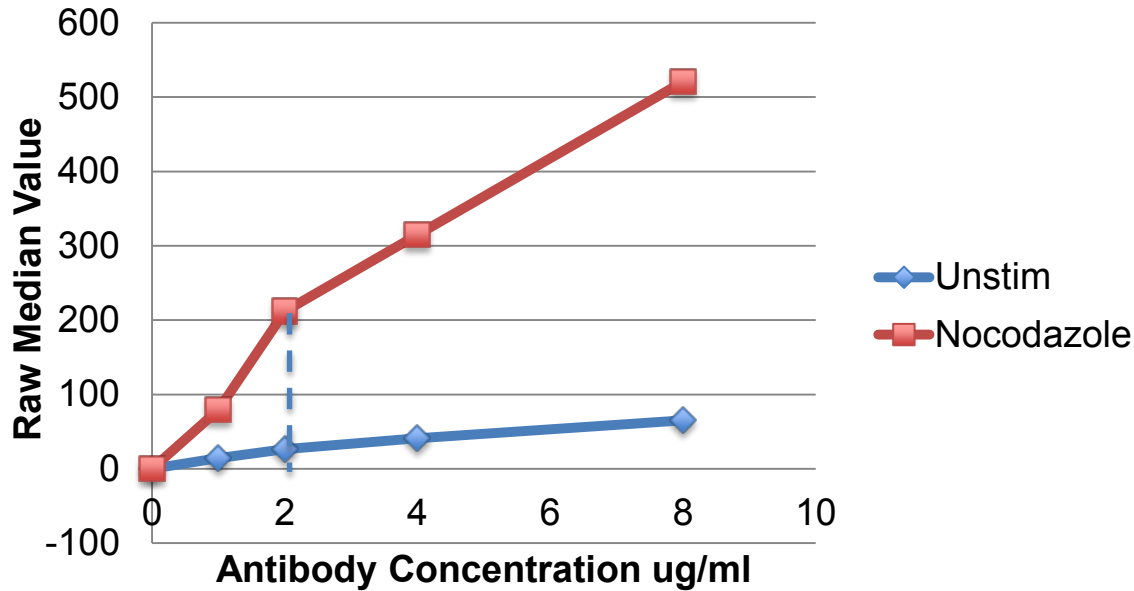
Date Conjugated: 2/13/13
 Titration: 2/14/13
 Millipore 05-636
 Clone: JBW301

Selected Conc. : 4ug/ml

	0ug/ml	1ug/ml	2ug/ml	4ug/ml	8ug/ml
Jurkats	-0.5	150.98	169.84	173.41	214.81
Etoposide	-0.49	504.49	605.9	836.7	887.14



148 (Nd): Cyclin B1

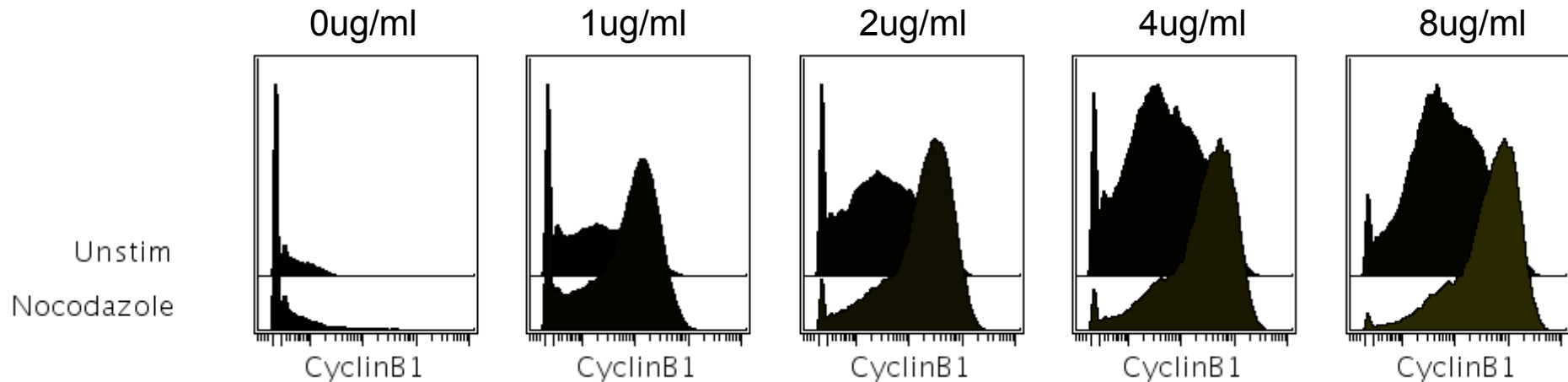


Nd (148): Cyclin B1

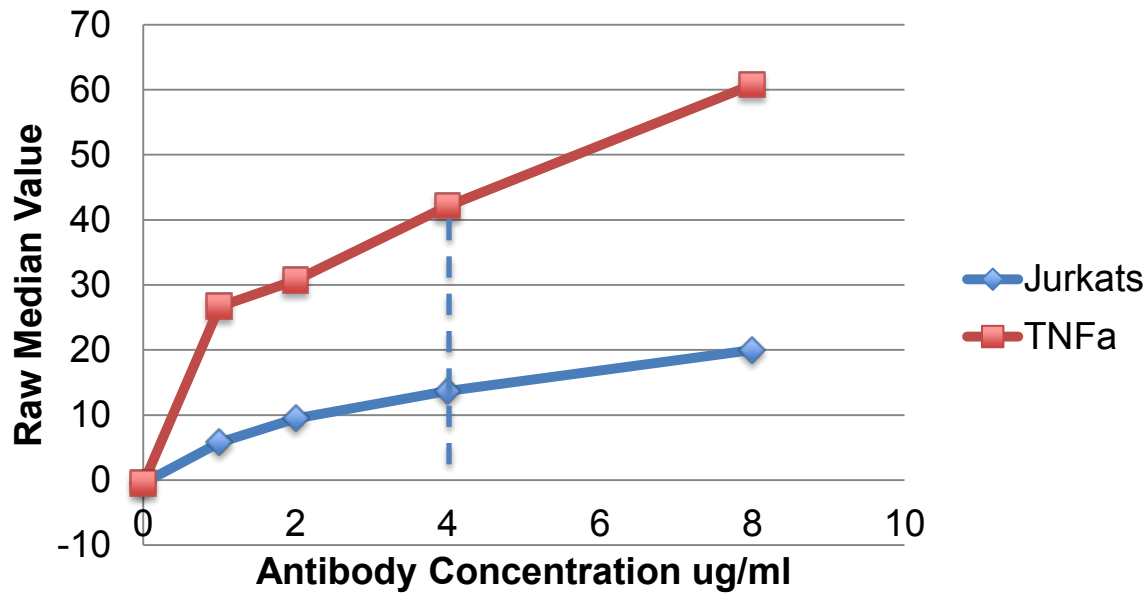
Conjugated: 9/19/12
 Titration: 10/3/12
 BD 554176
 Clone: GNS-1

Selected Conc. : **2ug/ml**

	0ug/ml	1ug/ml	2ug/ml	4ug/ml	8ug/ml
Unstim	-0.06	14.21	26.44	40.83	65.3
Nocodazole	0.09	79.39	212.07	314.73	520.4



149 (Sm): p65Rel-A (pS529)

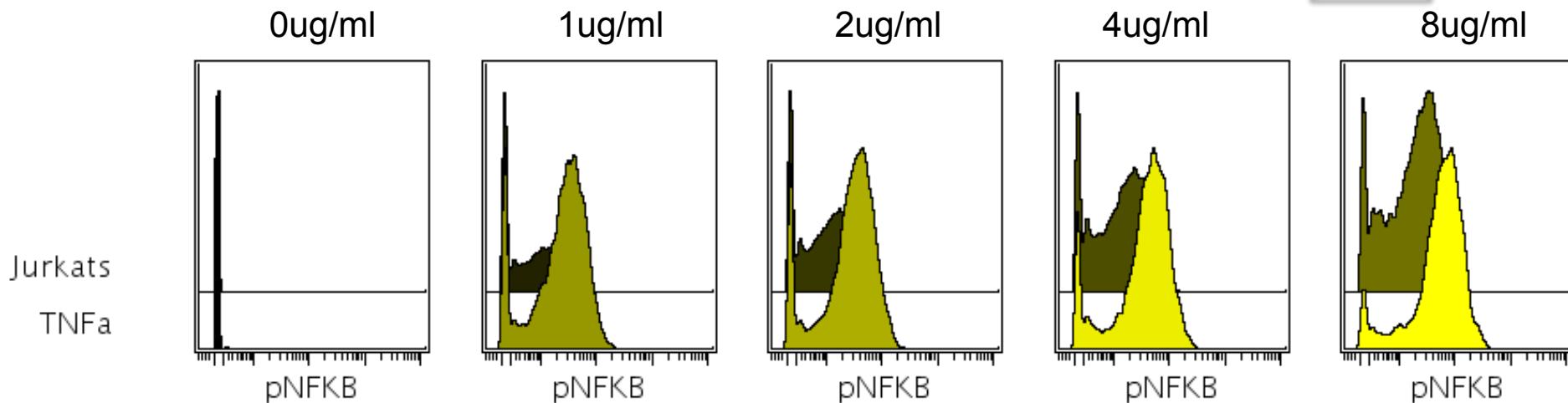


149 (Sm): p65Rel-A (pS529)

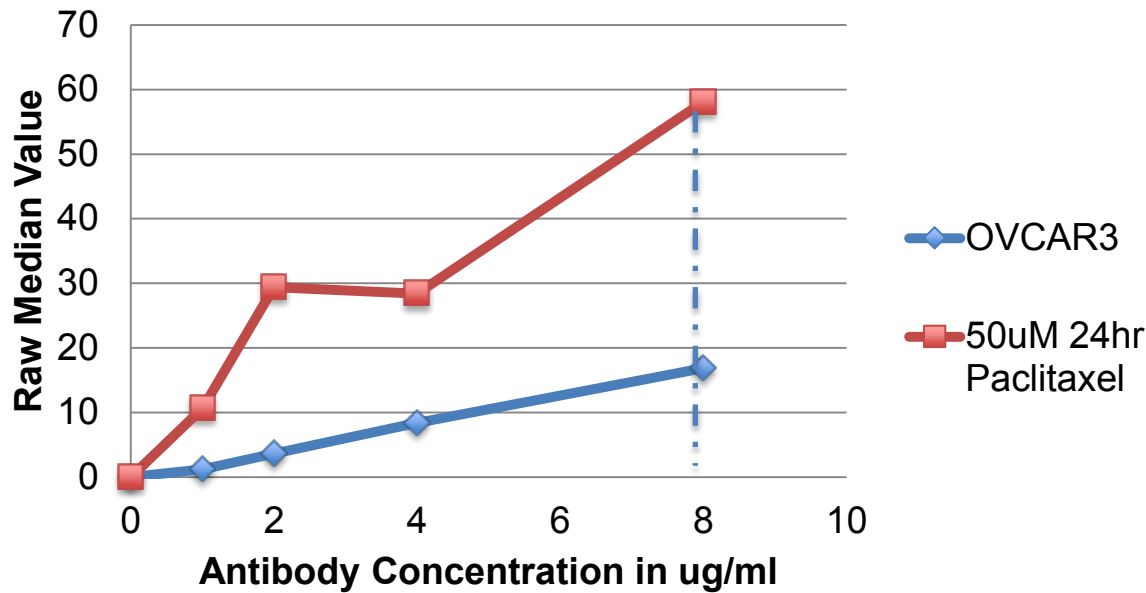
Conjugated: 9/19/12
 Titration: 9/28/12
 BD 558393
 Clone: K10-895.12.50

Selected Conc. : **4ug/ml**

	0ug/ml	1ug/ml	2ug/ml	4ug/ml	8ug/ml
Jurkats	-0.49	5.75	9.47	13.68	19.98
TNFa	-0.49	26.67	30.71	42.13	60.76



150 (Nd): BCL2 (pS70)



150 (Nd): pBCL2 (pS70)

Conjugated: 5/7/2013
 Titration: 5/10/13
 CST 2827
 Clone: 5H2

Selected Conc. : **8ug/ml**

	0ug/ml	1ug/ml	2ug/ml	4ug/ml	8ug/ml
OVCAR3	X	1.23	3.63	8.39	16.84
50uM 24hr Paclitaxel	6.02	10.65	29.39	28.4	58.08

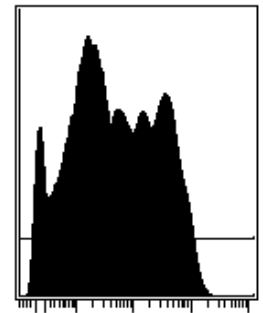
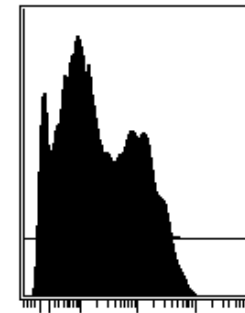
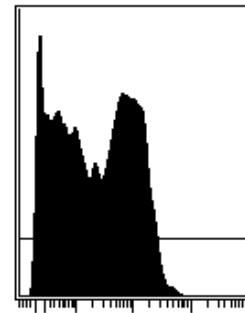
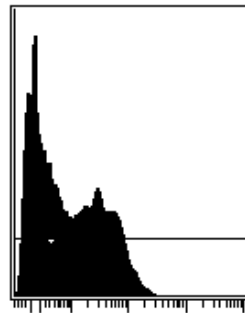
0ug/ml

1ug/ml

2ug/ml

4ug/ml

8ug/ml



OVCAR3

50uM 24hr Paclitaxel

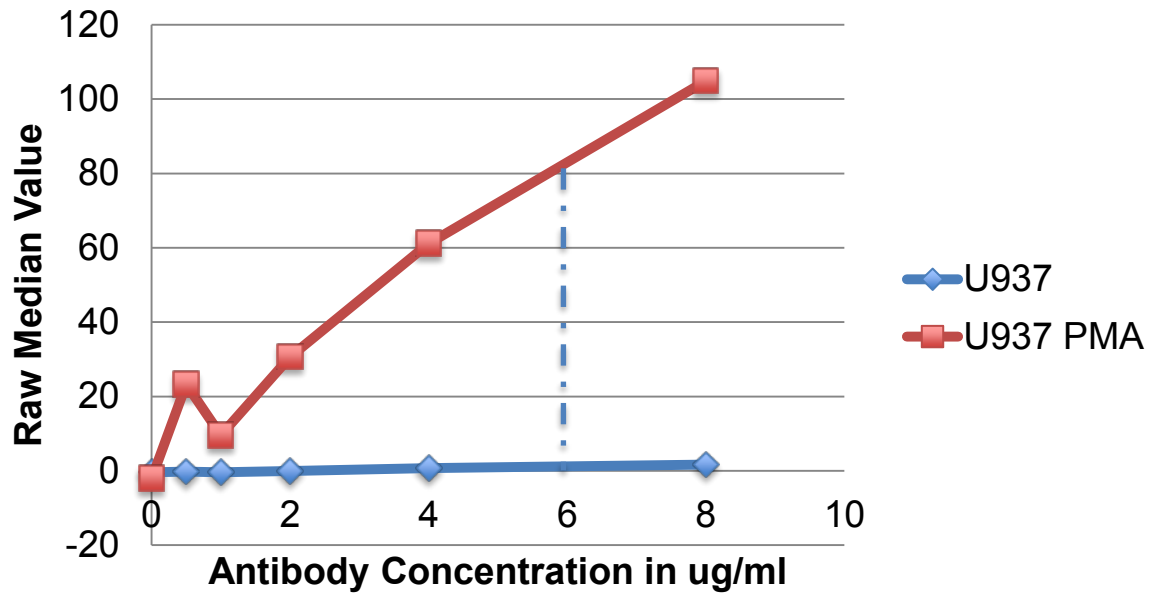
pBCL2

pBCL2

pBCL2

pBCL2

151 (Eu): pERK (pT202/pY204)

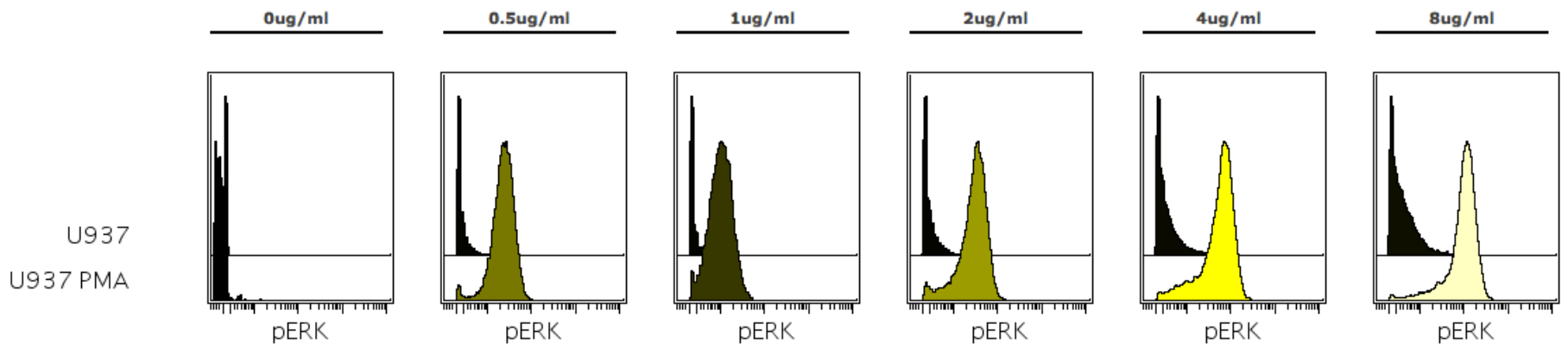


151 (Eu): pERK (pT202/pY204)

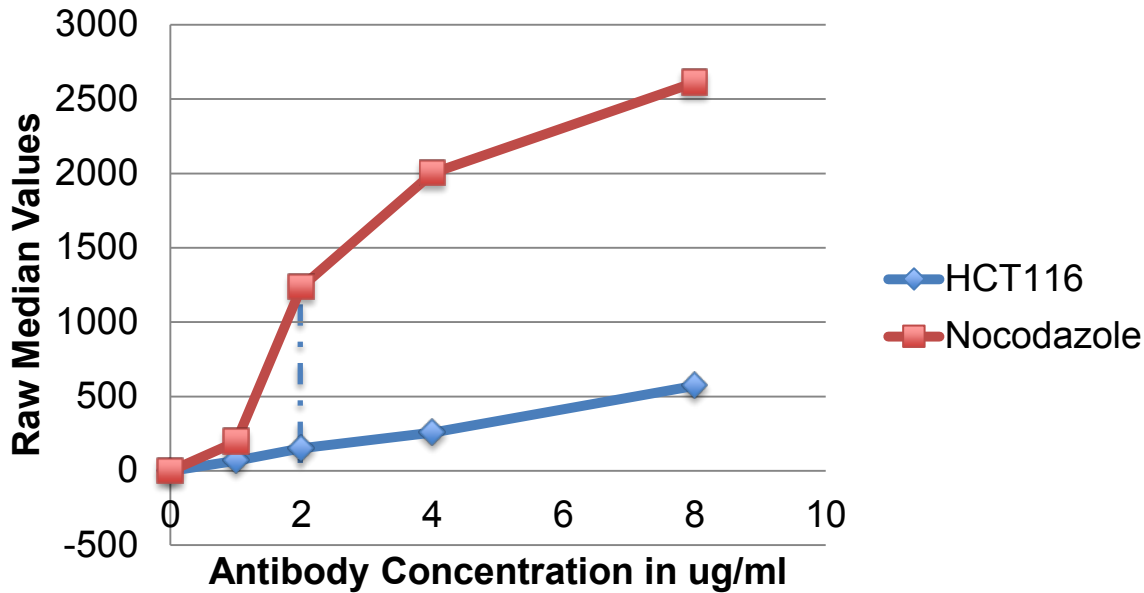
Date Conjugated: 2/12/2013
 Titrated: 10/01/2013
 BD 624084
 Clone: 20A

Selected Conc. : **6ug/ml**

	0ug/ml	0.5ug/ml	1ug/ml	2ug/ml	4ug/ml	8ug/ml
U937	-0.43	-0.2	-0.38	-0.08	0.69	1.63
U937 PMA	-2.0	23.27	9.57	30.69	61.14	104.86



152 (Sm): Ki67

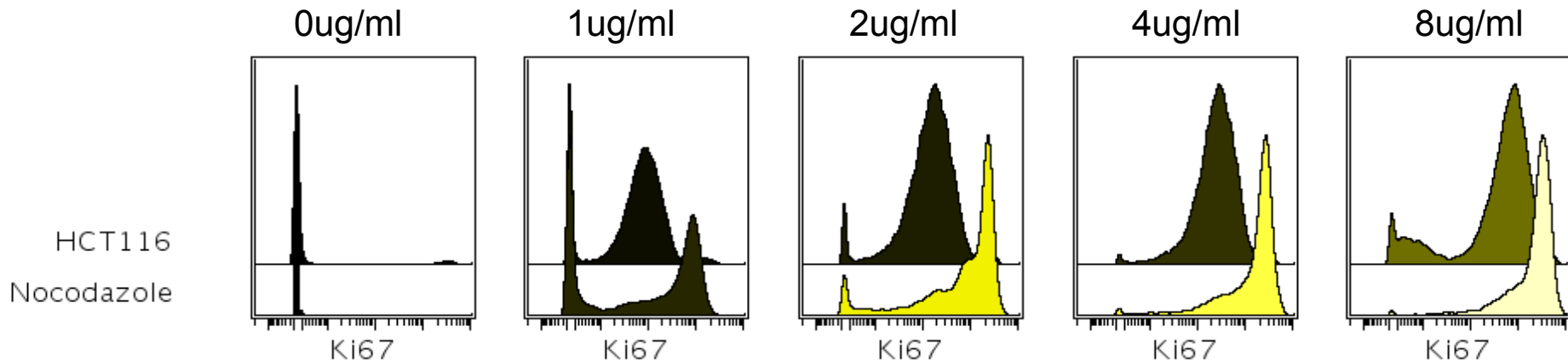


152 (Sm): Ki67 Total

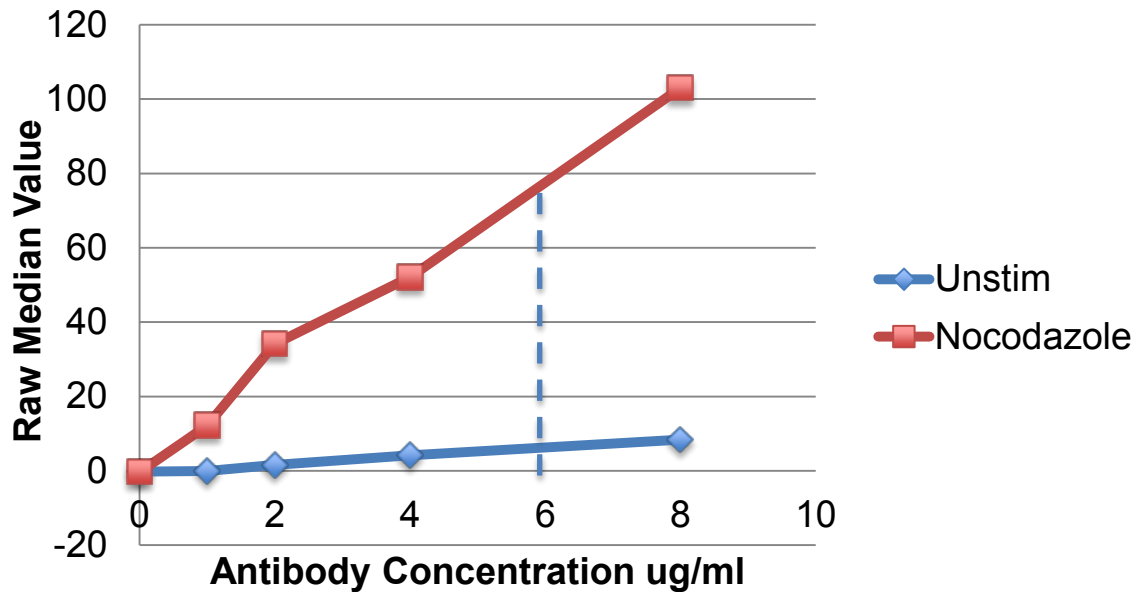
Conjugated: 3/15/2013
 Titration: 3/21/13
 BD 556003
 Clone: B56

Selected Conc. : 2ug/ml

	0ug/ml	1ug/ml	2ug/ml	4ug/ml	8ug/ml
HCT116	-0.37	67.89	151.33	256.66	571.46
Nocodazole	-0.49	194.5	1235.78	2001.93	2611.07



153 (Eu): pCHK2 (pT68)



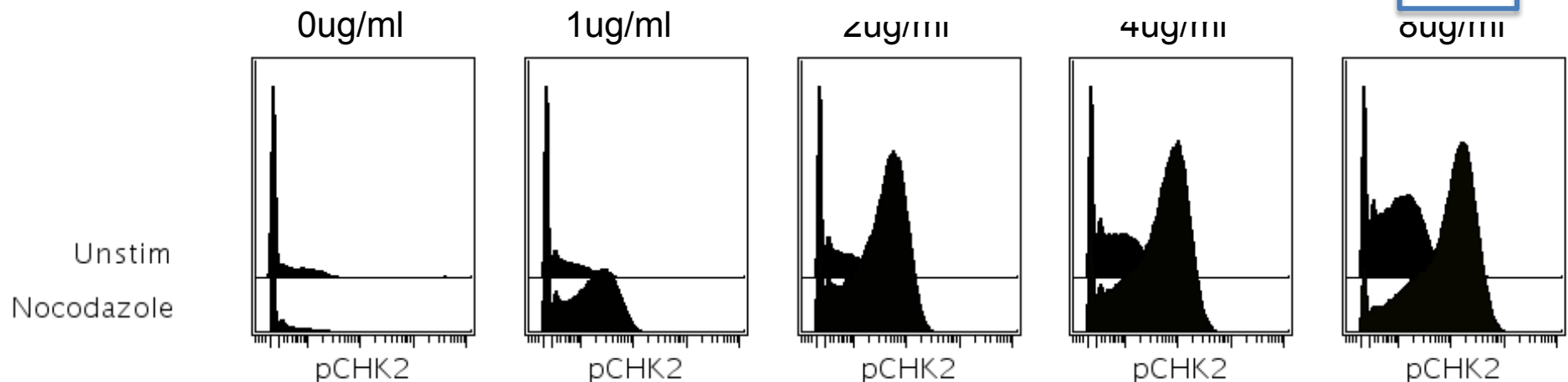
153 (Eu): pCHK2 (pT68)

Conjugated: 9/21/12
 Titration: 10/3/12
 CST 2661
 Clone: C13C1

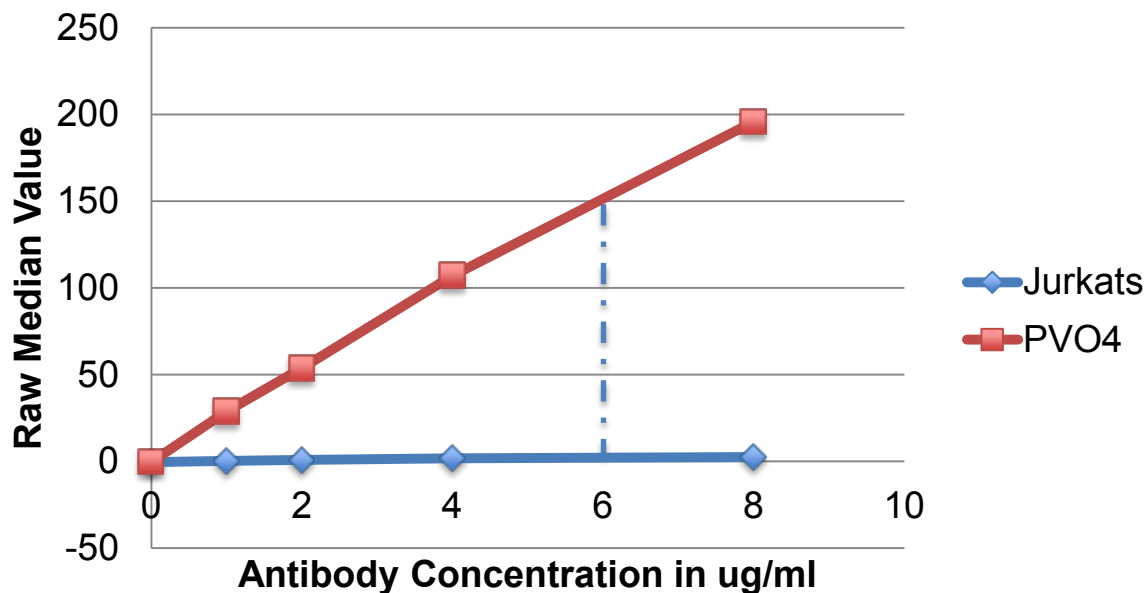
Selected Conc. : **6ug/ml**

	0ug/ml	1ug/ml	2ug/ml	4ug/ml	8ug/ml
Unstim	-0.2	-0.04	1.58	4.17	8.34
Nocodazole	-0.33	12.16	34.08	52.14	103.0

6µg



154 (Sm): STAT3

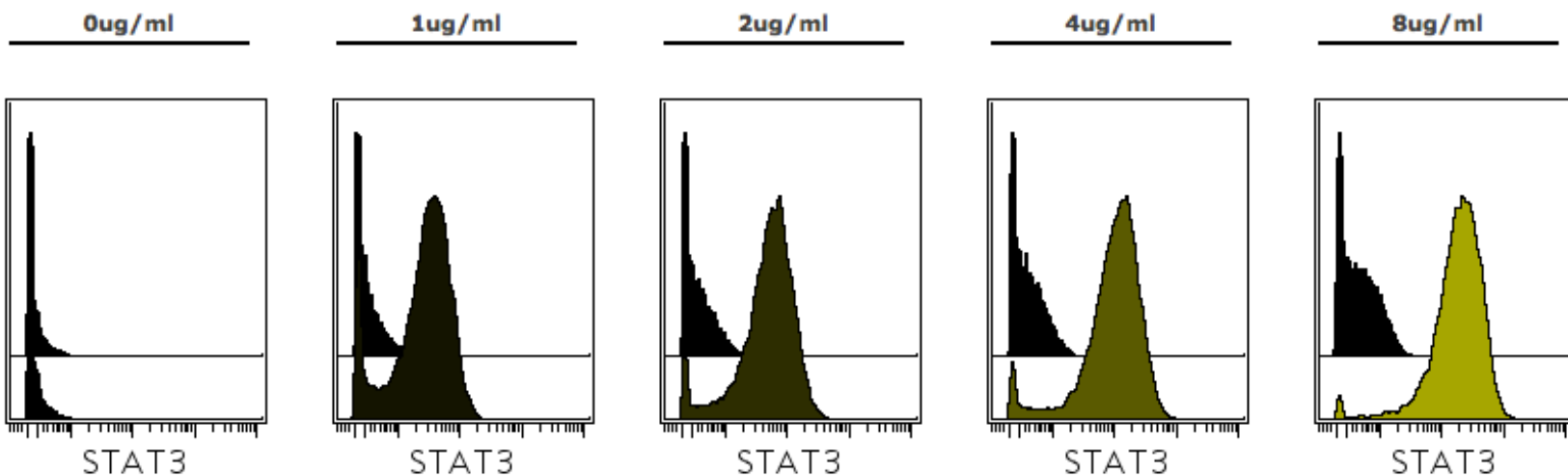


154 (Sm): pSTAT3

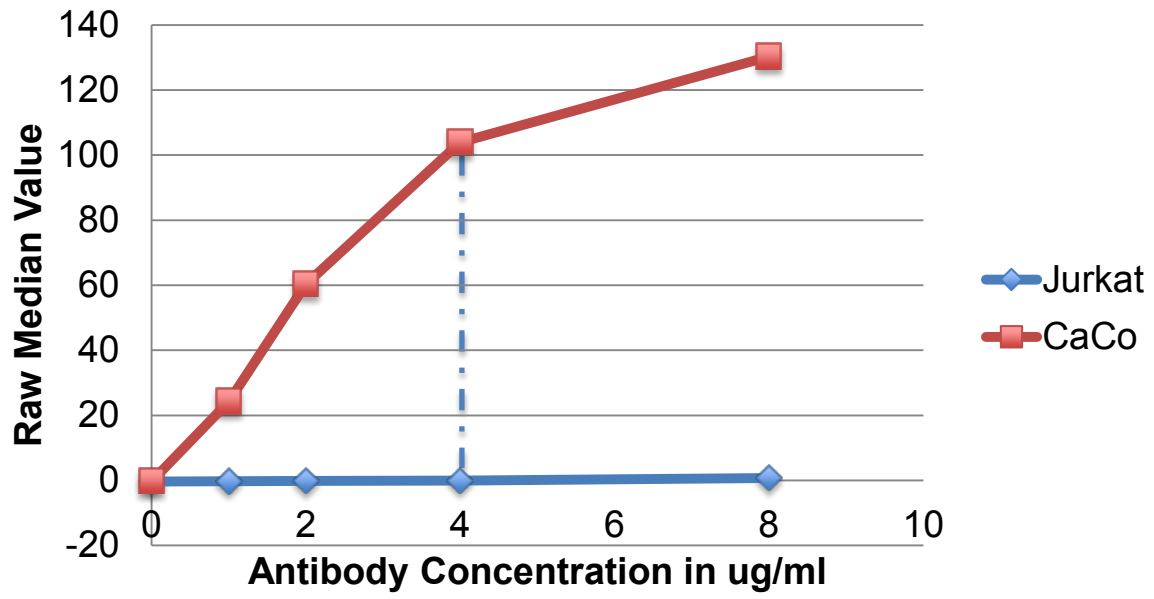
Date Conjugated: 7/16/13
 Titration: 8/16/13
 BD 624084
 Clone: NA

Selected Conc. : **6ug/ml**

	0ug/ml	1ug/ml	2ug/ml	4ug/ml	8ug/ml
Jurkats	-0.35	0.36	0.93	1.69	2.48
PVO4	-0.33	28.87	53.75	107.17	195.9



155 (Gd): CD133

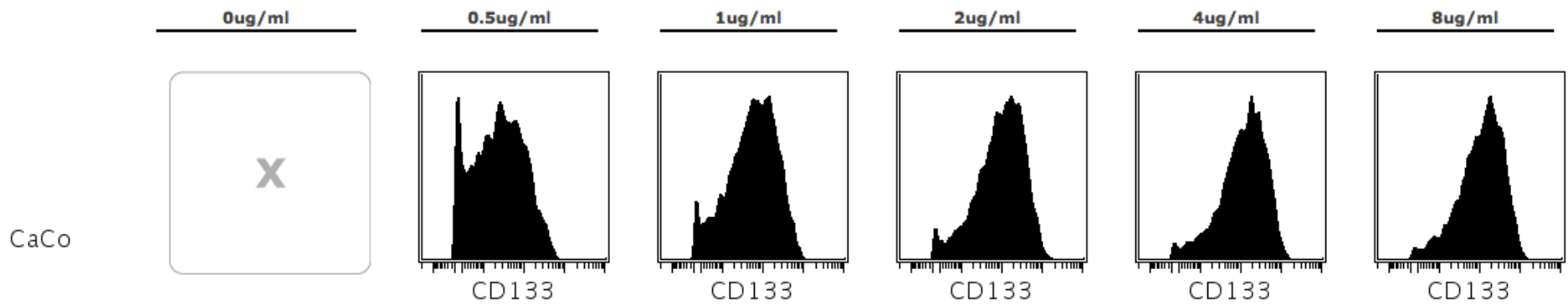


155 (Gd): CD133

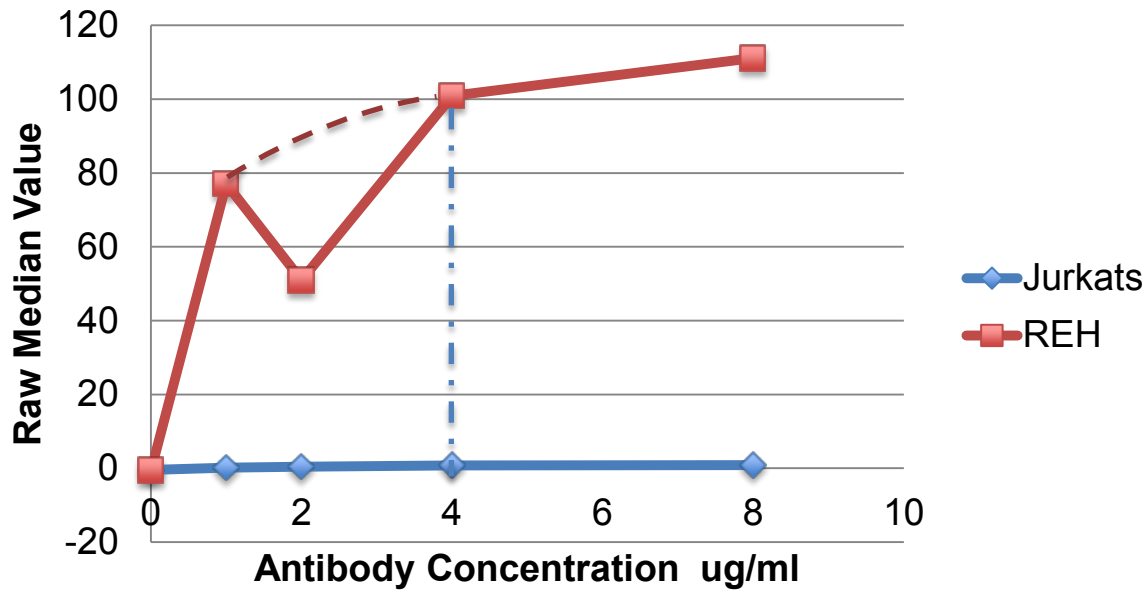
Date Conjugated: 7/22/13
 Titration: 9/10/13
 Miltenyi 130-090-422
 Clone: AC133

Selected Conc. : 4ug/ml

	0ug/ml	0.5ug/ml	1ug/ml	2ug/ml	4ug/ml	8ug/ml
Jurkats	-0.4	-0.29	-0.12	-0.02	0.69	1.58
CaCo	X	24.21	60.32	103.89	130.29	124.91



156(Gd) : CD10

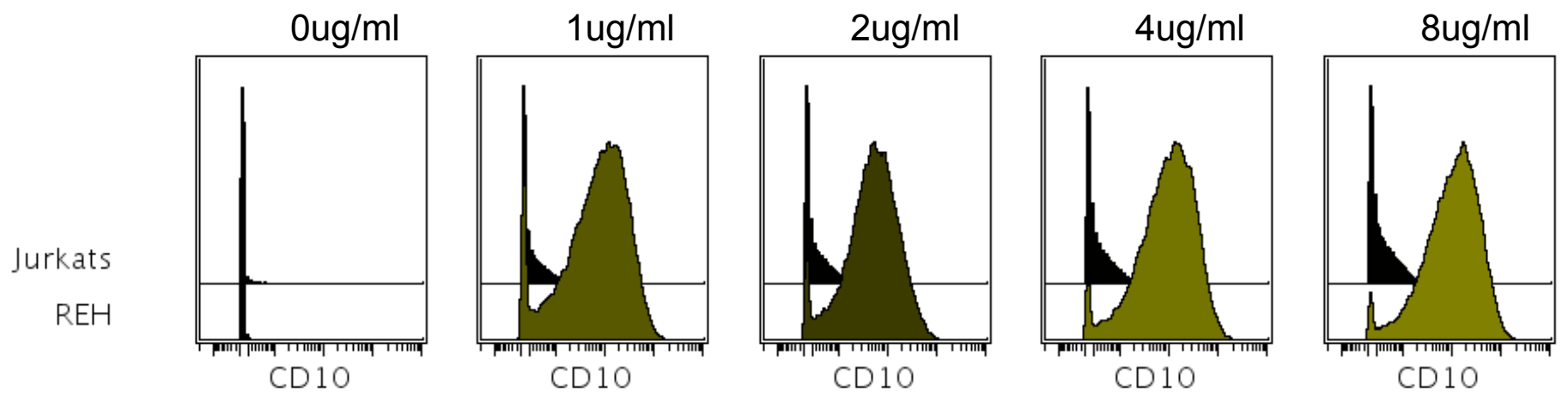


156 (Gd): CD10

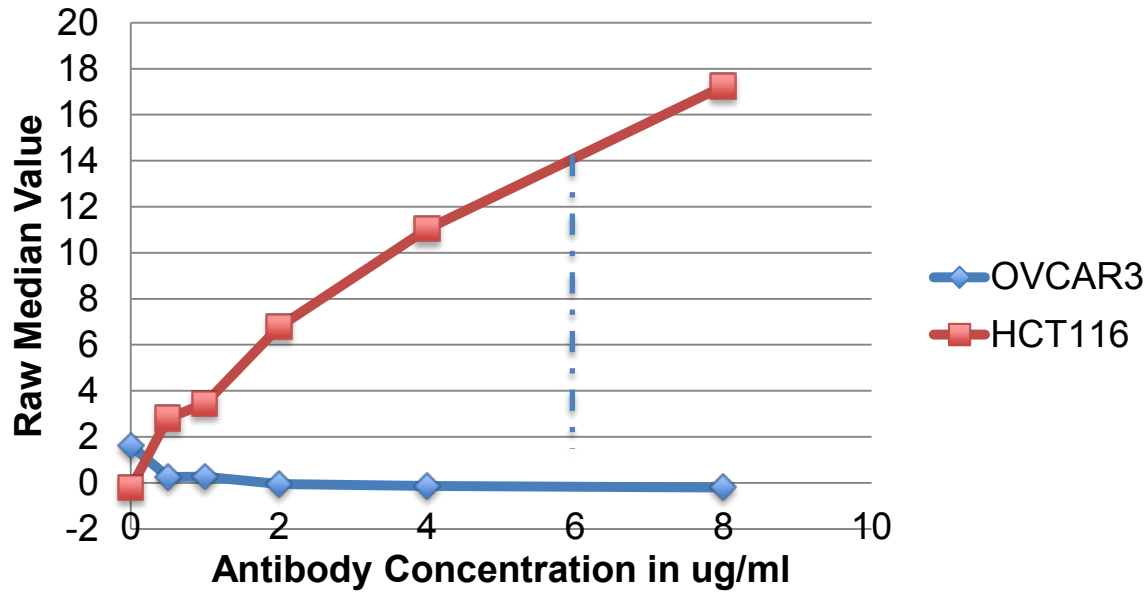
Date Conjugated: 2/13/2013
 Titration 2/26/13
 Biolegend 312202
 Clone: HI10a

Selected Conc. : **4ug/ml**

	0ug/ml	1ug/ml	2ug/ml	4ug/ml	8ug/ml
Jurkats	-0.4	0.21	0.39	0.74	0.89
REH	-0.5	77.04	51.0	100.93	111.15



157 (Gd): SNAIL



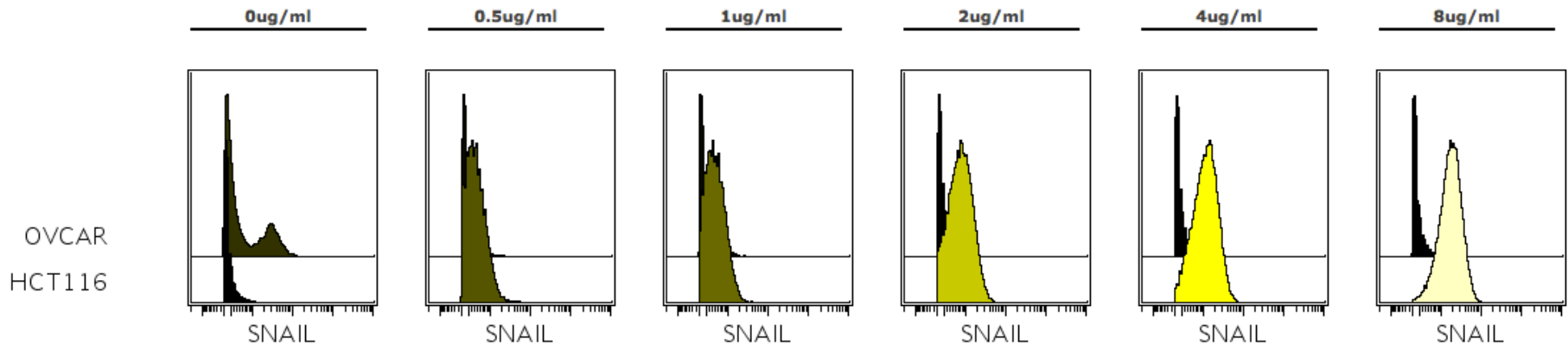
157(Gd): SNAIL

Date Conjugated: 8/28/13
 Titration: 9/10/13
 eBiosciences 14-9859-82
 Clone: 20C8

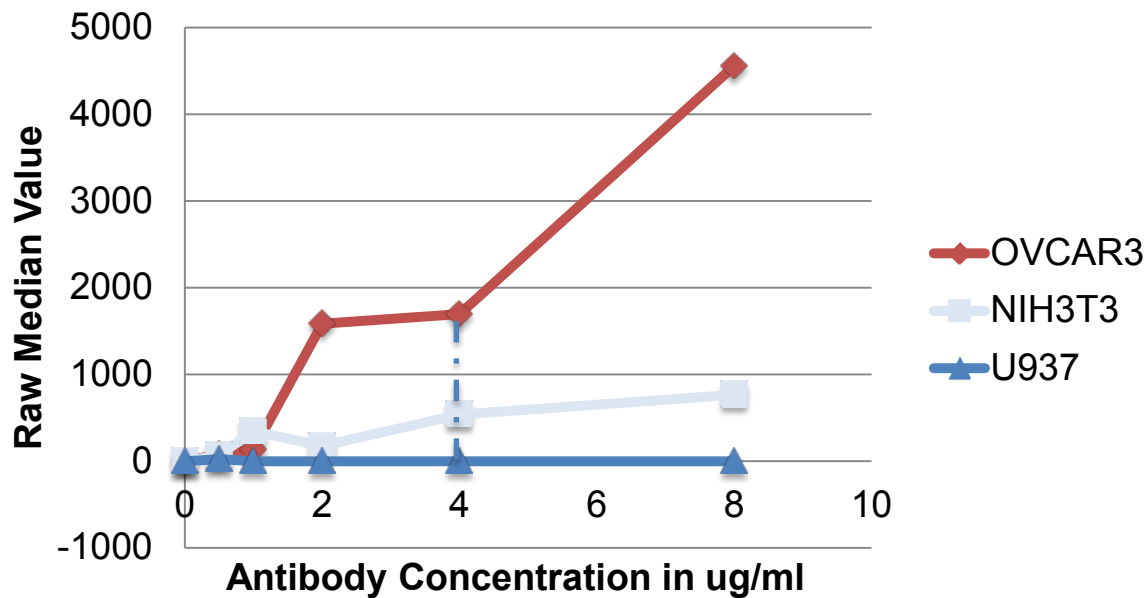
Selected Conc. : **6ug/ml**

	0ug/ml	0.5ug/ml	1ug/ml	2ug/ml	4ug/ml	8ug/ml
OVCAR	1.62	0.25	0.27	-0.05	-0.13	-0.2
HCT116	-0.22	2.82	3.44	6.78	11.04	17.24

6µg



158 (Gd): E-Cadherin



158 (Nd): E-Cadherin

Date Conjugated: 7/16/13

Titration: 9/24/13

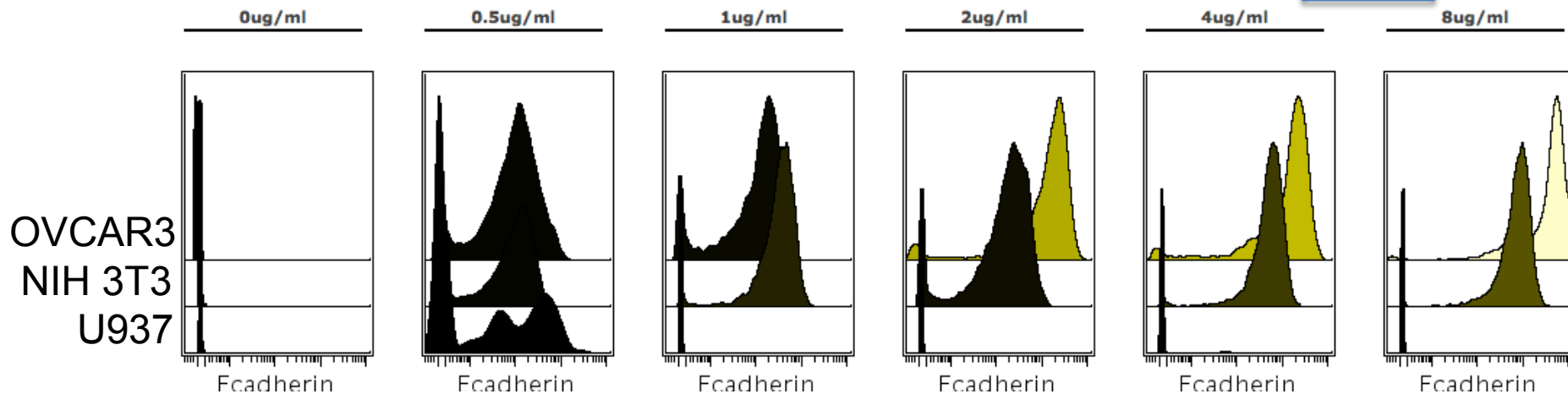
CST 3195BF

Clone: 2.40e11

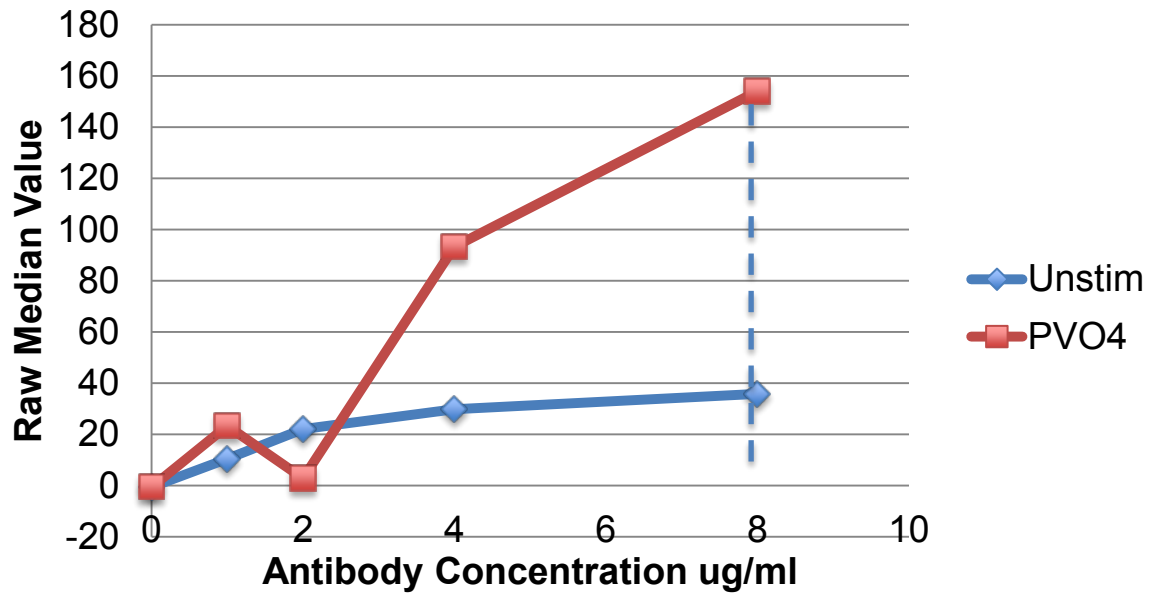
Selected Conc. : 4ug/ml

OVCAR3
NIH 3T3
U937

	0ug/ml	0.5ug/ml	1ug/ml	2ug/ml	4ug/ml	8ug/ml
OVCAR3	-1.07	84.38	130.73	1584.63	1696.38	4554.96
NIH 3T3	-0.51	70.8	344.73	177.37	535.94	767.28
U937	-0.4	25.11	-0.49	-0.49	-0.44	-0.49



159 (Tb): pAKT (pS473)



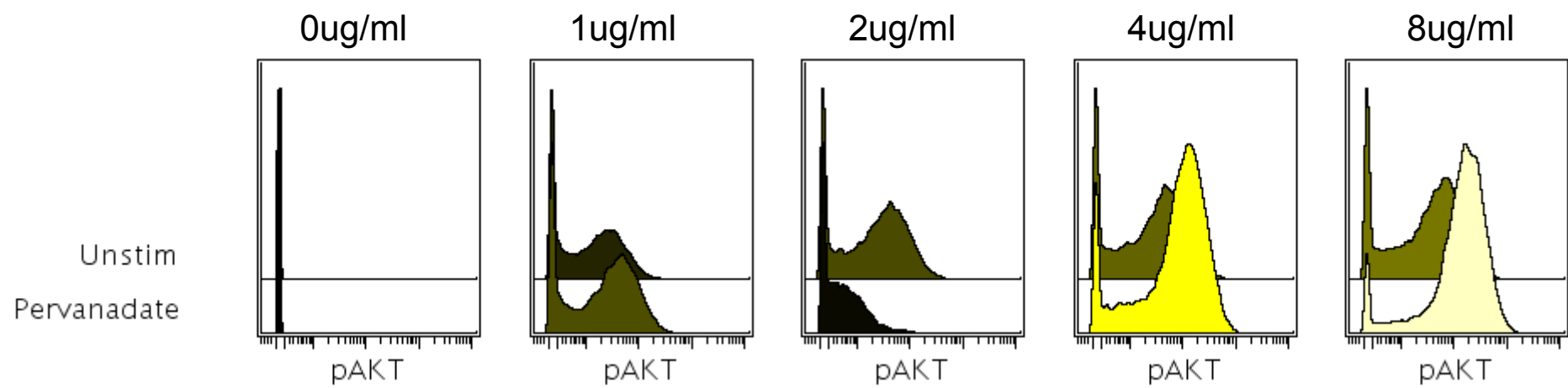
159 (Tb): pAKT (pS473)

Conjugated: 9/21/12
 Titration: 10/18/12
 CST 4060
 Clone: D9E

Cell Line: Jurkat Cells
 Stim: 125uM PV04 for 10min

Selected Conc. : **8ug/ml**

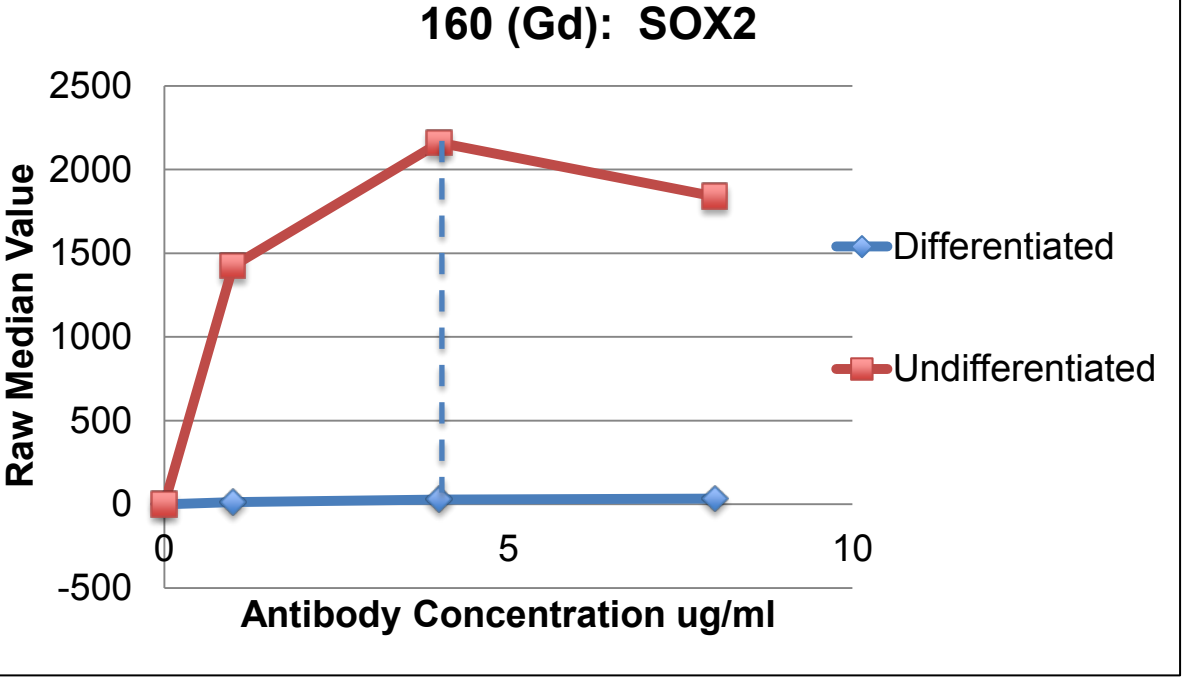
	0ug/ml	1ug/ml	2ug/ml	4ug/ml	8ug/ml
Unstim	-0.49	10.49	22.07	29.8	35.8
Pervanadate	-0.49	23.35	2.81	93.27	154.08



160 (Gd): SOX2

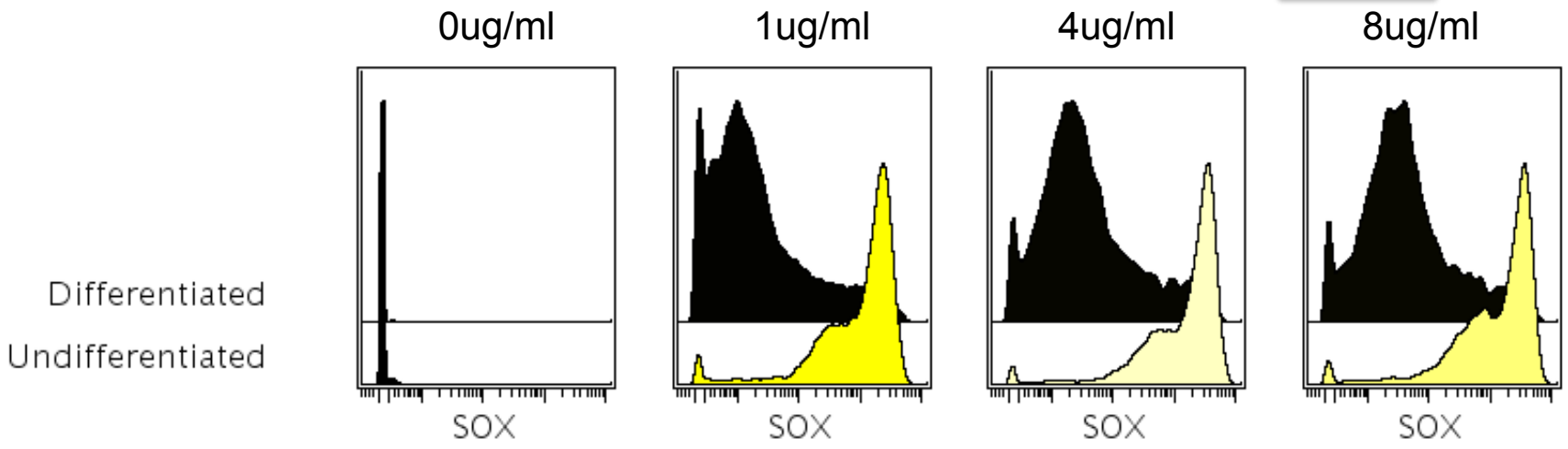
Lab Stock
 Titration Date: 8/16/2012
 BD 561469
 Clone: 030-678

Cells: MESC treated with LIF

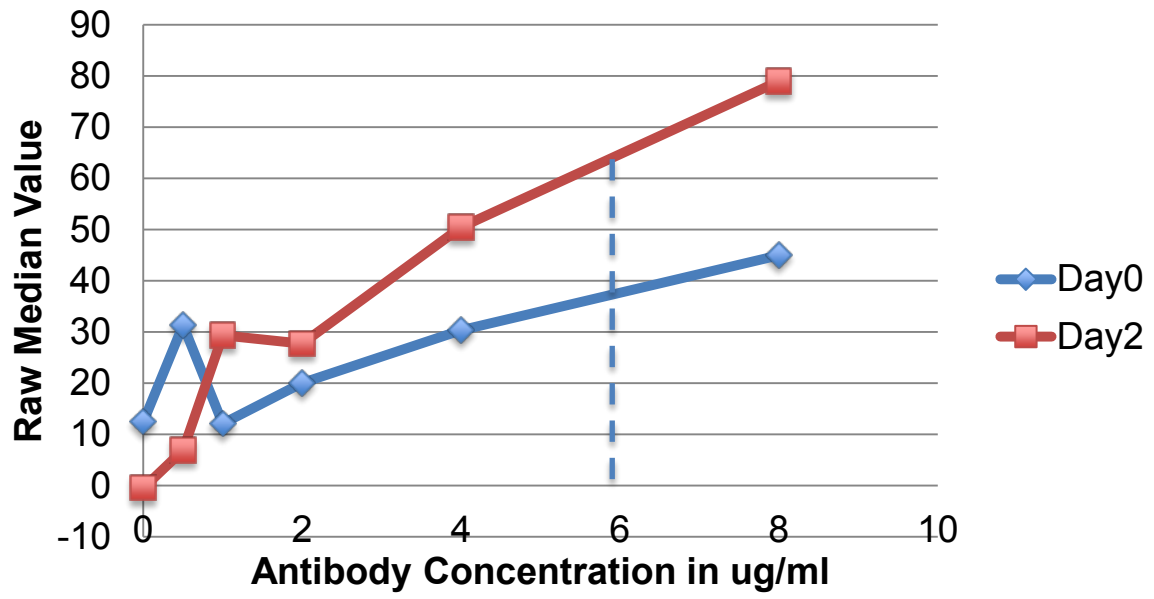


Selected Conc. : 4ug/ml

	0ug/ml	1ug/ml	4ug/ml	8ug/ml
Differentiated	-0.48	13.52	27.28	34.29
Undifferentiated	-0.44	1424.12	2159.02	1839.33



161 (Dy): cMYC



161 (Dy): cMYC

Date Conjugated: 8/28/13

Titration: 9/10/13

CST 5605BF

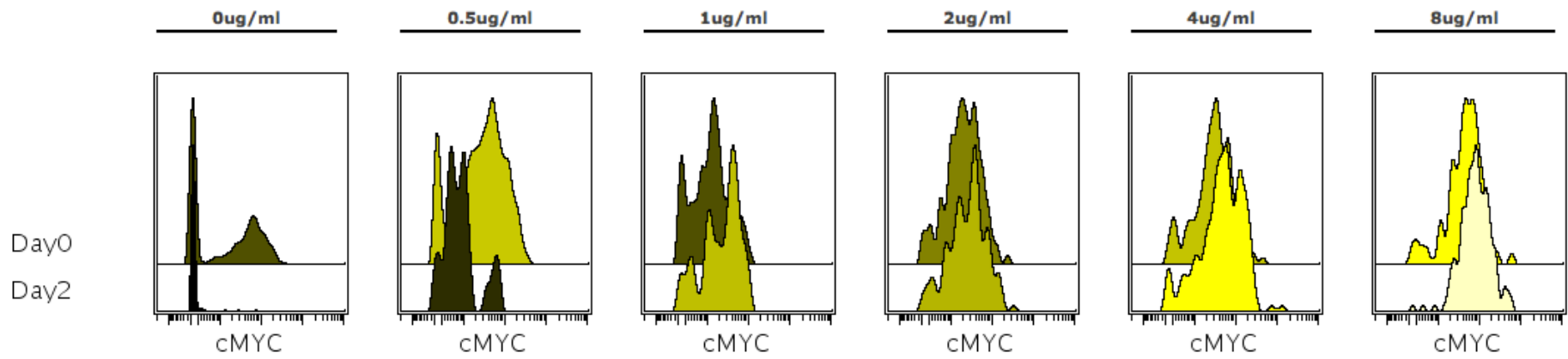
Clone: D84C12

Cells: MES C treated with LIF

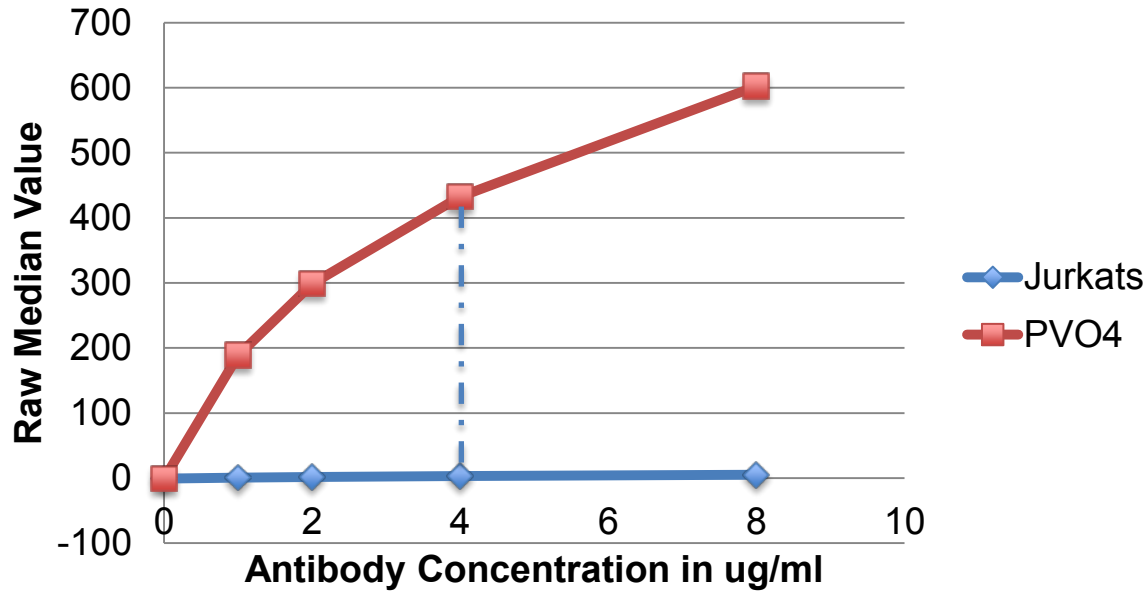
6 μ g

Selected Conc. : 6ug/ml

	0ug/ml	0.5ug/ml	1ug/ml	2ug/ml	4ug/ml	8ug/ml
Day0	12.48	31.38	12.12	20.05	30.35	44.96
Day2	-0.47	6.94	29.35	27.7	50.47	78.96



162 (Dy): STAT5

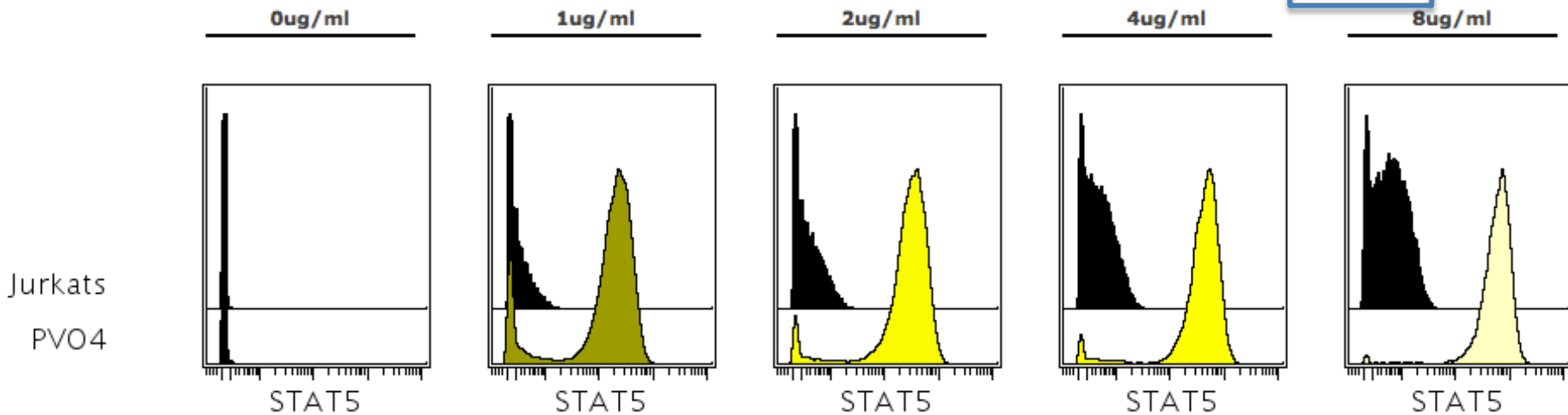


162 (Yb): pSTAT5

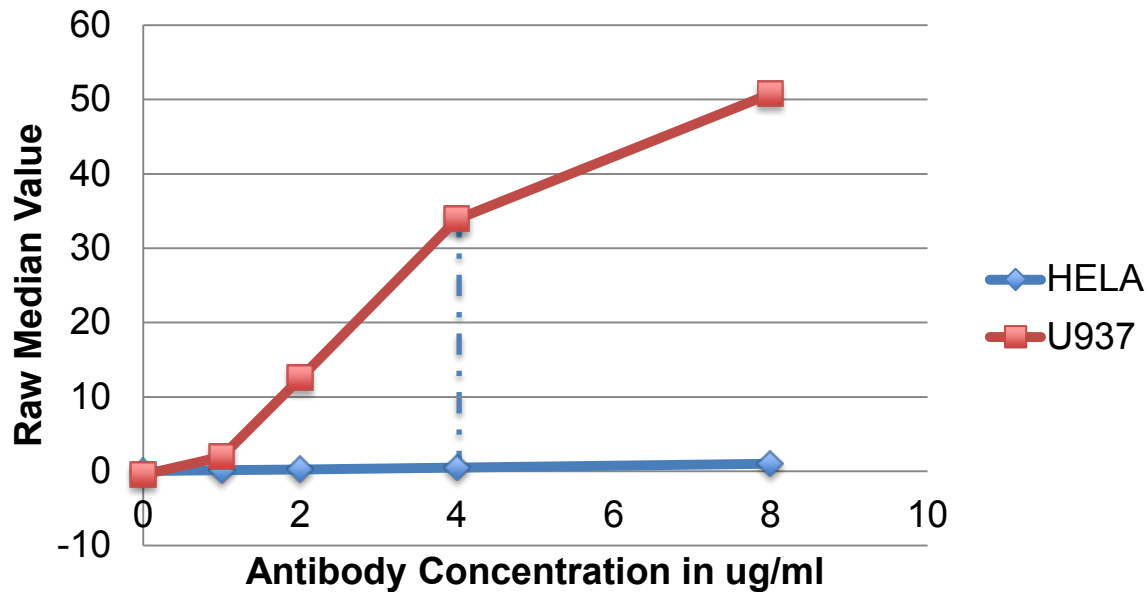
Date Conjugated: 7/16/13
 Titration: 8/16/13
 BD 624084
 Clone: NA

Selected Conc. : 4ug/ml

	0ug/ml	1ug/ml	2ug/ml	4ug/ml	8ug/ml
Jurkats	-0.58	0.54	1.58	3.06	4.87
PVO4	-0.59	188.56	299.01	432.66	602.37



163 (Dy): Endoglin



163 (Dy): Endoglin

Conjugated: 8/28/13

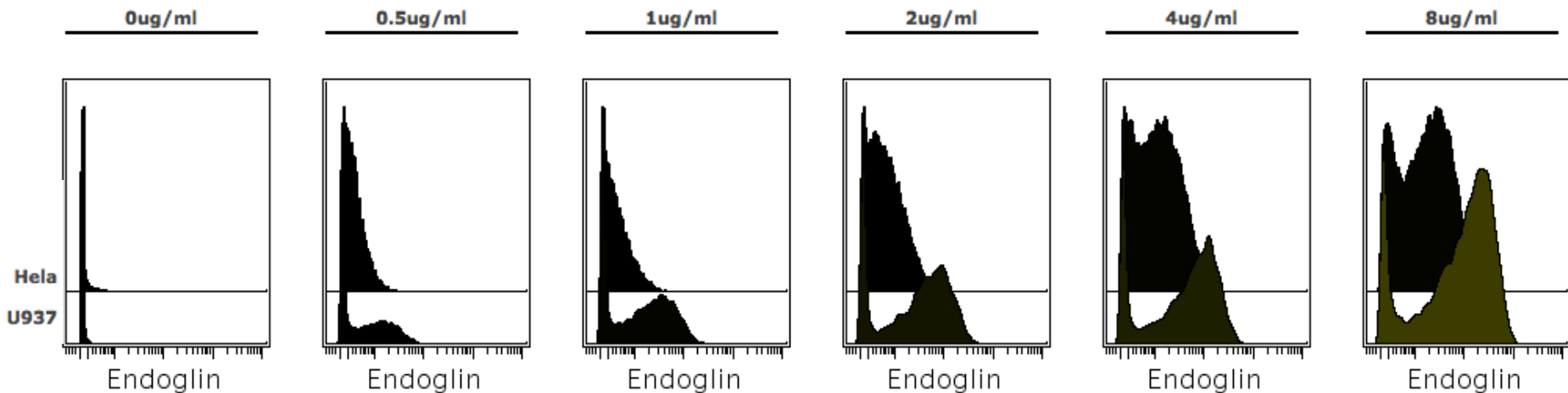
Titration: 9/3/13

Biolegend 323202

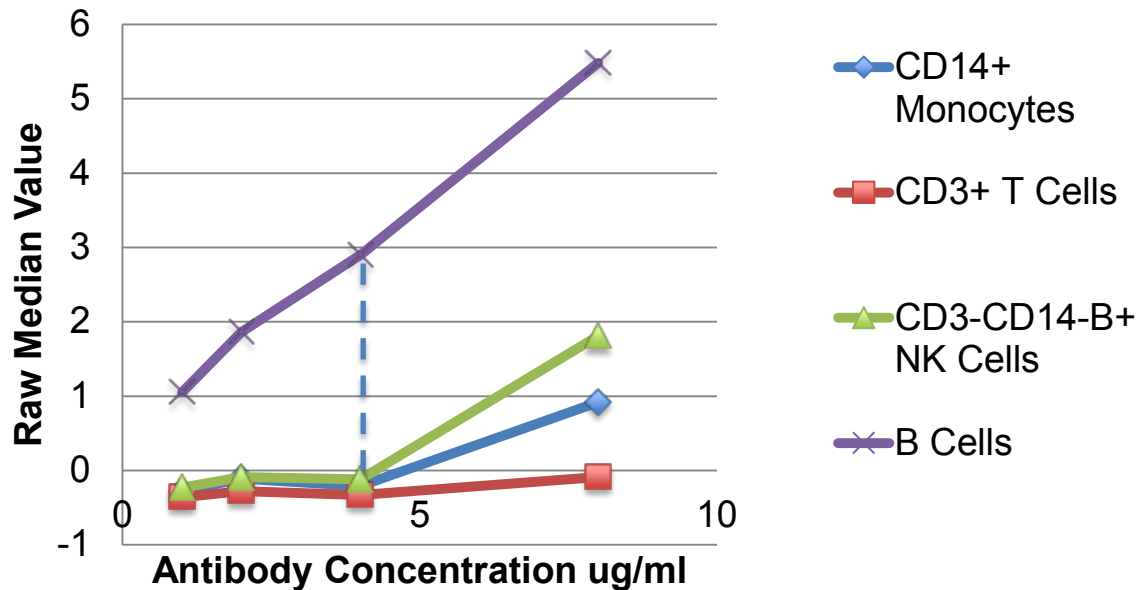
Clone: 43A3

Selected Conc. : 4ug/ml

	0ug/ml	0.5ug/ml	1ug/ml	2ug/ml	4ug/ml	8ug/ml
Hela	-0.41	1.64	1.94	4.78	9.86	16.05
U937	-0.46	1.96	12.48	33.87	50.76	105.78



164 (Dy): Titration of CD24 in PBMCs

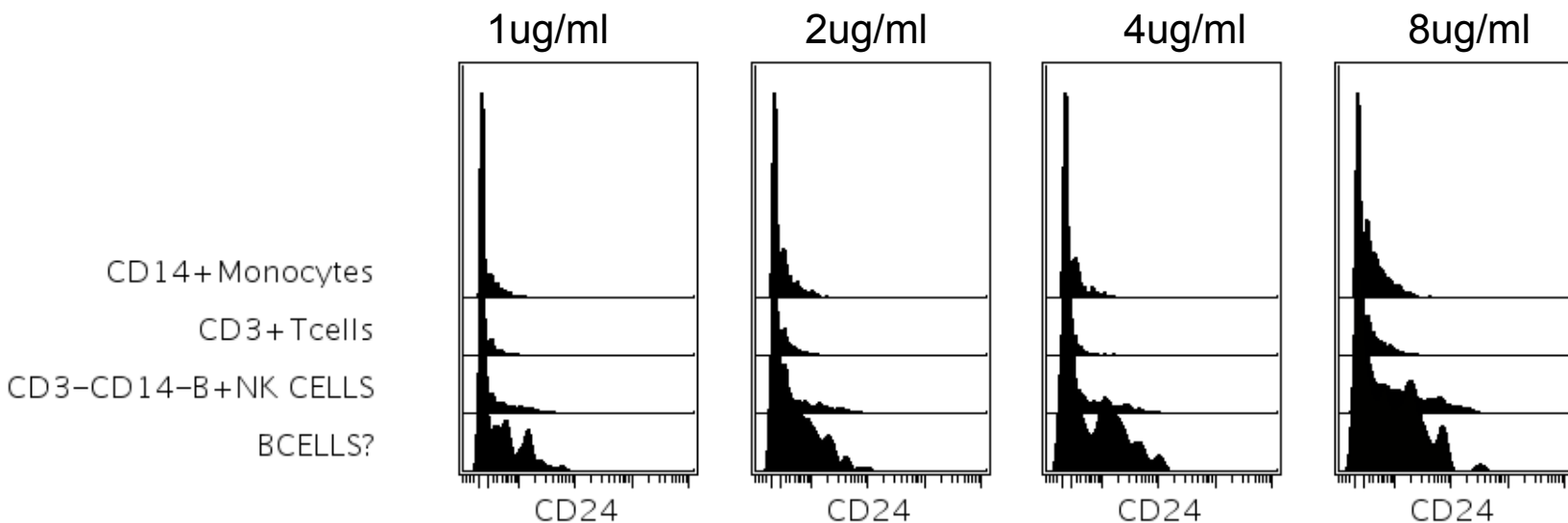


164 (Dy): CD24

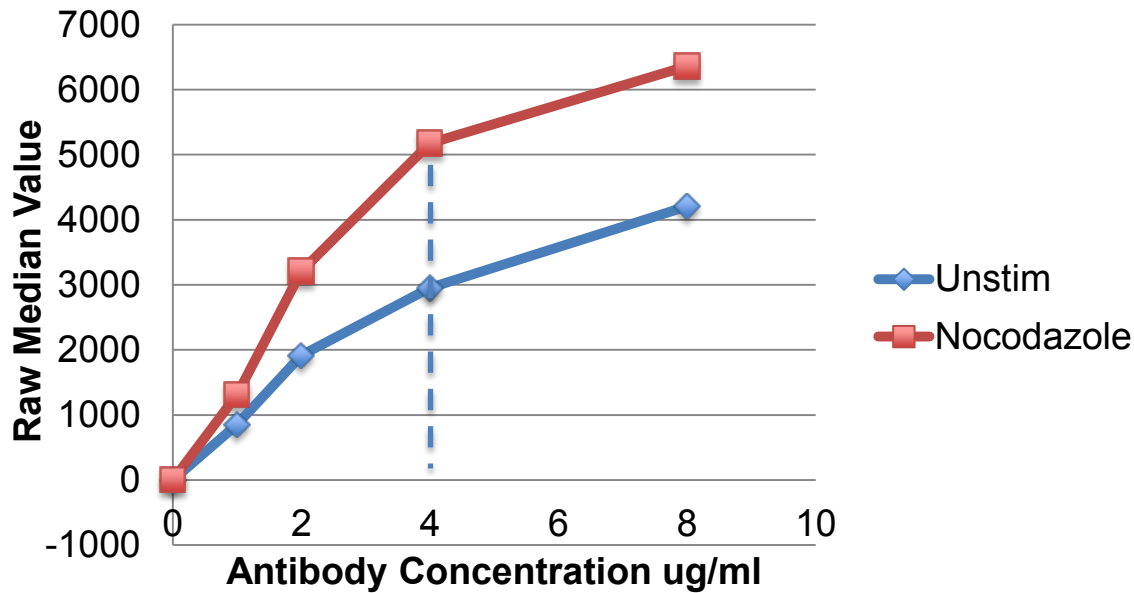
Lab Stock
 Titration Set 1
 8/21/2012
 Biolegend 311102
 Clone: ML5

	1ug/ml	2ug/ml	4ug/ml	8ug/ml
CD14+Monocytes	-0.28	-0.11	-0.21	0.92
CD3+Tcells	-0.36	-0.28	-0.33	-0.09
CD3-CD14-B+NK CELLS	-0.23	-0.09	-0.12	1.81
BCELLS?	1.05	1.86	2.9	5.48

Selected Conc. : **4ug/ml**



165 (Ho): pRb (pS807/811)



165 (Ho): pRb (pS807/811)

Conjugated: 9/21/12

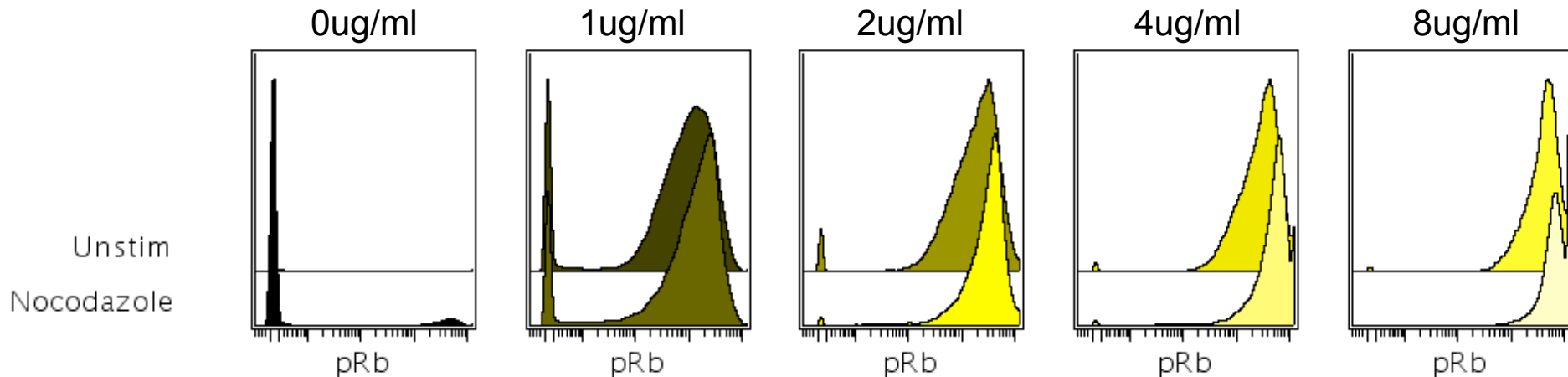
Titration: 10/3/12

BD 558389

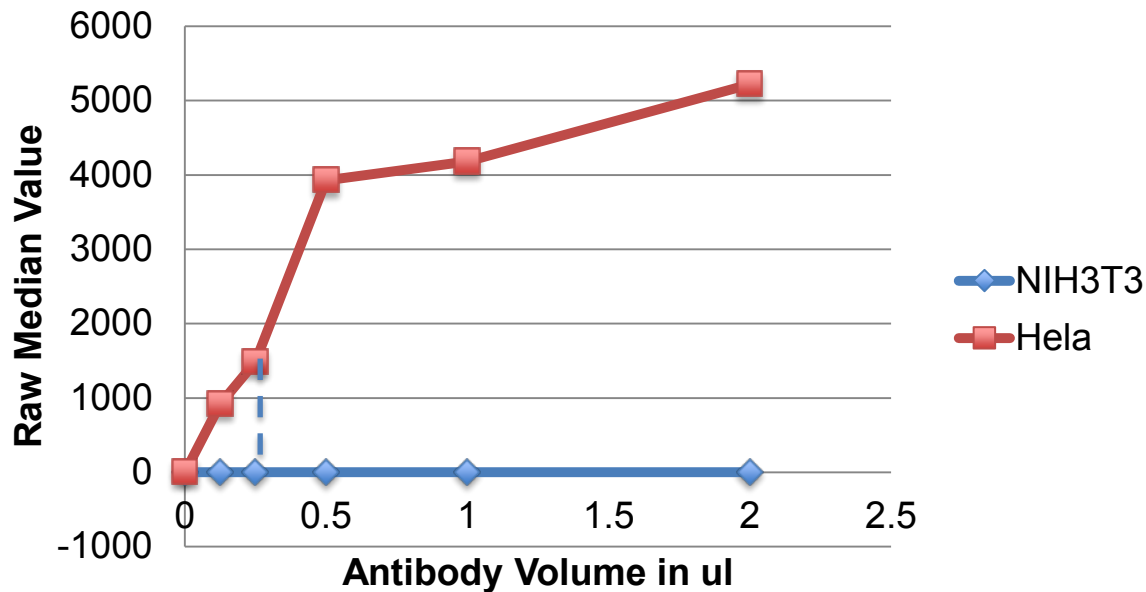
Clone: J112-906

Selected Conc. : 4ug/ml

	0ug/ml	1ug/ml	2ug/ml	4ug/ml	8ug/ml
Unstim	-0.48	852.86	1915.69	2952.27	4209.32
Nocodazole	-0.39	1310.4	3209.37	5175.0	6361.9



166 (Er): CD44

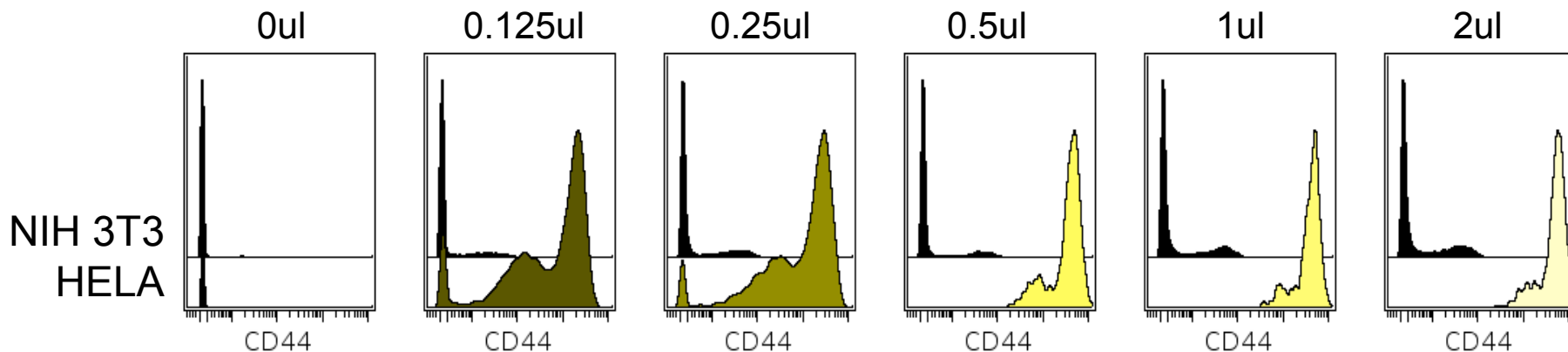


166 (Er): CD44

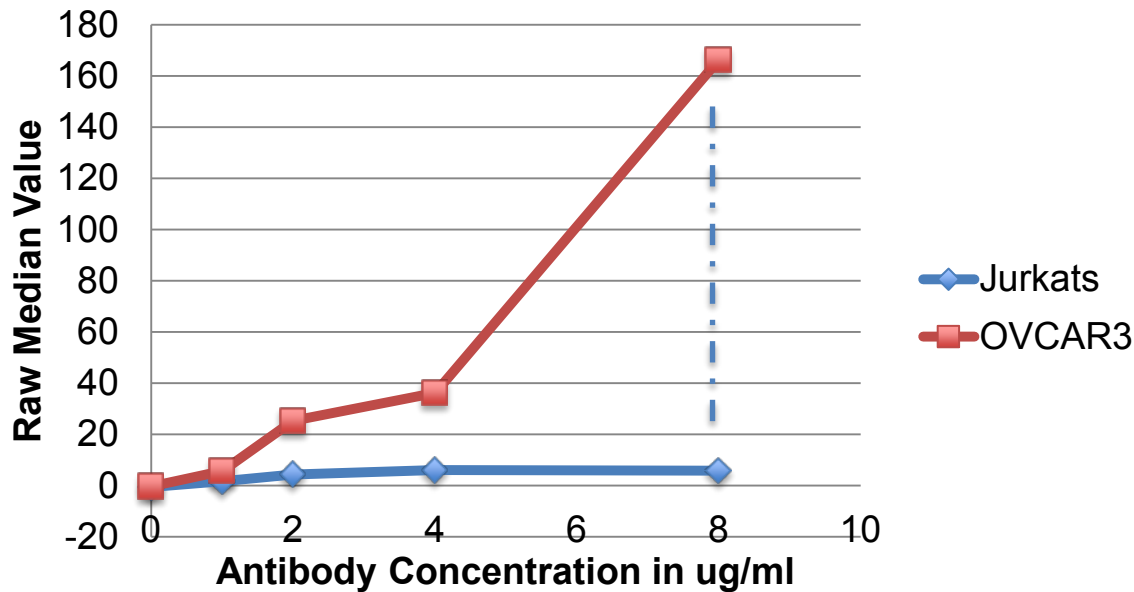
Date Conjugated: DVS
 Titration: 9/24/13
 DVS 3166001B
 Clone: BJ18

Selected Conc. : **0.25ul**

	0ul	0.125ul	0.25ul	0.5ul	1ul	2ul
NIH 3T3	-0.48	-0.44	-0.16	-0.27	-0.13	-0.03
HELA	-0.38	917.72	1486.94	3925.72	4180.42	5217.41



167 (Er): PAX8

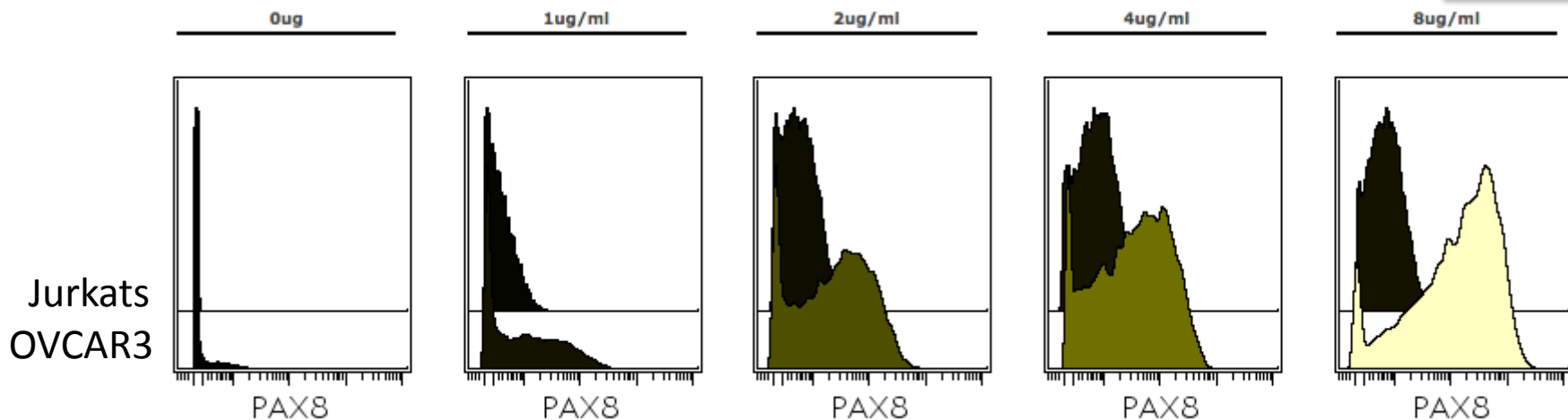


167 (Er): PAX8

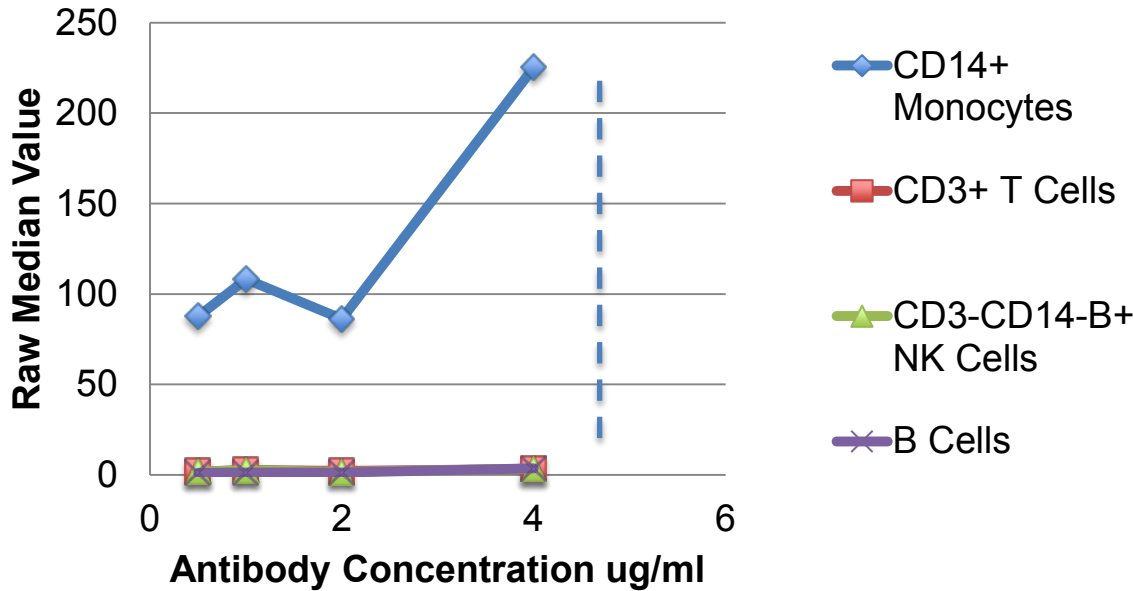
Conjugated: 6/20/2013
 Titration: 6/21/13
 ProteinTech 10336-1-AP
 Clone: Polyclonal

Selected Conc. : **8ug/ml**

	0ug	1ug/ml	2ug/ml	4ug/ml	8ug/ml
Jurkats	-0.54	1.69	4.3	6.11	5.83
OVCAR3	-0.3	5.75	25.31	36.21	166.26



168 (Er): Titration of CD13 in PBMCs



168 (Er): CD13

Conjugated: 9/21/12

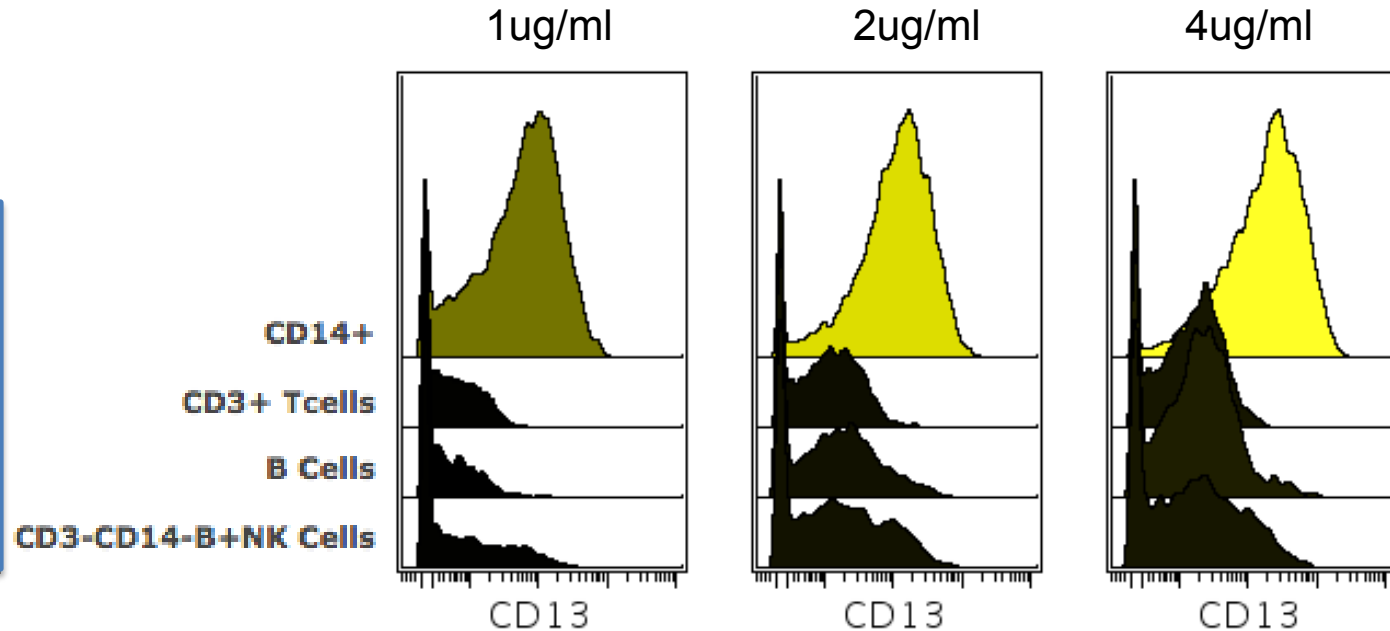
Titration: 10/3/12

BD 624084

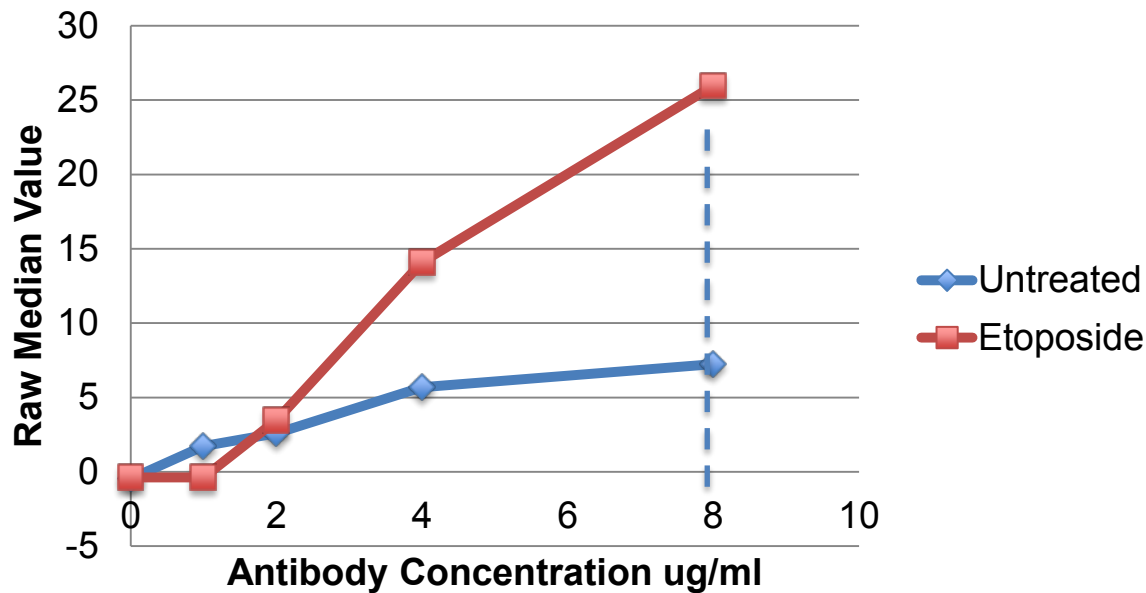
Clone: L138

Selected Conc. : **4ug/ml**

1ug/ml	2ug/ml	4ug/ml
62.61	117.11	198.43
2.79	8.67	13.11
1.41	10.44	17.29
2.84	11.24	13.28



169 (Tm): pCHK1 (pS345)

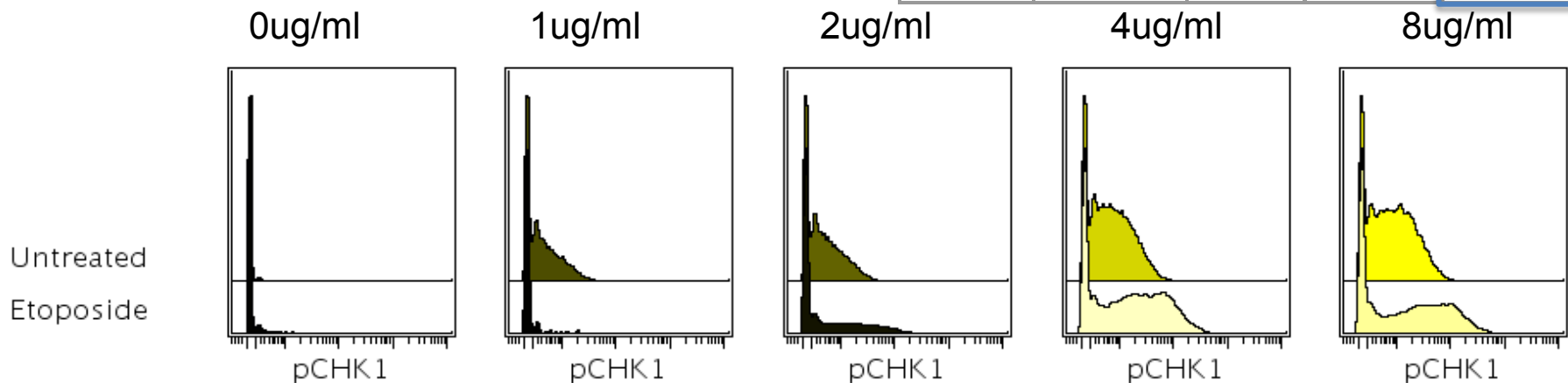


169 (Tm): pCHK1 (pS345)

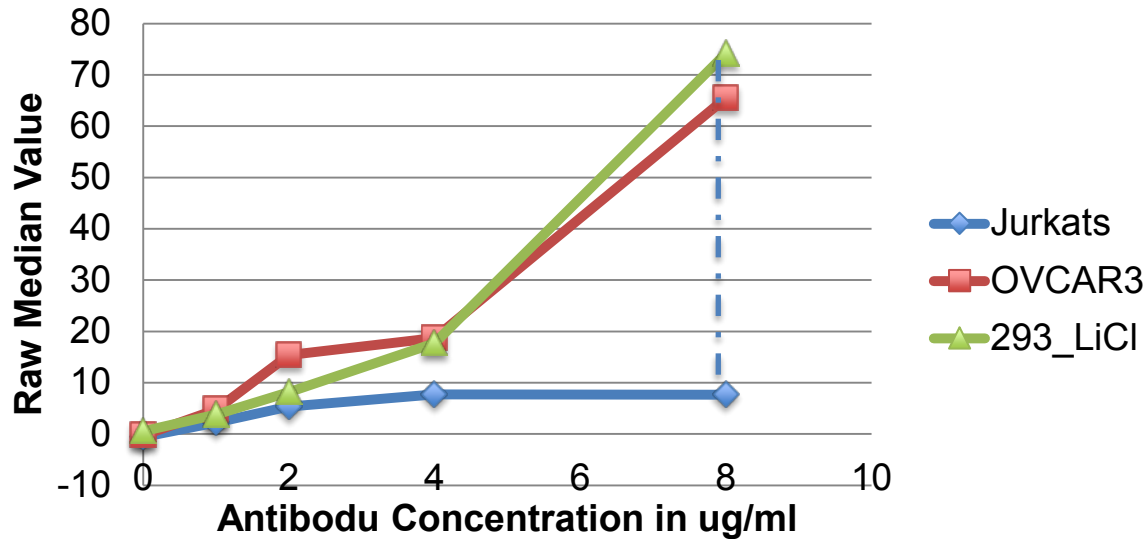
Lab Stock
 Titration Set 1
 8/16/2012
 CST 2535
 Clone: 40H19

Selected Conc. : **8ug/ml**

	0ug/ml	1ug/ml	2ug/ml	4ug/ml	8ug/ml
Untreated	-0.47	1.58	2.16	5.11	6.38
Etoposide	-0.39	-0.4	0.05	12.95	11.79



170 (Er): Active Non-Phosphorylated B-Catenin



170 (Er): Non Phosphorylated Beta Catenin

Conjugated: 6/20/2013

Titration: 6/21/13

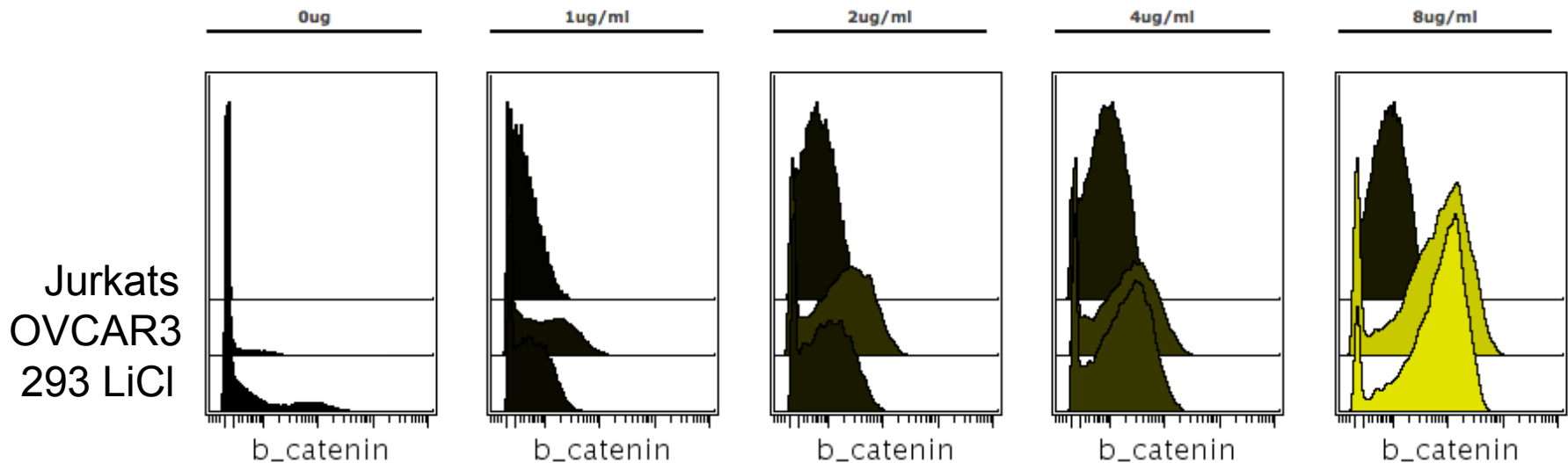
CST 8480

Clone: D10A8

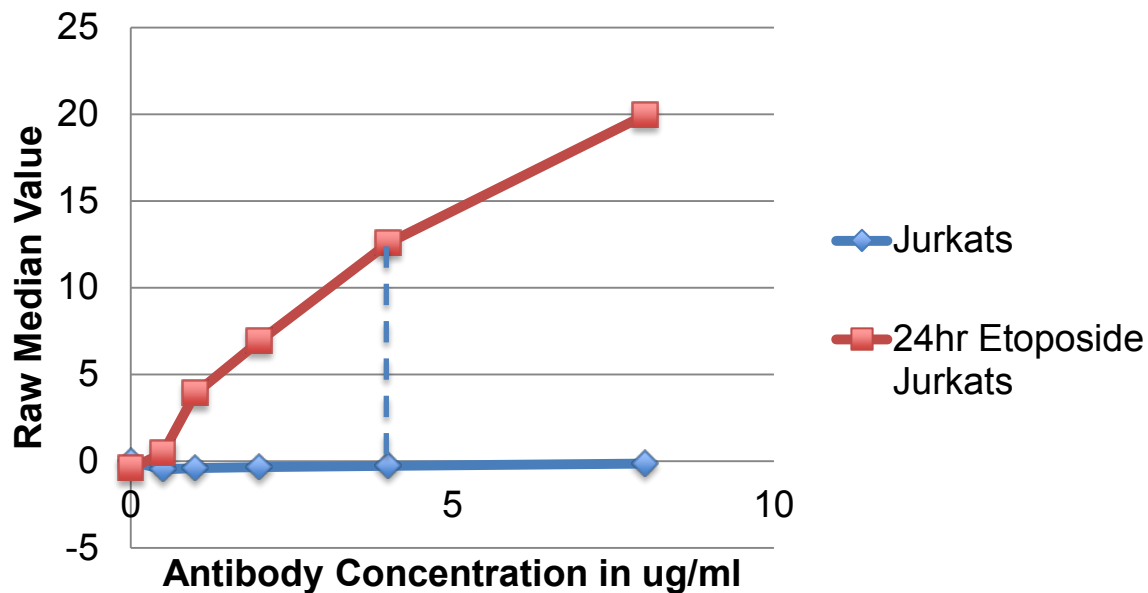
Selected Conc. : 8ug/ml

Jurkats
OVCAR3
293 LiCI

	0ug	1ug/ml	2ug/ml	4ug/ml	8ug/ml
Jurkats	-0.54	2.25	5.36	7.7	7.68
OVCAR3	-0.28	4.72	15.43	18.69	65.51
293 LiCI	0.54	3.79	8.17	17.72	74.18



171 (Yb): cPARP



171 (Yb): cPARP

Date Conjugated: 8/21/13

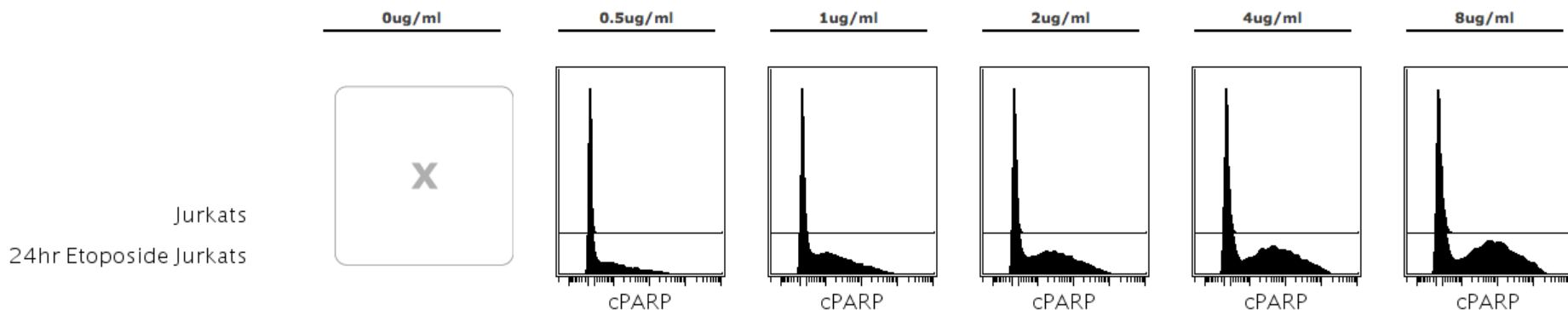
Titration: 9/10/13

BD 624084

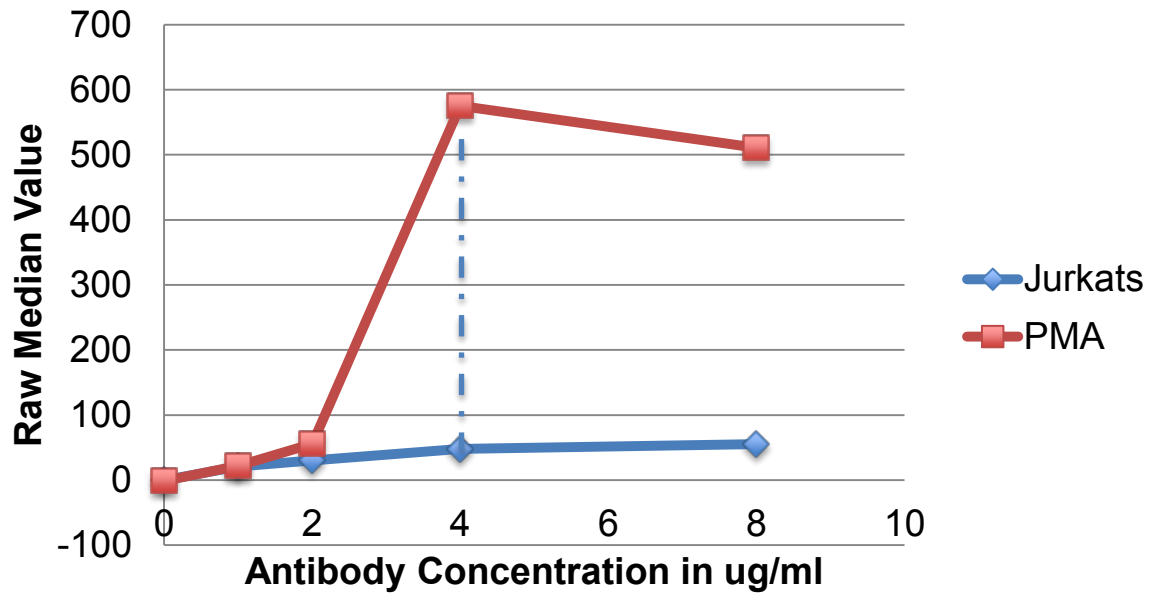
Clone: NA

Selected Conc. : **4ug/ml**

	0ug/ml	0.5ug/ml	1ug/ml	2ug/ml	4ug/ml	8ug/ml
Jurkats	X	-0.46	-0.39	-0.33	-0.26	-0.14
24hr Etoposide Jurkats	-0.42	0.47	3.91	6.93	12.57	19.95



172 (Yb): pS6 (pS235/pS236)

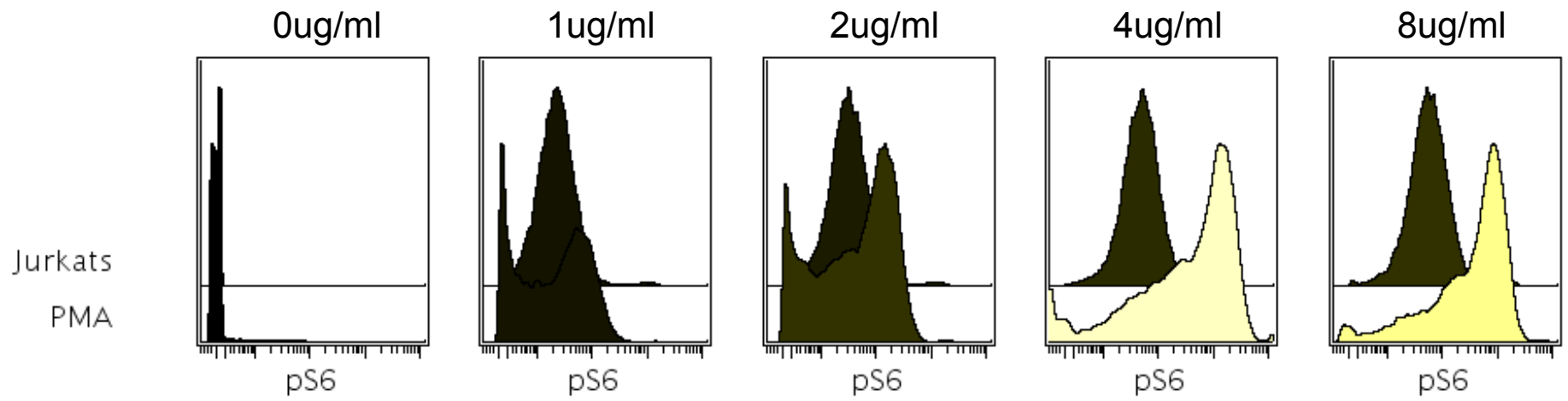


172 (Yb): pS6 (pS235/pS236)

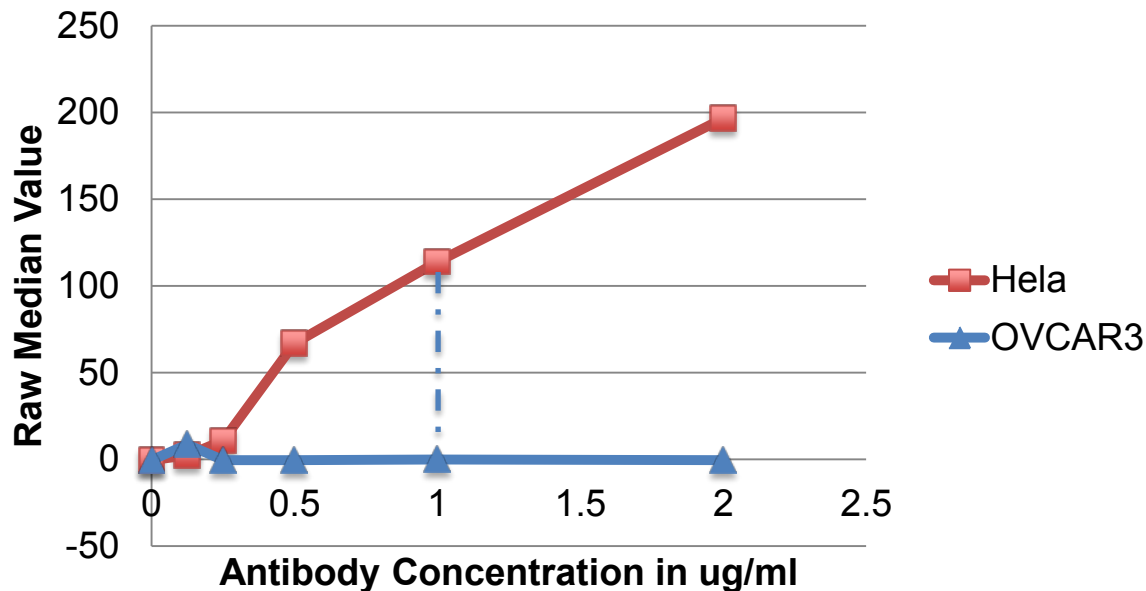
Conjugated: 4/10/2013
 Titration: 4/15/13
 BD 624084
 Clone: N7-548

Selected Conc. : **4ug/ml**

	0ug/ml	1ug/ml	2ug/ml	4ug/ml	8ug/ml
Jurkats	-0.37	21.06	30.42	47.9	55.17
PMA	-1.19	21.98	55.86	575.43	511.01



173 (Yb): Mesothelin

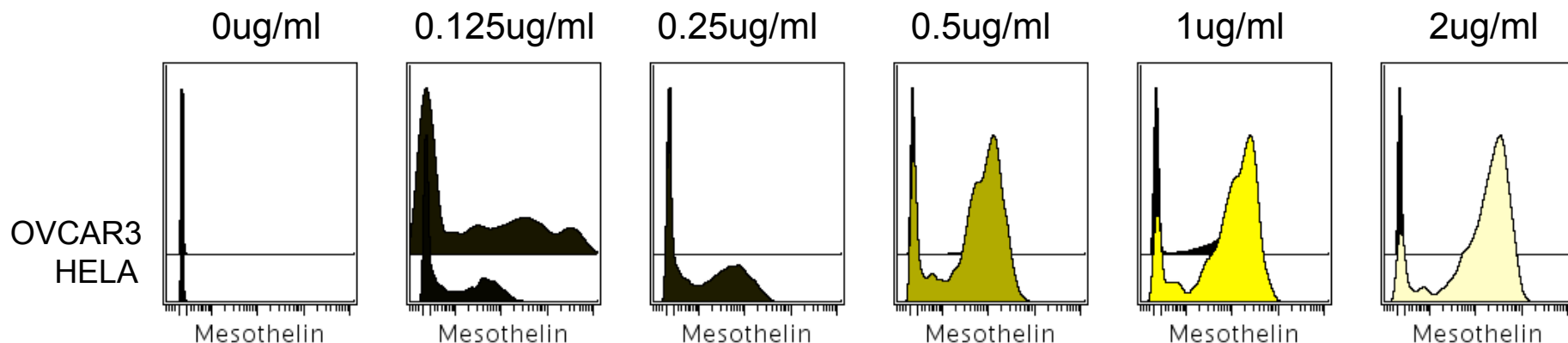


173 (Yb): Mesothelin

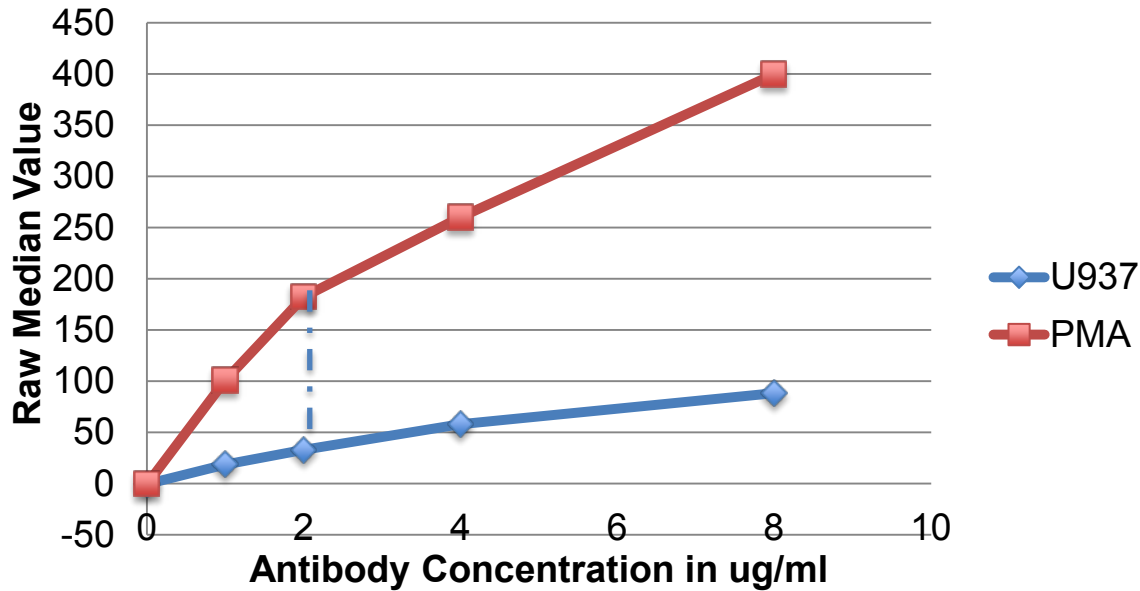
Date Conjugated:
 Titration: 9/24/13
 Rockland 200-301-A87
 Clone: MB-G10

Selected Conc. : **1ug/ml**

	0ug/ml	0.125ug/ml	0.25ug/ml	0.5ug/ml	1ug/ml	2ug/ml
OVCAR3	-0.41	8.53	-0.5	-0.39	-0.09	-0.49
HELA	-0.39	2.34	10.88	66.83	113.98	196.65



174 (Yb): pCREB



174 (Yb): pCREB (S133)

Date Conjugated: 7/22/13

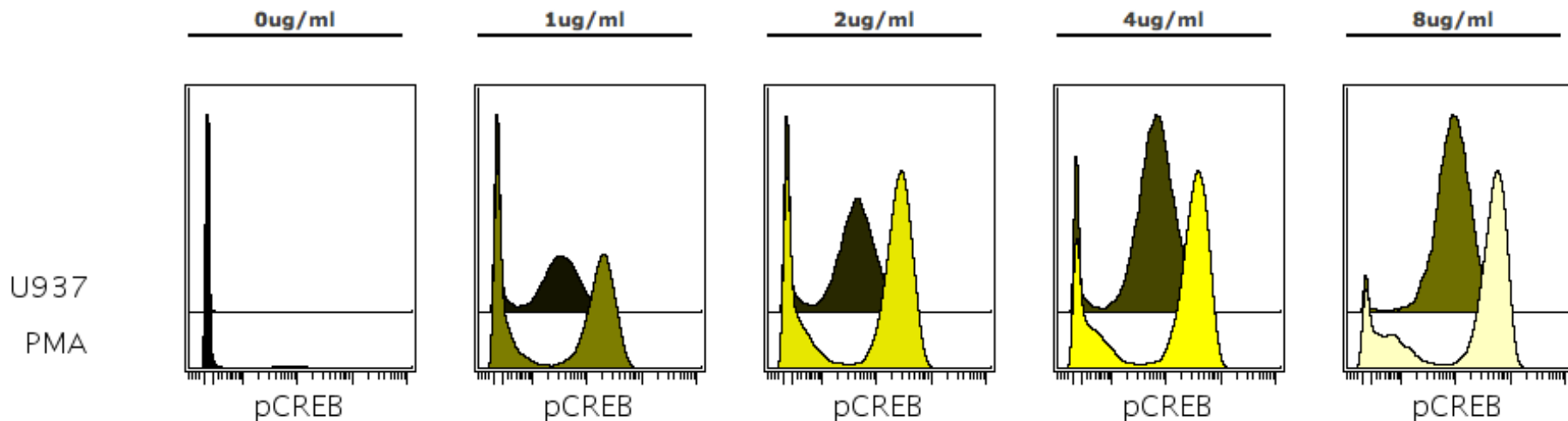
Titration: 8/16/13

CST 9198BF

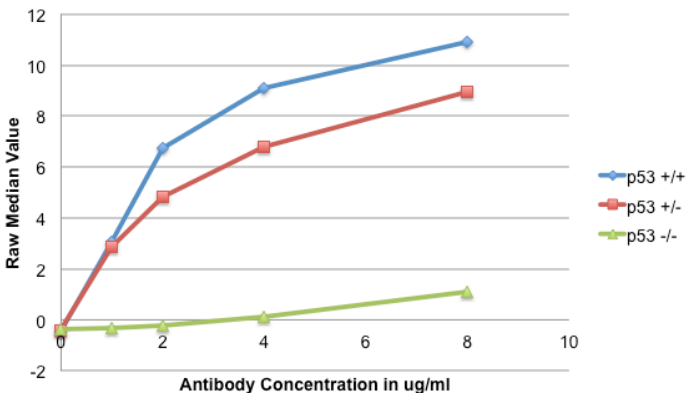
Clone: 8763

Selected Conc. : **2ug/ml**

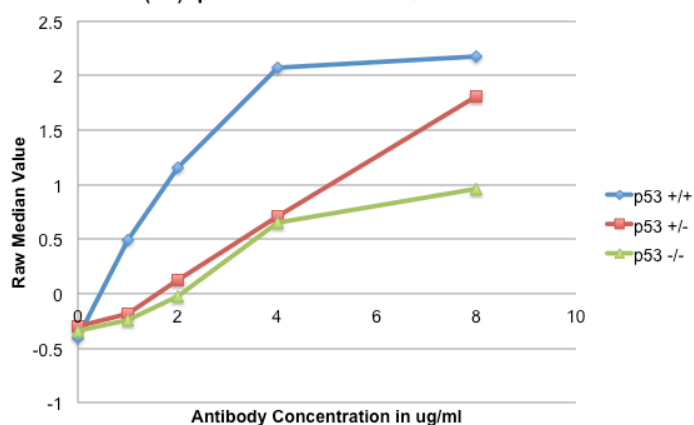
	0ug/ml	1ug/ml	2ug/ml	4ug/ml	8ug/ml
U937	-0.46	18.57	33.0	58.01	88.48
PMA	-0.37	101.07	182.36	260.27	399.95



175 (Yb): p53 Total Titration in 20mM 24hr HydroxyUrea Treated Cells



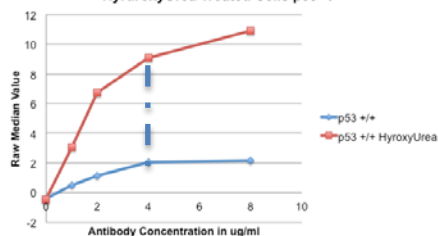
175 (Yb): p53 Total Titration in Unstimulated Cells



175 (Yb):
Total p53

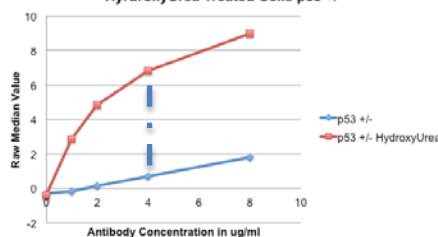
Conjugated: 5/7/2013
Titration Set 3
CST 2524
Clone: 1C12

175 (Yb): p53 Total Titration in 20mM 24hr HydroxyUrea Treated Cells p53 +/+

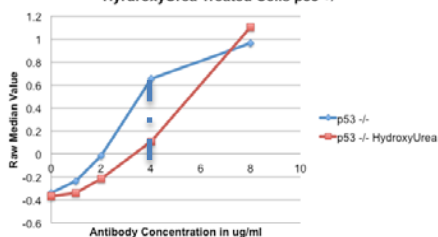


Selected Conc. : 4ug/ml

175 (Yb): p53 Total Titration in 20mM 24hr HydroxyUrea Treated Cells p53 +/-



175 (Yb): p53 Total Titration in 20mM 24hr HydroxyUrea Treated Cells p53 -/-

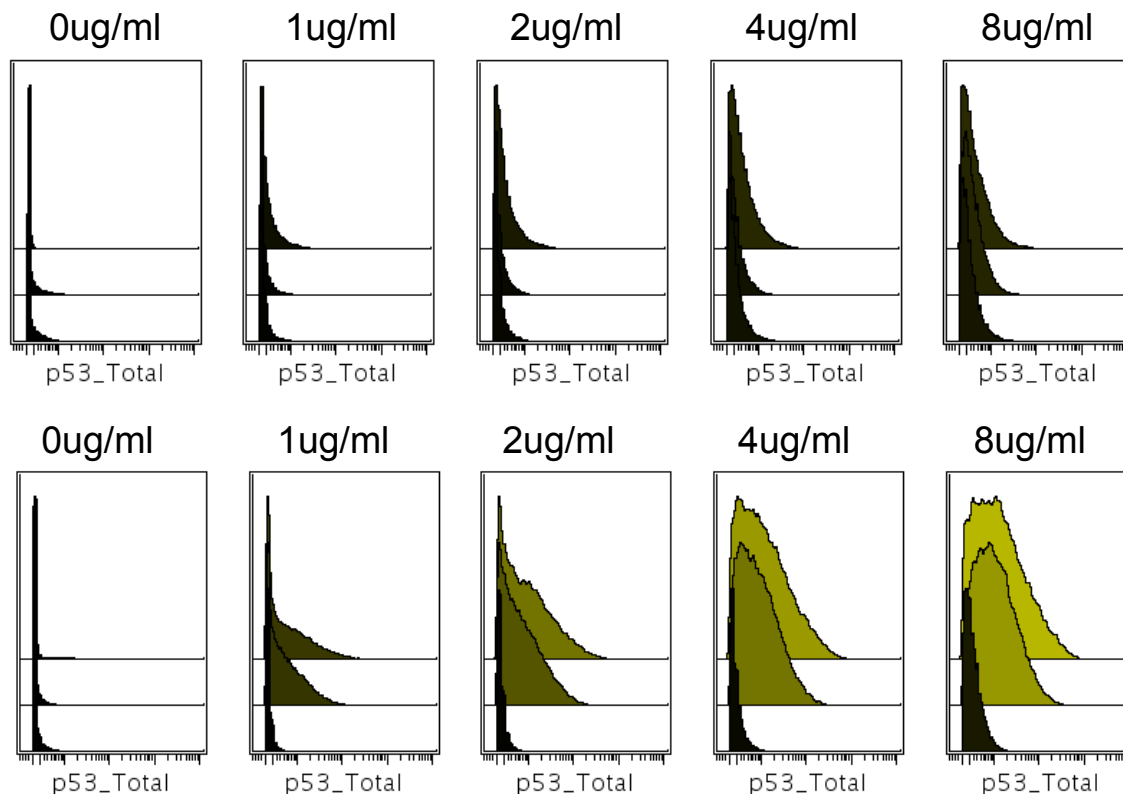


Unstim

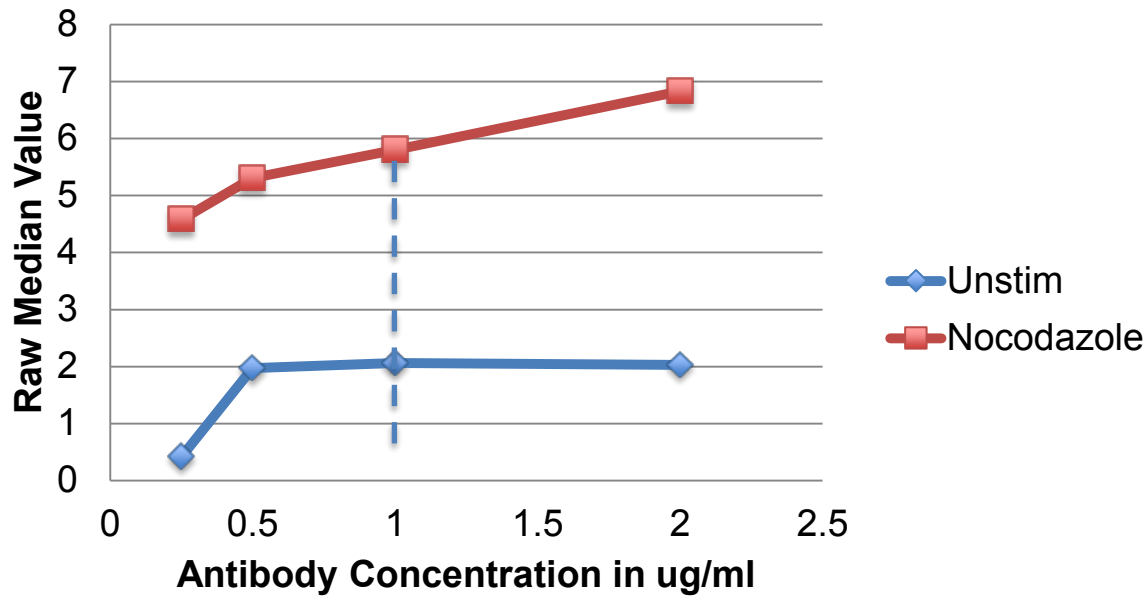
p53 +/+
p53 +/-
p53 -/-

20mM HU

p53 +/+
p53 +/-
p53 -/-



176 (Yb): pHH3



176 (Yb): pHH3 (pS28)

Lab Stock
 Titration Set 1
 8/21/2012
 Biolegend 641002
 Clone: HTA28

0.25ug/ml 0,5ug/ml 1ug/ml 2ug/ml

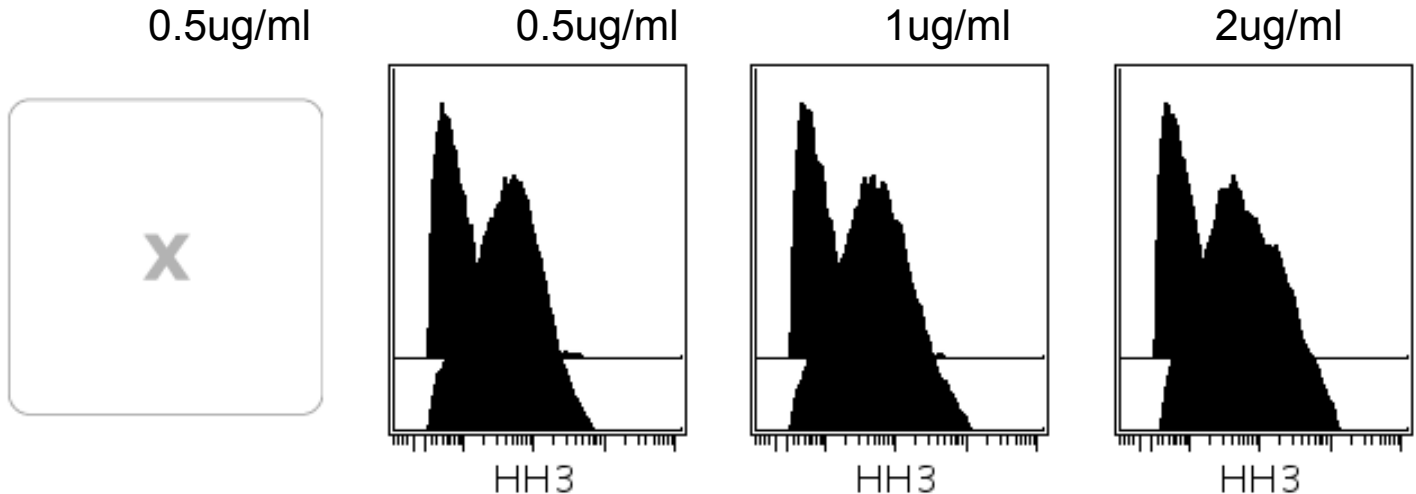
Selected Conc. : **1ug/ml**

Unstim

Nocodazole

X	1.97	2.06	2.03
4.58	5.31	5.8	6.83

Unstim
 Nocodazole



Appendix C —

OVCAR — Immune Panel

Titration 2012-2013

OVCAR Immune Panel 1 – Metal assignation

In113	CD235/CD61
In115	HLA-DR
La139	CD45
140Ce	NKG2D
Pr141	CCR6
Nd142	pMAPKAPK2 (pT334)
Nd143	pSTAT1 (pY701)
Nd144	CD11b
Nd145	CD4
Nd146	CD8
Sm147	p-H2AX (pS139)
Nd148	CD123
Sm149	p-NFkB (pS529)
Nd150	CD206
Eu151	p-ERK (pT202/pY204)
Sm152	Ki67 (total)
Eu153	CD45RA
Sm154	pSTAT3
Gd155	CD19
Gd156	BDCA2

Gd157p	CD11c
Gd158	CD33
Tb159	CCR7
Gd160	CD14
Dy161	CD66b
Dy162	pSTAT5
Dy163	CXCR3
Dy164	ICOS
Ho165	CD16
Er166	FoxP3
Er167	CD163
Er168	CD68
Tm169	CD25
Er170	CD3
Yb171	cleaved-PARP (@N214)
Yb172	pS6 (pS235/pS236)
Yb173	LAG-3
Yb174	CREB
Lu175	PD-1
Yb176	CD56

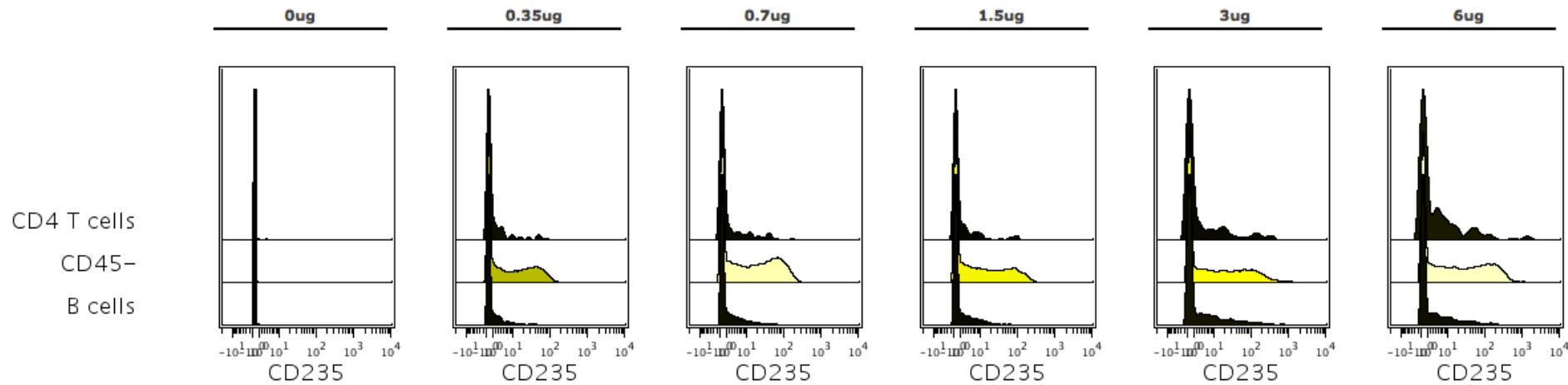
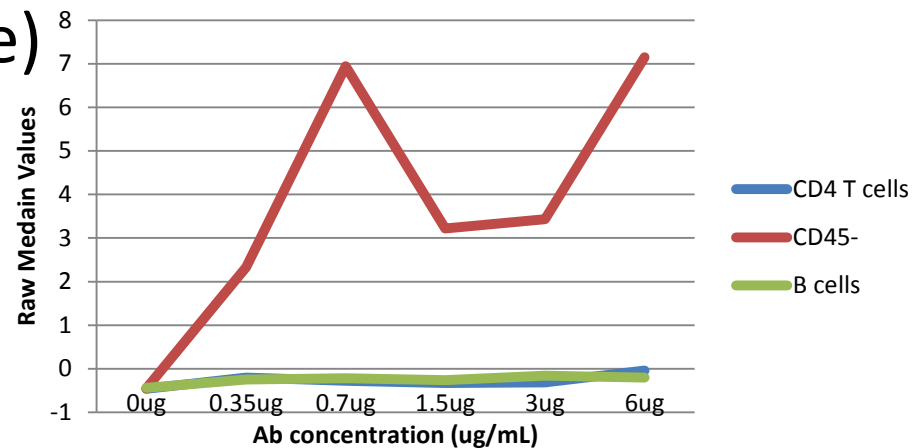
CD235a/b 113In (Surface)

Clone: HIR2 (Biolegend)
 Conjugation: 2013-01-24
 Titration: 2013-03-15

Human Bone Marrow

Staining conc.: 1.5ug/mL

CD235 113In



Raw Median Values

95th percentile

	0ug	0.35ug	0.7ug	1.5ug	3ug	6ug
CD4 T cells	-0.46	-0.2	-0.28	-0.33	-0.31	-0.04
CD45-	-0.45	2.33	6.94	3.22	3.43	7.15
B cells	-0.44	-0.25	-0.22	-0.26	-0.16	-0.2

	0ug	0.35ug	0.7ug	1.5ug	3ug	6ug
CD4 T cells	-0.03	25.83	35.5	28.58	136.93	121.47
CD45-	-0.04	74.02	127.41	138.61	262.24	303.99
B cells	-0.04	15.11	24.7	23.73	157.69	65.52

CD61 113In(Surface)

Clone: VI-PL2 (BD)

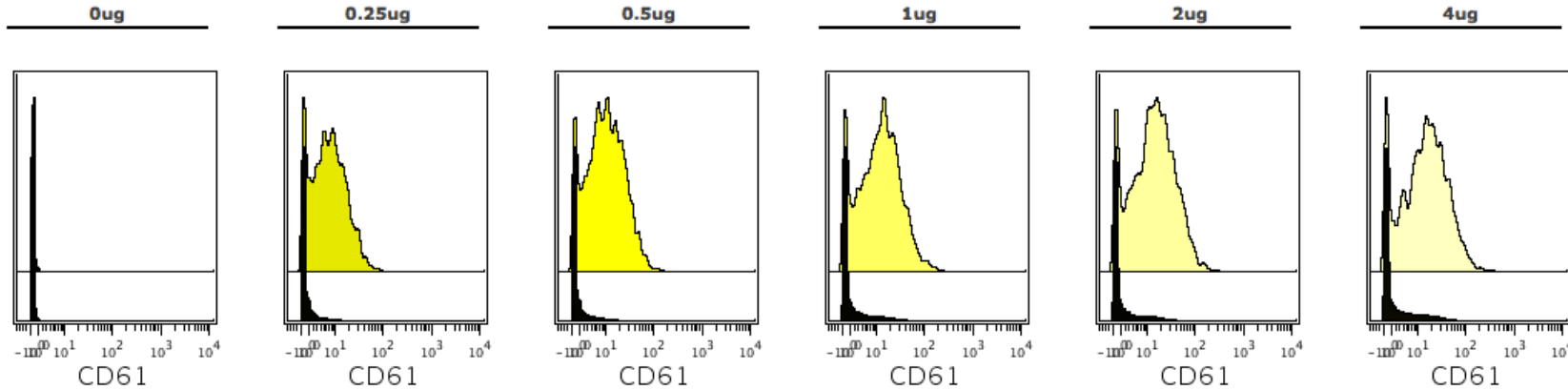
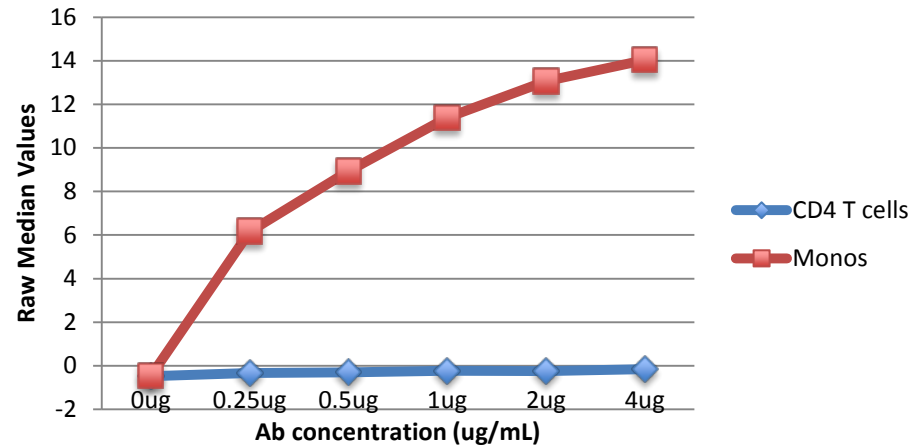
Conjugation: 2013-01-24

Titration: 2013-04-26

PBMCs – Live/frozen, thawed - rested 3h

Staining conc.: **1ug/mL**

CD61 113In



Raw Median Values

	0ug	0.25ug	0.5ug	1ug	2ug	4ug
Monos	-0.47	6.16	8.93	11.39	13.07	14.03
CD4 T cells	-0.48	-0.33	-0.31	-0.23	-0.24	-0.16

95th percentile

	0ug	0.25ug	0.5ug	1ug	2ug	4ug
Monos	-0.02	28.81	40.49	53.47	65.56	70.37
CD4 T cells	-0.03	5.98	9.0	19.32	20.81	28.01

HLA-DR 115In (Surface)

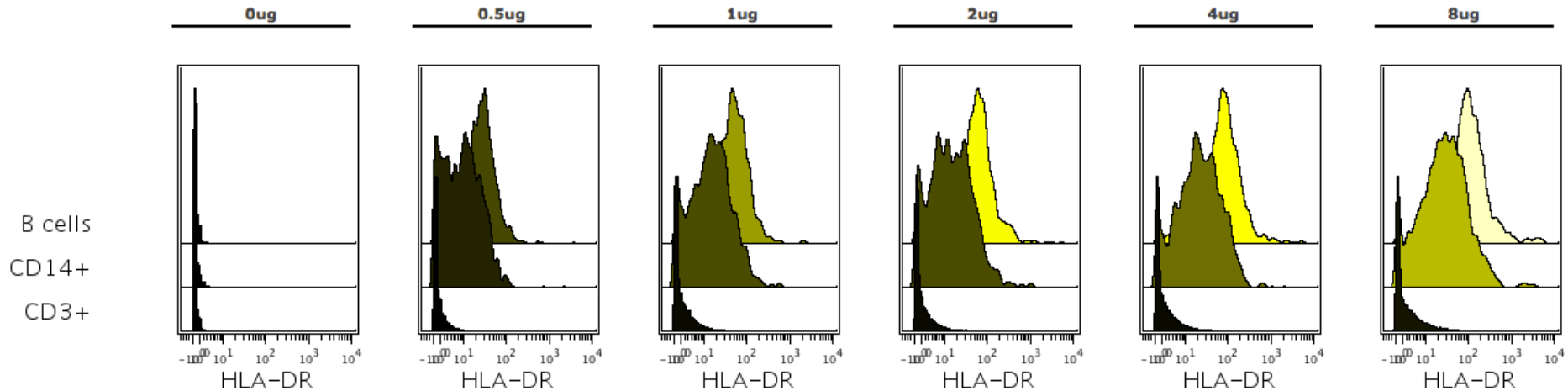
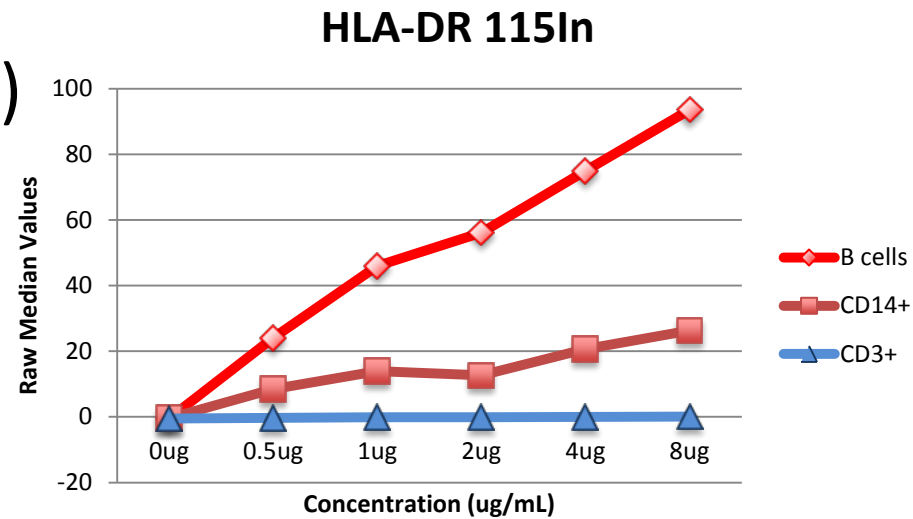
Clone: L243 (Biolegend)

Conjugation: 2013-08-19

Titration: 2013-09-05

PBMCs – Live/frozen, thawed - rested 3h

Staining conc.: **2ug/mL**



Raw Median Values

	0ug	0.5ug	1ug	2ug	4ug	8ug
B cells	-0.46	24.04	45.98	56.14	74.96	93.54
CD14+	-0.43	8.49	13.93	12.65	20.66	26.27
CD3+	-0.45	-0.32	-0.08	-0.08	-0.02	0.05

95th percentile

	0ug	0.5ug	1ug	2ug	4ug	8ug
B cells	0.8	84.92	181.0	287.59	366.37	581.56
CD14+	0.89	44.6	88.77	90.22	127.82	212.01
CD3+	0.73	5.01	13.39	12.19	15.95	24.97

CD45 139La (Surface)

Clone: HI30 (Biolegend)

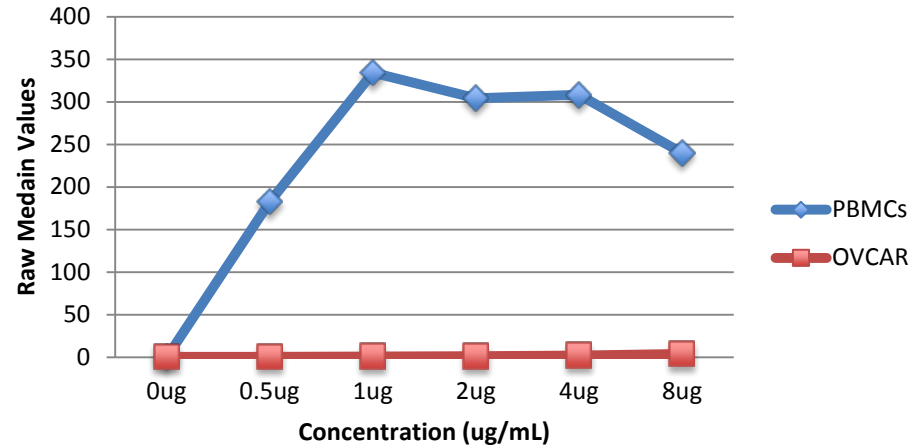
Conjugation: 2013-08-19

Titration: 2013-09-05

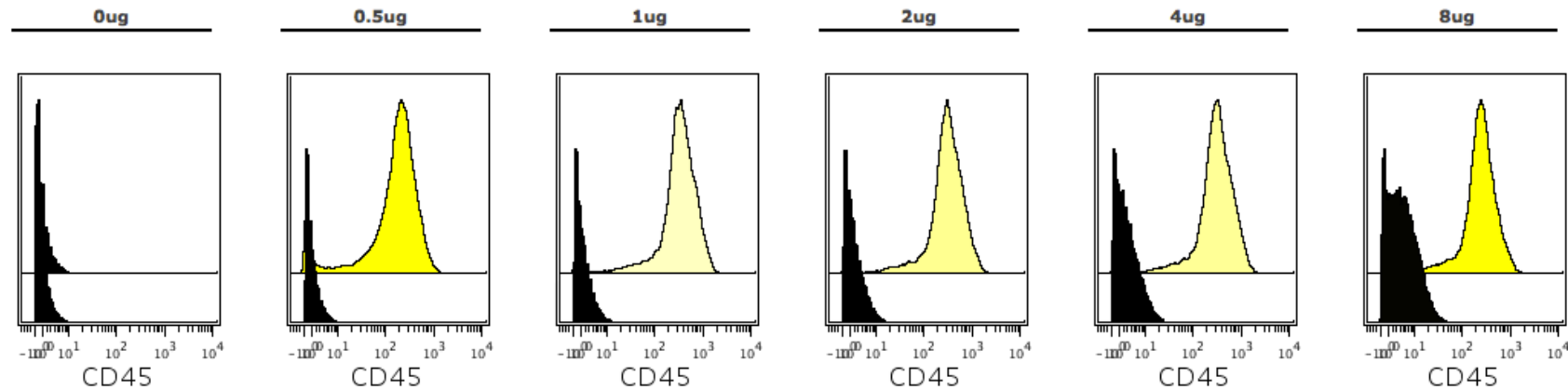
PBMCs – Live/frozen, thawed - rested 3h

OVCARs – Fixed/Frozen

CD45 139La



Staining conc.: **1ug/mL**



Raw Median Values

95th percentile

	0ug	0.5ug	1ug	2ug	4ug	8ug
PBMCs	0.1	182.69	334.14	304.13	308.33	239.82
OVCAR	0.27	0.33	0.68	1.07	2.06	3.91

	0ug	0.5ug	1ug	2ug	4ug	8ug
PBMCs	4.33	562.88	971.35	906.75	944.79	707.91
OVCAR	4.11	4.22	5.71	7.01	10.95	17.41

NKG2D 140Ce (Surface)

Clone: ()

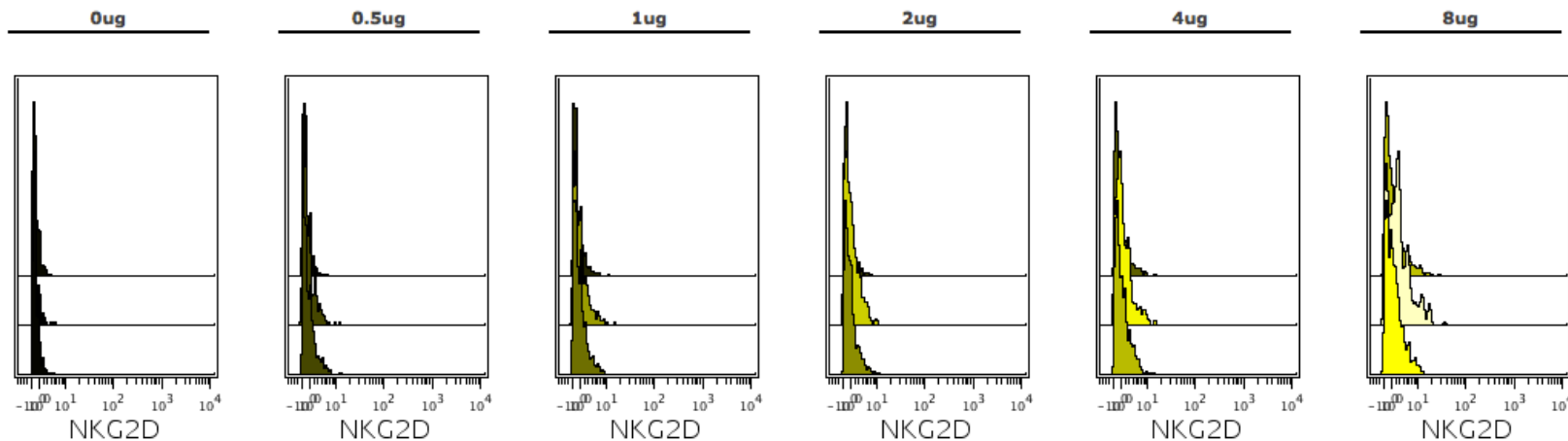
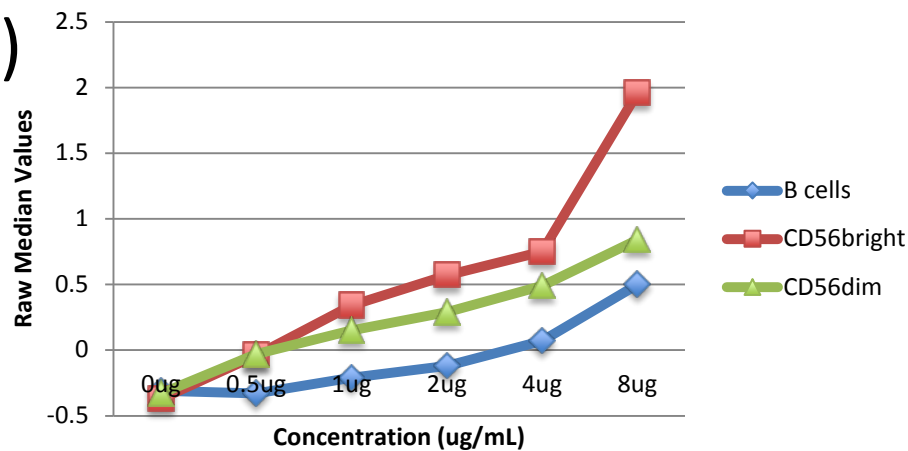
Conjugation: 2013-08-19

Titration:

PBMCs – Live/frozen, thawed - rested 3h

Staining conc.: **8ug/mL**

NKG2D 140Ce



Raw Median Values

	0ug	0.5ug	1ug	2ug	4ug	8ug
B cells	-0.31	-0.33	-0.21	-0.12	0.07	0.5
CD56bright	-0.37	-0.04	0.34	0.57	0.75	1.96
CD56dim	-0.33	-0.03	0.15	0.29	0.49	0.84

95th percentile

	0ug	0.5ug	1ug	2ug	4ug	8ug
B cells	1.65	1.83	3.15	2.86	5.27	9.24
CD56bright	1.86	3.72	5.51	5.03	7.04	12.33
CD56dim	1.46	4.34	4.38	4.35	5.19	6.81

CCR6 141Pr (Surface)

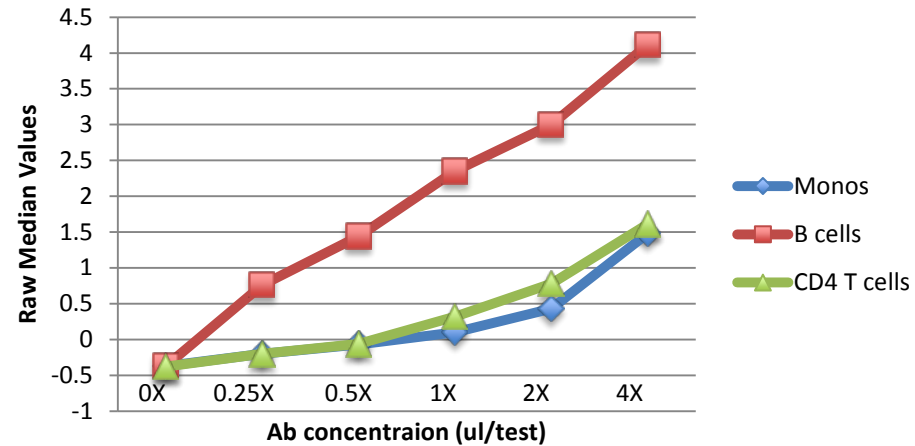
Clone: G034E3 (DVS)

Conjugation: DVS

Titration: 2013-08-27

PBMCs – Live/frozen, thawed - rested 3h

CCR6 141Pr



CCR6 - Panel 2

0X

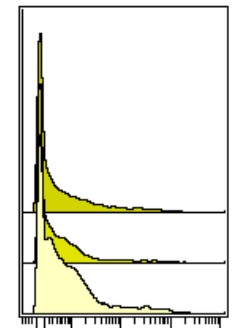
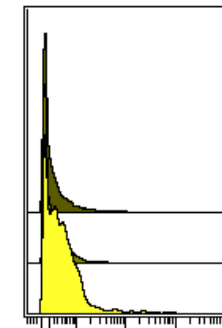
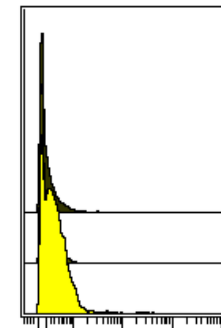
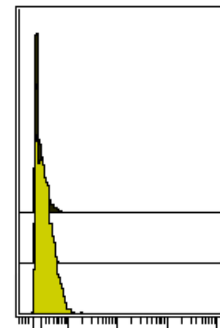
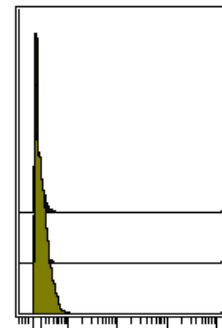
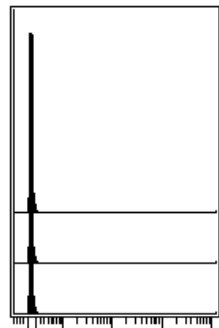
0.25X

0.5X

1X

2X

4X



Monos

CD4 T cells

B cells

1127

1127

1127

1127

1127

1127

Raw Median Values

95th percentile

0X 0.25X 0.5X 1X 2X 4X

0X 0.25X 0.5X 1X 2X 4X

Monos	-0.37	-0.2	-0.07	0.1	0.43	1.48
CD4 T cells	-0.38	-0.2	-0.06	0.32	0.78	1.61
B cells	-0.37	0.76	1.44	2.35	3.0	4.11

Monos	0.1	2.13	3.82	13.56	44.63	275.09
CD4 T cells	-0.01	1.92	3.21	8.71	33.76	253.76
B cells	0.01	4.56	6.64	15.18	53.34	306.46

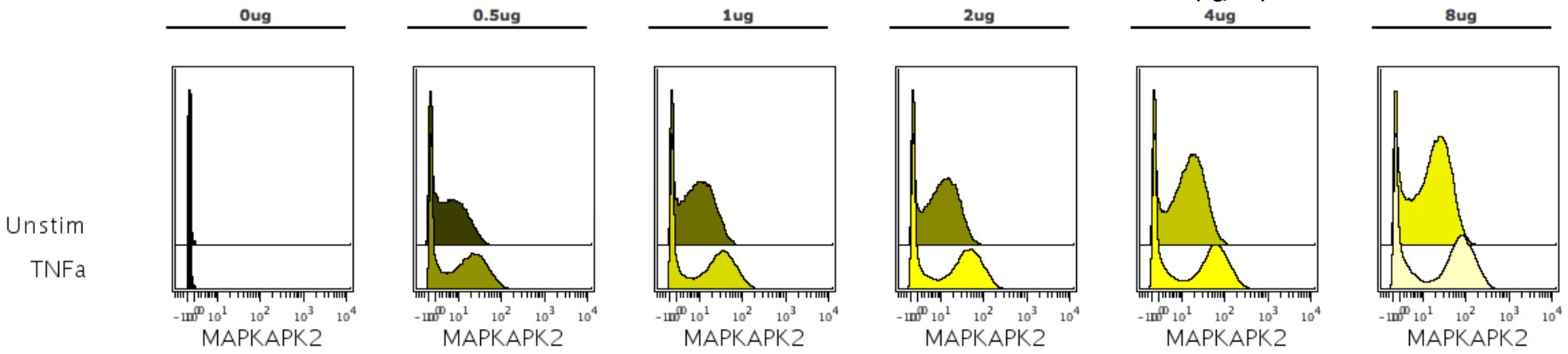
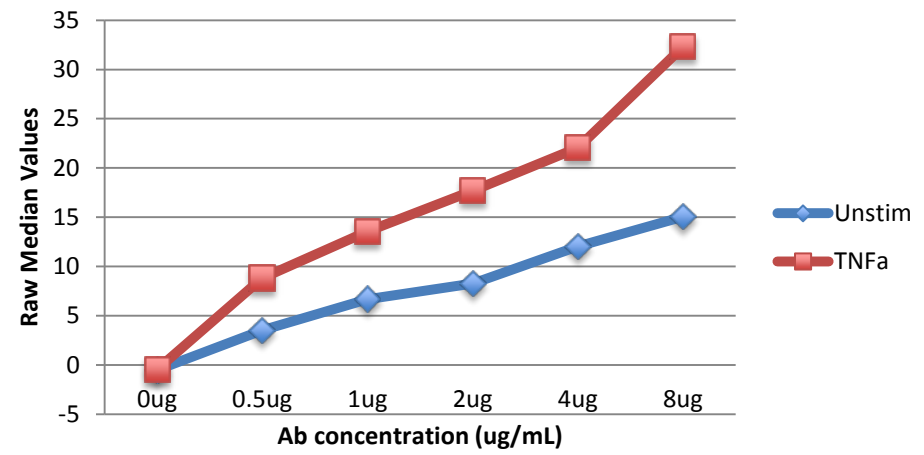
pMAPKAPK2 142Nd (ICS)

Clone: 27B7 pT334 (CST)
 Conjugation: 2013-08-26
 Titration: 2013-10-10

U937, TNFa stim, fixed/frozen

Staining conc.: 2ug/mL

pMAPKAPK2 142Nd



Raw Median Values

95th percentile

	0ug	0.5ug	1ug	2ug	4ug	8ug
Unstim	-0.51	3.52	6.68	8.26	12.04	15.06
TNFa	-0.45	8.82	13.57	17.69	22.04	32.3

	0ug	0.5ug	1ug	2ug	4ug	8ug
Unstim	-0.01	23.52	31.79	36.18	47.98	61.01
TNFa	0.92	60.92	88.98	120.47	155.63	201.58

pSTAT1 143Nd (ICS)

Clone: 4a pY701 (BD)

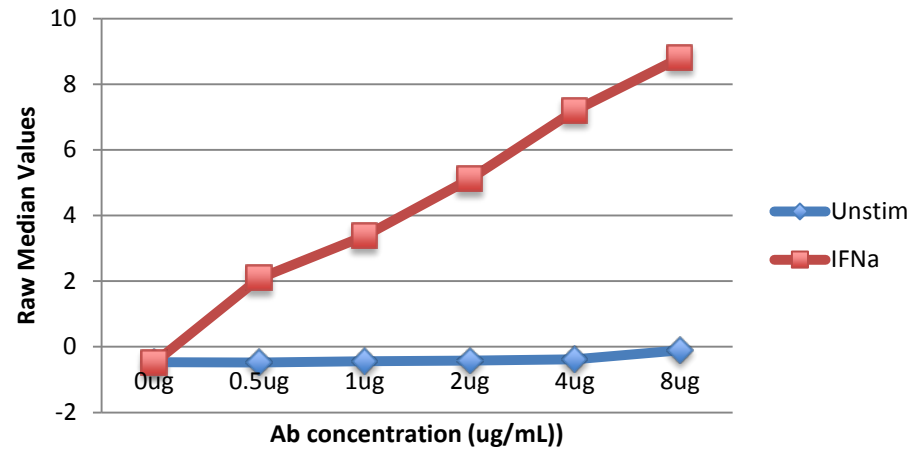
Conjugation: 2013-08-21

Titration: 2013-10-10

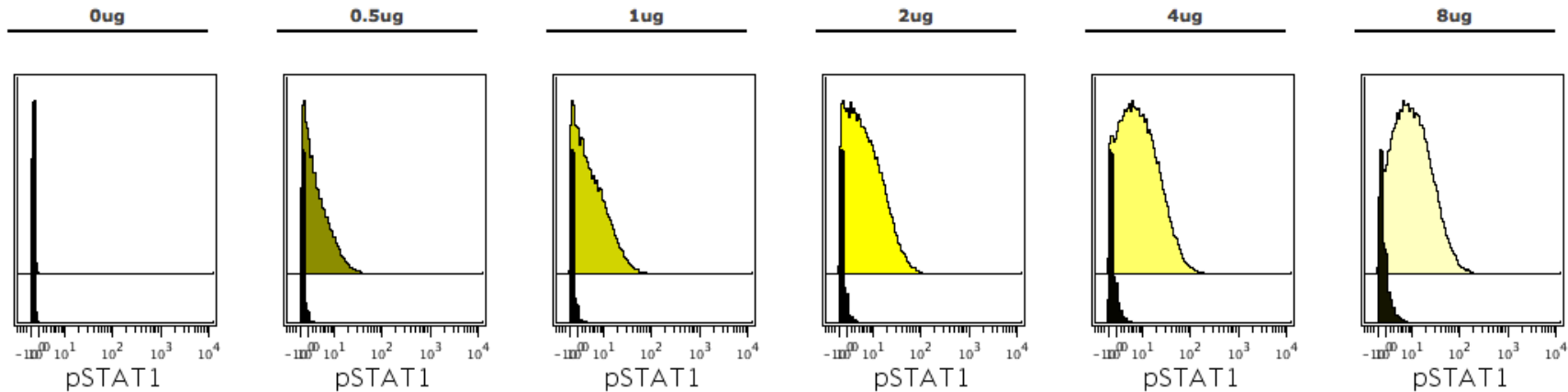
Splenocytes, IFNa stimulated, fixed/frozen

Staining conc.: 4ug/mL

pSTAT1 143Nd



IFNa
Unstim



Raw Median Values

95th percentile

0ug 0.5ug 1ug 2ug 4ug 8ug

0ug 0.5ug 1ug 2ug 4ug 8ug

	0ug	0.5ug	1ug	2ug	4ug	8ug
IFNa	-0.49	2.09	3.37	5.11	7.19	8.8
Unstim	-0.47	-0.48	-0.44	-0.42	-0.38	-0.11

	0ug	0.5ug	1ug	2ug	4ug	8ug
IFNa	-0.04	14.07	22.16	30.38	42.5	48.32
Unstim	-0.03	0.55	0.87	1.38	2.11	3.32

CD11b 144Nd (Surface)

Clone: IRCF44 (DVS)

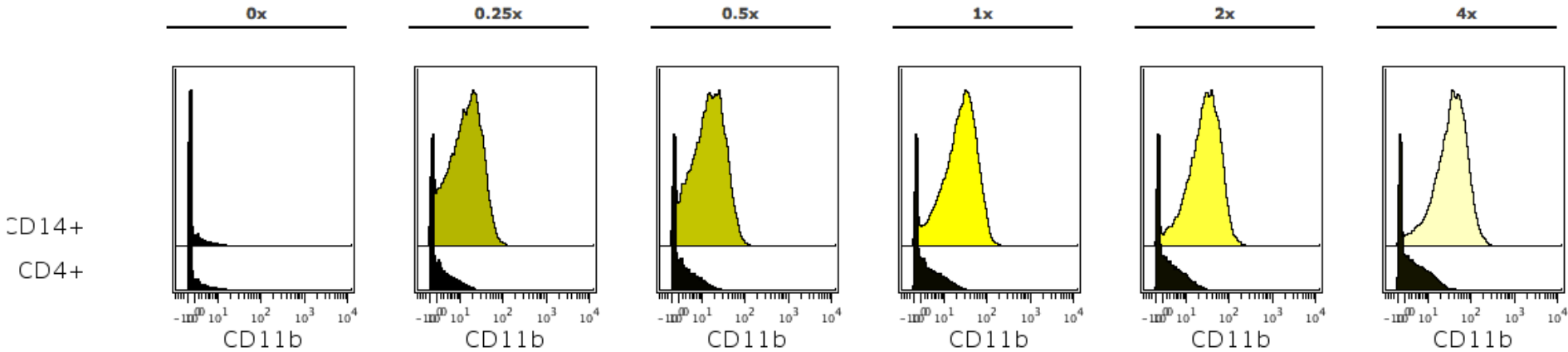
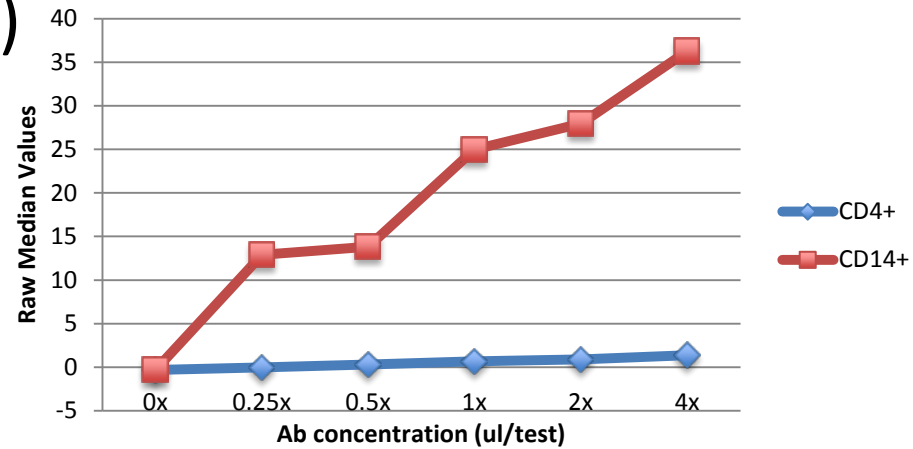
Conjugation: DVS

Titration: 2012-08-16

PBMCs – Live/frozen, thawed - rested 3h

Staining conc.: **1ul/test**

CD11b 144Nd



Raw Median Values

95th percentile

	0x	0.25x	0.5x	1x	2x	4x
CD14+	-0.32	12.91	13.82	25.0	27.96	36.26
CD4+	-0.33	-0.01	0.32	0.68	0.91	1.36

	0x	0.25x	0.5x	1x	2x	4x
CD14+	7.0	44.63	48.71	78.77	84.97	111.03
CD4+	6.71	11.57	12.23	15.02	14.36	17.69

CD4 145Nd (Surface)

Clone: RPA-T4 (DVS)

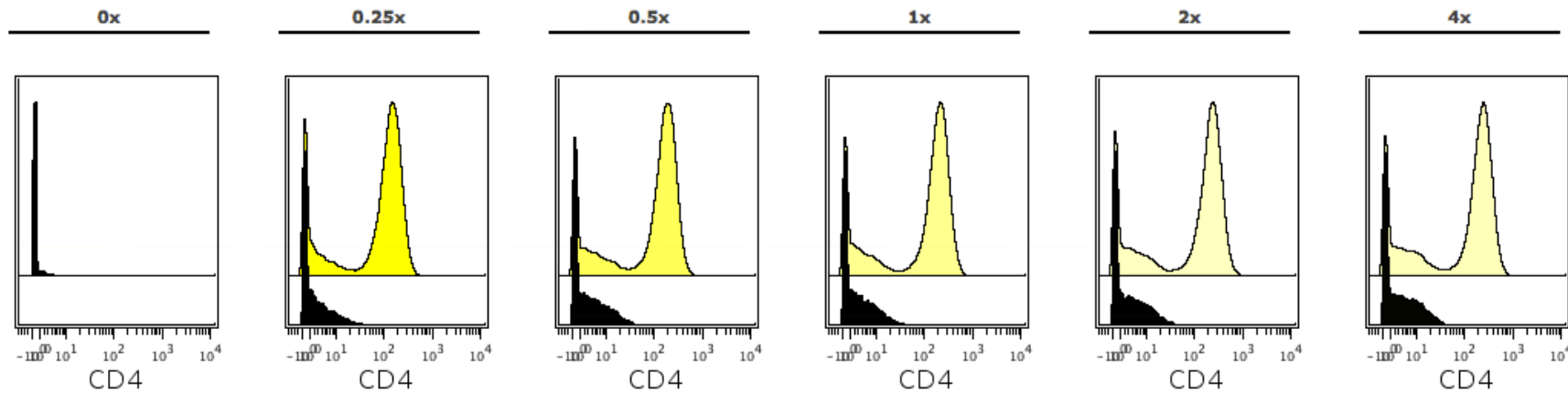
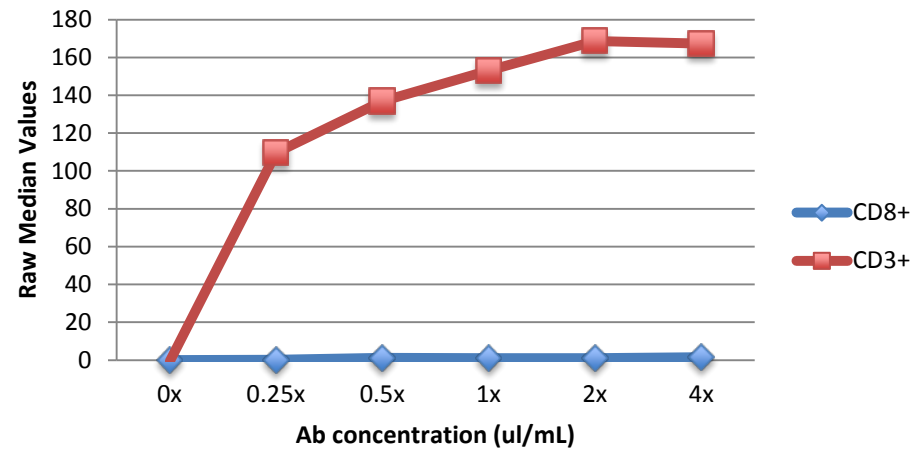
Conjugation: DVS

Titration: 2012-08-16

PBMCs – Live/frozen, thawed - rested 3h

Staining conc.: **0.5ul/test**

CD4 145Nd



Raw Median Values

95th percentile

	0x	0.25x	0.5x	1x	2x	4x
CD3+	-0.44	109.7	136.83	153.05	168.63	167.41
CD8+	X	0.18	1.15	0.96	1.1	1.53

	0x	0.25x	0.5x	1x	2x	4x
CD3+	1.95	262.06	324.45	364.92	415.74	413.56
CD8+	X	13.33	17.86	15.35	17.21	18.57

CD8 146Nd (Surface)

Clone: RPA-T8 (DVS)

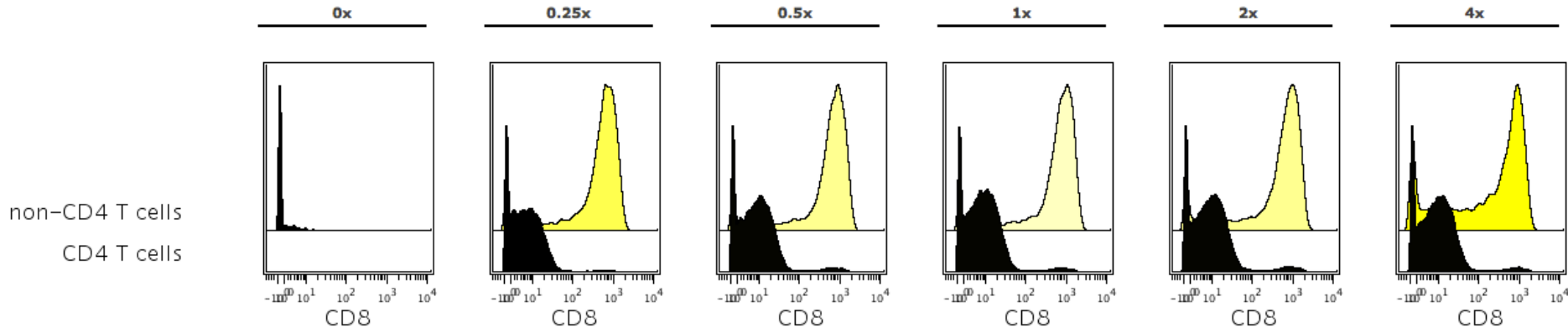
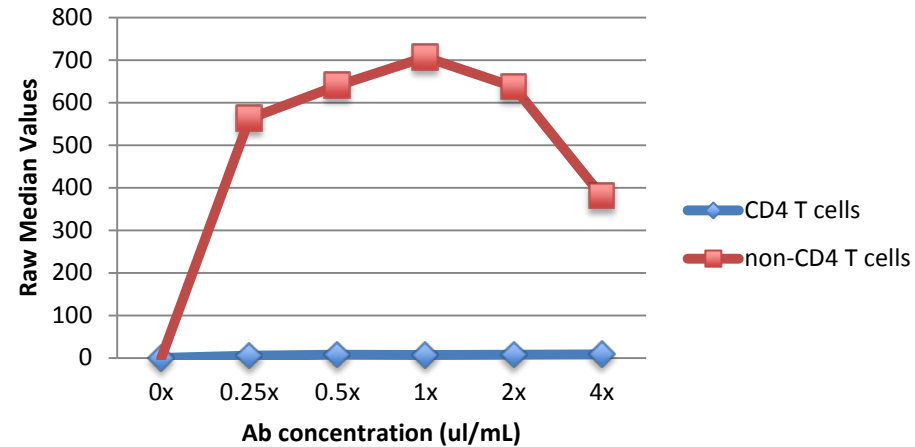
Conjugation: DVS

Titration: 2012-08-16

PBMCs – Live/frozen, thawed - rested 3h

Staining conc.: **0.5ul/test**

CD8 146Nd



Raw Median Values

	0x	0.25x	0.5x	1x	2x	4x
non-CD4 T cells	-0.43	562.52	639.59	706.93	636.96	380.24
CD4 T cells	X	5.17	7.31	7.15	7.68	8.01

95th percentile

	0x	0.25x	0.5x	1x	2x	4x
non-CD4 T cells	5.08	1387.04	1567.0	1709.86	1640.7	1373.62
CD4 T cells	X	30.43	53.65	47.39	119.97	66.44

pH2AX 147Sm (ICS)

Clone: JBW301 pS139 (Millipore)

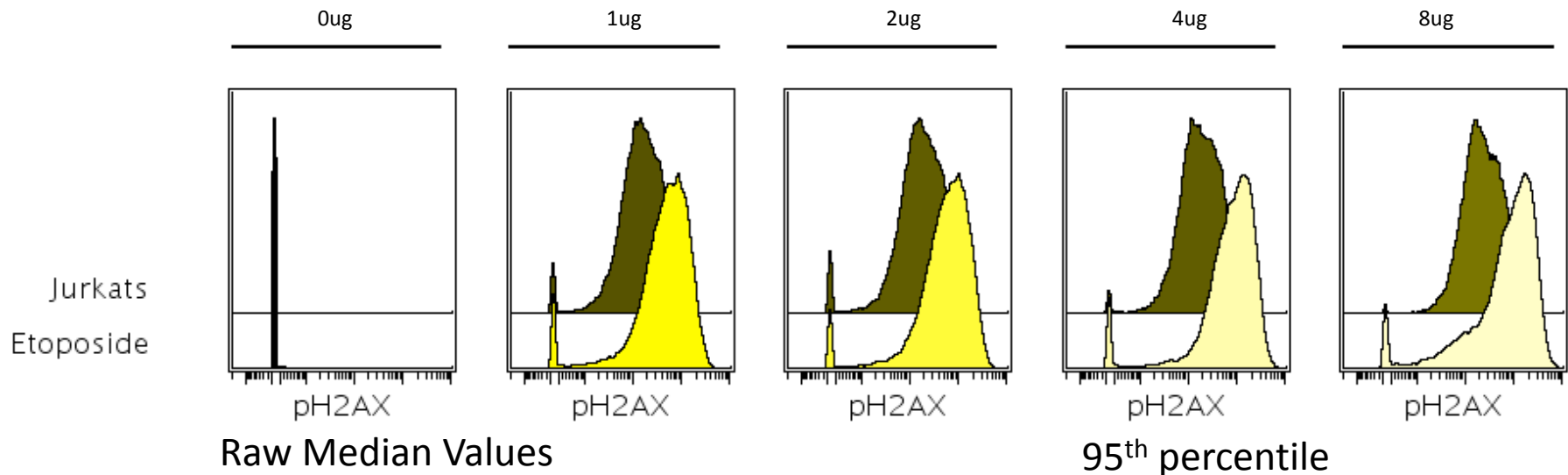
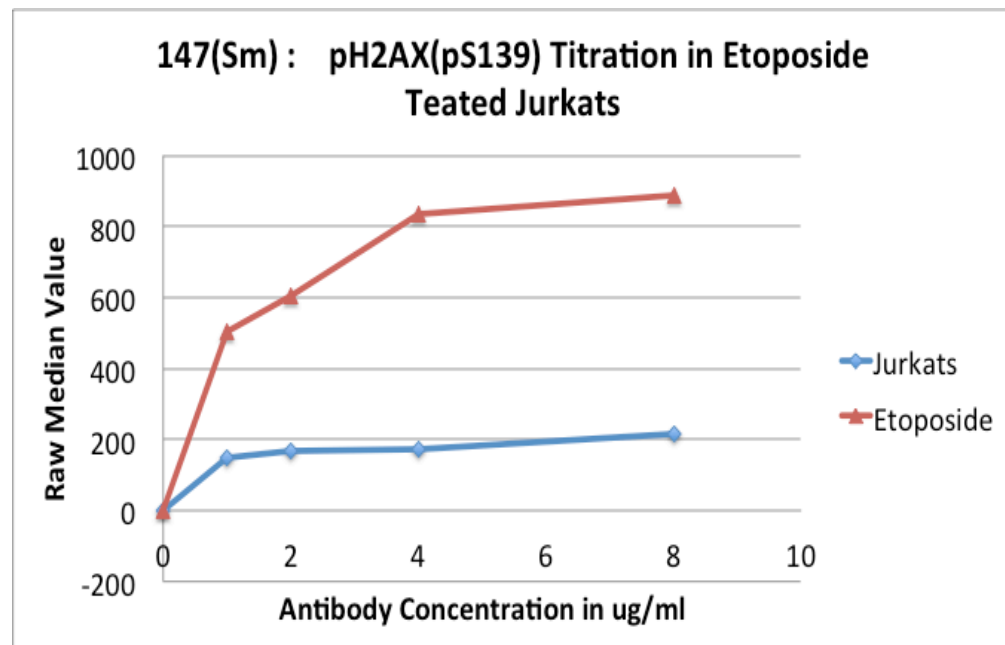
Conjugation: 2013-02-13

Titration: 2013-02-14

Jurkat – Etoposide treated

Staining conc.: **4ug/mL**

Am re-conjugating/re-titrating



	0ug	1ug	2ug	4ug	8ug
Jurkats	-0.5	150.98	169.84	173.41	214.81
Etoposide	-0.49	504.49	605.9	836.7	887.14

CD123 148Nd (Surface)

Clone: 6H6 (Biolegend)

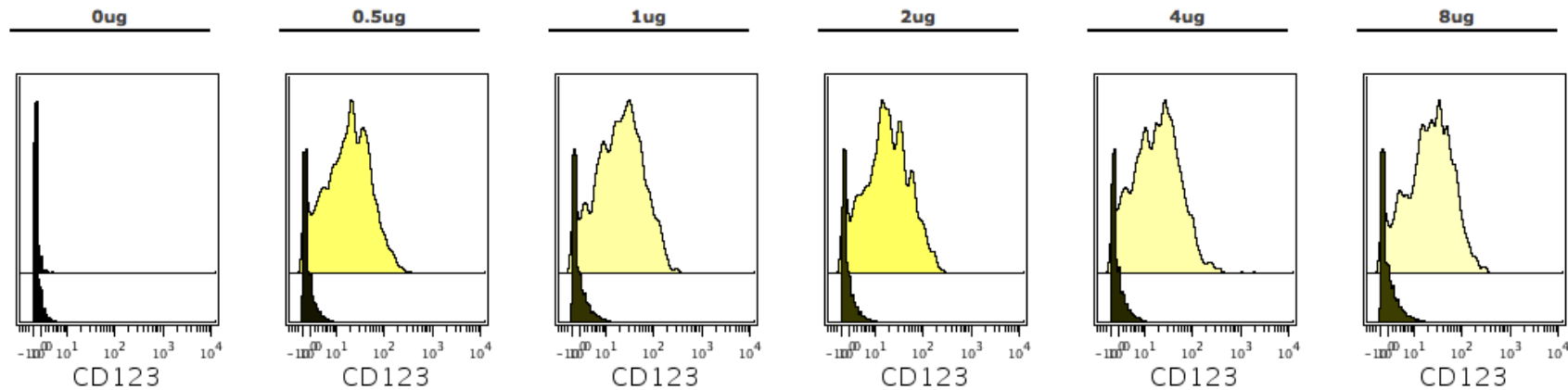
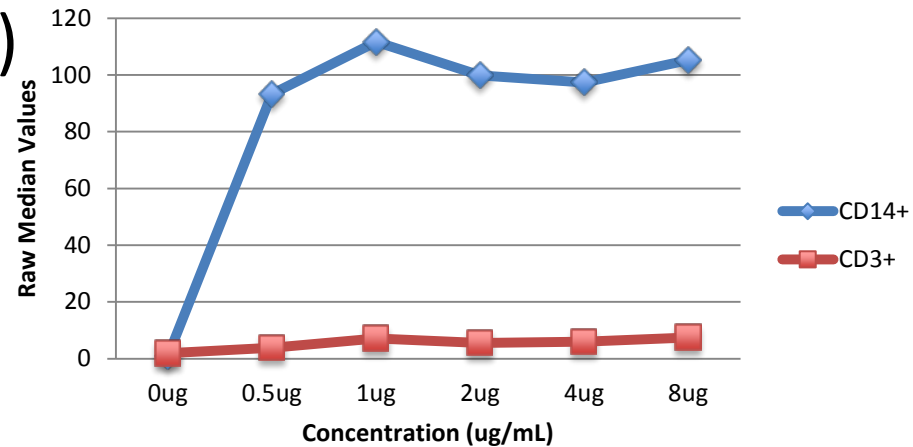
Conjugation: 2013-08-26

Titration: 2013-08-27

PBMCs – Live/frozen, thawed - rested 3h

Staining conc.: **1ug/mL**

CD123 148Nd



Raw Median Values

95th percentile

	0ug	0.5ug	1ug	2ug	4ug	8ug
CD14+	-0.45	17.91	19.95	16.46	17.78	21.88
CD3+	-0.34	-0.28	-0.16	-0.14	-0.11	-0.06

	0ug	0.5ug	1ug	2ug	4ug	8ug
CD14+	0.88	93.34	111.71	99.78	97.39	105.25
CD3+	1.89	3.87	7.14	5.53	5.93	7.48

pNFkB 149Sm (ICS)

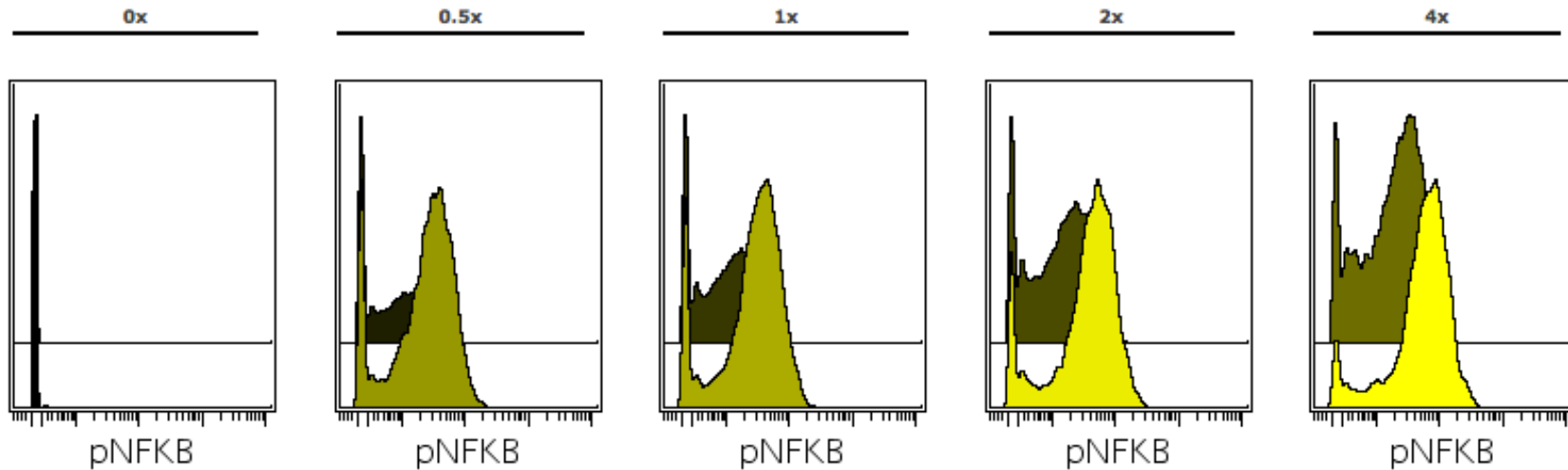
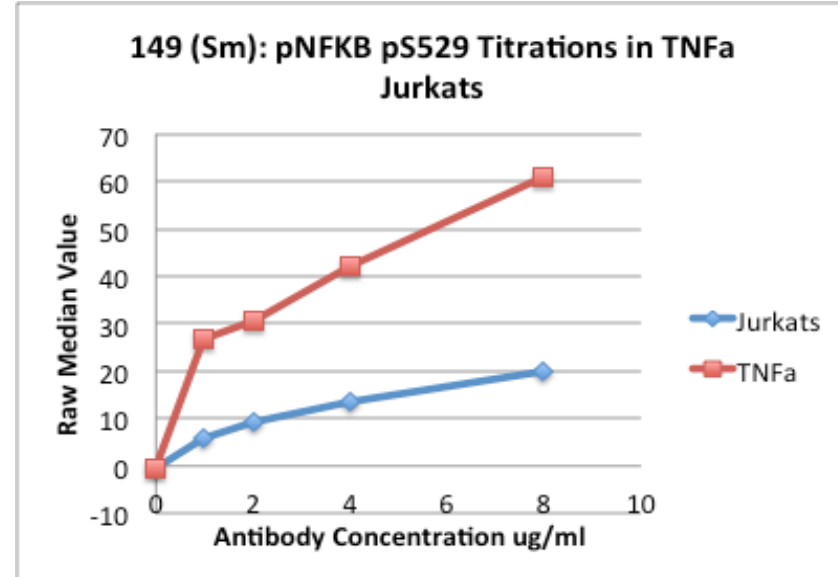
Clone: K10-895.12.50 pS529 (BD)

Conjugation: 2012-09-19

Titration: 2012-09-28

Jurkat – TNFa stim

Staining conc.: **4ug/mL**



Raw Median values

95th percentile

0x 0.5x 1x 2x 4x

Jurkats	-0.49	5.75	9.47	13.68	19.98
TNFa	-0.49	26.67	30.71	42.13	60.76

CD206 150Nd (Surface)

Clone: 19.2 (BD)

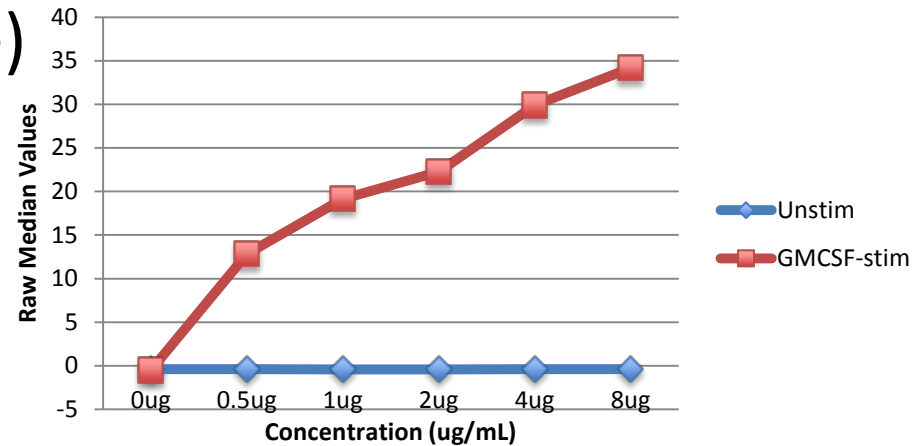
Conjugation: 2013-08-26

Titration: 2013-09-09

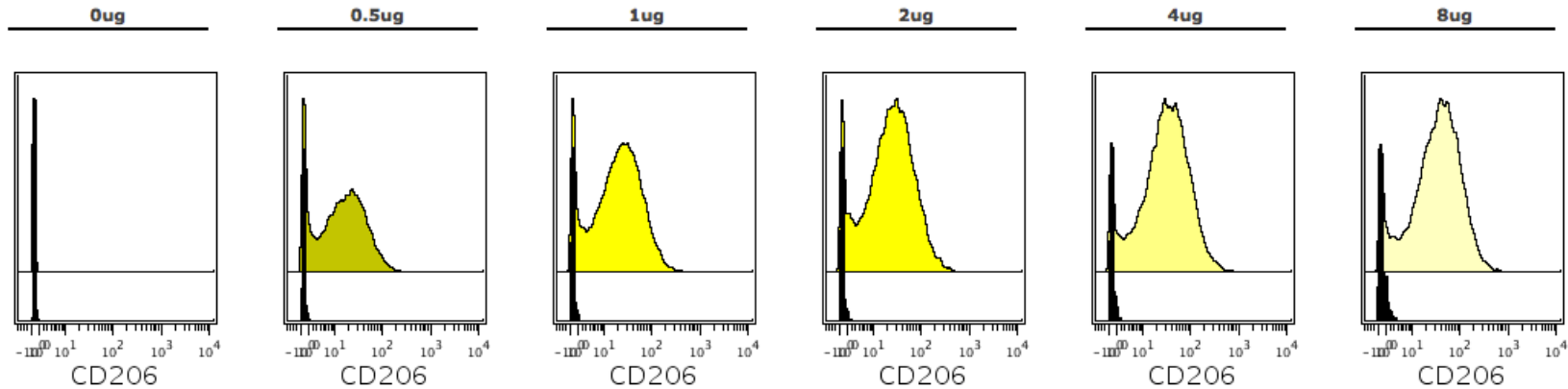
PBMCs – Unstim : Fixed/frozen

Stim: GMCSF 10ng/mL 3 days

CD206 150Nd



Staining conc.: **2 ug/mL**



Raw Median Values

	0ug	0.5ug	1ug	2ug	4ug	8ug
GMCSF-stim	-0.51	12.84	19.15	22.26	29.89	34.17
Unstim	-0.38	-0.39	-0.43	-0.43	-0.39	-0.4

95th percentile

	0ug	0.5ug	1ug	2ug	4ug	8ug
GMCSF-stim	-0.04	72.36	99.09	116.86	151.65	162.92
Unstim	-0.03	0.0	0.29	0.43	0.71	1.51

pERK 151Eu (ICS)

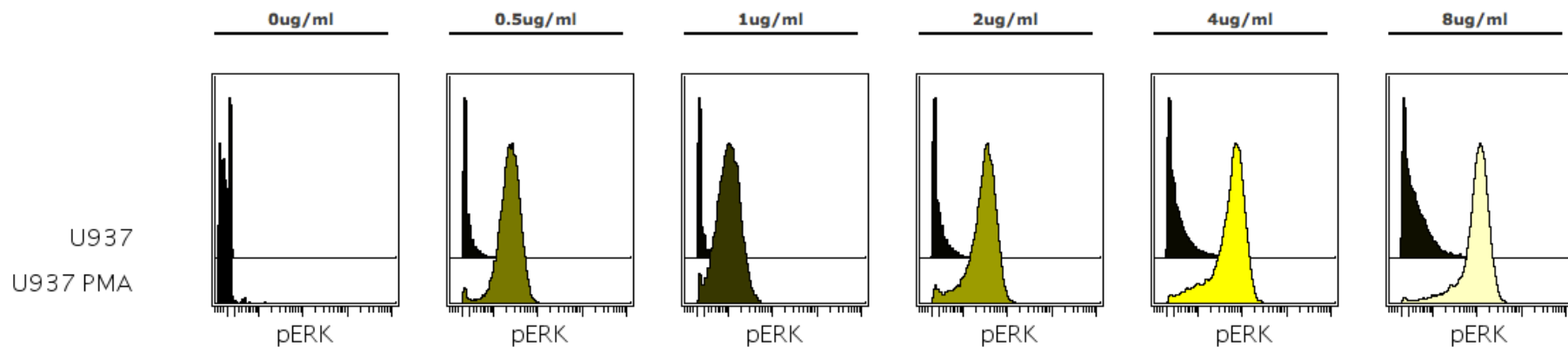
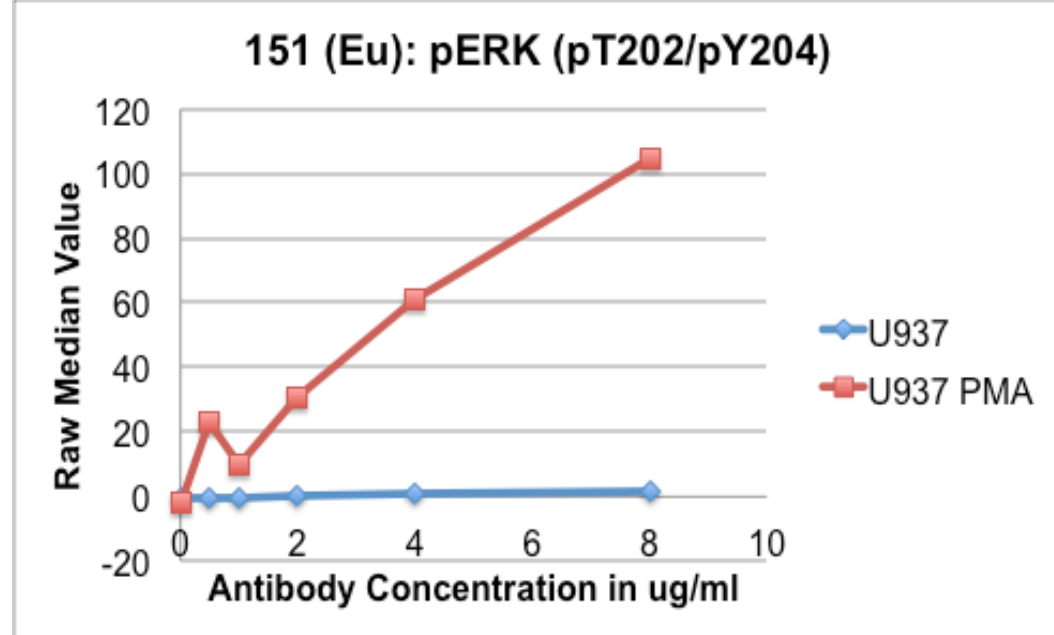
Clone: 20A pT202/Y204 (BD)

Conjugation: 2013-02-12

Titration: 2013- 10-01

U937 – PMA Stim

Staining conc.: **2 ug/mL**



Raw Median Values

95th percentile

	0ug/ml	0.5ug/ml	1ug/ml	2ug/ml	4ug/ml	8ug/ml
U937	-0.43	-0.2	-0.38	-0.08	0.69	1.63
U937 PMA	-2.0	23.27	9.57	30.69	61.14	104.86

Ki67 152Sm (ICS)

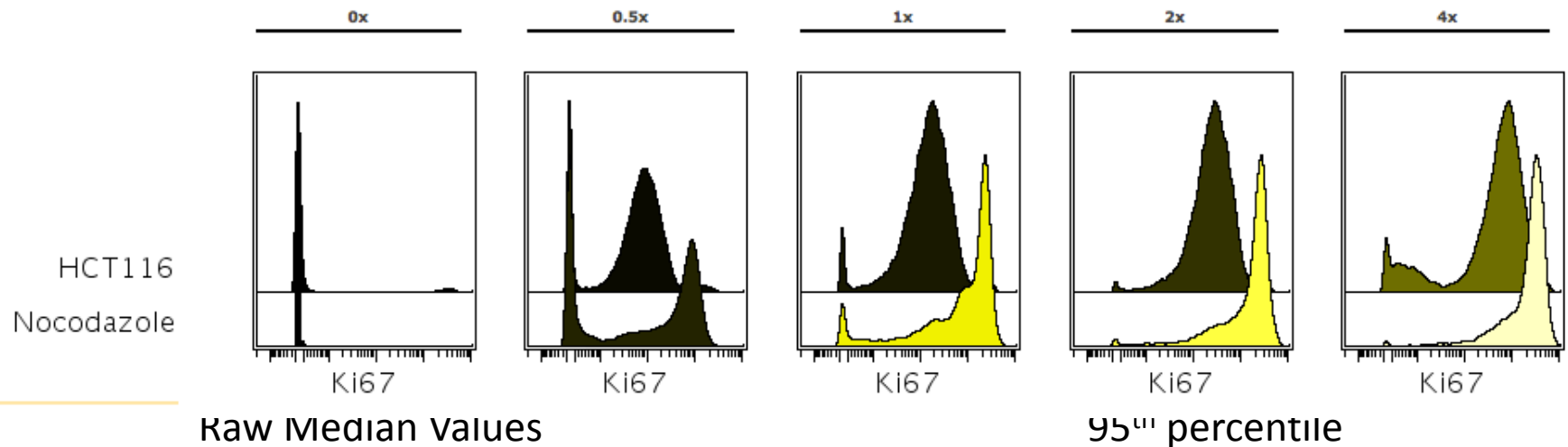
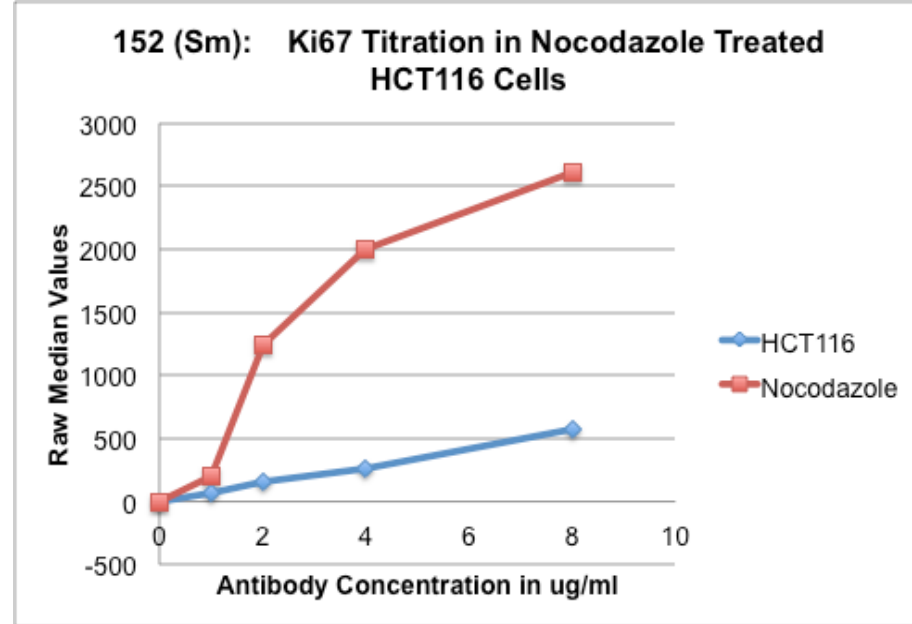
Clone: B56 totalKi67 (BD)

Conjugation: 2013-03-15

Titration: 2013-03-21

HCT116 – Nocodazole treated

Staining conc.: **2ug/mL**



	0x	0.5x	1x	2x	4x
HCT116	-0.37	67.89	151.33	256.66	571.46
Nocodazole	-0.49	194.5	1235.78	2001.93	2611.07

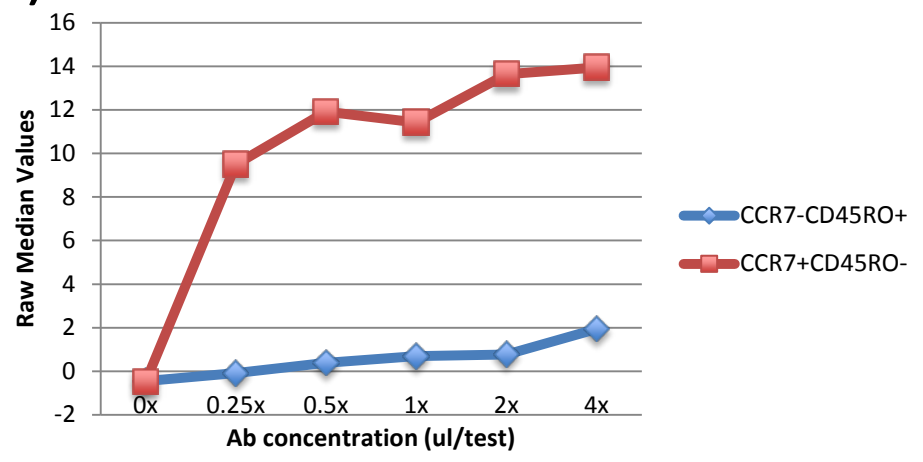
CD45RA 153Eu (Surface)

Clone: HI100 (DVS)
 Conjugation: DVS
 Titration: 2012-10-24

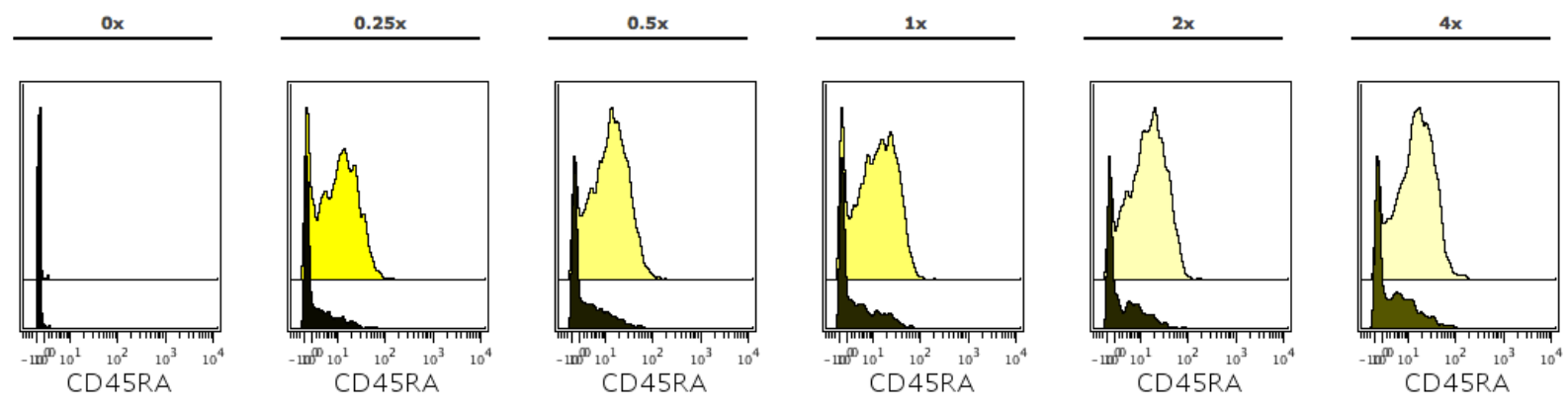
PBMCs – Live/frozen, thawed - rested 3h

Staining conc.: **0.5ul/test**

CD45RA 153Eu



CD8 T cells
 CCR7+CD45RO-
 CCR7-CD45RO+



Raw Median Values

95th percentile

	0x	0.25x	0.5x	1x	2x	4x
CCR7+CD45RO-	-0.48	9.49	11.92	11.42	13.63	13.94
CCR7-CD45RO+	-0.45	-0.08	0.39	0.69	0.77	1.95

	0x	0.25x	0.5x	1x	2x	4x
CCR7+CD45RO-	-0.01	38.44	46.48	46.09	50.65	49.16
CCR7-CD45RO+	0.46	19.77	23.0	26.08	23.1	33.77

pSTAT3 154Sm (ICS)

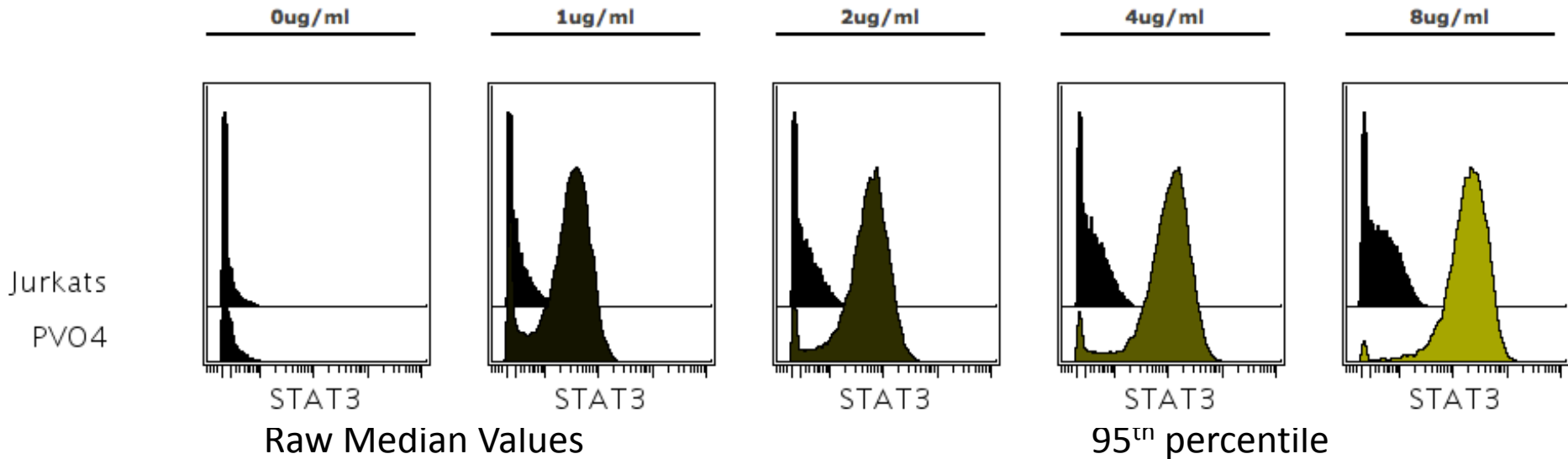
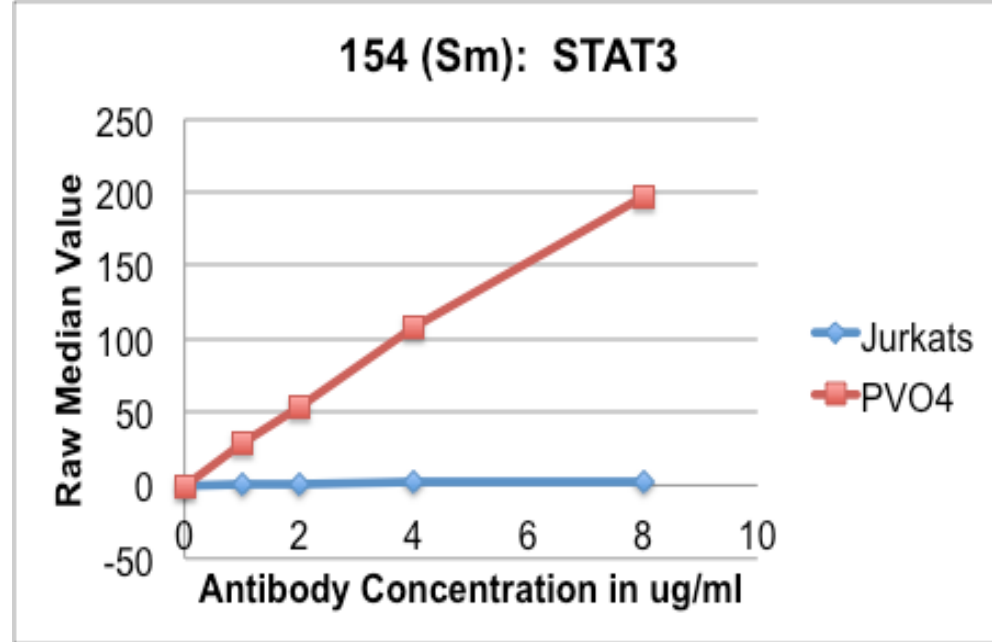
Clone: 4P STAT-3 pY705 (BD)

Conjugation: 2013-07-16

Titration: 2013-08-16

Jurkat – PVO4 Stim

Staining conc.: **6ug/mL**



	0ug/ml	1ug/ml	2ug/ml	4ug/ml	8ug/ml
Jurkats	-0.35	0.36	0.93	1.69	2.48
PVO4	-0.33	28.87	53.75	107.17	195.9

CD19 155Gd (Surface)

Clone: HIB19 (BD)

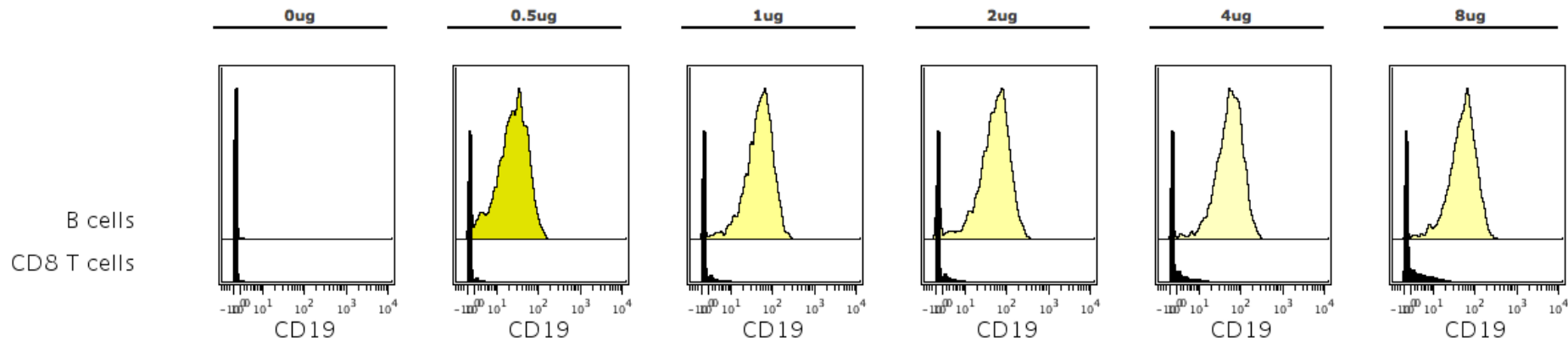
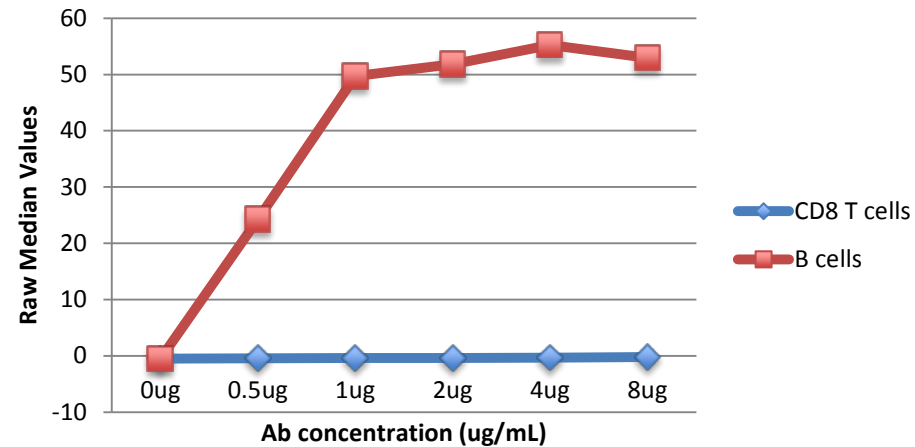
Conjugation: 2012-10-26

Titration: 2012-11-01

Staining conc.: **1ug/mL**

PBMCs – Live/frozen, thawed - rested 3h

CD19 155Gd



Raw Median Values

95th percentile

	0ug	0.5ug	1ug	2ug	4ug	8ug
B cells	-0.47	24.25	49.74	51.83	55.22	52.93
CD8 T cells	-0.48	-0.46	-0.41	-0.39	-0.33	-0.24

	0ug	0.5ug	1ug	2ug	4ug	8ug
B cells	-0.01	74.62	132.74	153.48	147.37	143.84
CD8 T cells	-0.01	1.68	4.24	5.18	8.27	13.33

BDCA2 (CD303) 156Gd (Surface)

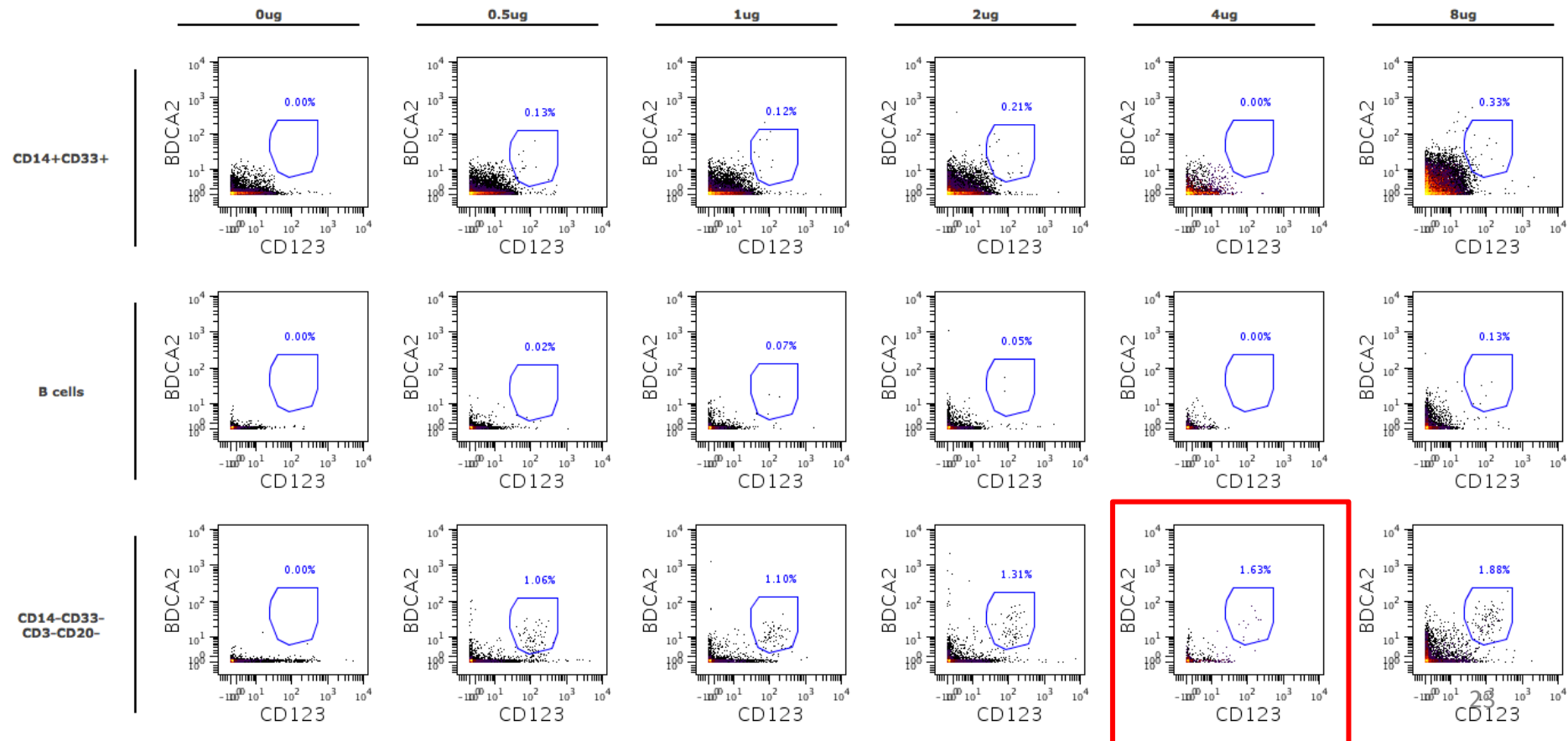
Clone: 201A (Biolegend)

Conjugation: 2013-05-17

Titration: 2013-05-22

Staining conc.: **4ug/mL**

PBMCs – Live/frozen, thawed - rested 3h



CD11c 157Gd (Surface)

Clone: 3.9 (Biolegend)

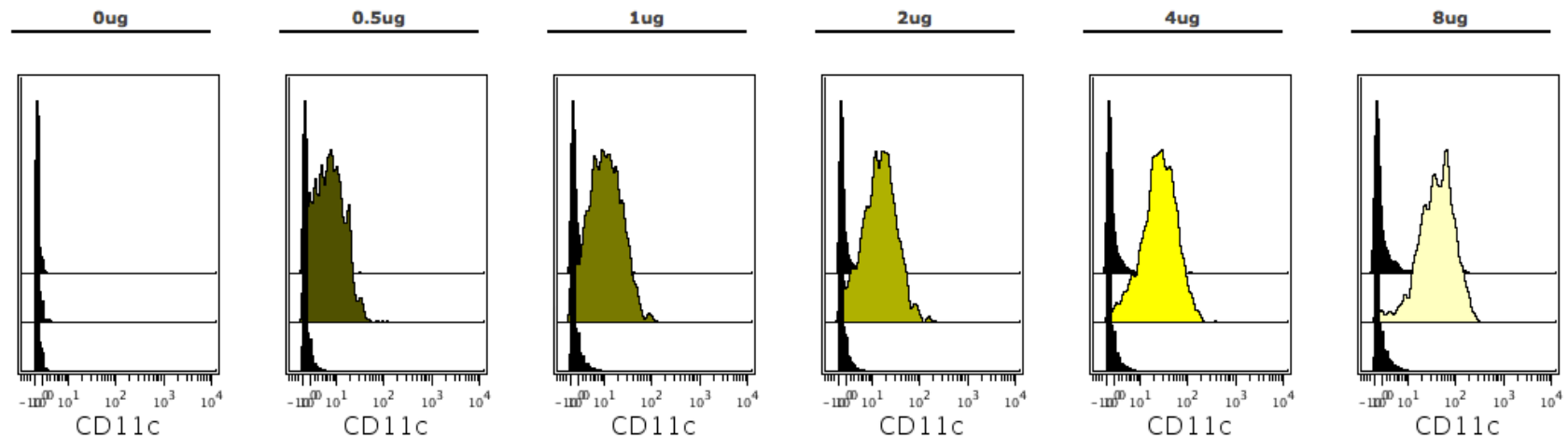
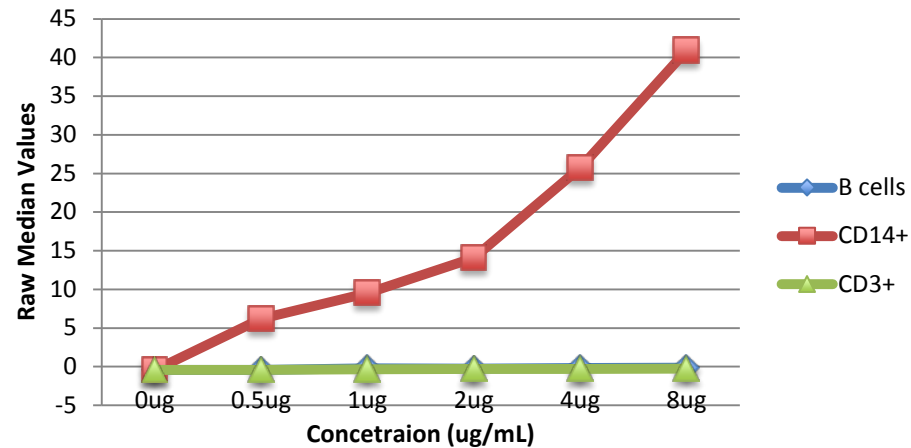
Conjugation: 2013-08-19

Titration: 2013-08-27

Staining conc.: 4ug/mL

PBMCs – Live/frozen, thawed - rested 3h

CD11c 157Gd



Raw Median Values

	0ug	0.5ug	1ug	2ug	4ug	8ug
B cells	-0.44	-0.42	-0.2	-0.27	-0.17	-0.14
CD14+	-0.46	6.2	9.52	14.07	25.74	40.89
CD3+	-0.44	-0.43	-0.33	-0.29	-0.28	-0.27

95th percentile

	0ug	0.5ug	1ug	2ug	4ug	8ug
B cells	0.7	5.03	14.03	9.37	21.32	55.95
CD14+	0.85	21.73	38.02	51.97	90.24	141.72
CD3+	0.83	1.91	3.78	3.27	3.74	4.67

CD33 158Gd (Surface)

Clone: WM53 (DVS)

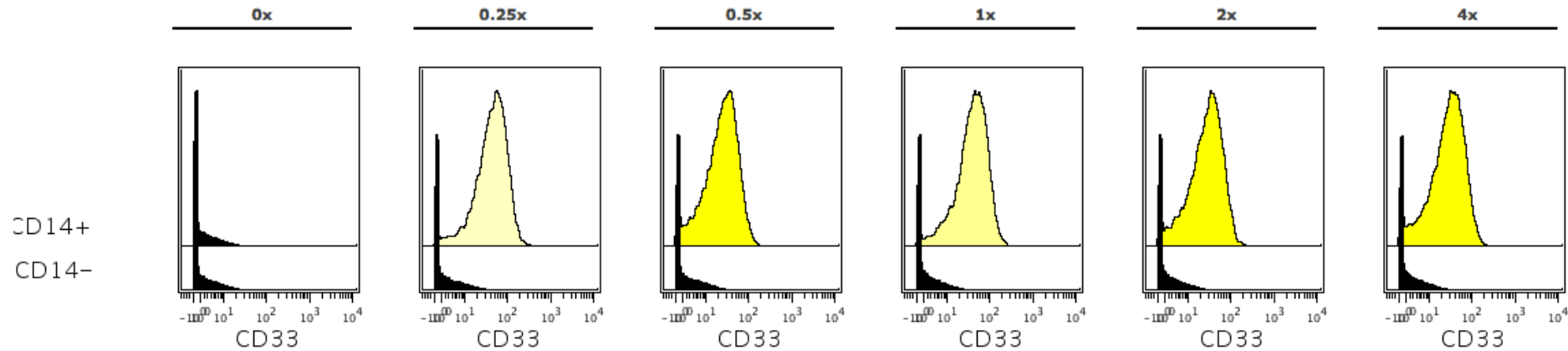
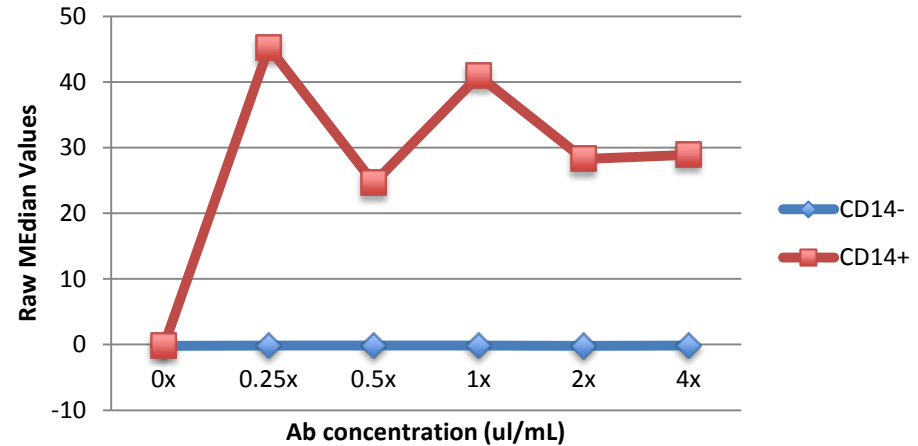
Conjugation: DVS

Titration: 2012-08-16

PBMCs – Live/frozen, thawed - rested 3h

Staining conc.: **0.5ul/test**

CD33 158Gd



Raw Median Values

	0x	0.25x	0.5x	1x	2x	4x
CD14+	-0.22	45.3	24.59	40.95	28.28	28.91
CD14-	-0.22	-0.17	-0.17	-0.15	-0.18	-0.16

95th percentile

	0x	0.25x	0.5x	1x	2x	4x
CD14+	10.98	124.94	74.69	115.08	84.66	89.22
CD14-	10.85	14.28	13.44	12.18	12.17	12.12

CCR7 159Tb (Surface)

Clone: 150503 (R&D systems)

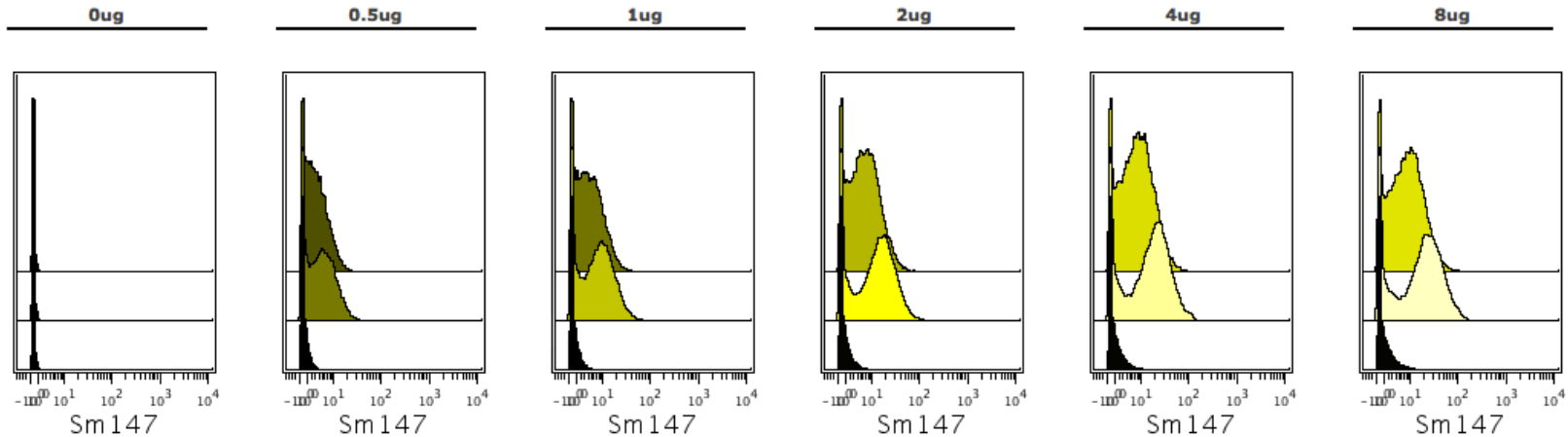
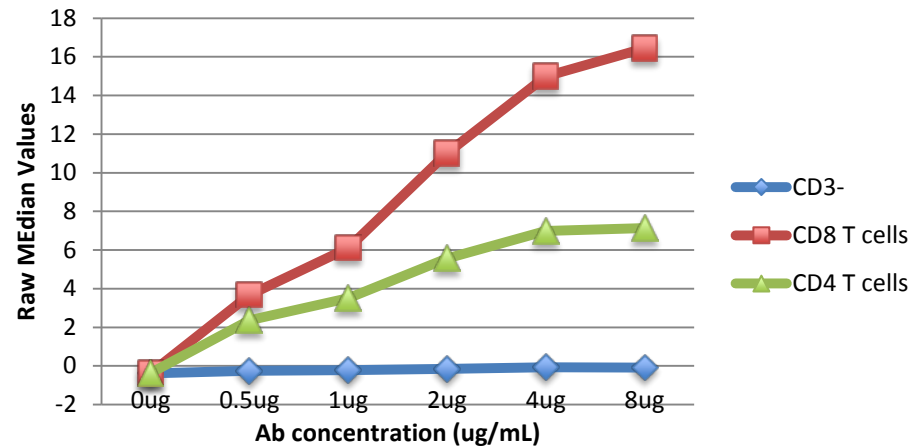
Conjugation: 2013-08-26

Titration: 2013-08-27

PBMCs – Live/frozen, thawed - rested 3h

Staining conc.: **3ug/mL**

CCR7 159Tb



Raw Median Values

	0ug	0.5ug	1ug	2ug	4ug	8ug
CD4 T cells	-0.37	2.36	3.5	5.57	6.99	7.13
CD8 T cells	-0.37	3.67	6.11	11.02	14.98	16.44
CD3-	-0.38	-0.25	-0.22	-0.15	-0.07	-0.08

95th percentile

	0ug	0.5ug	1ug	2ug	4ug	8ug
CD4 T cells	0.06	10.69	15.0	23.06	27.77	29.3
CD8 T cells	0.1	15.58	24.79	42.95	57.7	67.7
CD3-	0.02	1.7	2.27	3.45	5.17	6.38

CD14 160Gd (Surface)

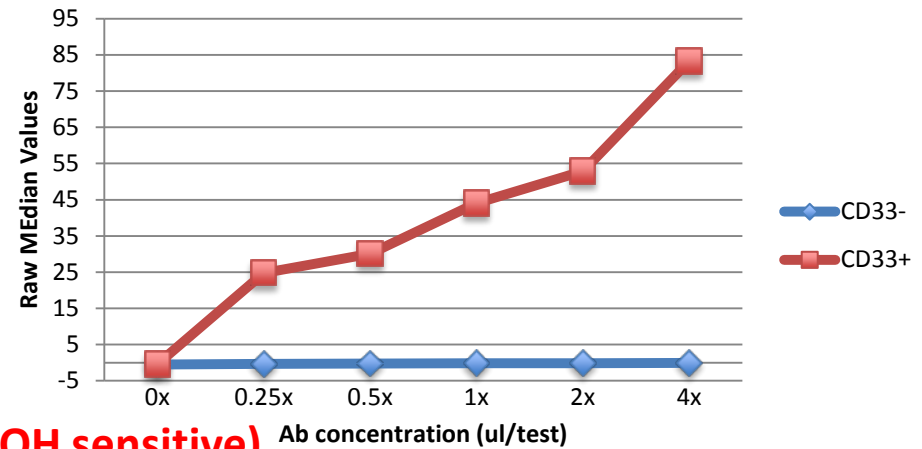
Clone: M5E2 (DVS)

Conjugation: DVS

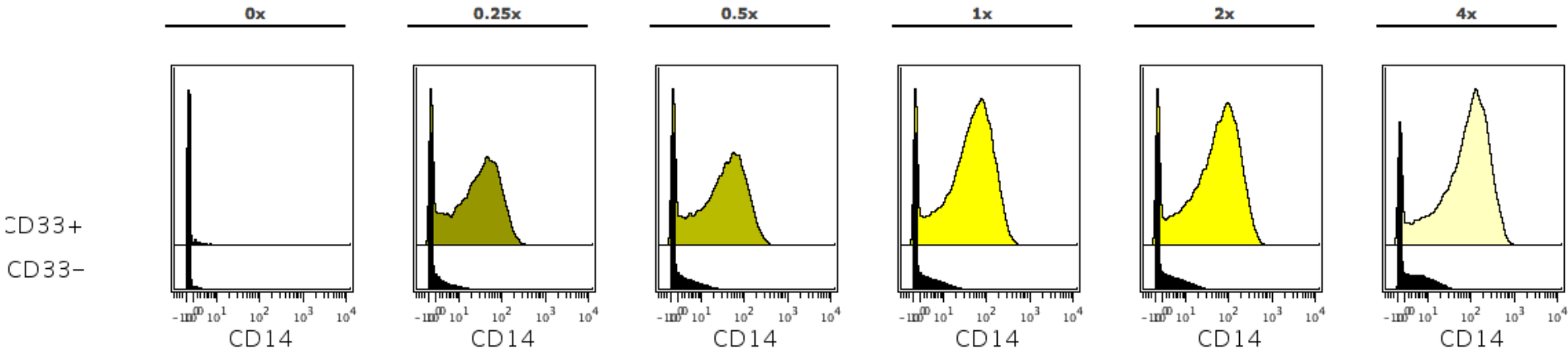
Titration: 2012-08-16

PBMCs – Live/frozen, thawed - rested 3h

CD14 160Gd



Staining conc.: **1.5ul/test (epitope is MeOH sensitive)**



Raw Median Values

95th percentile

	0x	0.25x	0.5x	1x	2x	4x
CD33+	-0.44	24.81	30.04	44.07	52.84	83.25
CD33-	-0.46	-0.28	-0.2	-0.17	-0.12	-0.04

	0x	0.25x	0.5x	1x	2x	4x
CD33+	2.8	125.86	153.39	198.72	248.99	356.03
CD33-	1.27	7.94	12.01	12.73	14.73	18.63

CD66b 161Dy (Surface)

Clone: G10F5 (Biolegend)

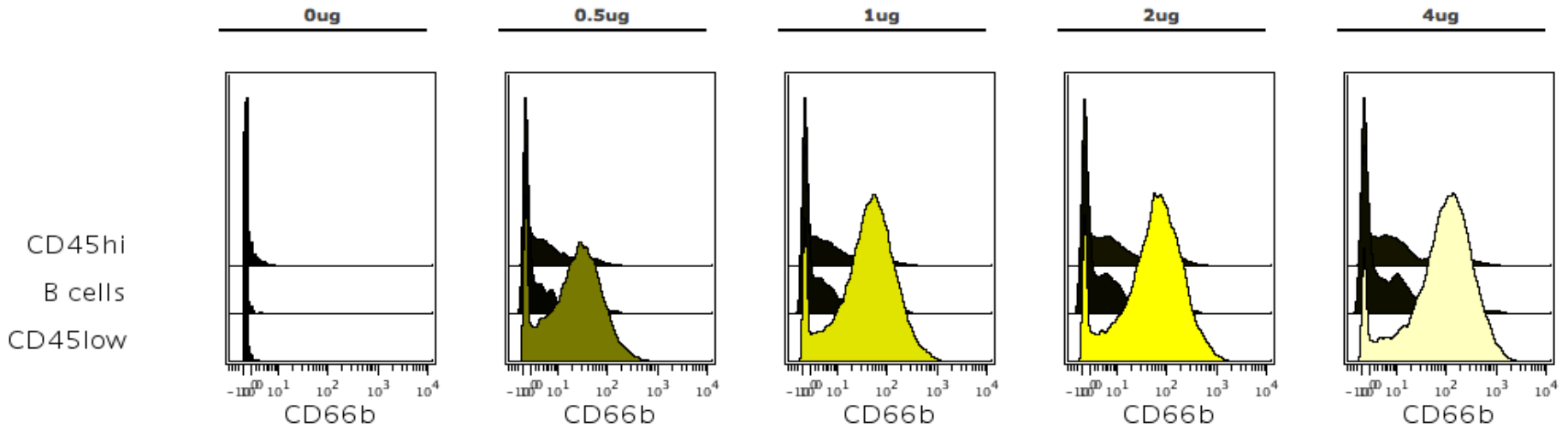
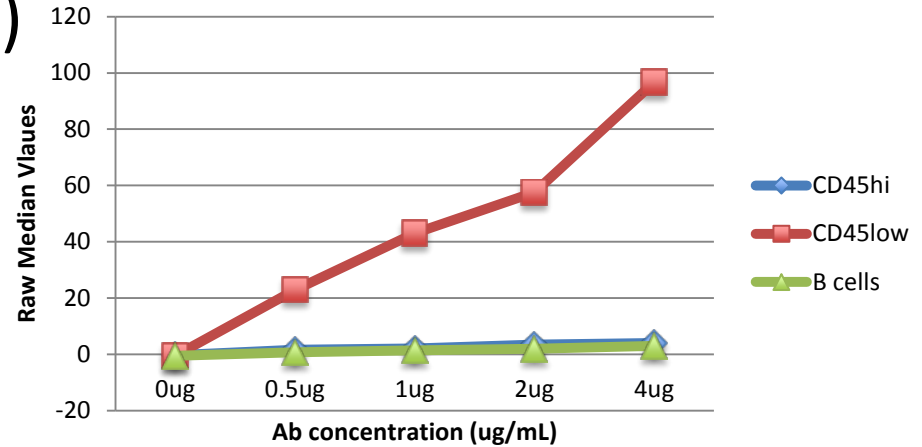
Conjugation: 2013-05-01

Titration: 2013-05-10

Whole Blood – Smart tube buffer treated

Staining conc.: **2ug/mL**

CD66b 161Dy



Raw Median Values

95th percentile

	0ug	0.5ug	1ug	2ug	4ug
CD45hi	-0.35	1.58	2.13	3.41	4.03
B cells	-0.52	0.73	1.45	1.96	2.95
CD45low	-0.49	22.89	43.03	57.55	96.7

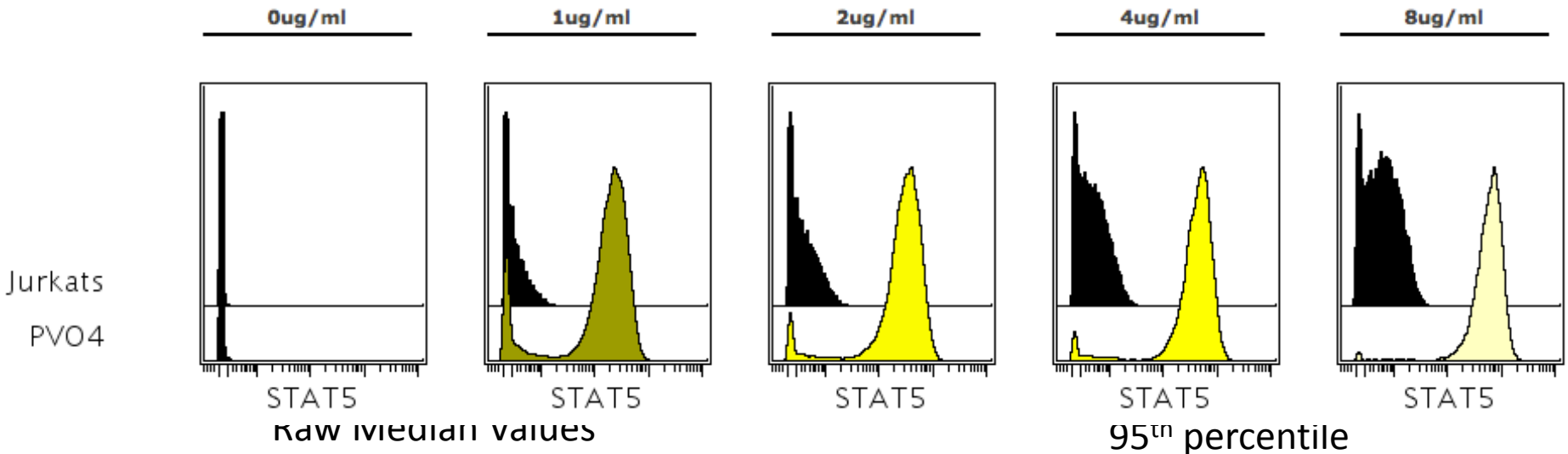
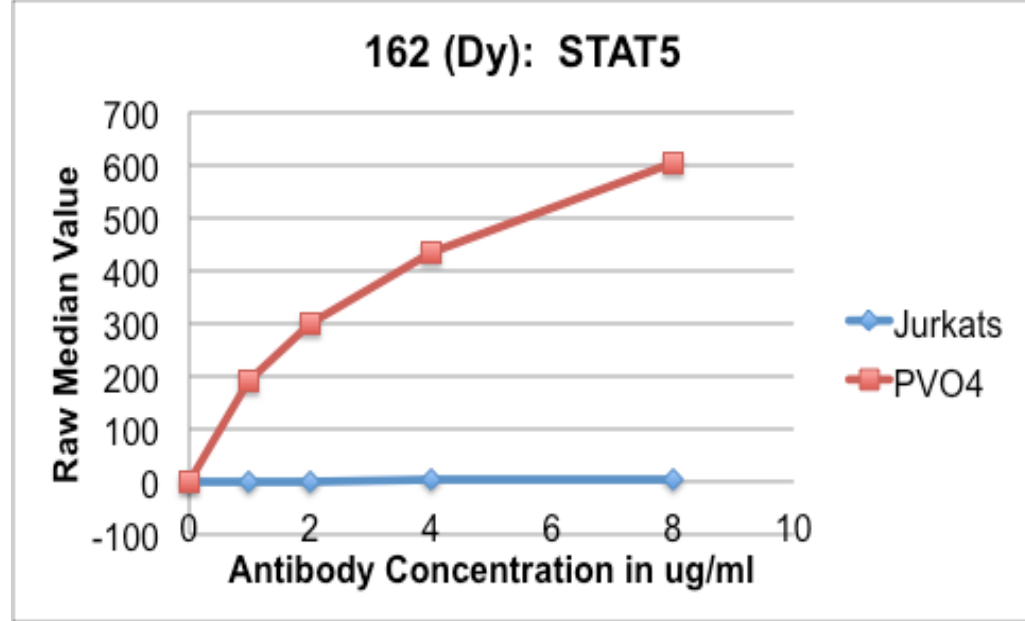
	0ug	0.5ug	1ug	2ug	4ug
CD45hi	3.12	60.81	107.54	177.77	263.03
B cells	0.23	55.96	88.15	156.87	257.43
CD45low	0.58	135.19	260.08	362.57	585.28

pSTAT5 162Dy (ICS)

Clone: 47 pY694 (BD)
 Conjugation: 2013-07-16
 Titration: 2013-08-16

Jurkat – PVO4 Stim

Staining conc.: **4ug/mL**



	0ug/ml	1ug/ml	2ug/ml	4ug/ml	8ug/ml
Jurkats	-0.58	0.54	1.58	3.06	4.87
PVO4	-0.59	188.56	299.01	432.66	602.37

CXCR3 163Dy (Surface)

Clone: G025H7 (Biolegend)

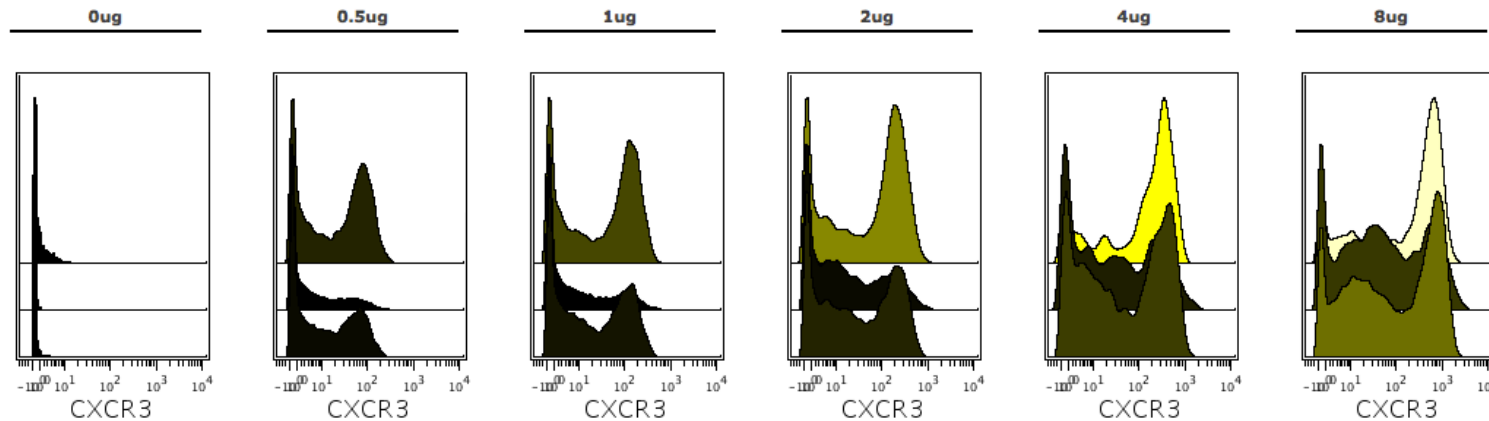
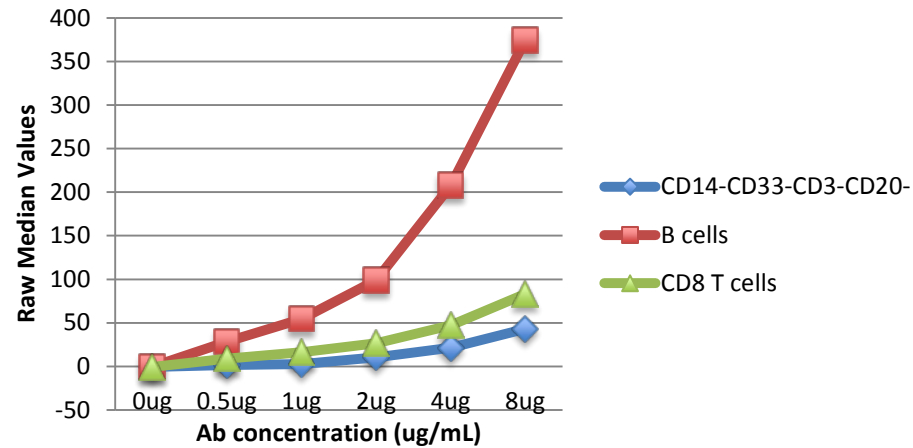
Conjugation: 2013-05-17

Titration: 2013-05-22

PBMCs – Live/frozen, thawed - rested 3h

Staining conc.: **2ug/mL**

CXCR3 163Dy



Raw Median Values

	0ug	0.5ug	1ug	2ug	4ug	8ug
B cells	-0.19	28.28	54.34	98.77	207.78	374.18
CD14-CD33-CD3-CD20-	-0.46	1.43	2.86	10.34	21.58	42.93
CD8 T cells	-0.44	9.06	16.15	26.47	47.26	83.24

95th percentile

	0ug	0.5ug	1ug	2ug	4ug	8ug
B cells	5.54	150.94	263.58	427.43	650.17	1096.53
CD14-CD33-CD3-CD20-	-0.01	95.42	187.91	360.0	647.73	1195.7
CD8 T cells	0.92	113.99	216.52	388.68	664.2	1191.4

ICOS 164Dy (Surface)

Clone: C398.4A (Biolegend)

Conjugation: 2013-08-19

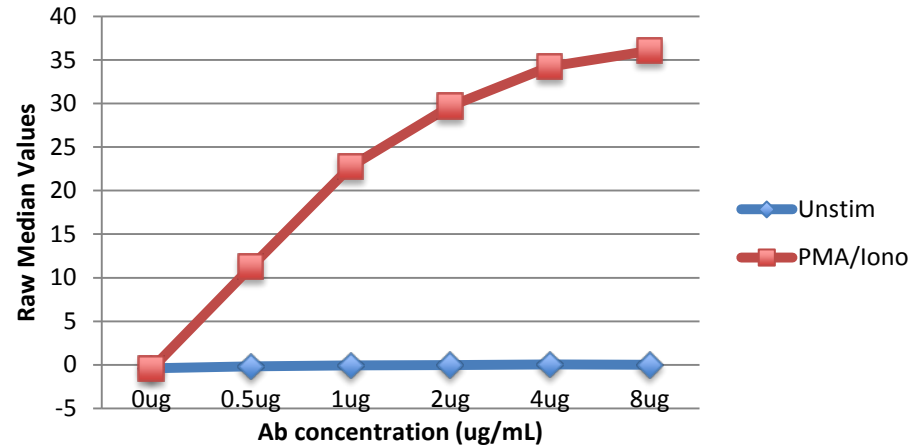
Titration: 2013-09-05

PBMCs – Live/frozen, thawed

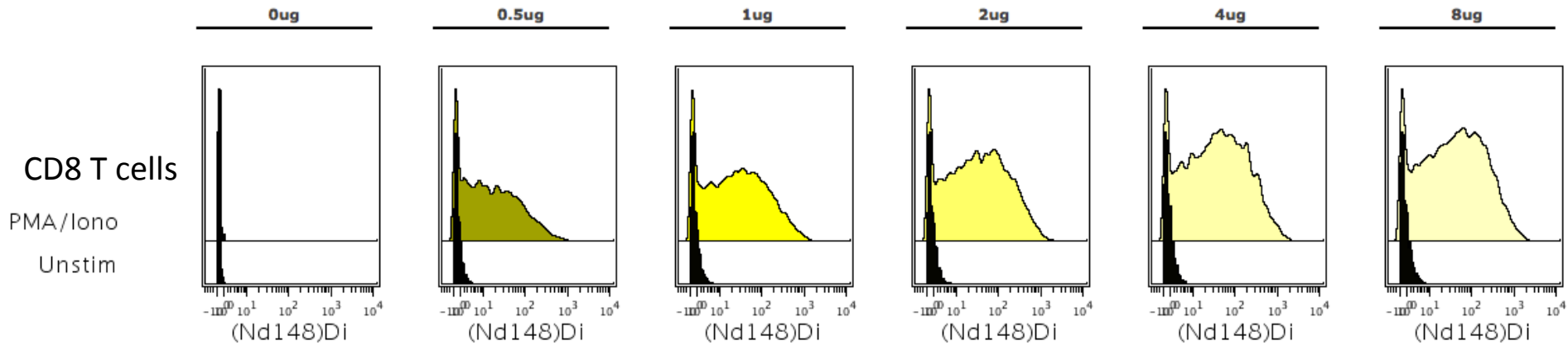
– 24h stim PMA/Iono

Staining conc.: **2ug/mL**

ICOS 164Dy



ICOS - Panel 1



Raw Median Values

	0ug	0.5ug	1ug	2ug	4ug	8ug
PMA/Iono	-0.48	11.25	22.78	29.68	34.25	36.05
Unstim	-0.41	-0.18	-0.07	-0.04	0.05	0.0

95th percentile

	0ug	0.5ug	1ug	2ug	4ug	8ug
PMA/Iono	0.13	199.77	355.04	418.24	464.28	480.5
Unstim	-0.01	2.12	2.71	2.7	2.99	3.4

CD16 165Ho (Surface)

Clone: 3G8 (DVS)

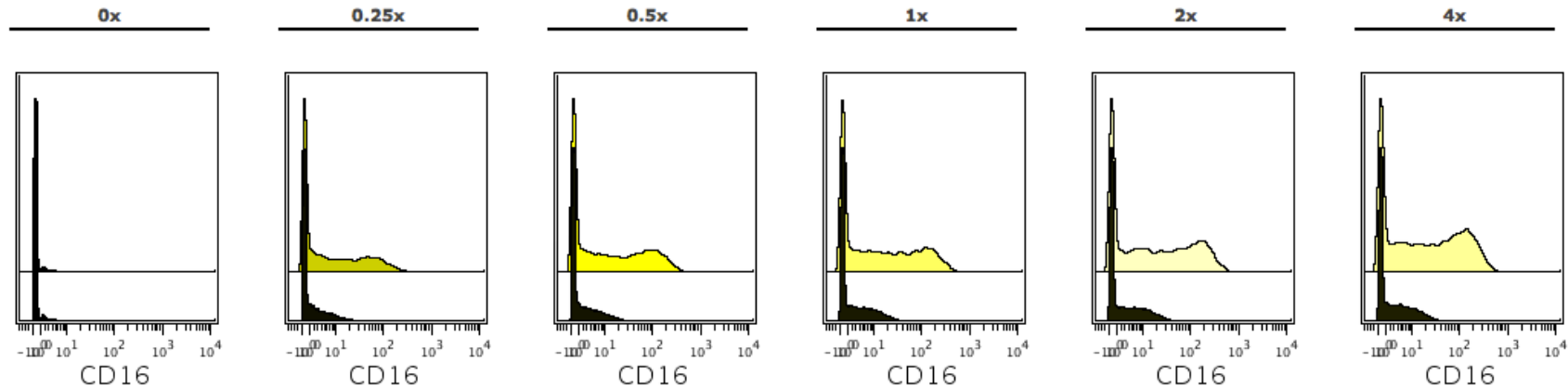
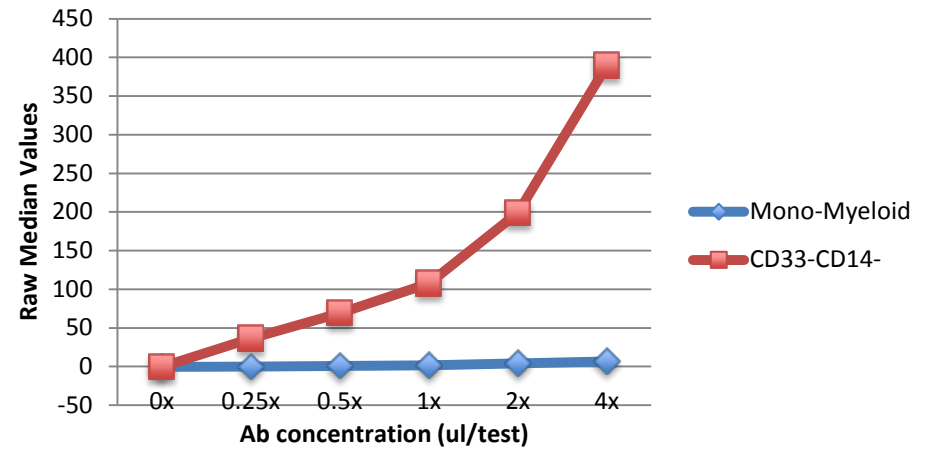
Conjugation: DVS

Titration: 2012-08-16

PBMCs – Live/frozen, thawed - rested 3h

Staining conc.: **1ul/test**

CD16 165Ho



Raw Median Values

95th percentile

	0x	0.25x	0.5x	1x	2x	4x
CD3-	-0.45	2.11	5.2	6.96	10.12	13.25
CD4+	-0.44	-0.23	-0.18	-0.11	-0.1	-0.05

	0x	0.25x	0.5x	1x	2x	4x
CD3-	2.07	107.81	181.14	215.65	261.9	239.98
CD4+	2.29	10.33	12.94	16.4	19.29	17.42

FoxP3 166Er (ICS)

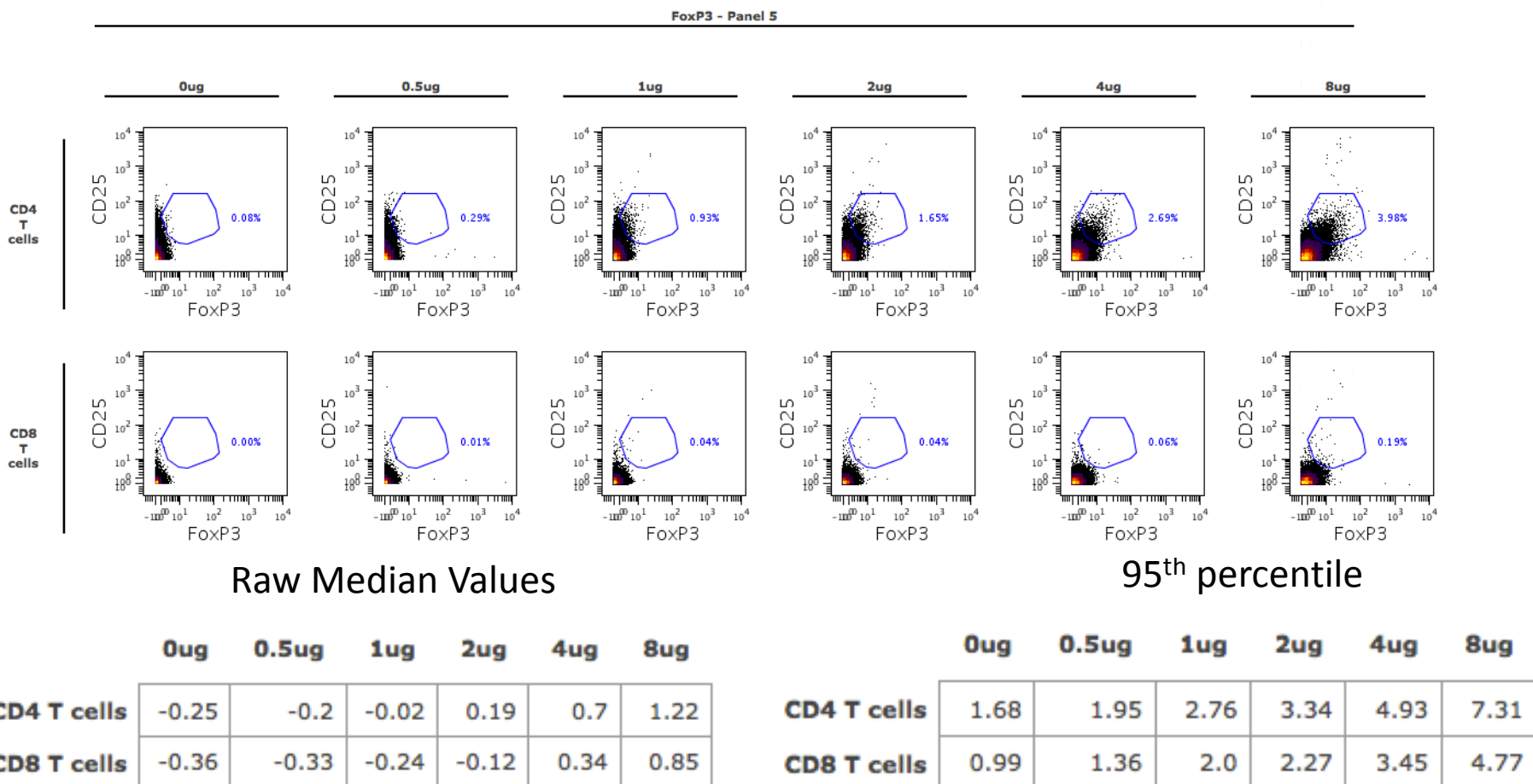
Clone: PCH101 (Ebioscience)

Conjugation: 2013-08-26

Titration: 2013-08-27

Staining conc.: **8ug/mL**

PBMCs – Live/frozen, thawed - rested 3h



CD163 167Er (Surface)

Clone: GHI/61 (BD)

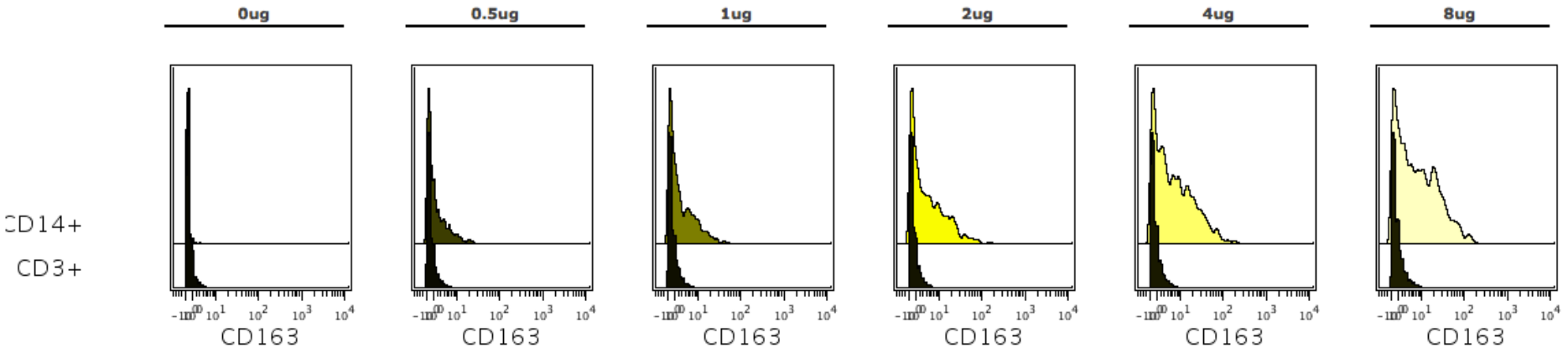
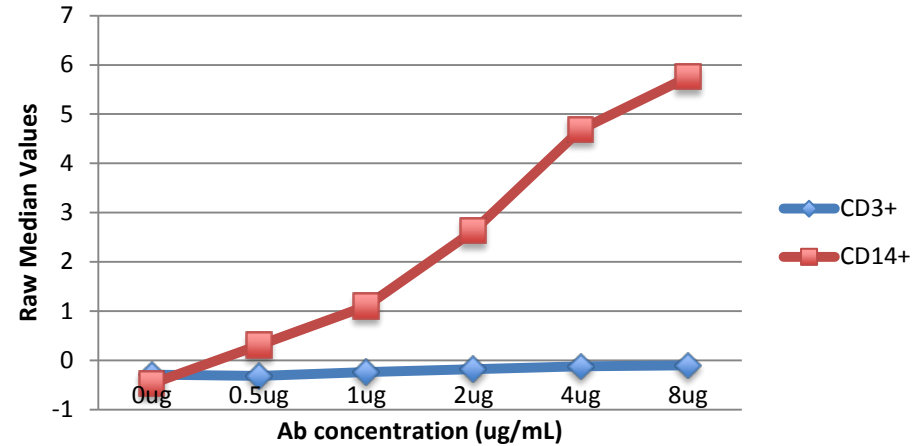
Conjugation: 2013-08-26

Titration: 2013-09-05

PBMCs – Live/frozen, thawed - rested 3h

Staining conc.: **6 ug/mL**

CD163 167Er



Raw Median Values

95th percentile

	0ug	0.5ug	1ug	2ug	4ug	8ug
CD14+	-0.47	0.31	1.1	2.63	4.69	5.75
CD3+	-0.29	-0.32	-0.24	-0.18	-0.12	-0.1

	0ug	0.5ug	1ug	2ug	4ug	8ug
CD14+	-0.01	10.57	16.71	33.18	49.23	57.05
CD3+	1.97	2.61	3.13	2.97	3.68	4.23

CD68 168Er (ICS)

Clone: Y1/82A (Biolegend)

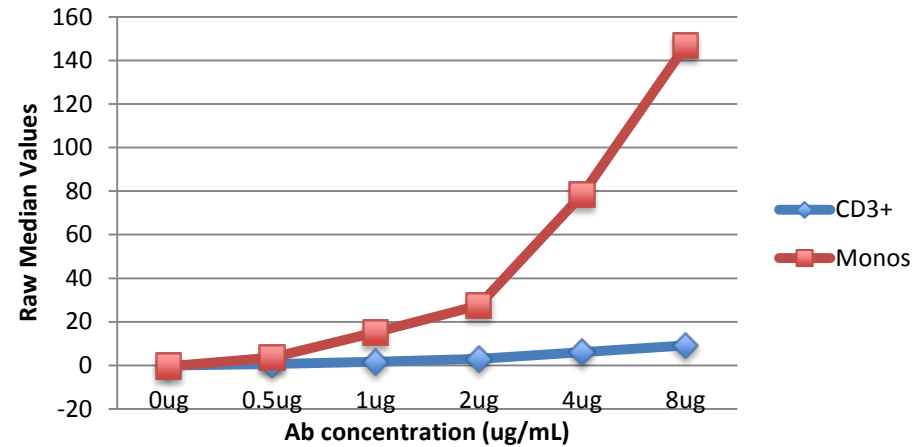
Conjugation: 2013-08-26

Titration: 2013-08-27

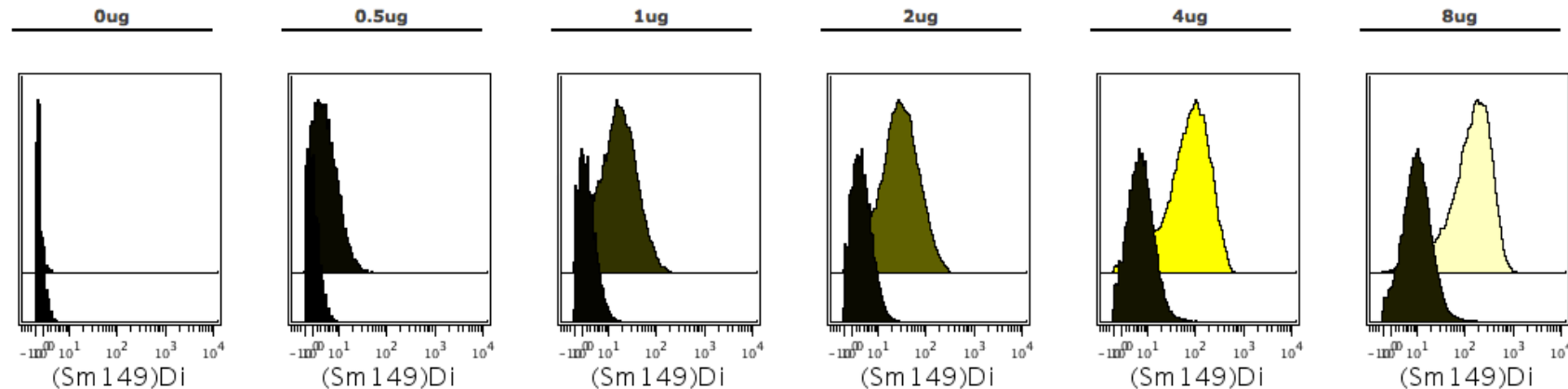
PBMCs – Live/frozen, thawed - rested 3h

Staining conc.: **6 ug/mL**

CD68 168Er



CD68 - Panel 5



Raw Median Values

	0ug	0.5ug	1ug	2ug	4ug	8ug
Monos	-0.41	3.53	15.19	27.46	78.45	146.82
CD3+	-0.12	0.62	1.67	2.97	6.11	9.2

95th percentile

	0ug	0.5ug	1ug	2ug	4ug	8ug
Monos	1.29	14.65	63.97	117.47	285.24	463.01
CD3+	2.06	4.03	7.14	10.44	20.53	31.53

CD25 169Tm (Surface)

Clone: 2A3 (DVS)

Conjugation: DVS

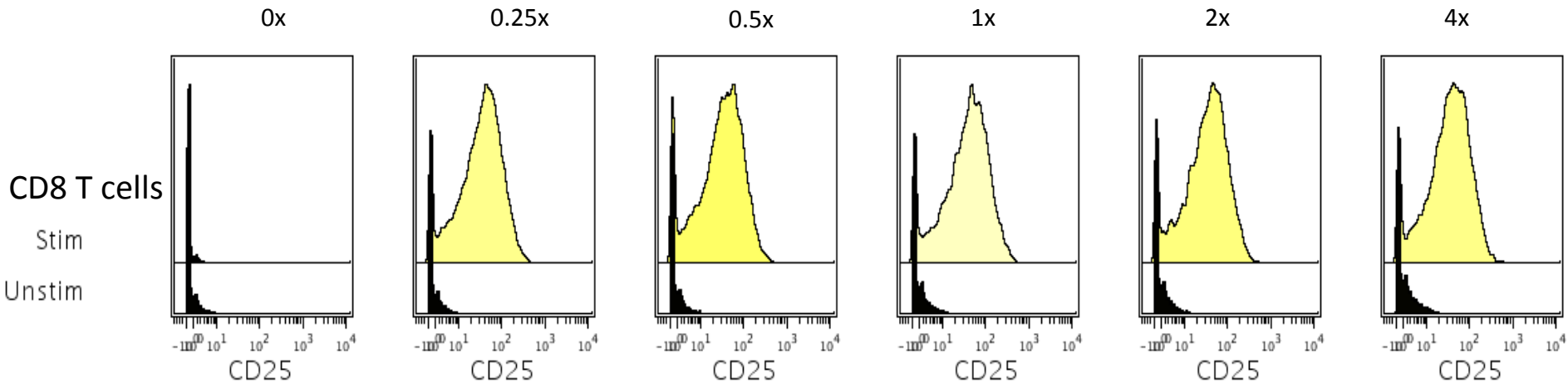
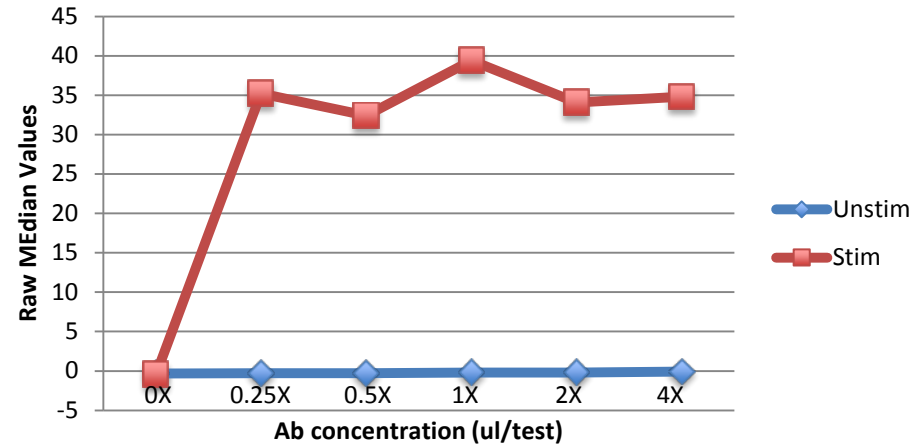
Titration: 2012-12-12

PBMCs – Live/frozen, thawed

– 24h stim PMA/Iono

Staining conc.: **1ul/test**

CD25 169Tm



Raw Median Values

95th percentile

	0x	0.25x	0.5x	1x	2x	8x
Stim	-0.43	35.2	32.42	39.41	34.09	34.83
Unstim	-0.33	-0.3	-0.28	-0.2	-0.19	-0.09

	0x	0.25x	0.5x	1x	2x	8x
Stim	1.64	154.86	147.81	178.73	154.24	156.12
Unstim	3.69	3.86	4.75	6.19	6.27	8.72

CD3 170Er (Surface)

Clone: UCHT1 (DVS)

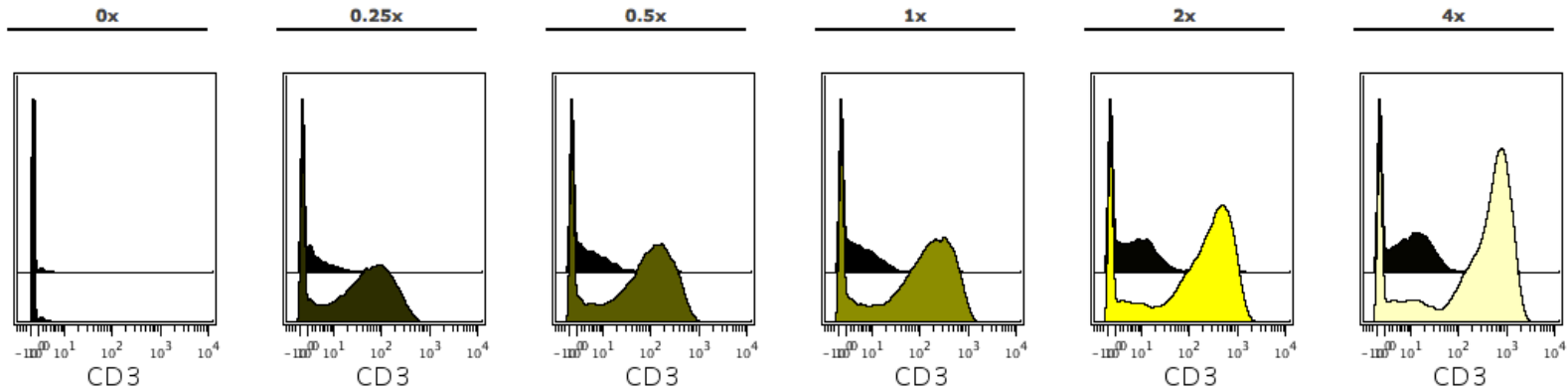
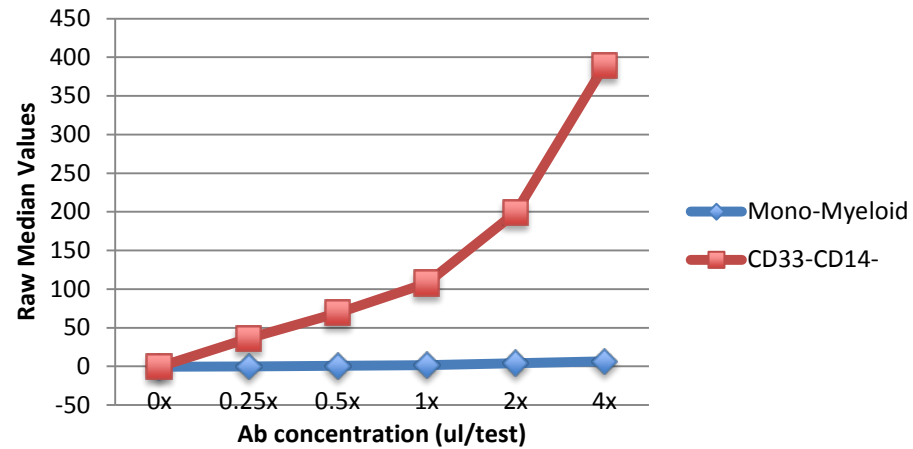
Conjugation: DVS

Titration: 2012-08-16

PBMCs – Live/frozen, thawed - rested 3h

Staining conc.: **0.5ul/test**

CD3 170Er



Raw Median Values

95th percentile

	0x	0.25x	0.5x	1x	2x	4x
Mono-Myeloid	-0.45	-0.09	0.89	1.51	3.85	6.43
CD33-CD14-	-0.45	36.35	68.91	107.47	199.1	389.8

	0x	0.25x	0.5x	1x	2x	4x
Mono-Myeloid	1.91	29.73	117.66	172.81	364.06	436.12
CD33-CD14-	1.83	257.99	423.1	676.11	988.06	1430.68

cPARP 171Yb (ICS)

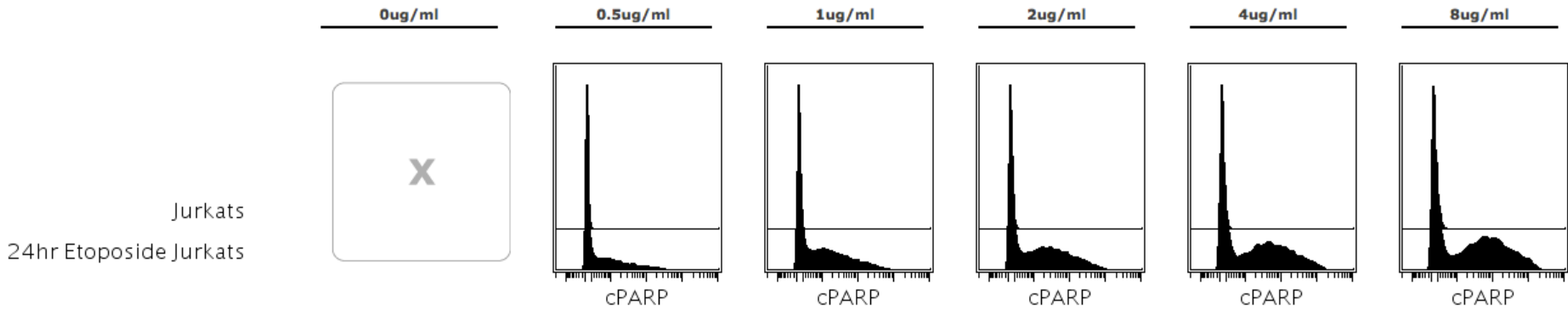
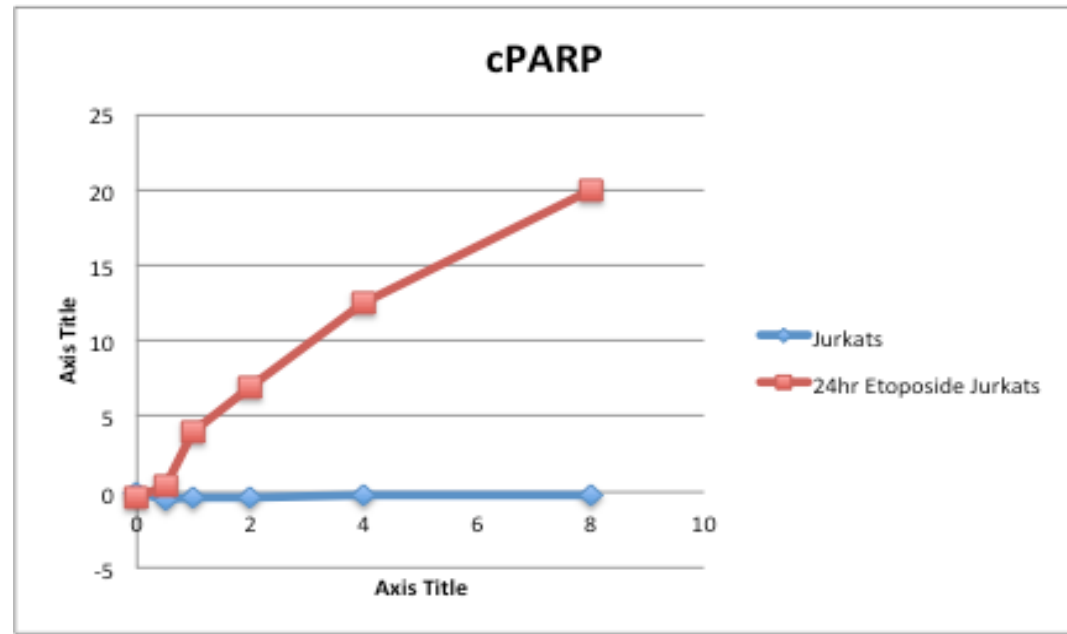
Clone: F21- 852 (BD)

Conjugation: 2013-08-21

Titration: 2013-9-10

Jurkat, – 24h Etoposide

Staining conc.: **4ug/mL**



Raw Median Values

95th percentile

	0ug/ml	0.5ug/ml	1ug/ml	2ug/ml	4ug/ml	8ug/ml
Jurkats	X	-0.46	-0.39	-0.33	-0.26	-0.14
24hr Etoposide Jurkats	-0.42	0.47	3.91	6.93	12.57	19.95

pS6 172Yb (ICS)

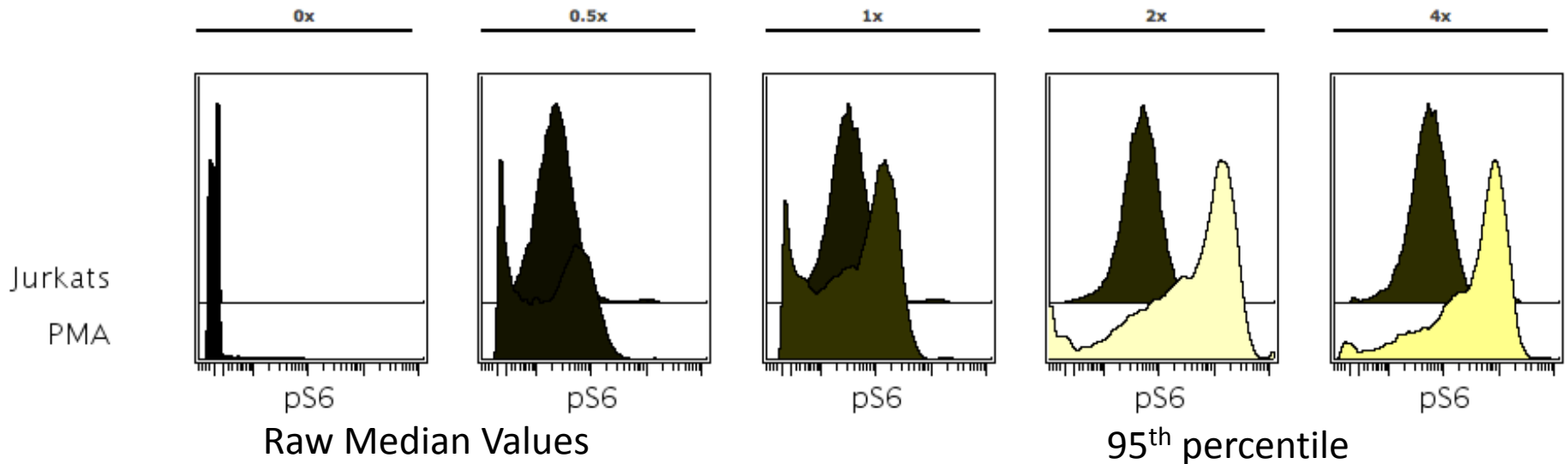
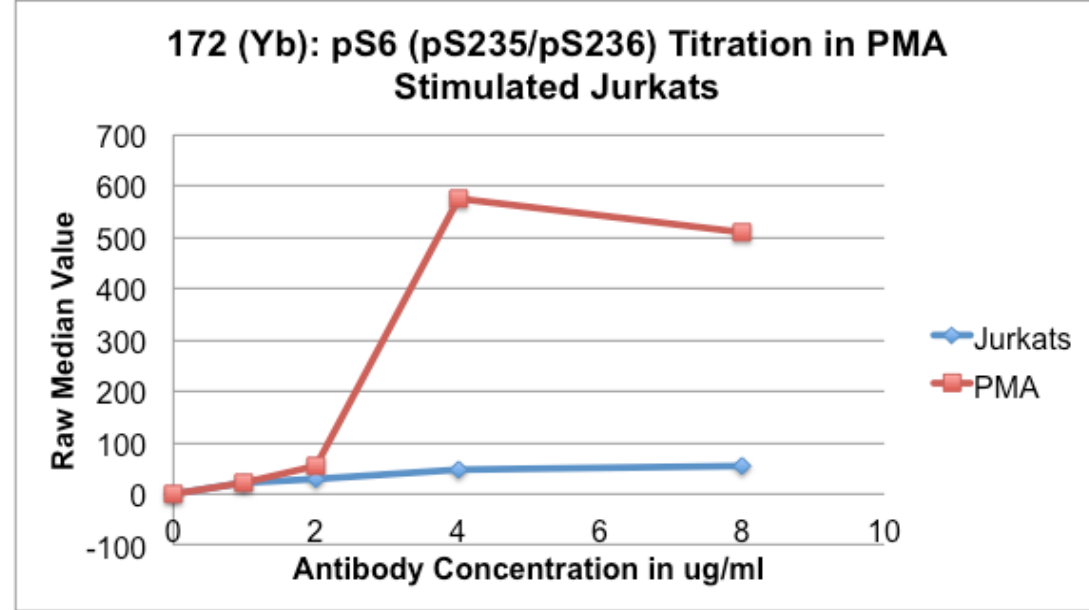
Clone: N7-548 pS235/S236 (BD)

Conjugation: 2013-10-04

Titration: 2013-04-15

Jurkat – PMA stim

Staining conc.: **4ug/mL**



	0x	0.5x	1x	2x	4x
Jurkats	-0.37	21.06	30.42	47.9	55.17
PMA	-1.19	21.98	55.86	575.43	511.01

LAG-3 173Yb (Surface)

Clone: N/A (R&D systems)

Conjugation: 2013-08-19

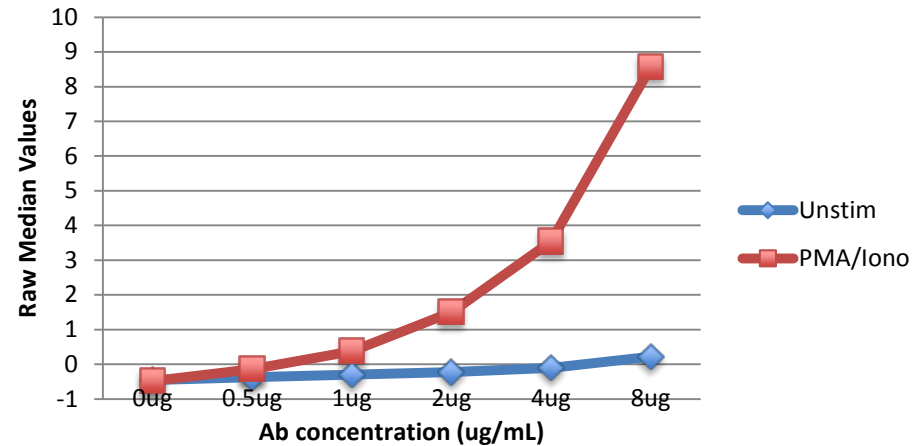
Titration: 2013-09-05

PBMCs – Live/frozen, thawed

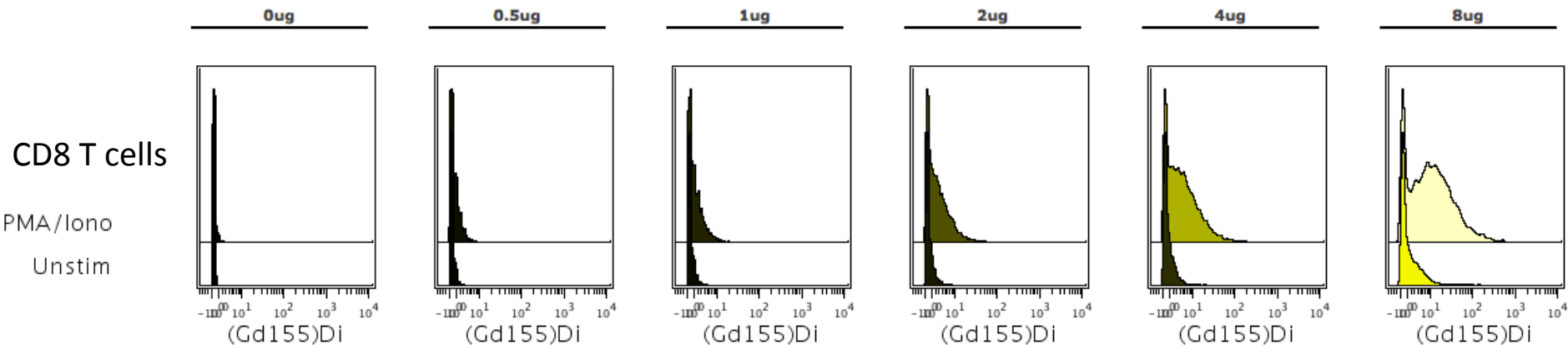
– 24h stim PMA/Iono

Staining conc.: **6ug/mL**

LAG3- 173Yb



LAG3 - Panel 1



Raw Median Values

95th percentile

	0ug	0.5ug	1ug	2ug	4ug	8ug
PMA/Iono	-0.48	-0.14	0.38	1.5	3.54	8.57
Unstim	-0.45	-0.37	-0.3	-0.22	-0.1	0.22

	0ug	0.5ug	1ug	2ug	4ug	8ug
PMA/Iono	0.69	3.18	6.31	13.14	29.22	83.73
Unstim	-0.04	0.99	2.24	4.35	7.91	40.87

pCREB 174Yb (ICS)

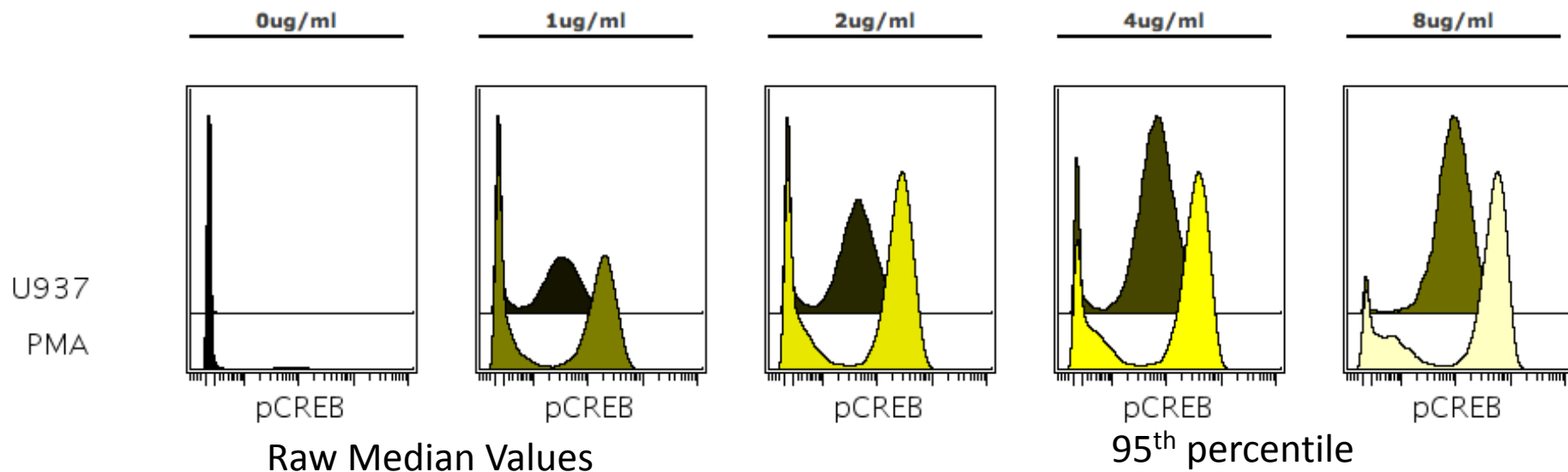
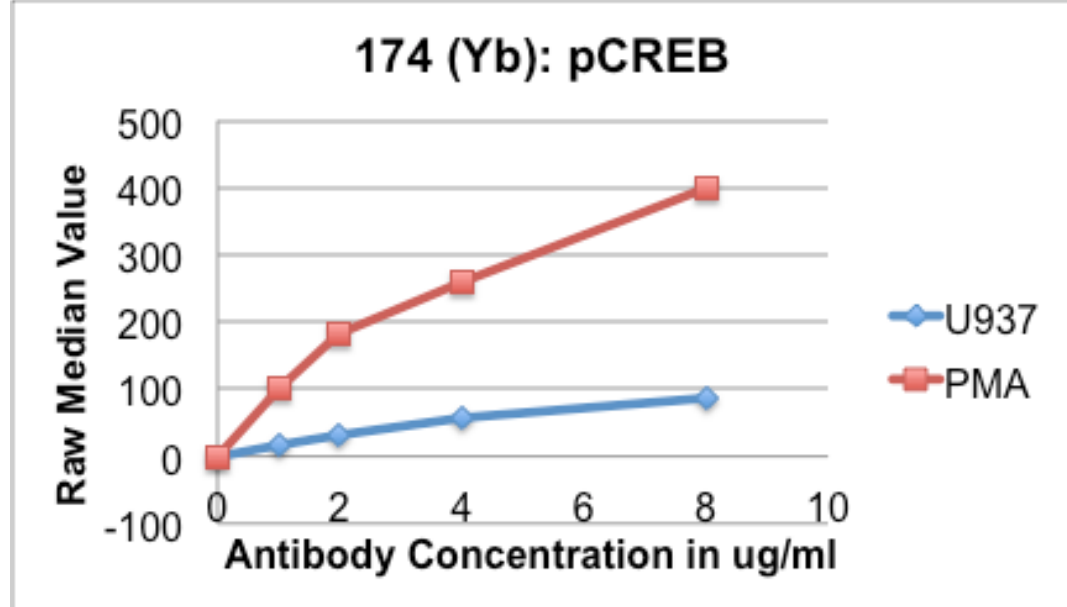
Clone: 87G3 pS133 (CST)

Conjugation: 2013-7-22

Titration: 2013-8-16

U937 - PMA stim

Staining conc.: **2ug/mL**



	0ug/ml	1ug/ml	2ug/ml	4ug/ml	8ug/ml
U937	-0.46	18.57	33.0	58.01	88.48
PMA	-0.37	101.07	182.36	260.27	399.95

PD-1 175Lu (Surface)

Clone: EH12.2H7 (DVS)

Conjugation: DVS

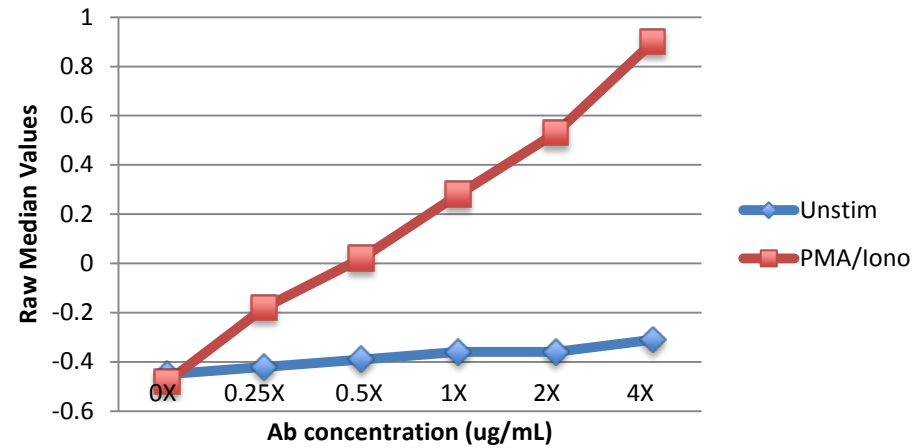
Titration: 2013-09-05

PBMCs – Live/frozen, thawed

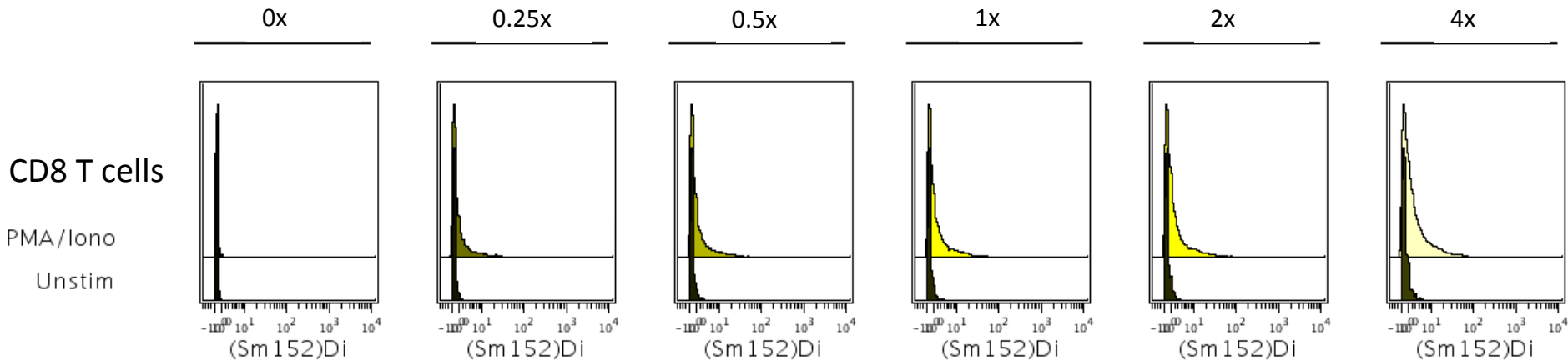
– 24h stim PMA/Iono

Staining conc.: **2ul/test**

PD-1 175Lu



PD1 - Panel 1



Raw Median Values

0x 0.25x 0.5x 1x 2x 4x

PMA/Iono	-0.48	-0.18	0.02	0.28	0.53	0.9
Unstim	-0.45	-0.42	-0.39	-0.36	-0.36	-0.31

95th percentile

0x 0.25x 0.5x 1x 2x 4x

PMA/Iono	-0.02	11.8	14.57	15.53	16.77	18.89
Unstim	-0.04	0.61	1.08	1.24	1.57	2.19

CD56 176Yb (Surface)

Clone: NCAM16.2 (BD)

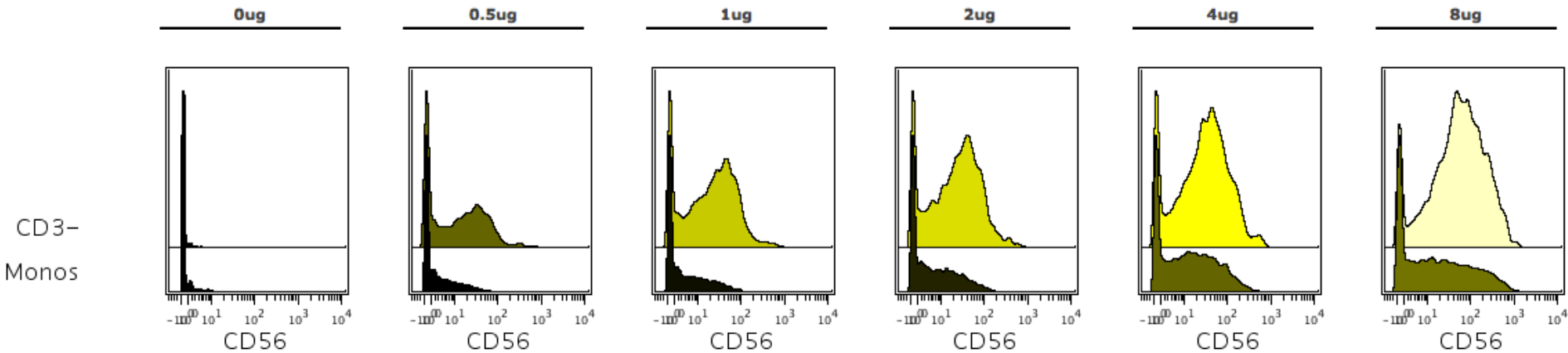
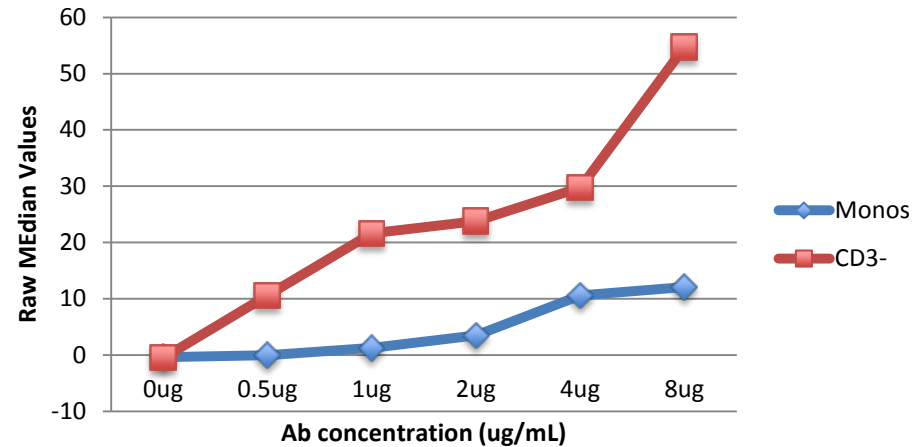
Conjugation: 2013-01-24

Titration: 2013-01-26

PBMCs – Live/frozen, thawed - rested 3h

Staining conc.: **1ug/mL**

CD56 176Yb



Raw Median Values

95th percentile

0ug 0.5ug 1ug 2ug 4ug 8ug

0ug 0.5ug 1ug 2ug 4ug 8ug

CD3- -0.47 10.58 21.65 23.81 29.75 54.71

CD3- 1.39 106.78 133.97 148.9 201.57 407.62

Monos -0.39 -0.02 1.28 3.49 10.61 12.08

Monos 4.69 28.51 45.61 65.24 139.91 352.34

CD56 176Yb (Surface)

Clone: NCAM16.2 (BD)

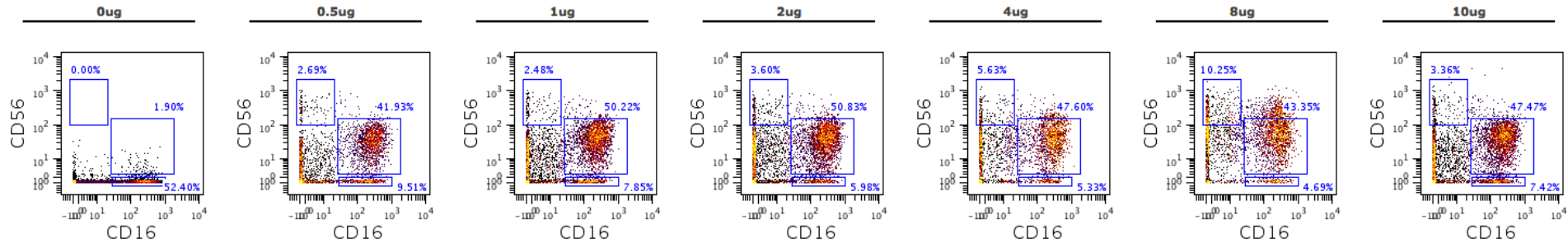
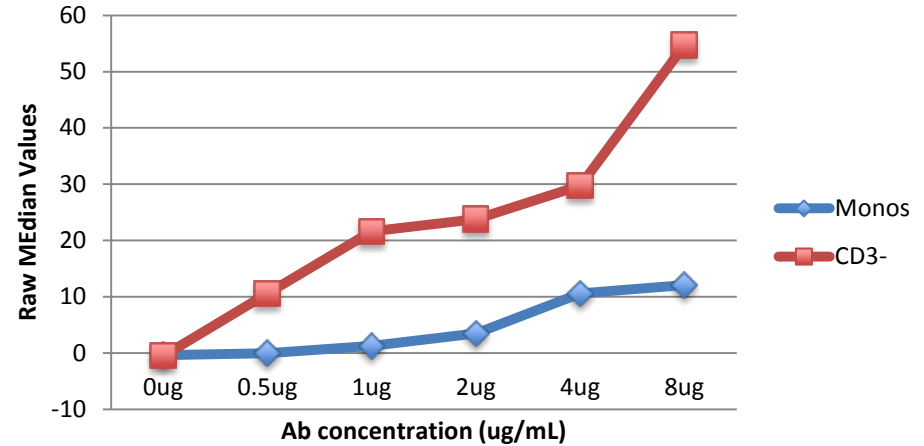
Conjugation: 2013-01-24

Titration: 2013-01-26

PBMCs – Live/frozen, thawed - rested 3h

Staining conc.: **1ug/mL**

CD56 176Yb



Raw Median Values

95th percentile

0ug 0.5ug 1ug 2ug 4ug 8ug

0ug 0.5ug 1ug 2ug 4ug 8ug

CD3- -0.47 10.58 21.65 23.81 29.75 54.71

CD3- 1.39 106.78 133.97 148.9 201.57 407.62

Monos -0.39 -0.02 1.28 3.49 10.61 12.08

Monos 4.69 28.51 45.61 65.24 139.91 352.34